

Newcastle
University



Characterising the invasion of *Streptococcus mutans* into an oral community using *in vitro* and *in silico* modelling

School of Engineering

Jay Awtar Singh Sangha BSc (Hons), MSc (Hons)

Thesis submitted in partial fulfilment of the requirements for the degree of Doctor of Philosophy

December 2022

Abstract

The transition of a commensal dental biofilm, to one overpopulated with acidogenic species, e.g. *Streptococcus mutans*, is associated with caries development. Approaches to understand this dysbiosis have not balanced representing the complexity of dental biofilms, with defining the factors underpinning caries development, including interspecies interactions and pH influence. This research aimed to characterise *S. mutans* invasion into a synthetic oral community, to better understand the factors contributing to colonisation, using modelling approaches in a defined environment.

A 4-species synthetic oral community, comprised of *Streptococcus gordonii*, *Actinomyces oris*, *Neisseria subflava*, and *Veillonella parvula*, was exposed to *S. mutans*. Biofilms were grown on hydroxyapatite coupons in continuous flow bioreactors, using a developed chemically defined medium, supplemented with glucose and lactic acid. Biofilm and planktonic growth were simulated with a 2-D Individual-based model (IbM) and a 0-D continuous reactor model, respectively.

High glucose and lactic acid concentrations resulted in a significant pH drop and *S. mutans* dominating the biofilm and planktonic communities. In substrate-limited environments, the community composition, measured by qPCR and *fluorescence in situ hybridization*, was more balanced. The IbM simulated *S. mutans* dominance at high glucose concentrations, using kinetic parameters collected experimentally. When the influence of pH on the bacterial growth kinetics was considered, rather than just on chemical speciation, the simulations corroborated with *in vitro* and *in vivo* findings.

I have developed *in vitro* and *in silico* models characterising *S. mutans* invasion of a 4-species commensal community, improving on previous attempts to represent the complexity of the dental biofilm. These models have advanced knowledge of the importance of pH in *S. mutans* invasion and considering pH in growth kinetics within simulations. Models will assist safe oral care product development by enabling the impact of antibacterial agents on the dental biofilm to be studied without *in vivo* assessment.

Acknowledgements

I would not have been able to complete my research and this thesis without the support and generosity of so many people during my time in Newcastle. I would like to thank my supervisors for their guidance during my studies. Firstly, I would like to thank Dana for helping me in the modelling aspect of my research, with scientific writing throughout the project, and for allowing me to develop as a researcher. I want to thank Nick for giving me a home in the dental school, where I have grown enormously as a scientist and met so many great people. Thank you also for your support regarding everything microbiology related. Tom, I would like to thank you for your overall support and guidance, particularly at the ISME conference. I would like to thank both of my supervisors over at Unilever, Aline, and Paul. I appreciate your help during these studies, including keeping perspective of the impact of my research, and for hosting me at the Safety and Environmental Assurance Centre at Unilever. I would also like to give a special thank you to Valentina, who has helped me enormously with the modelling aspect of this research when you did not have to. I will forever be grateful and hope to one day repay the generosity. I would like to thank my funding bodies the Engineering and Physical Sciences Research Council, and the Safety and Environmental Assurance Centre at Unilever, for funding my research over the course of the last 4 years.

I thank everyone from the level 7 lab for keeping me sane during my time conducting experiments and making me feel at home from the very first day. I want to thank my lab sisters Nadia and Zella. Nadia for reigning me in and giving advice when I fell into bad habits of overworking to the point of burning out and Zella for all the food breaks. My mental health thanks you, even if my bank balance does not. I would also like to thank Jamie and Chris for all your support, both for experimental advice and for being present as very good friends. I would also like to thank my friends over in Merz court for keeping me company during my time in the Biolab and whilst writing the annual reports. There are too many of you to mention, but specifically Obaidullah for being a fantastic desk buddy and for the wonderful home-cooked food, and James for the two years of being a flatmate during Covid, ranting about the stresses of PhD life. I would like to thank the laboratory technicians for their support. Manpreet and Paul, I appreciate all your help autoclaving my reactors and carboys in engineering. I want to thank the city of Newcastle, which will always feel like home, due to the fantastic memories, generosity of the people, and plethora of amazing food places.

I would like to thank my family for all their support during the last 4 years. Firstly, my mum and dad for assuring me that I will finish my research, in times when I thought I was not capable of doing so. I would like to thank my Pinder and Rani Dhadi, for all the life advice. Without this, I would not have even taken this project. I thank my siblings for always being the inspiration to push myself to become better in every facet, including my research. I would like to thank the people who are no longer with us, including my Baba and Dhadi ma, who will always be with me and whom I hope to have made proud by getting to this point through all the obstacles that I have faced. Finally, I would like to thank Surina for all the support in the good times and bad during this PhD. The goal of spending our lives together after this project kept me going every time I have been ready to throw in the towel.

I dedicate this project and everything else that I achieve in life, to my brother and best friend Rajan. I have an endless amount of stories to share with you one day over a glass of milk and a PlayStation controller. Until then, I hope that I am making you proud.

Conference attendance, publications, and awards

Conference presentations:

Cold Spring Harbor Laboratory, virtual conference, 20-23rd October 2020

Poster presentation- The development of a chemically defined medium for a synthetic oral microbial community and its characterisation with FISH.

Oral Microbiology and Immunology Group, virtual conference, 24th-29th March 2021

Poster presentation-The development of a chemically defined medium for a synthetic oral microbial community and its characterisation with FISH.

Microbiology Society 2022, Belfast, Ireland, 4th-7th April 2022

Poster presentation- The effect of glucose on *Streptococcus mutans* invasion of an *in vitro* synthetic community of oral bacteria.

International Symposium on Microbial Ecology, Laussane, Switzerland, 14th-19th August 2022

Oral presentation-Modelling *Streptococcus mutans* invasion of an *in vitro* synthetic community of oral bacteria.

Publications:

Paper 1 (in process of submission)-

Characterising the invasion of *Streptococcus mutans* into an oral multispecies community using an *in vitro* model.

Paper 2: (in process of submission)-

Mathematical models of multispecies dental biofilm stress the importance of considering pH in modelling growth.

Awards:

Unilever Safety and Environmental Assurance Centre, Bedford, 13-15th June 2022

PhD prize award; runner up.

Table of contents

| | |
|--|------------------------------|
| Abstract | i |
| COVID-19 impact statement | Error! Bookmark not defined. |
| Acknowledgements | iii |
| Conference attendance, publications, and awards | vi |
| Table of contents | vii |
| List of Figures | xi |
| List of Tables | xv |
| List of abbreviations | xvi |
| Chapter 1- Introduction and literature review | 1 |
| 1.1 Dental caries, a global health and economic burden | 1 |
| 1.2 The oral microbiome, role in health and disease | 4 |
| 1.2.1 <i>The complexity of the oral microbiome</i> | 4 |
| 1.2.2 <i>Structure and function of dental biofilms</i> | 6 |
| 1.2.3 <i>Health-associated oral species in dental biofilms</i> | 8 |
| 1.2.4 <i>Disease-associated oral species in dental biofilms</i> | 10 |
| 1.3 Experimental-based modelling approaches to study dental biofilms..... | 13 |
| 1.3.1 <i>The use of bacterial communities to understand dental biofilm in caries</i> | 13 |
| 1.3.2 <i>In vivo modelling of dental biofilms</i> | 15 |
| 1.3.3 <i>In vitro modelling of dental biofilms</i> | 15 |
| 1.3.4 <i>Different types of nutritional sources used in in vitro models</i> | 20 |
| 1.4 <i>In silico</i> modelling approaches to characterising dental biofilms | 21 |
| 1.5 Aims and objectives | 30 |
| 1.6 Importance of the research..... | 31 |
| Chapter 2. Material & Methods | 32 |
| 2.1 Materials used in research | 32 |
| 2.1.1 <i>List of bacterial strains</i> | 32 |
| 2.2 List of equipment | 33 |
| 2.2 Culturing and storage of bacterial strains | 35 |
| 2.2.1 <i>Routine culturing of bacterial strains</i> | 35 |
| 2.2.2 <i>Preparation of glycerol stocks</i> | 36 |
| 2.2.3 <i>Colony forming unit counts</i> | 36 |
| 2.3 Experiments defining synthetic community | 37 |
| 2.3.1 <i>Growth experiments</i> | 37 |
| 2.3.2 <i>Development of AFMC medium</i> | 37 |

| | |
|--|-----------|
| 2.3.3 Carbohydrate utilisation | 38 |
| 2.3.4 Calscreener™ experiments | 38 |
| 2.4 Molecular biology techniques | 39 |
| 2.4.1 Agarose gel electrophoresis..... | 39 |
| 2.4.2 NanoDrop™ for DNA quantification..... | 39 |
| 2.4.3 Genomic DNA extraction from bacterial species | 39 |
| 2.4.4 Plasmid extraction from <i>E. coli</i> | 40 |
| 2.4.5 PicoGreen™ for double-stranded DNA quantification of plasmids..... | 40 |
| 2.4.6 qPCR primers and probes..... | 40 |
| 2.4.7 Cloning of targets into <i>E.coli</i> | 41 |
| 2.4.8 Validation of successful cloning of targets into <i>E. coli</i> | 42 |
| 2.4.9 qPCR and multiplex qPCR..... | 42 |
| 2.5 Flow cytometry for live and dead analysis | 43 |
| 2.6 Microscopy | 44 |
| 2.6.1 Gram staining | 44 |
| 2.6.2 Fluorescence in situ hybridization (FISH) | 45 |
| 2.6.3 Live dead staining for imaging of biofilms..... | 46 |
| 2.7 CDC reactor invasion experiments | 47 |
| 2.7.1 Reactor system setup..... | 47 |
| 2.7.2 Inoculation strategy..... | 49 |
| 2.7.3 Sampling from invasion experiments | 49 |
| 2.8 <i>In silico</i> modelling of the synthetic community..... | 50 |
| 2.8.1 Flux balance analysis | 51 |
| 2.8.2 Stoichiometry considered for the bacterial species | 52 |
| 2.8.3 Growth kinetics for each bacterial species | 54 |
| 2.8.4 pH influence on growth | 57 |
| 2.8.5 Continuum stirred tank reactor (CSTR) model..... | 60 |
| 2.8.6 Implementation of the CSTR model..... | 61 |
| 2.8.7 Individual based model..... | 62 |
| 2.8.8 IbM implementation and solving algorithm | 67 |
| 2.9 Statistical analysis..... | 69 |
| Chapter 3. Development of a synthetic microbial community model..... | 70 |
| 3.1 Introduction..... | 70 |
| 3.2 Aims and objectives..... | 73 |
| 3.3 Results | 74 |
| 3.3.1 Selection of a synthetic community of oral bacteria and <i>in vitro</i> growth model | 74 |
| 3.3.2 The development of a CDM to support the growth of the oral synthetic community..... | 77 |

| | |
|--|------------|
| 3.3.3 Determining the kinetic parameters of the oral bacterial species | 83 |
| 3.3.4 Substrate utilisation by the synthetic community | 86 |
| 3.3.5 Growth of oral species and acid production at different pH | 89 |
| 3.3.6 Synthetic community visualisation through fluorescence in situ hybridization | 91 |
| 3.3.7 Development of a qPCR method to quantify bacterial species | 98 |
| 3.3.8 Using qPCR and FISH to develop inoculation strategy | 103 |
| 3.4 Discussion | 105 |
| Chapter 4. <i>In vitro</i> modelling approaches to characterise the invasion of <i>Streptococcus mutans</i> into an oral commensal community | 111 |
| 4.1 Introduction..... | 111 |
| 4.2 Aims and objectives | 113 |
| 4.3 Results | 114 |
| 4.3.1 Description of <i>in vitro</i> invasion experiments | 114 |
| 4.3.2 Observing turbidity of the reactor bulk over time | 117 |
| 4.3.3 Quantifying the glucose and sucrose concentration of the reactor bulk over time | 119 |
| 4.3.4 Quantifying the lactic acid concentration of the reactor bulk over time | 122 |
| 4.3.5 Quantifying changes in the pH of the reactor bulk over time | 125 |
| 4.3.6 Quantifying the relative abundance of the synthetic community species in the reactor bulk | 128 |
| 4.3.7 Quantifying the relative abundance of the synthetic community species in biofilms | 133 |
| 4.3.8 Imaging the synthetic community biofilm using fluorescence in situ hybridization | 139 |
| 4.3.9 Assessing the viability of bacteria within the reactor system | 143 |
| 4.4 Discussion | 148 |
| Chapter 5- <i>In silico</i> modelling approaches to characterise the invasion of <i>Streptococcus mutans</i> into an oral commensal community | 154 |
| 5.1 Introduction..... | 154 |
| 5.2 Aims and objectives | 157 |
| 5.3 Results | 158 |
| 5.3.1 Description of <i>in silico</i> modelling experiments | 158 |
| 5.3.2A The glucose concentration of the reactor bulk | 161 |
| 5.3.2B The lactic acid concentration of the reactor bulk..... | 164 |
| 5.3.2C The pH of the reactor bulk..... | 167 |
| 5.3.2D Species relative abundance in the bulk | 169 |
| 5.3.3A The pH and substrate concentrations of the synthetic biofilm | 173 |
| 5.3.3B The relative abundance of bacterial species in the synthetic biofilm | 175 |
| 5.3.4 Influence of bacterial seeding on species relative abundance in the community biofilm .. | 180 |
| 5.4 Discussion | 184 |

| | |
|--|------------|
| Chapter 6. Conclusions | 190 |
| 6.1 General discussion..... | 190 |
| 6.2 Future work | 197 |
| 6.3 Concluding remarks..... | 201 |
| References | 203 |
| Appendix A- AFMC medium components..... | 230 |
| Appendix B- Gibbs free energy of formation for chemical species | 232 |
| Appendix C- Stoichiometry table for synthetic community species..... | 233 |
| Appendix D- Dissociation constants for chemical species | 234 |
| Appendix E- Code and functions for <i>in silico</i> models | 235 |

List of Figures

| | |
|--|----|
| Figure 1.1 Illustration of caries development through cariogenic biofilm formation..... | 2 |
| Figure 1.2 Microbial diversity in the oral environment..... | 6 |
| Figure 1.3 Processes governing dental biofilm <i>formation</i> | 7 |
| Figure 1.4 Metabolic pathways of oral bacteria..... | 11 |
| Figure 1.5 Figure demonstrating the abundance of bacteria at phylum, genus, and species level..... | 12 |
| Figure 1.6 Different types of models used to grow dental biofilms..... | 14 |
| Figure 1.7 An IBM used for wastewater systems..... | 25 |
| Figure 2.1 Flow cytometry gating to determine live and dead cells..... | 44 |
| Figure 2.2 Schematic of CDC reactor setup..... | 47 |
| Figure 2.3 Setup of the CDC reactors..... | 48 |
| Figure 2.4 Sampling of coupons in the laminar flow hood..... | 50 |
| Figure 2.5 Two mathematical modelling approaches are used in this research to describe the behavior of the synthetic community..... | 51 |
| Figure 2.6 Schematic representation of the sub-domains included in the IBM..... | 63 |
| Figure 2.7 Workflow for solving the algorithm for the IBM and the interactions between the model's modules..... | 68 |
| Figure 3.1 A CDC bioreactor setup, recently used for dental biofilm research..... | 78 |
| Figure 3.2 Imaging the members of the synthetic community on THYE + lactic acid medium..... | 80 |
| Figure 3.3 Growth curves of the oral bacteria over 24 h on FMC medium..... | 81 |
| Figure 3.4 Reaction flux of <i>V. parvula</i> growth..... | 82 |
| Figure 3.5 Growth curves of the oral bacteria over 24 h in AFMC medium..... | 84 |
| Figure 3.6 Substrate affinity constants (K_s) for <i>S. gordonii</i> , <i>S. mutans</i> , <i>A. oris</i> , and <i>N. subflava</i> | 86 |
| Figure 3.7 Substrate affinity constant (K_s) for <i>V. parvula</i> | 87 |
| Figure 3.8 Growth and substrate utilisation of the synthetic community members over 24 h on AFMC, supplemented with either glucose or sucrose..... | 88 |
| Figure 3.9 Growth of <i>S. mutans</i> on AFMC supplemented with different sugars..... | 89 |
| Figure 3.10 Heat output from <i>S. gordonii</i> , <i>S. mutans</i> , and <i>N. subflava</i> on glucose and sucrose over 24 h recorded using a microcalorimeter..... | 90 |

| | |
|--|-----|
| Figure 3.11 Maximum OD _{600nm} of the synthetic community members at different initial pH over 48 h on AFMC medium.. | 91 |
| Figure 3.12 The final pH of the AFMC medium after 48 h of growth for each species of oral bacteria..... | 92 |
| Figure 3.13 Fluorophores selected to optimise minimal overlap..... | 93 |
| Figure 3.14 <i>A. oris</i> planktonic cells visualised using FISH..... | 94 |
| Figure 3.15 Members of the synthetic community visualised as monoculture planktonic cells using FISH..... | 95 |
| Figure 3.16 Members of the synthetic community visualised as monoculture biofilms using FISH..... | 97 |
| Figure 3.17 Visualising <i>S. gordonii</i> and <i>S. mutans</i> in a mixed-species biofilm using confocal microscopy..... | 98 |
| Figure 3.18 Imaging the 5 species synthetic community biofilm using FISH, aided by spectral fingerprinting..... | 99 |
| Figure 3.19 Validating the amplification of gDNA target using designed cloning primers..... | 100 |
| Figure 3.20 Analysis of pDNA species extracts-post cloning using the NanoDrop™..... | 101 |
| Figure 3.21 Standard curve generated using the PicoGreen™ assay kit..... | 102 |
| Figure 3.22 Amplification of genomic DNA from each species in wells using multiplex qPCR..... | 103 |
| Figure 3.23 Visualising <i>A. oris</i> and <i>S. mutans</i> mixed-species biofilms grown anaerobically on AFMC..... | 104 |
| Figure 3.24. Number of cells per 72 h biofilm, quantified using multiplex qPCR, to confirm an appropriate inoculation strategy..... | 105 |
| Figure 4.1 Overview of the reactor strategy and goals of Chapter 4..... | 117 |
| Figure 4.2. The OD _{600nm} readings recorded over 9 days for all reactor experiments..... | 119 |
| Figure 4.3 The change in glucose concentration in the reactor bulk over time for all reactor experiments..... | 122 |
| Figure 4.4 The change in lactic acid concentration in the reactor bulk over time for all reactor experiments..... | 124 |
| Figure 4.5 The pH variation in the CDC reactor bulk for each condition for all reactor experiments..... | 125 |
| Figure 4.6. Relative abundance of each synthetic community member in the reactor bulk for reactor experiment 1..... | 130 |

| | |
|---|-----|
| Figure 4.7. Relative abundance of each synthetic community member in the reactor bulk for reactor experiment 2..... | 131 |
| Figure 4.8. Relative abundance of each synthetic community member in the reactor bulk for reactor experiment 3..... | 132 |
| Figure 4.9. Relative abundance of each synthetic community member in the reactor bulk for reactor experiment 4..... | 133 |
| Figure 4.10. Relative abundance of each synthetic community member in the reactor bulk for reactor experiment 5..... | 134 |
| Figure 4.11. Relative abundance of each species in the synthetic community for reactor experiment 1..... | 135 |
| Figure 4.12. Relative abundance of each species in the synthetic community for reactor experiment 2..... | 136 |
| Figure 4.13. Relative abundance of each species in the synthetic community for reactor experiment 3..... | 137 |
| Figure 4.14. Relative abundance of each species in the synthetic community for reactor experiment 4. | 138 |
| Figure 4.15. Relative abundance of each species in the synthetic community for reactor experiment 5. | 139 |
| Figure 4.16. Imaging of the synthetic community biofilm over time for reactor experiment 1 using FISH..... | 141 |
| Figure 4.17. Imaging of the synthetic community biofilm over time for each reactor condition using FISH..... | 143 |
| Figure 4.18 Viability of the synthetic community in both the reactor bulk and biofilm for reactor experiment 1..... | 144 |
| Figure 4.19 Viability of the synthetic community in both the reactor bulk and biofilm for reactor experiment 2..... | 145 |
| Figure 4.20 Viability of the synthetic community in both the reactor bulk and biofilm for reactor experiment 3..... | 146 |
| Figure 4.21 Viability of the synthetic community in both the reactor bulk and biofilm for reactor experiment 4..... | 147 |
| Figure 4.22 Viability of the synthetic community in both the reactor bulk and biofilm for reactor experiment 5..... | 148 |

| | |
|---|-----|
| Figure 5.1 Overview of the <i>in silico</i> strategy and goals in Chapter 5 to characterise <i>S. mutans</i> invasion..... | 161 |
| Figure 5.2 Glucose concentrations with and without pH influence on the growth rate of synthetic community members..... | 164 |
| Figure 5.3 Lactic acid concentrations with and without pH influence on the growth rate of synthetic community members..... | 167 |
| Figure 5.4 The pH of the bulk with and without pH influence on the growth rate of synthetic community members..... | 169 |
| Figure 5.5 Simulation of relative abundances in the reactor bulk without pH correction.... | 171 |
| Figure 5.6 Simulation of relative abundances in the reactor bulk with pH correction..... | 173 |
| Figure 5.7 Representation of a biofilm, its corresponding glucose, and lactic acid concentrations, and pH profile..... | 175 |
| Figure 5.8 Simulation of relative abundances in the synthetic community biofilm without pH correction..... | 178 |
| Figure 5.9 Simulation of relative abundances in the synthetic community biofilm with pH correction..... | 180 |
| Figure 5.10 Relative abundance of each synthetic community member simulated in the biofilm, plotted with abundances from experimental data. Simulations were with seeding of cells clustered by species..... | 182 |
| Figure 5.11 Relative abundance of each synthetic community member simulated in the biofilm, plotted with abundances from experimental data. Seeding strategy matched the reactor runs..... | 184 |
| Figure 6.1 Strategy for using the modelling approaches to combat caries development..... | 200 |

List of Tables

| | |
|---|-----|
| Table 2.1 All bacterial strains used in this research, including the genotype and reference..... | 32 |
| Table 2.2 All equipment used in this research, including the device application, name, and manufacturer..... | 33 |
| Table 2.3 All qPCR primers and probes used in this research project..... | 41 |
| Table 2.4 Reaction steps for the qPCR experiments..... | 43 |
| Table 2.5 All FISH probes used in this research project..... | 45 |
| Table 2.6. The kinetic parameter for each bacterial species used in mathematical models... | 56 |
| Table 2.7 The boundaries for each of the bacteria species considered in the pH correction for species kinetic parameters..... | 60 |
| Table 2.8 Diffusion coefficients for the soluble components considered in the lbM..... | 66 |
| Table 3.1 Selection of the synthetic community of oral bacteria, including names of strains, justification of selection, and references..... | 76 |
| Table 3.2 Development of the AFMC medium to support the growth of the whole synthetic community..... | 81 |
| Table 3.3 The μ_{max} and K_s values for all oral bacterial species..... | 85 |
| Table 3.4 Inoculation strategy to be used for the <i>in vitro</i> experiments..... | 106 |
| Table 4.1 Reactor experiment conditions used in Chapter 4..... | 115 |
| Table 4.2 A summary of the OD _{600nm} readings across all reactor experiments..... | 120 |
| Table 4.3. A summary of the glucose concentrations across all reactor experiments..... | 122 |
| Table 4.4. A summary of the lactic acid concentrations across all reactor experiments..... | 125 |
| Table 4.5 The pH recording across the 9-day reactor experiments for all conditions..... | 128 |
| Table 5.1 Conditions tested using simulations in Chapter 5..... | 159 |
| Table 6.1 Summary of key findings and applications from all results chapters..... | 193 |

List of abbreviations

| | |
|------------------|---|
| [prod] | Concentration of reaction products |
| [S] | Substrate concentration |
| °C | Degrees Celsius |
| 3D | Three dimensions |
| Ach | Acetate |
| ANOVA | Analysis of variance |
| ATP | Adenosine 5'-triphosphate |
| BHI | Brain Heart Infusion |
| Bp | Base pairs |
| $C_3H_5O_3^-$ | Lactate |
| $C_3H_6O_3$ | Lactic acid |
| CDM | Chemically defined medium |
| CFU | Colony forming unit |
| CLSM | Confocal Laser Scanning Microscopy |
| Cm | Centimetre |
| CO ₂ | Carbon dioxide |
| CSTR | Continuous stirred-tank reactor |
| CV | Crystal violet |
| D _{eff} | Effective diffusion of chemical species |
| EDTA | Ethylenediaminetetraacetic acid |
| EPM | Extracellular polymeric matrix |
| et. al | and others |
| FBA | Flux balance analysis |
| FISH | <i>Fluorescence in situ hybridization</i> |
| Form | Formate |
| g | Gram |
| G _{ana} | Gibbs free energy of anabolism |
| G _{cat} | Gibbs free energy of catabolism |
| G _{DIS} | Gibbs free energy of dissociation |
| gDNA | Genomic DNA |

| | |
|--------------------------------|-----------------------------------|
| GL ⁻¹ | Gram/litre |
| h | Hour(s) |
| H ⁺ | Hydrogen ions |
| H ₂ | Hydrogen |
| H ₂ CO ₃ | Carbonic acid |
| H ₂ O | Water |
| H ₂ O ₂ | Hydrogen peroxide |
| HCl | Hydrochloric acid |
| IBM | Individual-based model |
| K | Kelvin |
| k _{eq} | Equilibrium constant |
| K _j | Kilojoule |
| K _s | Monod substrate affinity constant |
| L | Litre |
| M | Molar |
| M _{bac} | Maintenance term |
| Mg | Magnesium |
| min | Minute |
| mm | Millimetre |
| mM | Millimolar |
| mmol L ⁻¹ | Millimole per litre |
| NaOH | Sodium hydroxide |
| NH ₃ | Ammonia |
| nm | Nanometres |
| nM | Nanomolar |
| O ₂ | Oxygen |
| OD | Optical density |
| OH ⁺ | Hydroxyl ion |
| OVG | Overall growth equation |
| PBS | Phosphate buffered saline |
| PCR | Polymerase chain reaction |
| pDNA | Plasmid DNA |

| | |
|-------------------------------|--|
| PFA | Paraformaldehyde |
| pH _{max} | Maximum pH boundary |
| pH _{min} | Minimum pH boundary |
| pH _{opt} | Optimum pH boundary |
| Prop | Propionate |
| qPCR | Quantitative polymerase chain reaction |
| rpm | Revolutions per minute |
| rRNA | Ribosomal RNA |
| s | Second(s) |
| SD | Standard deviation |
| SDS | Sodium dodecyl sulphate |
| T | Temperature |
| TAE | Tris-acetate-EDTA |
| THYE | Todd Hewitt Yeast Extract |
| UK | United Kingdom |
| USA | United States of America |
| UV | Ultraviolet |
| v/v | Volume/volume |
| xg | G-force |
| Y _{xs} | Growth yield |
| μ | Micro |
| μ (Bacterial growth kinetics) | Growth rate |
| μL | Microlitre |
| μm | Micrometre |
| μM | Micromolar |
| μ _{max} | Maximum specific growth rate |
| μw | Microwatt |
| τ | Residence time |

Chapter 1- Introduction and literature review

1.1 Dental caries, a global health and economic burden

Dental caries, also known as tooth decay, is characterised by the localised destruction of mineral tissues of teeth. Caries is the most prevalent, non-communicable disease worldwide (Pitts et al., 2021b), with an estimated 2.3 billion untreated cases globally (Bernabé & Marcenes, 2020). Caries develops when a high frequency of sugar is eaten, leading to acid production from oral bacteria, and a lack of fluoride, which is a natural element that strengthens teeth and prevents decay (Medjedovic et al., 2015). Caries progression can lead to endodontic infections and acute pain when oral hygiene is not maintained using safe products i.e., toothbrushes and fluoridated toothpaste, and an excess of sugar is consumed (Paredes et al., 2021). The estimated global treatment costs attributed to caries is approximately \$298 billion per annum (Listl et al., 2015). Caries has been known to be a psychological burden, directly affecting quality of life. This cascades into a knock-on effect, as those suffering from poor mental health, are more likely to neglect their oral hygiene, leading to disease progression (Knapp et al., 2021).

Caries is associated with biofilms that form on teeth, known clinically as dental plaque. These dental biofilms remain relatively stable in species composition over time, a term called microbial homeostasis, which is maintained by a balance in synergistic and antagonistic interactions between microbes (Marsh, 2006). Diets that are high in sugar concentration and frequency, along with poor oral hygiene, lead to oral dysbiosis. Here, the microbial composition changes. In these conditions, acid production from commensal organisms, i.e., those belonging to the genera *Streptococcus* and *Actinomyces*, paves the way for acidogenic species, including *Streptococcus mutans* and *Scardovia wiggsiae*, to overpopulate dental biofilms (Takahashi & Nyvad, 2016) (Figure 1.1). These acidogenic species produce more acid, which can demineralise teeth at a pH of approximately 5.5 (known as the critical pH level) and below (Dawes, 2003). The loss of calcium and phosphate in the early stages is reversible, as these ions can deposit into the crystal lattice from saliva (Hamba et al., 2020). Persistent acid production and the resulting demineralisation lead to white spot lesions, the first clinical signs of caries development (Khoroushi & Kachuie, 2017). Progression of caries leads to the structural integrity of the tooth being compromised, resulting in cavities (Roberts et al., 2022).

Once cavities form, bacteria invade dentinal tubules, causing endodontic infection (Love & Jenkinson, 2016). This leads to severe pain and inflammation. If untreated, oral bacteria access the base of the tooth, resulting in periapical abscess formation. These can prove life-threatening (Erazo & Whetstone, 2022). Later stages of caries development also have a detrimental effect on other parts of the mouth. The waste products from fermentation, including acid production, contribute to gingivitis, gum recession and inflammation (Nyvad & Takahashi, 2020).

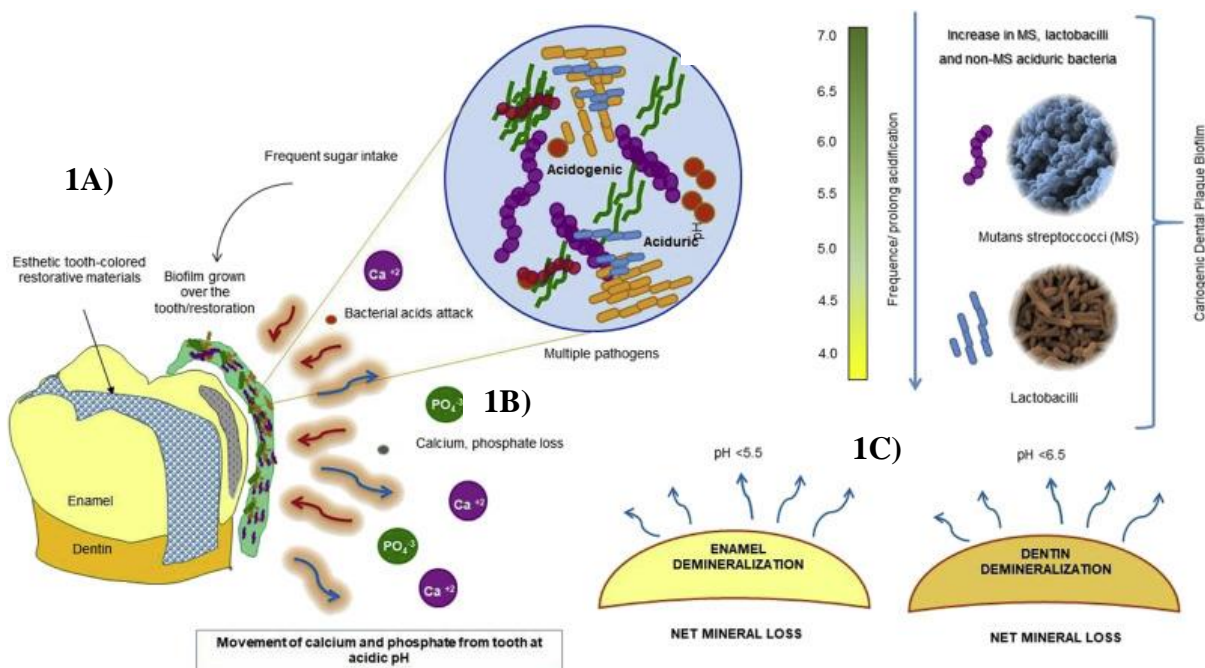


Figure 1.1 Illustration of caries development through cariogenic biofilm formation. A) Cariogenic dental biofilm, comprised of an overpopulation of acidogenic species e.g., *S. mutans*, lowers the local pH. B) This leads to demineralisation of teeth, particularly the loss of calcium and phosphate. C) This net loss occurs at an approximate pH of 5.5 for enamel and 6.5 for dentin, known as the critical pH level. Figure adapted with permission through creative common license (Balhaddad et al., 2019).

Numerous oral hygiene products are used to combat the global health and economic problems arising from caries, by reducing the progression before severe problems develop. The most common method is the use of toothbrushes to remove dental biofilms (Otten et al., 2012). The mechanical motion of biofilm disruption and removal is effective at controlling dental biofilm development in areas that the bristles can not access. Successful removal using manual toothbrushes varies significantly based on technique (Slot et al., 2012). The use of

electric toothbrushes is also used to fight caries, but whilst they negate some of the variances in success seen with manual toothbrushes resulting from human error in technique, an improvement in efficacy is not universally agreed upon. In one study, electronic toothbrushes showed an 86% reduction in plaque index vs 85% with manual toothbrushes (Slot et al., 2012). The use of dental floss is effective at removing interproximal plaque that toothbrushes do not have access to, but difficulty in technique leads to a low compliance of between 10-30% among adults (Sambunjak et al., 2019). These products can be combined with fluoridated toothpaste. The use of fluoride reduces demineralisation, as the enamel recovers lost minerals as fluorapatite. Fluorapatite forms when fluoride is present in an acidic environment and reacts with hydroxyapatite (Daruich & Brizuela, 2022). Hydroxyapatite is a naturally occurring mineral form of calcium apatite and the main component of dentin and enamel (O'Hagan-Wong et al., 2022; Habibah et al., 2022). Fluoride also acts as an antimicrobial by inhibiting F-ATPase, a group of enzymes that bacteria use to catalyse the hydrolysis of phosphate bonds to form adenosine triphosphate (Zhang et al., 2019). Fluoride affects the synthesis of extracellular polymeric substances (EPS), which are important in biofilm formation.

Oral supplementation strategies have been researched for their anti-cariogenic effect. The use of xylitol as a replacement for sugars, or the supplementation of xylitol in the diet, has been associated with a significant reduction in caries incidence (Horst et al., 2018). This anti-caries was linked to the reduction of *S. mutans* concentration in the saliva, where the species metabolised xylitol-5-phosphate, shown to be toxic to the cell (Tanzer et al., 2006.). Recent evidence suggests that previous studies on the positive effects of xylitol were flawed. There is a lack of evidence in human cases and use in animal models has previously resulted in hyperglycaemia and intestinal dysbiosis (Janket et al., 2019). The use of probiotics and probiotic-related bacteria, including *Lactobacillus reuteri* (now *Limosilactobacillus reuteri*) have also been shown to reduce *S. mutans* invasion of dental biofilms (Baca-Castañón et al., 2015), but the efficacy of these treatments and the ability to get probiotic bacteria to establish has varied in success (Cagetti et al., 2013).

Approaches to combat caries can be assisted with the use of microbial risk management to prevent caries development. Studies have demonstrated that diet, bacterial profile i.e., the amount of *S. mutans* or *S. wiggisiae* in plaque, fluoride intake, and brushing/flossing teeth, all intervened in caries development in those undergoing orthodontic treatment (Beheshti, 2021). The resilience of the oral microbiome is identified as a criterion for characterising a

healthy microbiome. This is particularly relevant to the oral microbiome as oral products are routinely used and microbial dysbiosis is strongly linked to caries development (McBain et al., 2019). Microbial risk assessments (MRA) have been used to help prevent the undesirable effects of products on the oral microbiome (Métris et al., 2022). Understanding the effect of fluoride-containing toothpaste on microbial perturbation, the reversibility of perturbations and the understanding of preserving desirable species in the dental biofilm, all help in offsetting the contribution of oral dysbiosis in caries development. This means that the development of oral MRA is important as they help further our understanding of how to protect a commensal oral microbiome. Protecting commensal species that have health benefits (Section 1.2.3) and preventing the overpopulation of cariogenic species (Section 1.2.4) through the use of antimicrobial actives, would help prevent caries progression (Inquimbert et al., 2019; Philip et al., 2018).

1.2 The oral microbiome, role in health and disease

1.2.1 *The complexity of the oral microbiome*

The oral microbiome is an open, natural microbial system. It is the second most diverse microbiome in the body, consisting of over 700 different species of bacteria, as well as fungi, archaea protozoa and viruses (Kilian et al., 2016). The bacteria found within the oral environment were some of the first observed. This dates back to initial observations of dental biofilms, using primitive microscopes, by Van Leeuwenhoek in 1680 (He & Shi, 2009).

The colonisation of the oral environment occurs at or very soon after birth, before hard tissues i.e., teeth are present. The microbial diversity begins at birth, where the delivery method can affect the oral microbial composition (H. Li et al., 2019). As hard tissues start to form, pioneering colonisers e.g., *Streptococcus*, *Actinomyces*, *Neisseria* and *Veillonella* populate the tooth surface and salivary pellicle (Huang et al., 2011). The oral cavity is the primary route of entry into the digestive system and respiratory tracts for both commensal and pathogenic microorganisms. Up to 10^8 microbes are present per millilitre of saliva (Philip D Marsh et al., 2015). The diversity of the oral microbiome is contributed to by constant contact with food intake and breathing. Bacterial cells are present as either free-living planktonic cells or assembled into a biofilm. They populate different tissue surfaces within the oral environment, e.g., the tongue, gums, and teeth.

The oral environment itself consists of several different tissue types and varying compositions of the oral mucosa. Areas of the oral cavity have varying microenvironments, contributing to the diversity and complexity of the oral microbiome. The tooth surface is the only non-shedding surface in the oral cavity. This provides an opportunity for biofilm formation, leading to a higher diversity of species compared to saliva or the tongue. The presence of multiple microenvironments within the mouth leads to species abundance in sample collections differing, depending on where they are taken from (Krishnan et al., 2017). Species abundance differs not only within different sites of the same human host but also from person to person. The advancement of new technologies, including next-generation genomic sequencing (Caselli et al., 2020a), has shed light on the microbial populations in different areas of the mouth (Figure 1.2), and the complexity of interspecies interactions. Anaerobes, including *Actinomyces*, *Veillonella*, and *Fusobacterium*, are found in higher abundance in subgingival dental biofilms compared to supragingival biofilms, as there is a lower concentration of oxygen in this environment (Caselli et al., 2020b). *Rothia dentocariosa* and *Streptococcus gordonii* preferentially colonise teeth, whilst *Streptococcus salivarius* has been predominantly found on the tongue dorsum. *Streptococcus mitis* populate numerous areas of the oral cavity and are almost universally found in patient samples (Aas et al., 2005), whilst *Clostridia* species have been found to reside preferentially in the tongue dorsum (Dong et al., 2018). Furthermore, species that have close metabolic interactions, e.g., that between *Streptococcus* and *Veillonella*, are often found in similar microenvironments within the oral cavity (Abram et al., 2022). The latter is not able to metabolise carbohydrates to grow and relies on lactic acid produced by other oral species e.g., those belonging to the *Streptococcus* genus, to grow in the mouth. Overall, the diversity of the oral microbiome shows the importance of defining microbial relationships and their effect on the oral environment i.e., acid production leading to enamel demineralisation.

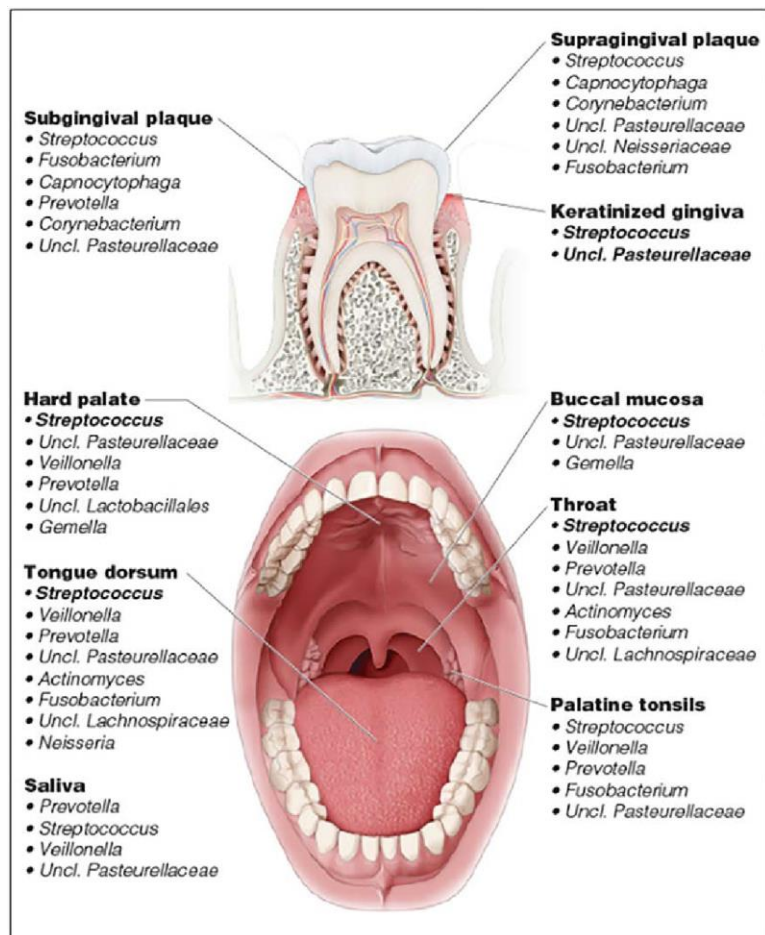


Figure 1.2 Microbial diversity in the oral environment. Genera of bacteria populate different areas of the oral cavity. *Streptococcus*, *Neisseria* and *Veillonella* are abundant in numerous areas of the oral cavity, whilst *Gemella* is associated with specific areas, including the buccal mucosa (Withers, 2019). Figure adapted with permission through creative common license.

1.2.2 Structure and function of dental biofilms

Bacterial biofilms are believed to be the preferred mode of bacterial existence in nature and can exist as either monospecies or multispecies. Almost all biofilms found within the body e.g., dental biofilms, are multispecies and are formed when cells adhere to a surface and/or each other within a self-produced extracellular polymeric matrix (EPM). The EPM can constitute up to 90% of the dry mass of biofilms (Bogino et al., 2013). The protection offered by this matrix allows the cells to thrive when compared to planktonic cells. There are numerous advantages for cells to exist within a biofilm structure, including the recycling of nutrients and enhanced intracellular communication (Flemming & Wuertz, 2019). Furthermore, the matrix maintains cells near host tissue, which facilitates interactions between microorganisms and the host. This can impact health and disease (Jakubovics et al., 2021). The bacterial composition of the

biofilm affects both its physical and chemical characteristics and influences how it affects the surrounding tissue.

There are several steps in the formation of dental biofilms (Figure 1.3), governed by numerous physical, biological, and chemical processes. Initial stages of dental biofilm formation on teeth, following brushing, include early coloniser bacteria, e.g., *Actinomyces* and *Streptococcus*, coming into contact with the enamel surface. This surface is coated by a conditioning layer known as the salivary pellicle. The pellicle is formed of proteins, glycoproteins, and lipids (Chawhuaveang et al., 2021). Initial adherence of cells to the pellicle occurs. The reversible attachment of bacteria develops into irreversible attachment through the use of surface proteins. This initial attachment is variable depending on the presence of nutrients, competitor cells, etc. A three-dimensional layer can be established. This adds to the structural complexity of dental biofilms, where microchannels and gradients of nutrients, oxygen and heat appear (Proctor & Relman, 2017; Simón-Soro et al., 2013). Cells aggregate and spread to nearby environments and the formation procedure can then occur again (Melaugh et al., 2016).

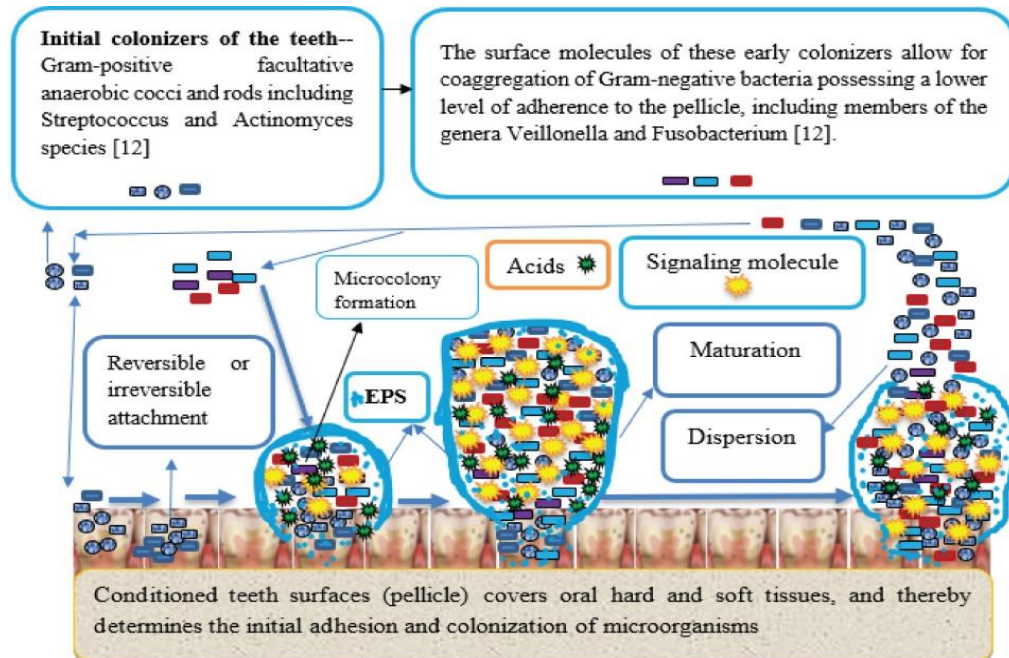


Figure 1.3 Processes governing dental biofilm formation. Salivary pellicles form on teeth after saliva comes into contact with the enamel surface. This pellicle influences the adhesion and colonisation of bacteria to the enamel surface. Both reversible and irreversible cell attachment of early coloniser bacteria occurs. Bacteria within the dental biofilm are involved in physical interactions and the exchange of nutrients as maturation occurs. Micro-colonies develop into macro-colonies, and dispersal from the dental biofilm occurs (Gedif Meseret, 2021). Figure adapted with permission through creative common license.

The depth and structure of dental biofilms contribute to their protection against antibiotics and disinfectants. This is due to the difficulty of penetrating the biofilm and killing off cells in the deeper layers (Kouidhi et al., 2015). Cells within the dental biofilm are between 10-1000 times more resistant to antibiotics than their planktonic counterparts (Sharma et al., 2019). This means understanding dental biofilm behaviour is important in combatting their role in oral diseases i.e., caries and periodontitis. As these biofilms mature, they can infect tissues surrounding the tooth, causing inflammation (Jakubovics & Kolenbrander, 2010; Strauss et al., 2019). Uncontrolled dental biofilms can also influence peri-implant mucositis, characterised by inflammation and bleeding, and peri-implantitis (Mombelli & Décaillot, 2011), which results in bone destruction. This included bone that supports dental implants, often leading to implant failure.

1.2.3 Health-associated oral species in dental biofilms

In a health-associated oral environment, dental biofilms consist of a balanced microbial cohort, where commensal organisms help prevent the domination of cariogenic species (Oh et al., 2020). Commensal oral bacteria are those that exist in the oral environment in a balanced state, not driven towards disease and dysbiosis (Khan et al., 2019). They prevent pathobionts (opportunistic organisms) from dominating the oral microbiota. Oral commensal bacteria include species e.g., *Actinomyces oris*, an early coloniser of freshly cleaned teeth (Mishra et al., 2010), and *S. gordonii* (Nairn et al., 2021). These were found to be in high abundance in normal, healthy dental biofilms by Palmer *et al.*, (2014), who studied the microbiome composition using 16S rRNA gene analysis. Similar levels of these genera were also observed in a study by Takahashi and Nyvard *et al.*, (2008). The proportion of bacterial sequences was similar across individuals classified as possessing a healthy oral microbiome. This supports the concept of a core microbiome in health (Zaura et al., 2009).

These commensal organisms are often found in high abundance in dental biofilms and once they have bound to the tooth surface, offer a more complex environment that other species can bind to (Baker & Edlund, 2019). Certain oral species, including *S. gordonii*, *Streptococcus oralis* and *S. sanguinis*, can produce hydrogen peroxide. This is antagonistic to other bacterial growth, including that of cariogenic-related species e.g., *S. mutans* (Zheng et al., 2011). Whilst numerous commensal bacteria produce acid, contributing towards caries development, species e.g., *S. salivarius*, *Actinomyces naeslundii* and *S. gordonii* can utilise arginine to elevate

the local pH (Burne & Marquis, 2000). *S. gordonii* and *S. sanguinis* produce ammonia from the hydrolysis of ammonia and urea, increasing the pH of the local environment, which contributes towards tooth remineralisation (Nascimento et al., 2009). Furthermore, early colonisers restrict access to the host epithelium, by competing with cariogenic species for nutrients and directing foreign microbes away from enamel via saliva (Valm, 2019a). The activity of these commensal microorganisms means they play an important role in preventing dysbiosis by preventing the overpopulation of aciduric species. Understanding the interactions between commensal, early colonisers, and later cariogenic species, as well as preventing a shift in abundance away from the health-associated bacteria, is important in preventing caries development.

Commensal bacteria within dental biofilms have been associated with positive health effects outside of caries prevention. Genera i.e., *Veillonella* and *Neisseria*, are capable of the denitrification of nitrate to nitrite, and then to nitrogen, using bacterial nitrate reductases (Doel et al., 2005). Saliva is rich in nitrate, particularly after the consumption of green vegetables, indicating that the mouth is a favourable environment to see the benefits of these denitrifying species (Ma et al., 2018). Acidified nitrite has been shown to have an antimicrobial effect on oral pathogens that contribute towards periodontitis. This includes *Fusobacterium nucleatum* (Allaker et al., 2001). Evidence suggests that nitric oxide produced at significant enough levels can play a regulatory role in inflammatory disorders of gum tissue (Schreiber et al., 2010). Nitric oxide has been shown to help with lowering blood pressure and reducing ischemia-reperfusion damage. When the oral microbiota was disrupted with mouthwash, some of these health benefits were lost (Petersson et al., 2009a). Koch *et al.*, (2017) demonstrated that disruption of the oral microbiome by using an antibacterial mouthwash led to a reduction in nitrate reduction, and an increase in blood pressure in treated hypersensitive men and women. These studies provide evidence that oral species involved in dental biofilms have health benefits beyond the local environment. Protecting commensal microorganisms within the mouth is important in reducing the progression of diseases. Therefore, there have been strategies to increase the concentration of several bacteria. Genera that offset oral disease-associated activity and have been of interest to increase through probiotic treatment, include *Bifidobacterium* (Invernici et al., 2018). They do so by reducing some of the inflammatory effects of *Porphyromonas gingivalis*, which contributes towards periodontitis (Y. Zhang et al., 2022a). *Lactobacillus acidophilus* LA5, has also been of

interest in probiotic treatment as it has been observed to downregulate *mfa1* and *fimA*, which are virulence factors implicated in gingivitis (Y. Zhang et al., 2022b).

1.2.4 Disease-associated oral species in dental biofilms

Despite commensal oral bacteria in dental biofilms providing health benefits to the local environment and beyond, they can also contribute to negative health outcomes. *A. oris* and *Actinomyces israelii* are early colonisers of freshly cleaned teeth and are considered commensal microorganisms universally found in the common oral microenvironment. However, on rare occasions, these species can lead to actinomycosis, leading to abscess formation and pain (Valour et al., 2014). A study of mouse models linked *A. naeslundii* peptidoglycan to the induction of inflammatory cytokine production. This led to bone loss, comparable to that induced by *P. gingivalis* (Sato et al., 2012). It should be considered that mouse models do not directly relate to the human oral environment.

Oral bacteria form complex networks with intricate metabolic, physical, and chemical interactions between species (Figure 1.4). This includes interactions between commensal bacteria and pathobionts. The production of acids by early colonisers paves the way for acidogenic species to thrive. Poor oral hygiene and ecological factors in the oral environment, i.e., high sugar concentrations occurring through eating a sugar-rich diet, can lead to the colonisation and overpopulation of dental biofilms by these acidogenic species, including *S. mutans* and *S. wiggsiae* (Keller et al., 2017).

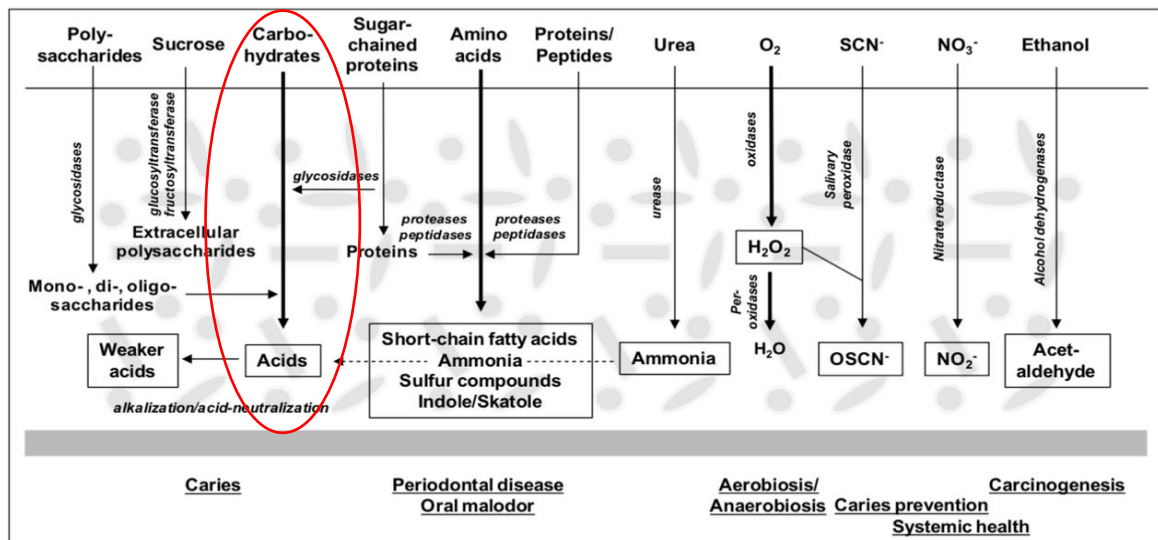


Figure 1.4 Metabolic pathways of oral bacteria are complex and have varying effects on caries development. In this Figure, pathways are represented by arrows and the associated health effects related to these pathways can be seen at the bottom. One example is the metabolism of carbohydrates, leading to the production of acids that can be broken down further into weaker acids (red). This overall process had been related to caries development (Takahashi, 2015). Figure adapted with permission through creative common license.

S. mutans produces exopolysaccharides from sucrose. This does not occur when grown on other sugars e.g., glucose (Costa Oliveira et al., 2021a). This makes *S. mutans* suited to thrive within dental biofilms, as EPS production by *S. mutans* on sucrose improves the ability to adhere to surfaces and increases the physical integrity/stability of the biofilm (Cai et al., 2018). The lowering of pH by these cariogenic species favours aciduric bacteria, which produce even more acid. Acid production, leading to low pH, leads to bacterial cell stress, including compromising the structural integrity of cell membranes (Guan & Liu, 2020a). This leads to microbial dysbiosis in a positive feedback loop which drives caries progression, as aciduric microorganisms e.g., *S. mutans* and *Bifidobacteria* thrive in this lowered pH environment (Valm, 2019b). *S. mutans* can adapt to acidic conditions, due to an acid adaptation response, where it can alkalinize the cytoplasm to reduce cell stress (Baker et al., 2017a). *S. mutans* is protected against hydrogen peroxide, produced by commensal oral species, by *Veillonella parvula*, which thrives by consuming the lactic acid produced by *S. mutans* (Zhou et al., 2021a). This synergistic relationship likely contributes to the increased abundance of *V. parvula* in caries-associated dental biofilms (Dame-Teixeira et al., 2021). The prevalence of *S. mutans* and *V. parvula* in caries-associated patients was also observed by Gross *et al.*, (2012). In this study, PCR and 16S rRNA gene sequence identification was used on samples from 72 patients, 36 with caries and 36 healthy control patients (Figure 1.5). The results also found a decrease

in species diversity within and between patients' dental biofilms as caries progressed. This co-association was also observed more recently by Abram *et al.*, (2022), who found that *V. parvula*, *S. mutans*, *A. naeslundii* and *Capnocytophaga gragranulosa* were present in significantly higher levels within the diseased roots of 7 different people with caries lesions, although abundance varied dramatically.

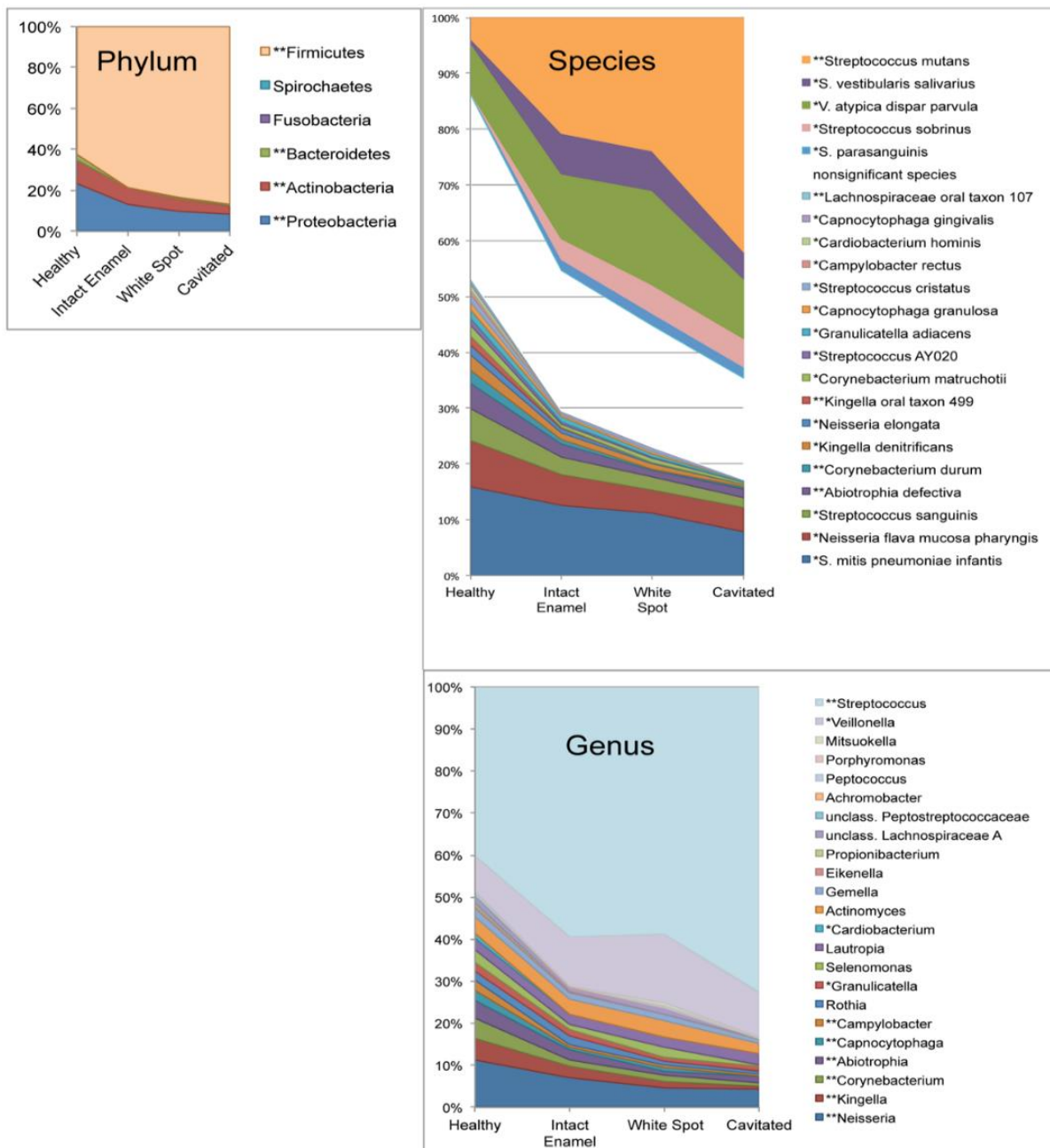


Figure 1.5 Figure demonstrating the abundance of bacteria at phylum, genus, and species level. These were quantified using PCR and 16S rDNA sequence identification at different stages of caries from a study of 72 patients by Gross (2012). *S. mutans* and *V. parvula* were two species found in elevated abundances in caries-associated patients, whilst *Proteobacteria* and *Actinobacteria* generally decreased during the progression of caries. Figure adapted with permission through creative common license.

1.3 Experimental-based modelling approaches to study dental biofilms

1.3.1 *The use of bacterial communities to understand dental biofilm in caries*

Understanding the behaviour of dental biofilms that contribute to caries progression, requires the use of bacterial communities. These have varied from complex, mammalian-derived communities, to single species grown in the laboratory.

Sampling microbial communities straight from human patients offers an understanding of species' behaviour in the host environment. A study by Cruz de Jesus *et al.*, (2021) took supragingival plaque and swab samples from 80 children (40 caries-free and 40 with caries) to understand the microbial composition differences. This study was able to determine that the fungal species *Candida dubliensis* and *Candida tropicalis* were more abundant in non-caries associated patients. An alternative to sampling from humans is the use of animal models. A study by Crowley *et al.*, (1999) used rat models to inoculate *S. mutans* into the oral microbiome and track caries progression in extracted teeth using x-ray spectrometry. This study provided information on what occurred *in situ*, when compared to the more artificial, *in vitro* models, but did not reflect the human oral environment as well as the study by de Jesus *et al.*, (2021). This is because of the difference in the host response and species behaviour between human and animal models (Bibiloni, 2012; Shi et al., 2019). Also, there is an ethical aspect to consider when using animal models, such as in this study. These research studies often cause an induced disease state and, in many cases, the animals must be euthanised.

Microcosm biofilm models, where communities are derived from human samples, are often used to study dental biofilms. They aim to achieve a bacterial diversity and composition similar to that found *in vivo*. These models can offset some of the ethical implications seen in human and animal models. Culturing artificial biofilms allow for far more sampling opportunities, as a significant number of biofilms can be cultured from minimal saliva samples. A study by Li *et al.*, (2021) investigated the influence of nutrient and surface properties on microbial composition. This research demonstrated that the biofilm cultured from saliva collected from a patient, had several species struggle to thrive on a rich brain heart infusion medium without the addition of growth factors i.e., vitamin K. This showed that the medium type influences species diversity. The study also found that substrate type influenced the community composition. Using reconstructed human gingiva instead of hydroxyapatite or titanium, led to

a more similar microbial profile to that of saliva. This demonstrated that the human host environment plays an important role in oral ecology.

To eliminate the ethical implications of human and animal models, synthetic biofilms are often used. These biofilms do not fully resemble extracted dental plaque, but they allow for selecting specific species of interest to study and choosing the number of species within a community. Furthermore, they allow for the introduction of oral species into the biofilm at controlled times. This level of control allows for the simplification of biofilms, which is particularly useful when the research aims to understand drivers of microbial composition changes and inter-species interactions. Synthetic communities that have been used to study caries development have varied significantly. This includes studying *S. mutans* genes involved in biofilm formation using gene deletion (Yoshida & Kuramitsu, 2002). These simple models are useful in characterising the species of interest, which can be used to help elucidate what their role *in vivo* might be, but they are too simple to capture any inter-microbial interactions which are core to dental biofilms. Furthermore, species behave differently in monoculture and so findings on isolated species may not be the same as they would in a mixed-species environment. To circumvent this problem, multi-species synthetic biofilms have been used. Studies that use these synthetic biofilms include the testing of phytochemicals on a mixed-species biofilm comprising species from the *Streptococcus* and *Rothia* genera (Sateriale et al., 2020). The difference in resistance to antimicrobial actives between single and multi-species biofilms in this study highlighted the need to include a sufficient number of oral species within *in vitro* biofilm models. A study by Lyu et al., (2021) showed ursolic acid effectively inhibited the growth of a synthetic community containing several oral *Streptococci*, including *S. mutans*, by reducing EPS synthesis. Complex communities containing 14 species, including *Streptococcus gordonii*, *Actinomyces oris*, and *Veillonella parvula*, have been used to test the ability of glycerol at different concentrations in strengthening the probiotic effect of *Limosilactobacillus reuteri* on dental biofilms. This study by Van Holm et al., (2022) used a chemostat model and concluded that there was a synergistic relationship between glycerol and *L. reuteri*. Glycerol supplementation led to the reduction of pathobionts in the dental biofilm, including *P. gingivalis* and *F. nucleatum*. The use of numerous species in this study was more representative of the dental biofilm, which has a diverse representation of oral species, compared to those using simple biofilm i.e., that by Yoshida et al., (2002). These studies show the promise of synthetic oral communities in defining drivers of disease over

dental biofilm samples. Also in testing antimicrobial actives, provided they are complex enough to represent the microbial ecology occurring in the *in vivo* environment.

1.3.2 *In vivo* modelling of dental biofilms

In vivo models are often used in the growth and characterisation of dental biofilms to best characterise their role in caries. These models attempt to understand changes in response to different anti-cariogenic products, within the natural environment that they reside.

One study used nail varnishes containing different compounds including fluoride on bovine enamel surfaces that were worn intra-orally (Salomão et al., 2016). This was to monitor the effectiveness of these compounds on species implicated in the carious demineralisation of enamel. This study was useful as the sample was exposed directly to the oral environment. This avoided the use of synthetically controlled parameters e.g., the use of artificial media instead of saliva. These models are invasive and require compliance from enough patients. Combinatory approaches between *in vivo* and *in vitro* models have also been attempted as a balance between the two (Klug et al., 2016). A mouth-to-model approach was used to demonstrate that biofilms from the *in vivo* environment, could be cultured in the laboratory under more simplified conditions. This study cultivated dental biofilms using a drip flow reactor and noted that *Streptococci* and *Veillonella* remained dominant after this transfer, with anaerobic species including *Actinomyces*, *Prevotella* and *Rothia* increasing in abundance. This demonstrated the sensitivity of oral composition to changes in environment between *in vivo* and *in vitro*, but also suggests that oxygen is an important parameter to consider in such models.

1.3.3 *In vitro* modelling of dental biofilms

In vitro models have been used to study the role of dental biofilm communities in caries development, discussed in Section 1.3.1. These models avoided the ethical implications and difficulty with obtaining samples that come with *in vivo* model. *In vitro* models routinely used include continuous flow models and more modern models e.g., microfluidic devices. Both can supply constant nutrients to microbial communities. Commonly used growth models also include static biofilm models i.e., microtiter plates that do not have this constant media supply (Figure 1.6) The type of models used are selected based on the goals of the research study they are employed in. They help characterise the activity of bacteria in different conditions,

to help us understand their impact on each other and the local environment. These factors can contribute towards disease *in vivo* i.e., acid production and demineralisation.

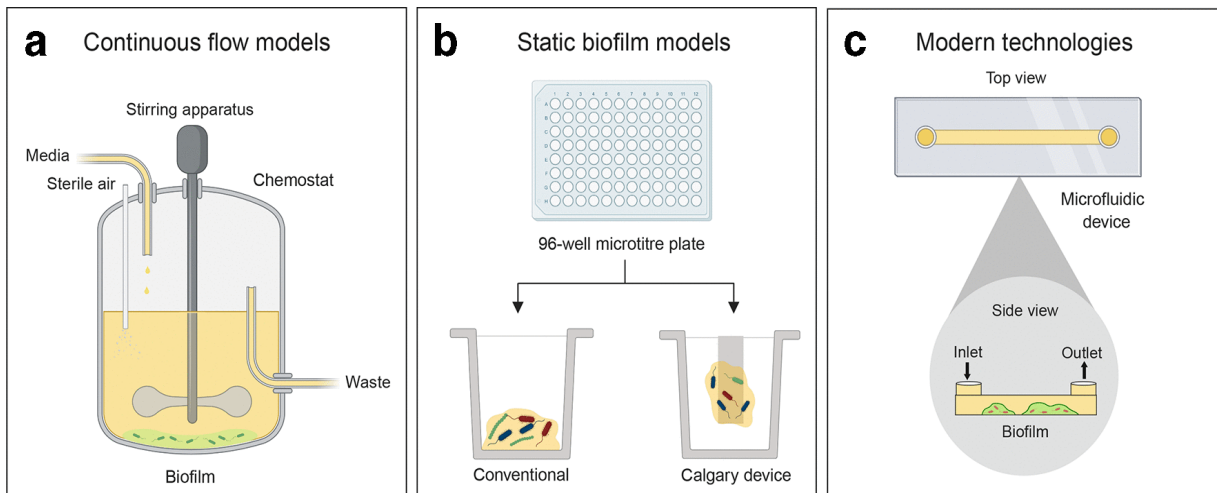


Figure 1.6 Different types of models used to grow dental biofilms. A) Chemostat models offer the ability to flow medium in and out of the reactor, but at the cost of low throughput. B) Cheaper, more cost-effective models exist including static microtiter plate models, but they lack characteristics of the *in vivo* environment, e.g., the flow of nutrients. C) The use of models is advancing, with microfluidic devices now becoming popular (J. L. Brown et al., 2019). Figure adapted with permission through creative common license.

Closed systems, where nutrients do not flow in or out of the model, are used for growth in some studies. They usually have a lower chance of contamination and are cost-effective. However, they do not resemble the oral environment, which is an open system, where nutrients are continuously fed and removed. One closed system commonly used is a microtiter plate or a multiple-well plate. These are used widely in dental biofilm research and have been utilised by Roberts *et al.*, (2002) for the growth of oral pathogens *S. mutans* and *P. gingivalis*. This study successfully grew biofilms comprising these two species, demonstrating a low-cost, albeit labour-intensive, reproducible laboratory model. Microtiter plates offer limited control over the flow rate, which is important in the *in vivo* environment, and feeding in batch is not representative of the supply of nutrients to dental biofilms from saliva in the mouth. The study by Roberts (2002) led to more rapid growth of *S. mutans* and *P. gingivalis* initially, then a fall due to nutrient limitation which is not seen in the oral environment. The model also only considered two species, insufficient in appropriately representing dental biofilms. This was in contrast with a study by Guggenheim *et al.*, (2004) who developed the Zurich model (multispecies microtiter plate studying dental biofilms) to grow 6 oral species. This model was used to observe the spatial arrangement and associative behaviour of multispecies biofilms,

using species-specific probes in multiplex *fluorescence in situ hybridization* (FISH). The Zurich model provided the framework for the research by Amann *et al.*, (2012). This study used a 10-species community (instead of 6) and different modified saliva media to identify the nutritional needs of subgingival biofilms. This research investigated biofilm composition and the use of FISH to observe biofilm structure. The results showed that *Treponema denticola* struggled to establish in a dental biofilm when using media containing low or no heat-inactivated human serum. Using 50% heat-inactivated human serum resulted in significantly thicker and more stable biofilms, and a species abundance more similar to that *in vivo* compared to media with less human serum. The model allowed for characterising interspecies independence, where *F. nucleatum* had a very strong dependency on *Streptococci* and needed them in the local environment to establish. *T. denticola*, *P. gingivitis* and *Tannerella forsythia* occupied the top layer of dental biofilms, demonstrating the promise of FISH in identifying the spatial preference of oral species.

Open systems are more prone to contamination; however, they better mimic the oral environment. They enable fresh culture medium to be supplied and better control over conditions e.g., flow rate and feeding profile of cells. A device that has been used in dental biofilm research is the Modified-Robbins device (MRD). The MRD is a biofilm model that allows for the formation of microbial biofilms on various substrates under controlled flow conditions. This has been used to study the removal efficacy of a disinfectant in oral medicine (Coenye *et al.*, 2008). This study found NitrAdine[®], an anti-bacterial agent, was effective in reducing the cell counts of *Candida albicans*, *Staphylococcus aureus*, *S. mutans*, and *Pseudomonas aeruginosa* in biofilms. This model allowed simultaneous biofilm formation by different bacteria and within this study, it was possible to test several different substrata and growth media. There are drawbacks to using the MRD as a growth model. Particularly, the presence of a substrate gradient along these devices and less control over variables, including pH monitoring. The constant depth film fermenter (CDFF) is a high throughput biofilm growth model that produces biofilms of defined thickness using a scraper. It allows for the continuous feeding of media into the reactor. A CDFF has been used by Roberts *et al.*, (2021) to show that starch and sucrose exposure to dental biofilms, led to significantly more demineralisation and mineral loss, compared to sucrose alone, in the presence of fluoride. This was not seen when fluoride was absent. CDFF reactors provide more control over the MRD or closed systems, including flow rate modification and reactor bulk agitation to prevent nutrient gradients. It

has the specific advantage of allowing for biofilm growth on a solid substratum, with nutrients being supplied continuously in a thin liquid that trickles over the surface. A drawback is that the size of the biofilm is predetermined. The physical intervention on exact biofilm size is something that is not controlled uniformly in the oral environment (although there is some level of natural control with mechanical movements e.g., the tongue over teeth). This does reduce the ability of the model to replicate the growth of dental biofilms similar to that in the environment.

The CDC biofilm is a continuously stirred tank reactor (CSTR) that has recently been shown to be useful in dental biofilm research. The reactor can hold up to 24 coupons for biofilm growth. The coupons can be composed of material relevant to dental biofilm research different i.e., hydroxyapatite, and provide multiple sampling opportunities. Furthermore, the conditions of the model are flexible. One example is the control of the shear stress on the biofilm through the controlled agitation speed of the magnetic stir bar. Greater control on the feeding profile, including medium flow rate, and feeding of multiple media types, allows for use of the model in investigating dental biofilm compositional changes under varying conditions. This includes sucrose pulsing, which has been utilised by Rudney *et al.*, (2012). The results showed that sucrose pulsing led to a decrease in oral species diversity, with the abundance of *Streptococcus* and *Veillonella* increasing. Whilst this study involved saliva, the reactor is also effective at growing pure-culture bacteria that are not human or animal-derived. This has been done by Song *et al.*, (2017), working with mono and mixed cultures of *F. nucleatum* and *P. gingivalis* under different flow rates. This research used varying flow rates and found that dynamic flow led to lower bacterial adherence and that flow rate did not affect the ability of chlorhexidine to decrease bacterial counts.

A study by An *et al.*, (2022) successfully used the CDC reactors to grow, maintain and test the reproducibility of a diverse oral microbiota. The reactors were operated under conditions mimicking the oral environment. This included maintaining a temperature of 37 °C, similar to that of the oral environment, using a flow rate of 0.5 mL min⁻¹ for the medium similar to that of saliva, and using hydroxyapatite disks as a surface for biofilm growth (mimicking enamel). In this model, saliva inoculum from 6 healthy volunteers, to represent the oral microbiome, was used to grow biofilms on supplemented brain heart infusion. The study was able to cultivate the six major phyla previously identified as the core saliva microbiome. This included *Firmicutes*, *Bacteroidetes*, *Proteobacteria*, *Actinobacteria*, *Spirochaetes* and *Fusobacteria*. The

growth model was used in combination with analytical techniques, including confocal laser scanning microscopy (CLSM) and 16s rRNA metagenomic analysis, to examine the bacterial community. CFU counting found that after an initial acclimatisation period, communities stabilised. The use of CLSM showed that aggregates formed between days 1-3. These colonised the surface and biofilms developed 3D structured masses between days 5-8. Continuous monitoring of pH found that there was a decrease from 7.0 to 5.8 over the first 24 h, before increasing to 6.8 on day 3 and remaining between 6.5-8 for the remainder of the experiment. The Stoodley research group (Stoodley, 2022) used this model to test the impact of antimicrobial actives on the oral microbiome. Chlorhexidine and triclosan were applied for 14 days to test the effect on the microbial composition daily to mimic the oral healthcare regime. The research used analytical techniques including CLSM and 16s rRNA metagenomic analysis to examine the bacterial community and found that *Streptococcus*, *Veillonella* and *Actinomyces* decreased in abundance over 9 days, whilst *Selenomonas*, *Campylobacter* and *Oribacterium* increased. Triclosan led to the diminished prevalence of *Fusobacterium*, whilst Chlorohexidine led to an increased prevalence of *Streptococcus* genera relative to the control. This research was an example of an *in vitro* system studying dental biofilms that can be used in testing antimicrobial actives. The model was useful in benchmarking antimicrobial actives against those that are well-characterised e.g., chlorohexidine, and tracking the resulting change in microbial ecology over time, to inform risk assessment and improve product safety.

There were advantages and disadvantages to all the laboratory models seen above. These *in vitro* models do not resemble naturally occurring dental biofilms as well as *in vivo* models, but offer far greater experimental control, allowing for the defining of biofilm characteristics. The ethical issues associated with animal models are not relevant when using *in vitro* models. Dental biofilms grown using these models can be analysed by techniques e.g., qPCR, which allows for bacterial quantification in dental biofilm samples (Bourgeois et al., 2017), and FISH, which allows for imaging spatial and structural patterns for mixed-species dental biofilms. (Xiao et al., 2017). The use of these techniques has allowed for characterising of defined biofilms using growth models, where previous analysis had been limited to the use of selective media (J. L. Brown et al., 2019).

1.3.4 Different types of nutritional sources used in *in vitro* models

The growth medium that oral models are maintained on is vital to characterising these oral communities. The behaviour of bacteria changes depending on the nutrients and growth factors metabolised, as described with *S. mutans* on sucrose compared to other sugars in Section 1.2.4. In the oral environment, bacteria consume nutrients provided by food, metabolites excreted from other species in the same environment, urea, serum proteins and other nutrients in the saliva.

To reflect the *in vivo* environment, these models are often fed with saliva as this is the case as found *in situ*. Research Lim (Lim et al., 2020) fed biofilm *in vitro* using saliva collected from both caries and caries-free associated patients, supplemented with basal mucin medium. This was to study the effect of caries activity on the composition of *S. mutans* in saliva-induced biofilms on bracket materials. The conclusion was that the caries-associated saliva feeding resulted in more *S. mutans* but less overall bacterial count. Other studies have used artificial saliva in growing mixed-species, *in vitro* models (Tabenski et al., 2014). Several oral species require the addition of further chemicals to artificial saliva, including growth factors to support growth. The use of artificial saliva is less variable than human saliva, which helps with keeping studies standardised and reduces variability. Furthermore, sourcing artificial saliva is easier than human saliva and does not require the same ethical hurdles and access to patients. There are other rich media, containing animal-derived products, used in dental biofilm growth models. One medium that is commonly used is brain-heart infusion (BHI) (Cristina Barbosa da Silva et al., 2008). Another that is used to culture a wide range of oral bacteria is SHI medium (Lamont et al., 2021). This supported a wide range of oral species and is easy to source from chemical companies. These media are generally easy to handle and store, provided they have been sterilised by methods e.g., autoclaving.

Chemically defined media (CDM) provide the advantage of knowing every chemical and its concentration used. CDM are devoid of undefined, animal-derived components e.g., bovine serum. They are therefore extremely useful in studying bacterial metabolism by quantifying the consumption of medium components. This untangles the complexity of the chemical environment, which is not possible on media comprising animal-derived products, as used in the models discussed in Section 1.3.3. The defined chemical nature of these media eliminates the batch-to-batch variation that can occur using media containing animal-derived

components. CDM has often been used to support the growth of oral species, including several *Streptococci* (Terleckyj et al., 1975). The FMC medium developed here has been used numerous times in dental biofilm research to understand the behaviour of oral species on varied carbon source concentrations (Guo et al., 2014; Renye et al., 2004; Zeng & Burne, 2021). A significant drawback is the artificial nature of the media, as it is very different in composition from the *in vivo* environment and the tedious nature of compiling media that can consist of over 60 different components.

1.4 *In silico* modelling approaches to characterising dental biofilms

In silico modelling approaches have been used to characterise dental biofilms. This includes the influence of bacterial species on each other and their role in oral diseases, including caries. *In silico* models help understand factors driving caries development, including predicting the growth of cariogenic species at different sugar concentrations, and acid production of a dental biofilm, which is directly implicated in enamel demineralisation. Furthermore, simulations help direct experimental strategies to characterise biofilm behaviour, in a cost and time-effective manner.

The oral microbiome contains a complex network of metabolic interactions between species. Interspecies interactions can have synergistic effects on some bacteria and antagonistic effects on others (see *Streptococci-Veillonella* interaction in Section 1.2.1 as an example). Understanding these metabolic interactions is vital for characterising microbial contributions towards oral diseases. Central to understanding these complex networks is the sequencing of bacteria. Several studies have taken advantage of the progression of genome sequencing technology to identify the abundance of taxa in various parts of the mouth (Caselli et al., 2020c). Once genomes have been sequenced, metabolic models can be constructed, and flux balance analysis (FBA) carried out to analyse the flow of metabolites through a metabolic network. This provides information on what reactions can happen in a cell, including metabolite consumption and production (Jensen et al., 2020). One study by Mazumdar (2009) used metabolic modelling strategies to quantitatively understand the metabolic network for *P. gingivalis*, which is largely implicated in periodontitis. A model was constructed to inform amino acid preference and cytotoxic by-product secretion. This enabled the potential targeting of knock-out genes that could inhibit this pathogen to be identified. This included the genes GMAND, a mannose dehydratase enzyme, and GFUCS, a fucose synthase enzyme.

These enzymes were found to help produce GDP-L-fucose, vital in LPS assembly and the detrimental immune response associated with *P. gingivalis*. Understanding which enzymes, belonging to disease-associated oral species, are responsible for detrimental oral health, is useful in identifying targets central to the production of antimicrobials for disease treatment. This study showed the potential benefit of such metabolic models in combatting oral pathogens. This framework shows promise for use in other oral pathogens for antibacterial target strategies.

Metabolic modelling has been used in caries research to understand the interactions between species in dental biofilms. *S. mutans* and *S. sanguinis* are prevalent in dental biofilm and understanding interactions between the two is important, as it is known that commensal *Streptococci* species play a role in preventing *S. mutans* overpopulation. Valdebenito *et al.*, (2018) performed genomic and metabolic pathway comparisons to understand the competition and antagonistic relationship between the two species. It was concluded that *S. sanguinis* contained an enzyme capable of neutralising hydrogen peroxide, an antibacterial chemical produced by itself and several other oral species, something that *S. mutans* lacks. This leads to *S. sanguinis* outcompeting *S. mutans* in dental biofilms. This research demonstrated the benefit of using metabolic modelling to better understand the competitive nature between commensal and cariogenic species within the same environment. Genome sequencing and annotation must be completed to construct an accurate metabolic model, as done in this research.

Understanding the nutritional requirements of oral species is important in characterising their role and ability to thrive in the oral environment. Metabolic modelling approaches can be used to develop CDM for oral species in a time and cost-effective manner, by directing laboratory experiments to formulate them. These CDM can be used to untangle complex environmental influences in dental biofilm behaviour. Jijakli *et al.*, (2019) manually constructed a genome-scale metabolic model of the cariogenic species *S. mutans* to better understand its metabolism. This helped uncover findings e.g., the ability of *S. mutans* to catabolise sorbitol and the requirement for the Leloir pathway to use substrates e.g., raffinose. This study used FBA to better understand the chemical requirements to produce a CDM to support growth, with simulations validated by experimental work. Manual curation helped improve the accuracy of the automatic reconstruction of the metabolic model. One drawback of this type of modelling in general is the use of gap filling for unknown metabolic pathways. The strain

used in this research was *S. mutans* UA159 which is fully sequenced. Whilst this work is promising in the production of a CDM and a better understanding of bacterial metabolism, the species needs to be fully sequenced.

Continuous models, often using differential equations applied to continuous data, have advanced knowledge of dental biofilms and their roles in caries development. Pioneering work by Dibdin and Reece *et al.*, (1990; 1984), developed a 1-D continuous model to understand factors contributing towards caries development. This included the modelling of sugar clearance in saliva, modelled separately from dental biofilm/saliva exchange of sugars. Sugar diffusion and utilisation were modelled using an iterative Crank-Nicolson central difference scheme with time steps of one second or less. Sugar utilisation and acid production were computed within this time step. Lactic acid and acetic acid production were considered within this model. The research showed the importance of the isoelectric point of oral bacteria in factors associated with caries development, including acid production. It was also shown that varying biofilm/saliva contact affected cariogenic development. The model also concluded that changing initial acetate in the dental biofilm from 10 mmol L⁻¹ to 60 mmol L⁻¹ did not lead to a significant difference in the Stephan curve but decreased mineral loss. The consideration of modelling salivary regarding characterising factors associated with caries was important. This is because saliva surrounds dental biofilms, providing nutrients and impacting the oral ecology (Simon-Soro *et al.*, 2022). To date, there are still limited modelling approaches in characterising microbial ecology in the saliva, including composition, response to substrate concentrations, and acid production. More recent continuous models have investigated the relationship between specific oral species. This includes modelling the relationship between *Streptococcus* species and those belonging to the *Veillonella* genus. Feng *et al.*, (2021) developed a 2-D, continuum model, considering the mass balance of biomass and two nutrients (saliva and lactic acid), to understand the symbiotic relationship between *S. gordonii* and *Veillonella atypica*. The primary focus was the consumption of lactic acid by *Veillonella*, which is produced by *S. gordonii*, and is antagonistic to *S. gordonii* growth. The model was informed with parameters specific to the two bacteria, including growth rates and growth yield on saliva. Microscopy was also used to examine that *S. gordonii* aggregated into clusters, where model simulations showed that this species rose within the biofilm to more nutritionally dense areas whilst competing for substrates. This model provides evidence that continuum modelling of the bulk is useful in the prediction of bacterial interactions, including

lactic acid consumption/production. One drawback of this model was the numerous assumptions, including the assumptions of kinetic parameters. These could have been determined experimentally. Furthermore, limited consideration for mechanical interactions between species was given.

Modelling biofilms pose different challenges to planktonic cells. Mechanical forces act between cells which impact the overall biofilm. Adhesion and competition for limited nutrients, as they diffuse through the biofilm in a non-homogenous environment, are important characteristics of biofilms not seen in planktonic cultures. This means that modelling approaches must consider these interactions to be able to characterise the ecology of biofilm systems more accurately. Individual-based modelling (IbM) allows for consideration of the chemical and mechanical properties of each cell and between bacteria within a biofilm. Each cell is represented as its agent, having individual properties i.e., mass and kinetic parameters. This is useful as species within a biofilm have independent effects on the overall structure and function of a biofilm i.e., acid production contributing to the overall pH of the local environment (Aruni et al., 2015). IbM can simulate these individual species characteristics, helping to simulate the heterogeneity in the biofilm, rather than assuming each cell acts the same within the model. There have been models developed that use IbM but do not consider such mechanical forces and only focus on the biological and chemical elements of biofilms. IBM have been used to characterise biofilms found within the ear, as developed by Brown *et al.*, (2019). This work simulated the difference in morphologies of *Haemophilus influenzae* biofilms formed *in vitro* and *in vivo*. The model reproduced surface fractal patterns that were observed *in vivo*. The results showed that the *in vivo* clusters were 10x smaller than *in vitro* clusters, due to the elimination of planktonic cells. This model did not consider mechanical interactions between agents, which is known to have a profound effect on biofilm formation (Stubbendieck et al., 2016). One model that considered the mechanical forces between cells in a domain containing a biofilm, homogenous bulk, and boundary domain, is that developed by Schluter *et al.*, (2015). Here, the effect of adhesion was studied, and they identified that growth within different locations of the biofilm affected the ability of the cells to thrive and outcompete, due to nutrient competition and resistance to sloughing. Simulated adhesive cells physically outcompeted less adhesive cells through pushing and this provided an advantage in a nutrient-limited system. This model showed the importance of considering mechanical forces between cells when characterising the evolution of a biofilm

under nutrient-limiting conditions when sloughing of the biofilm is considered. Another model that used IBM to model biofilms and considers mechanical interaction was developed by Jayathilake *et al.*, (Jayathilake et al., 2017) to analyse biofilms in wastewater. This model integrated bacterial cell biochemistry and physics to enable the quantification and prediction of a variety of properties of biofilms, including the effect of shear rate and biofilm growth (Figure 1.7). The model was based on the thermodynamic first law, and successfully integrated growth and mechanics, including adhesion and decay, by creating a microbiological adaptation of an open-source microbial simulator. The model took into consideration characteristics i.e., deformation and detachment of cells, which are both important in biofilm formation. This work also considered the resistance of agents to anti-bacterial agents/forces, not widely applied in IBM. Simulating large complex microbial systems can be challenging in terms of computational demand. One such work to do so was that by Li (2019) whose fully parallelised, 3-D model simulated biofilm formation and detachment considering fluid dynamics and several microbial functional groups and nutrients.

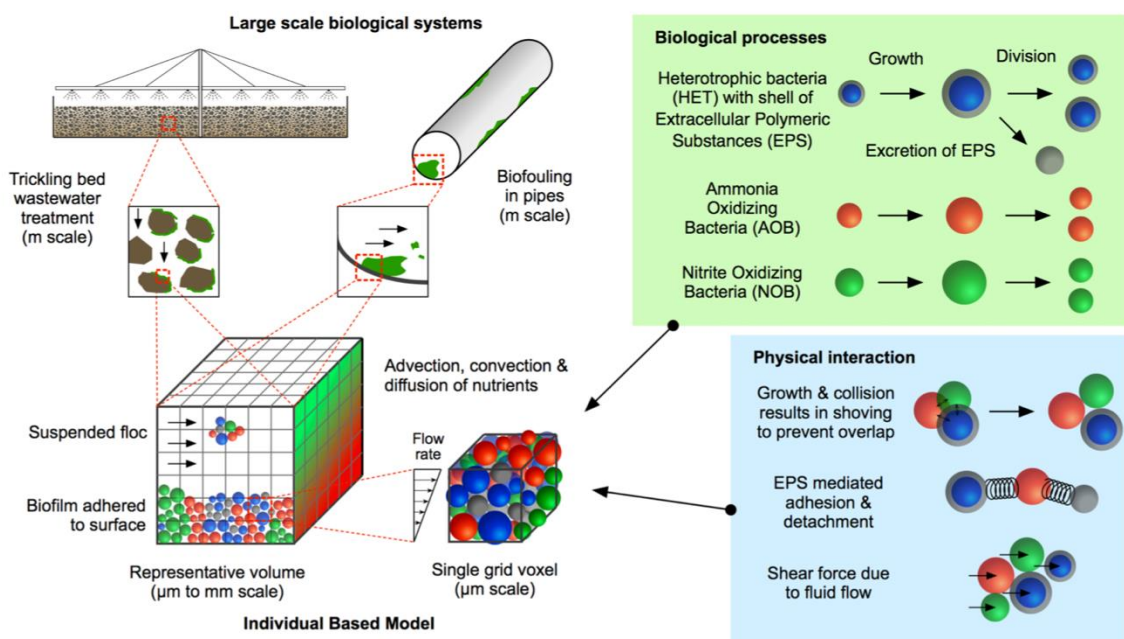


Figure 1.7 An IBM used for wastewater systems. This model, based on the first principle of thermodynamics, represented individual bacteria as spheres and takes into consideration several characteristics e.g., the collision of particles and shear force characteristics which are desirable in dental biofilm modelling (Jayathilake et al., 2017).

IbM models can simulate trophic interactions and population dynamics, considering several species with the same biofilm domain. A spatially resolved IBM model of microbial dynamics in soil was presented by Kim *et al.*, (2016). The research concluded that the effective water film thickness determined the microbial swimming speed across the biofilm surface and that swimming velocity was affected by the roughness of different regions of soils. This model considered two different nutrients and two species, where one species consumed by-products produced by the other. This model was therefore useful in providing a framework where mixed-community models on several substrates can be simulated in different environments within the same biofilm. This model did not, however, consider any characteristics specific to a bacterial species e.g., growth rates. This model would need expanding with kinetic parameters, thermodynamic considerations etc before the model could be applied to characterising a microbial community comprising specific bacteria. One model that considered these species-specific parameters was that developed by Gogulancea (2019). Using IbM, this model considered biological, chemical, and thermodynamic factors associated with biological growth to better simulate biofilm growth and the effect on the surrounding environment. Here, the stoichiometry of species as a thermodynamic approach was included, as well as Monod type kinetics, where species-specific growth rates and substrate affinity constants were defined. The model was able to simulate the local pH and substrate utilisation as the biofilm grew. The drawback of such models was the computational demand of simulating so many agents over long simulation times.

IBM are useful in dental biofilm research as the oral microbiome contains over 700 different species with complex interspecies interactions. It has allowed more complex dental models to be developed, advancing on pioneering work by Dibdin and Reece *et al.*, (1990; 1984), who developed 1-D and 2-D continuous models to calculate the pH profiles in the dental biofilm. Head (2021) used this type of modelling to determine the factors that governed biofilm composition and changes towards a cariogenic state under different conditions. He simulated the growth of two different populations and found that one would progressively disappear out of the system depending on the parameters defined for aciduric potential and nutrient uptake. The model did not consider the mass transfer limitations of glucose, so the populations were competing for space rather than for substrate. It was concluded that important parameters to consider were glucose concentration and acid buffering. This model did not define specific bacterial species or their kinetic/thermodynamic parameters, and

therefore lacked discrete information on how different bacteria would contribute to this environment in the tested carbohydrate change.

Mathematical and *in silico* modelling in dental biofilm research has become more popular. Head *et al.*, (2017) conducted *in silico* modelling to assess the effect of the frequency of sugar administration on supragingival plaque development. This was useful as the consumption of a high frequency of sugar is a primary driver of caries, due to the resulting acid production (Kawada-Matsuo *et al.*, 2017). This model can be used to inform dietary changes and further strengthen the known impact of sugar consumption on caries. The effect of saliva flow was neglected in the study to keep non-microbial factors limited. This is a parameter that plays an important role in the oral environment, as the salivary flow has a profound effect on pH buffering and sugar clearance within the mouth (Lynge Pedersen & Belstrøm, 2019a; Muddugangadhar *et al.*, 2015). One assumption made in this model was that the simulated biofilm was either always or never cariogenic, whereas dental biofilms potentially shift between the two states (Meyer *et al.*, 2021; Mark Steven & Charlie, 2009). Taking into consideration the dynamic nature of dysbiosis and how the microbiome changes from a healthy to a cariogenic state, is important in oral health and disease. This is generally lacking in modelling strategies.

Marsh *et al.*, (2015) developed a mathematical and *in silico* plaque simulation model. This was to predict changes in biofilm composition and growth under varying acid levels and antimicrobial agent concentrations. The model considered two bacterial populations, one aciduric and one non-aciduric. The simulation also included pulsing of glucose, leading to acid production. Microbes were modelled as discrete particles representing cell aggregates. The work concluded that reducing the frequency of acid challenge or terminal pH, by reducing bacterial growth, resulted in the protection of commensal microorganisms. This area of modelling, assessing whether environmental factors can modulate the dental biofilm without direct lethal microbial action, is very useful. This is because directly altering the microbiome can lead to the abolishment of positively contributing characteristics from specific oral bacterial species. This includes the denitrifying capacity of *Neisseria*. It also helps direct antimicrobial active use by targeting the more cariogenic species within a biofilm in this model. One area of research that should be expanded is looking at the impact of discrete bacterial species and considering more than two bacterial populations. This will help us

understand which species in a dental biofilm are sensitive to antimicrobial agents and pH changes.

A study by Martin *et al.*, (2017) involved the development of an IBM focused on interactions between *P. gingivalis* and *S. gordonii*. The former was shown to contribute towards dysbiosis. The model furthered knowledge of the bacterial interactions in biofilms that may happen during the transition between non-caries and caries. This model incorporated bacterial growth and yield into the model from experimental work and considered growth on different substrate concentrations. This allowed for simulations to resemble the *in vivo* environment more closely. The study utilised CLSM, which allowed for the assessment of biofilm architecture and characteristics of the two species. Nevertheless, an important limitation in this work concerning modelling dental biofilm was that the model produced was based on data from only two species. This limits research in an area where analysing numerous strains and having a more expansive model is important. The interaction between different bacterial species e.g., acid production and consumption, is key in dental biofilm research. Taking into consideration a very limited number of species does not represent the oral environment well. This model also did not consider bacterial cell death and detachment, which are important processes that occur continuously in any bacterial microbiome.

Mathematical models have also been used to understand the shape of carious lesions, to understand which parts of the tooth are important for caries development, and to understand the rate of caries progress. A 3-D model by Fabregas & Rubinstein (2014) considered diffusion of hydrogen and calcium ions, and reactions at the surface of enamel, in determining the rate of caries progression. This was done by quantifying the total volume change of enamel. The model was able to incorporate pH as a variable, simulating a pH drop mirroring that after eating. The model concluded that the outer prismless layer of enamel was vital in slowing down caries progression. This type of model provided information on the progression of the disease, not directly related to bacterial activity. Characterising tooth material better, it helped understand how fast caries progresses under certain conditions and gives more information on the specific parts of the tooth that need protecting to reduce caries progression. Another model built to characterise tooth enamel demineralisation was that by Ilie *et al.*, (2012). This model differed significantly from the model by Fabregas, as it put the focus on the modelling of the demineralisation of plaque through acid production from bacterial metabolism of substrates. This model focused on more species, including aciduric

Streptococci, non-aciduric *Streptococci*, *Actinomyces* and *Veillonella*, using their species-specific kinetic parameters. The use of several species within the oral model allowed it to better reflect dental biofilms compared to a simpler one or two-species system, as done by Martin (2017). This model found that *Veillonella* had a net negative effect on demineralisation due to consuming lactate, which the other species produced, increasing the pH. This research also demonstrated the importance of considering lactate consumption by bacteria in modelling caries formation. This was because the exposure of plaque to high glucose concentrations for 2 min led to glucose being present in the plaque for 25 min. The retention time in the saliva bulk was much lower, at 10 min. These types of oral models, where numerous species are considered, are becoming more popular as they better characterise the oral microbiota which is very diverse. One model that considered numerous species was a stochastic attachment model by Chathoth *et al.*, (2022). This research modelled the attachment of oral microcolonies of *P. gingivalis*, *S. gordonii* and *T. denticola*, to biotic and abiotic surfaces through intra and interspecies interactions. This was simulated under different iron concentrations. The research used three parameters, probability of attachment to the surface, horizontal attachment probability of bacteria, and vertical attachment probability. This data was collected experimentally, and the model was fitted to each species using this data. The model concluded that decreasing iron concentrations lead to lower horizontal attachment and higher vertical attachment. This model provided a useful tool for understanding caries progression, as bacterial adhesion to tooth surfaces is important in dental biofilm development. The modelling of three species was an improvement on two species models, as done by Martin (Martin *et al.*, 2017), although this is still too simple to capture the complexity needed from an oral community.

In silico approaches to understand species behaviour have shown to better reflect *in vivo* findings and *in vitro* data when validated by experimental data. This includes using pH corrections in species-specific bacterial growth kinetics, which has been done by Rosso (Rosso *et al.*, 1995). This research described μ_{max} as a function of temperature and pH, using three cardinal pH parameters (optimum pH, maximum pH where growth occurs and minimum pH where growth occurs). This resulted in better correspondence between mathematical simulations and experimental data. Whilst this was not directly applied to dental research, the consideration of pH on bacterial growth kinetics in oral species is important to consider, as there is often a drop in pH in the oral environment due to sugar fermentation (Kianoush *et al.*,

2014). Also, species have different tolerances to these acidic conditions (Boisen et al., 2021a). Studies utilising mixed *in vitro* and *in silico* approaches to understand dental biofilms activity in caries are limited, and those that have done so often consider few oral species (Rath et al., 2017; Martin et al., 2017) It is, therefore, desirable to use mixed *in vitro-in silico* approaches, where the use of a CDM (Section 1.3.4) would allow for testing the effect of one parameter at a time i.e. sugar concentration, on oral dysbiosis and caries progression.

1.5 Aims and objectives

In this research, I aimed to develop *in vitro* and *in silico* modelling approaches, to characterise and quantify the invasion of *S. mutans* into a 4-species, commensal dental biofilm. This involved modelling the transition to a cariogenic state, as seen *in vivo*. I aimed to model this transition in a defined environment. This was done using a CDM, to untangle complex chemical environmental influences. The CDM was used to support the growth of the synthetic community, representing dental biofilms. I aimed to use the combination of *in vitro* and *in silico* models (informed by experimental-collected kinetic parameters), to identify factors, including pH, glucose and lactic acid concentration, that influenced *S. mutans* invasion.

The objectives of this research were as follows:

- 1) Develop a chemically defined medium, supporting the growth of all members of a 5-species synthetic community of oral bacteria, to enable invasion experiments in a defined chemical environment.
- 2) Characterise the synthetic community of oral bacteria, including collecting the maximum specific growth rates (μ_{max}) and substrate utilisation constants (K_s) that will inform *in silico* modelling approaches.
- 3) Establish an *in vitro* reactor model capable of characterising the invasion of *S. mutans* into the pre-formed 4 species dental biofilm.
- 4) Use the *in vitro* model to characterise *S. mutans* invasion under different glucose and lactic acid concentrations, through optimised techniques i.e., qPCR and FISH. This included ascertaining the factors i.e., low pH, contributing towards *S. mutans* invasion and the effect of the commensal biofilm.
- 5) Develop *in silico* models to simulate the growth of these species under the same conditions used for the reactors, using experimentally collected kinetic parameters and considering the effect of pH on species kinetics.

1.6 Importance of the research

Modelling strategies that appropriately resemble the complexity of dental biofilms, whilst providing a defined environment to understand factors contributing to cariogenic species invasion, are limited. The models developed in this research fill this gap, allowing for the quantification of *S. mutans* invasion into a commensal dental biofilm, under different glucose and lactic acid concentrations, over time. The models considered the impact of invasion on a complex, commensal biofilm and the local environment. This included pH change, relevant to enamel demineralisation and caries progression. The *in vitro* model was a defined system, including the use of a CDM. This was developed to support the growth of a more diverse consortium of species, including the lactic acid-consuming species *V. parvula*, which is prevalent in dental biofilms. The *in silico* model, informed by experimentally-collected kinetic parameters, helped understand these caries-related factors by simulating dental biofilm invasion, local pH change and substrate consumption. The combined approaches of the *in vitro* and *in silico* models provide a framework, which will inform the production of safe products, including antimicrobial actives, toothpaste and risk assessment (Section 1.1) to help combat the significant global health and economic impact of dental caries.

Chapter 2. Material & Methods

2.1 Materials used in research

2.1.1 List of bacterial strains

The bacterial strains I used in this research project, including the name, genotype, and origin, were listed in Table 2.1. These were all wild type and comprised the synthetic community, excluding *Escherichia coli* TOP10, which were pre-made competent cells, used for cloning of plasmid inserts.

Table 2.1 All bacterial strains used in this research, including the genotype and reference. *Escherichia coli* TOP10 was used in plasmid cloning, all other species comprised the synthetic community.

| Bacterial strain | Genotype | Reference | NCBI reference for fully sequenced genomes |
|------------------------------------|--|---|--|
| <i>Streptococcus gordonii</i> DL1 | Wild type | (Jauregui et al., 2013) | (<i>Streptococcus gordonii</i> DL1/CH1 (ID 1021), Genome, NCBI, 2022) |
| <i>Streptococcus mutans</i> UA159 | Wild type | (Ajdic et al., 2002) | (<i>Streptococcus mutans</i> UA159 (ID 856), NCBI, 2022.) |
| <i>Actinomyces oris</i> MG1 | Wild type | (Mishra et al., 2007) | - |
| <i>Neisseria subflava</i> DSM17610 | Wild type | (German Collection of Microorganisms and Cell Cultures GmbH: 2019) | - |
| <i>Veillonella parvula</i> DSM2008 | Wild type | (German Collection of Microorganisms and Cell Cultures GmbH: 2019) | (<i>Veillonella parvula</i> DSM 2008 (ID 2471), NCBI, 2022.) |
| <i>Escherichia coli</i> TOP10 | F- <i>mcrA</i> Δ (<i>mrr-hsdRMS-mcrBC</i>) Φ 80 <i>lacZ</i> Δ M15 Δ <i>lacX74</i> <i>recA1</i> <i>araD139</i> Δ (<i>ara-leu</i>)7697 <i>galU</i> <i>galk</i> <i>rpsL</i> (StrR) <i>endA1</i> <i>nup</i> | (TOPOTM TA CloningTM Kit for Subcloning, with One ShotTM TOP10,2020.) | (<i>Escherichia Coli</i> (ID 167), NCBI, 2022.) |

1.2 List of equipment

The list of major equipment I used in this research project was listed in Table 2.2 This Table included the equipment type, device name, and manufacturer details. All equipment used was operated post-safety training and following the manufacturer's standard operating procedure.

Table 2.2 All equipment used in this research, including the device application, name, and manufacturer. In all instances, devices were operated post-safety training, where applicable.

| Equipment | Device | Manufacturer |
|----------------------------|--|--|
| Anaerobic cabinet | Whiteley DG250 | Don Whitley Scientific, Bingley, UK |
| Aerobic incubator | IKA KS 4000 | IKA, Cologne, Germany |
| Autoclave | Astell autoclave | Astell, Kent, UK |
| Swing out centrifuge | Sigma 3K10 | Sigma, MA, USA |
| Microcentrifuge | PrismR refrigerated microcentrifuge | Labnet, NJ, USA |
| Benchtop vortex | Starlab IR vortexer | Starlab, Brussels, Belgium |
| Laminar flow cabinet | Gelaire TC 48 | Gelaire, NSW, Australia |
| Water bath | JB1 | Grant instruments, Cambridge, UK |
| Biochrom spectrophotometer | Biochrom Libra S11 | Biochrom, Cambridge, UK |
| Calorimeter | Calscreener™ calorimeter | Symcel, Solna, Sweden |
| Agarose gel tank | Bio-Rad power pack 3000 | Bio-Rad, California, USA |
| Transilluminator | G box:Transilluminator | Syngene, Cambridge, UK |

| | | |
|--------------------------------|--------------------------|----------------------------------|
| NanoDrop™ spectrophotometer | ND-1000 Nanodrop™ | Thermo Fisher, MA, USA |
| Plate reader | Biotek Synergy HT | Biotek, Vermont, USA |
| qPCR thermocycler | QuantStudio qPCR studio | Thermo Fisher, MA, USA |
| Flow cytometer | Attune NxT | Thermo Fisher, MA, USA |
| Light microscope | Leica DM750 | Leica, Wetzlar, Germany |
| Fluorescence microscope | Olympus BX60 | Olympus, Tokyo, Japan |
| Confocal microscope | Zeiss 880 LSM | Zeiss, Jena, Germany |
| <i>In vitro</i> reactors | CBR 90-3 CDC bioreactor | Biosurface Technologies, USA |
| Benchtop pH probe/meter | Mettler Toledo Seveneasy | Mettler Toledo, Ohio, USA |
| Weighing scale | Ohaus Pioneer | Ohaus, NJ, USA |
| Autoclavable pH probe | F-695 Broadley James | Broadley James, California, USA |
| Raspberry Pi 3 with tentacle | Raspberry Pi 3 | RS components, London, UK |
| Peristaltic pump | 101 U/R low flow | Watson Marlow Falmouth, UK |
| Magnetic stirrer and hot plate | Biosurface hot plate | Biosurface Technologies, MT, USA |
| Camera | IXUS 220 HS | Canon, Tokyo, Japan |

2.2 Culturing and storage of bacterial strains

2.2.1 Routine culturing of bacterial strains

All bacterial species within this study were cultured using routine microbiological processes. *S. gordonii*, *S. mutans*, *A. oris* and *V. parvula* were all cultured anaerobically (80% N₂, 10% H₂, 10% CO₂) inside an anaerobic cabinet for 16 h at 37 °C. *N. subflava* and *E. coli* were cultured in aerobic conditions using an aerobic incubator. *E. coli* was cultured in Lysogeny Broth (Sigma Aldrich, Missouri, UK). All other species were cultured in THYE medium, containing 30 gL⁻¹ Todd Hewitt broth (Melford, Ipswich, UK) and 5 gL⁻¹ yeast extract (Melford). For *V. parvula*, this included the addition of 12.1 gL⁻¹ DL lactic acid. At all steps of culturing and at the end of all experiments, bacteria were checked for contamination using microscopy, Gram staining or visual inspection of colonies on agar plates. This included making sure that only one type of colony was observed during mono-culture experiments. Strain stocks were stored at -80 °C.

Agar was prepared by autoclaving THYE medium, supplemented with 13 gL⁻¹ Bacto agar (Melford), at 121 °C for 15 min. This medium was poured into sterile, empty Petri dishes (Thermo Fisher, MA, USA), which were cooled and stored at 4°C. Plates were inverted to stop condensation inside the dish. Agar plates used for the growth of *V. parvula* were reduced inside an anaerobic incubator for 24 h before use. Plates containing bacterial species were incubated overnight in either an anaerobic or aerobic incubator.

To prepare an overnight inoculum in preparation for experimentation, a single colony was taken from the agar plate using a sterile disposable inoculum loop. This was placed inside a universal bottle containing 20 mL of THYE medium and left for 16 h at 4 °C. For the growth of *V. parvula*, DL lactic acid syrup (Sigma Aldrich) was also included (final concentration 12.1 gL⁻¹) into the medium and agar, which were reduced anaerobically for 24 h before inoculation. *E. coli* was grown on LB broth (Sigma Aldrich) medium supplemented with 100 µg mL⁻¹ Ampicillin (Sigma Aldrich) to provide selection pressure for plasmid retention and expression.

2.2.2 Preparation of glycerol stocks

Glycerol stocks of each species were for use in all experiments involving the oral synthetic community members. Single colonies of bacterial strains were grown overnight in 20 mL of THYE medium. For *V. parvula*, this was supplemented with 12.1 gL⁻¹ lactic acid. Incubation of *A. oris*, *S. gordonii*, *S. mutans* and *V. parvula* took place in an anaerobic incubator for 16 h at 4 °C. *N. subflava* and *E. coli* were incubated inside an aerobic incubator. Following incubation, cells were harvested by centrifugation at 3,800 xg for 10 min at 4 °C using a swing-out rotor centrifuge. Pellets were resuspended in 2 mL of sterile, suitable medium, diluted 1:1 with 50% (v/v) glycerol (VWR, Pa, UK) for a final concentration of 25% glycerol. Suspensions were mixed using the bench-top vortex and 1 mL pipetted using filter pipette tips into sterile screw-top Eppendorf tubes (Thermo Fisher, MA, USA). Glycerol stocks were stored at -80 °C. Glycerol stocks at a higher bacterial concentration were produced for use in CDC bioreactor experiments by the method above but involved growing a 600 mL of overnight culture instead of 20 mL culture. All stocks were plated and checked for contamination before and after culture.

2.2.3 Colony forming unit counts

The number of cells per mL were calculated in glycerol stocks and overnight cultures using colony forming unit (CFU) counting. This was to standardise the inoculum for each species. Ten-fold serial dilutions of glycerol stock were created for each member of the synthetic community using 180 µL of sterile PBS (Sigma Aldrich) and 20 µL of culture. Dilutions ranged from 10⁻⁴ to 10⁻⁷. Samples were mixed using vortexing and 10 µL was pipetted onto pre-dried agar for each serial dilution. Drops were left to dry in the laminar flow cabinet, before being incubated for 24-48 h.

Plates were imaged using a Canon IXUS 200 (Canon, Tokyo, Japan), and colonies formed were counted using ImageJ (Fiji, Maryland, USA). The average number of colonies were calculated for dilutions, where between 10 and 100 colonies could be counted. The colony count was multiplied by the dilution factor and then by 100 (to account for volume) to calculate the number of cells per mL of glycerol stock or overnight culture.

2.3 Experiments defining synthetic community

2.3.1 Growth experiments

The oral species were grown individually to generate growth rates from the exponential phase. Sterile universal bottles containing 20 mL THYE were inoculated with a single colony of cells and incubated in the anaerobic workstation, *excluding N. subflava* which was incubated aerobically. After 16-20 h, the overnight cultures were each transferred into 50 mL Falcon tubes (Fisher Scientific) and centrifuged at 3,800 xg at 4 °C. The supernatant was discarded. Cells were suspended in 20 mL of altered FMC (AFMC), a chemically defined growth medium (CDM), (see Appendix A) and gently vortexed using a bench-top vortex. This culture was centrifuged at 3,800 xg and 20 °C to wash the cells of any residual medium. The cells were re-suspended in 20 mL AFMC and mixed with the vortex. 4.8 mL of medium was pipetted into each test tube and 0.2 mL of cell culture was added for a final dilution of 1:25. The test tubes were gently shaken and placed in a water bath for the duration of the experiment at a temperature of 37 °C, with the test-tube tops screwed tightly closed. At the end of the experiment, the test tubes were placed into the anaerobic workstation, *excluding N. subflava* and *E. coli*, which were incubated aerobically.

For the experiments performed to calculate the substrate affinity constants (K_s), the media used were kept constant, apart from varying concentrations of the limiting substrates (glucose, sucrose, and lactic acid).

2.3.2 Development of AFMC medium

AFMC was developed to support the growth of the synthetic community. The formulation of FMC medium (Terlecky et al., 1975) was supplemented with additional chemicals (see Appendix A) to support the growth of *A. oris* and *V. parvula*. When the growth of all species was supported, and each species was able to grow for at least 40 generations, this medium was known as AFMC. AFMC components were stored in aliquots at the appropriate temperature (see Appendix A). Flux balanced analysis (see 2.8.1) was used to validate that AFMC could support growth. FBA was used to model the metabolism of these species, and confirm growth, with and without the addition of chemicals e.g., lactic acid for *V. parvula*.

2.3.3 Carbohydrate utilisation

To understand the metabolic requirements of the synthetic community members and inform the IBM, growth experiments on different carbon sources were conducted. Bacterial strains were grown as described in 2.3.1. All chemicals used were from the Megazyme Sucrose/D-Glucose assay kit (Megazyme, Wicklow, Ireland). At the desired time point, 0.1 mL of bacterial culture was pipetted into each of the two Falcon tubes. To the first Falcon tube, 0.1 mL acetate buffer was added and 0.1 mL β -fructosidase was added to the other test tube. Both test tubes and all reagent blanks were incubated at 50 °C in a water bath for 20 min. After this time, 1.5 mL of glucose oxidase was added to each test tube, which were again incubated at 50 °C in a water bath. Finally, 1 mL of each test tube was pipetted into a cuvette (Fisher Scientific) and the optical density at a wavelength of 510 nm was recorded using the Biochrom spectrophotometer. To quantify the lactic acid concentration, 0.1 mL bacterial culture, containing between 0.5-30 μ g of lactic acid, was pipetted into a cuvette. 1.6 mL distilled water was added, along with 0.5 mL of solution 1 buffer, 0.1 mL NAD⁺ and 0.02 mL D-GPT (D-L Lactic acid assay kit, Megazyme, Ireland). The optical density was read at a wavelength of 340 nm after 5 min (A1). 0.02 mL D-LDH and 0.02 mL L-LDH (D-L Lactic acid assay kit, Megazyme, Ireland) were added to the cuvette and the optical density was measured after 10 min at 340 nm (A2). The lactic acid concentration was calculated, using these two values, from the equation detailed in the assay kit protocol.

2.3.4 Calscreeener™ experiments

For each species, the heat produced over 24 h was recorded using the Calscreeener™ (Symcel, Solna, Sweden) calorimeter. This was to observe any metabolic differences when grown on different carbon sources and between planktonic and biofilm morphologies. Cultures for each species were grown in preparation for experiments, as described in Section 2.3.1. Then, 0.1 μ L was pipetted into plastic wells containing 190 μ L of AFMC and inserted into the Calscreeener™ titanium wells (Symcel, Solna, Sweden). These were loaded into the Calscreeener™ plate loader and inserted into the Calscreeener™. Both the top and bottom rows of wells in the 48-well plate loader contained 200 μ L of AFMC as control samples. A 30 min incubation period was allowed for signal stabilisation. Using the provided Calview™ software (Symcel), the heat flow (μ W) was recorded over 24 h. Control samples were used to take a baseline of all culture samples.

2.4 Molecular biology techniques

2.4.1 *Agarose gel electrophoresis*

Agarose gel electrophoresis was used to identify the quality of DNA extracts and qPCR products. Gels also needed to be run so that cloned inserts and the correct amplified products in the qPCR could be identified. Gels were made by adding 1-2% agarose (Melford) in 50 mL of TAE buffer (Thermo Fisher) and heated using a microwave, until dissolved. This was cooled briefly, before adding 5 μ L of Ethidium Bromide (Thermo Fisher) and left to set in a cassette. 4 μ L of DNA sample was mixed with 1 μ L of 5x DNA loading buffer (Bioline Ltd, London, UK) and loaded into the gel. 5 μ L of Hyperladder V DNA ladder (Bioline) was loaded onto the gel into a separate well. Gels were run at 90 V for 60 min using the gel electrophoresis machine. The DNA samples in the gels were visualized under UV light using the Transilluminator.

2.4.2 *NanoDrop™ for DNA quantification*

NanoDrop™ spectrophotometry was used to quantify nucleic acid concentrations of bacterial gDNA and plasmids. This was also used to check for the quality of the DNA collected from the synthetic community species. A reading of nuclease-free water (Sigma) was taken and the appropriate elution buffer (included in the kits for the experiments conducted) was used as a blank. 1 μ L of the sample was used for all readings. Values were recorded in ng/ μ L. The purity of DNA was checked by confirming that the 260/280 nm values recorded on the NanoDrop NanoDrop™ were between 1.8-2.

2.4.3 *Genomic DNA extraction from bacterial species*

Genomic DNA was extracted using a DNeasy Powersoil Pro kit (Qiagen, Hilden, Germany). Cells were first suspended in a mixture of 180 μ L Tris-HCl (Thermo Fisher), 10 μ L Mutanolysin (50 U concentration) (Sigma Aldrich) and 10 μ L lysozyme (200 mg/mL) (Sigma Aldrich). The suspension was incubated at 37 °C for 1 h in a water bath. 2 μ L of Proteinase K (Thermo Fisher) at a concentration of 20 mg/mL was added. The suspension was vortexed and incubated at 65 °C for 45 mins. The rest of the protocol was followed according to the manufacturer's instructions. DNA was eluted in 50 μ L of elution buffer (Qiagen) and checked on the NanoDrop™ for yield (Section 2.4.2) as well as on an agarose gel (Section 2.4.1) for sample quality. DNA was stored at -20 °C.

2.4.4 Plasmid extraction from *E. coli*

Plasmids were extracted from *E. coli* using the QIAprep Spin Miniprep plasmid kit (Qiagen) in accordance with the manufacturer's instructions. Following the extraction, samples were eluted in 50 μ L of elution buffer (Qiagen). The plasmids were stored at -20 °C and used as standards in later qPCR experiments. Samples obtained were measured on the NanoDrop™ spectrophotometer (Section 2.4.2) to check yield and quality. Plasmids were run on an agarose gel (Section 2.4.1) to check the quality of the DNA.

2.4.5 PicoGreen™ for double-stranded DNA quantification of plasmids

The DNA concentration of plasmids extracted from *E. coli* was accurately quantified using a Quant-iT PicoGreen™ dsDNA Assay Kit (Thermo Fisher). The standard curve used was in the high range of 1 μ g/mL-200 ng/mL. The protocol was carried out as per the manufacturer's instructions. Samples in black 96 well plates (Greiner Bio-One, Kremsmunster, Germany) were incubated for 5 min in the dark and fluorescence values were recorded on a plate reader at excitation/emission of 480/520 nm. Triplicate values were taken from three independent experiments and their average was used for the quantification of DNA.

2.4.6 qPCR primers and probes

Primers and probes specific to each synthetic community member were needed to correctly quantify each species using qPCR. All qPCR primers and probes used in this study were listed in Table 2.3, along with the targeted region for amplification. Primers were ordered using DNA Oligo Synthesis Services (Thermo Fisher). For *N. subflava*, primers and probes for qPCR quantification were designed using Snapgene software (Dotmatics, MA, USA). Primers were designed such that the difference in annealing temperature within the same primer set was 5°C or less. Primers and the Gibbs free energy of bonds were checked for hairpins using IDT OligoAnalyser (IDT, Iowa, USA).

Table 2.3 All qPCR primers and probes used in this research project, as well as the origin of the sequence used. Primers were checked for hairpins and suitable annealing temperatures (gene copy number a-1 b-3 c-4)

| Bacterial strain | Target region | Forward primer | Reverse primer | Probe | Origin |
|------------------------------------|-----------------------|---|---------------------------------------|--|------------------------|
| <i>Streptococcus gordonii</i> DL1 | 23S rRNA ^c | CTG ATG TCA ACC TGA TTA ACG GCA | GCT TGG TCA GAC CCT GAA AAA TCA | CTT TGA GGG AGA TGC TGT CTA CTC CAT GTA | (Jones, 2019) |
| <i>Streptococcus mutans</i> UA159 | 16S rRNA ^a | GCC TAC AGC TCA GAG ATG CTA TTC T | GCC ATA CAC CAC TCA TGA ATT GA | TGG AAA TGA CGG TCG CCG TTA TGA A | (Yoshida et al., 2003) |
| <i>Actinomyces oris</i> MG1 | 23S rRNA ^b | GGT GGT CTC CAG CAC TGG G | ATC CTG TGC GGA CGT AAC GC | GGG TGA TGG GCA CCG AGG CGT A | (Jones, 2019) |
| <i>Neisseria subflava</i> DSM17610 | 23S rRNA ^c | AAC GTA TTC ACC GCA GTA TG | TGG AGC CAA TCT CAC AAA AC | AGT CCG GAT TGC ACT CTG CAA CTC G | (Ciric et al., 2010) |
| <i>Veillonella parvula</i> DSM2008 | 23S rRNA ^c | CGT TTA GGA ATG AGT ACA GCC GTA | CGG ATG GTG TTG AAG ACC CA | ATT CGT ACT GCT GAA TGT GCG GGA G | (Jones, 2019) |

2.4.7 Cloning of targets into *E.coli*

The amplified DNA targets of bacterial species were cloned into the PCR 2.1 TOPO™ vector using the TOPO™ TA cloning kit (Invitrogen, MA, USA). This was necessary so that qPCR standards for each species could be generated. One cloning reaction was set up per species. To set up the cloning reaction, between 0.5-4 µL of fresh PCR product was pipetted into an Eppendorf (quantity was based on PCR fragment size, with a molar ratio of vector to PCR product of 1:3 desired). To this tube, 1 µL salt solution, 1 µL TOPO™ vector and nuclease-free water (to make a total volume of 5 µL) were added. All chemicals used were from the TOPO™ cloning kit (Invitrogen). The solution was mixed gently and incubated at room temperature for 5 min. From this mix, 5 µL was pipetted into a vial of pre-prepared competent *E. coli* cells and

gently mixed. The cells were incubated on ice for 15 min and heat shocked in a water bath for 30 s at 42 °C. The cells were transferred to ice and 250 µL of SOC medium from the TOPO™ cloning kit was added. The tube was shaken horizontally at 200 rpm at 37 °C for 1 hr. 50 µL of cell suspension was pipetted and spread on LB agar supplemented with ampicillin (100 µg/mL). As a positive control, 1 µL of supplied pUC19 vector (Invitrogen) was used and no insert with plasmid was used as a negative control. Plates were incubated at 37 °C for 24 h. Six colonies from the plate were picked and re-streaked to ensure the purity of the samples. Glycerol stocks were prepared and stored at -80 °C. When needed, 10 µL of glycerol stock was cultured in 5 mL of LB supplement with ampicillin and incubated aerobically at 37 °C for 16-20 h. Plasmids were extracted and used as qPCR standards for qPCR experiments.

2.4.8 Validation of successful cloning of targets into E. coli

To confirm the successful cloning of targets into *E. coli*, cells were grown in LB medium for 16 h at 37 °C. Cells were centrifuged at 3,800 xg for 10 mins at 4 °C. Plasmids were extracted using the QIAprep Spin Miniprep plasmid kit (Qiagen) and stored at -20 °C. Samples were sent for sequencing at Eurofins Genomics UK (Eurofins, Luxembourg) using the Mix2seq sequencing kit (Eurofins). This involved pipetting 15 µL of plasmid with the forward probe provided in the kit and 15 µL with the reverse primer. Obtained sequences were aligned with the genomic sequence of the bacterial species using NCBI Blast (NCBI, Maryland, USA), along with the forward/reverse primers and the qPCR probe.

2.4.9 qPCR and multiplex qPCR

Each species had its own qPCR reaction with specific primers and probes. Each reaction mixture contained 300 nM of forward and reverse primer, 150 nM of probe, 12.5 µL of 2x Premix ExTaq mix (Takara, Shiga, Japan), 2 mM Rox (Takara) and nuclease-free water (Thermo Fisher) making a total volume per well of 23 µL. Mixtures were pipetted into 96 well qPCR plates (Eurogentecs, Seriang, Belgium). 1 µL of DNA sample was added to each well, with plasmid standards added for positive controls and nuclease-free water (Thermo Fisher) for negative control wells. All samples were tested in triplicate. The plate was sealed tightly using 96 well plate micro seals (BioRad) and loaded onto the qPCR system. The running protocol for all species consisted of the steps detailed in Table 2.4.

Table 2.4 Reaction steps for the qPCR experiments using the QuantStudio qPCR machine for all species.

| Step | Temperature (°C) | Time (s) | Number of cycles |
|-----------------------------|------------------|----------|------------------|
| Initial denaturation | 95 | 30 | 1 |
| Denaturation | 95 | 5 | 40 |
| Annealing | 60 | 30 | 40 |

After the experiment has finished, all samples were stored at 4 °C until analysed. Amplified products were run on a gel (Section 2.4.1) to check for correct amplification results and were analysed using the Thermo Fisher Connect Software (Thermo Fisher). This was also done for cloned targets from *E. coli*, to ensure the product was at the size expected.

2.5 Flow cytometry for live and dead analysis

Flow cytometry was used to quantify how much of the biofilm and planktonic culture in the reactors was viable. This was important in determining the “health” of the bacterial system. Biofilms were scraped off hydroxyapatite coupons (Biosurface technology, Bozeman, USA) and suspended in filter-sterilised PBS (Thermo Fisher). Cells were centrifuged at 12,000 xg in a microcentrifuge at 4 °C and resuspended in 1mL of PBS (Thermo Fisher). Serial dilutions were made of samples, so that the cell concentration was between 1×10^{-3} and 1×10^{-4} cells mL⁻¹. This was to prevent cell aggregates from passing by the laser undetected. Staining mixtures were made using 35 µL of SYTO 9 dye (1.67 mM) /Propidium Iodide (1.67 mM (compound A) and 35 µL of SYTO 9 (1.67 mM)/ Propidium iodide (18.3 mM) (component B). Compounds A and B were used from the Thermo Fisher BacLight™ live dead staining kit (Thermo Fisher). From this mixture, 0.6 µL of combined reagent was added to each sample and mix thoroughly with a pipette. Plates were incubated in the dark for 15 min. Samples were analysed on the Attune NxT flow cytometer following the manufacturer’s instructions. All samples were gated to determine the number of live and dead cells (Figure 2.1) BL1-H representing green fluorescence and live cells was plotted against BL3-H, representing dead cells. Samples containing PBS and dye, as well as samples containing dead cells, were used as controls to determine dead cells and residual cells. Gate settings were applied across all samples to ensure no bias in gating occurred.

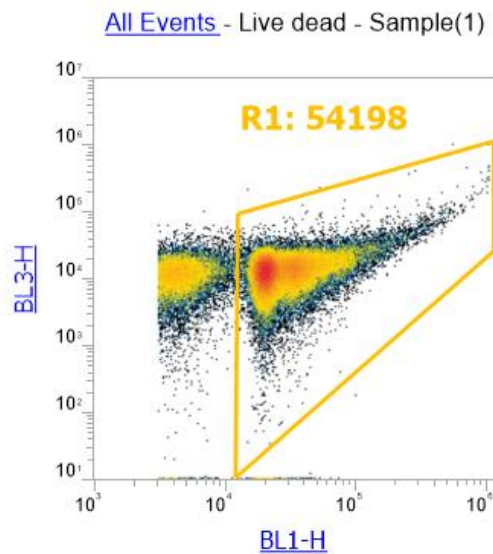


Figure 2.1 Gating using the NxT Attune flow cytometer was used to differentiate live cells (represented by BL1-H) and dead cells (represented by BL3-H). Samples containing PBS and dye, as well as dead cells, were used as controls to differentiate live from dead and machine remnants. All gate settings were kept constant across samples.

2.6 Microscopy

2.6.1 Gram staining

Gram staining and microscopy of samples were conducted to assess the potential contamination of samples and bacterial stocks. A 5 μ l of the cell sample of interest was pipetted onto a microscope slide. The bacteria were heat-fixed to the slide using a Bunsen burner. Filtered crystal violet (0.5 %) (Thermo Fisher) was applied to the microscope slide and left for 30 s. Excess crystal violet was washed off the slide using distilled water. Filtered Lugol's iodine (0.5 %) (Thermo Fisher) was pipetted onto the slide and left for 30 s, before 70% ethanol (Sigma) was gently sprayed onto the slide to de-stain and the slide was quickly washed in distilled water. The microscope slide was counter-stained using filtered safranin (0.5 %) (Thermo Fisher) and left for 2 min to stain. Excess safranin was washed off the slide, which was blot dried, assisted by a Bunsen flame. Samples were viewed using the Leica DM750 light microscope with a 100x objective, bright field setting, with a small drop of immersion oil placed on the sample. Images were recorded using Lumenera Infinity Analyze 3 (Lumenera, Ottawa, Canada) software.

2.6.2 Fluorescence *in situ* hybridization (FISH)

Fluorescent in situ hybridization (FISH) was used to identify each species in a mixed species biofilm and collect spatial information on the biofilm. Biofilms grown on hydroxyapatite coupons were washed gently with PBS (Thermo Fisher) to remove excess medium and planktonic cells. 1 mL of fixation buffer consisting of 4% paraformaldehyde in PBS, (Sigma Aldrich) was pipetted into each well and the biofilms were left to fix for 2 h at 4 °C. The biofilms were washed in PBS and 1 mL of dehydration buffer (50% ethanol in PBS) was added, and these were stored at -20 °C for 2 h. The biofilms were washed in PBS and incubated in 1mL lysozyme solution (1 mg/mL) (Thermo Fisher) for 15 min at 37 °C. Biofilms were again washed in PBS and hybridisation buffer was added (0.9 M NaCl, 20 mM Tris- HCl at pH 7.2, 0.01% SDS, 25% formamide) (chemicals sourced from Sigma Aldrich) containing 250 ng of the appropriate DNA probe (Table 2.5). The biofilms were protected from light by covering them with aluminium foil and were incubated for 3 h at 46 °C. After incubation, biofilms were washed with a wash buffer (10 mM Tris- HCl at pH 9.0, 1 mM EDTA) (chemicals sourced from Sigma Aldrich) and incubated in this buffer at 55 °C for 10 min. This step was repeated three times. All biofilms were kept in the dark until imaged. Images were taken using either the Olympus BX60 fluorescence microscope or the Zeiss 880 confocal microscope. All probes used in FISH experiments were listed in Table 2.5. Excitation intensity and any post-processing using Zen Black software (Zeiss, Jena, Germany) were recorded within the software for an accurate depiction of the signal received.

Alexa probes were selected using the Thermo Fisher Spectraviewer (Thermo Fisher), based on having as little overlap of emission/excitation as possible. Spectral fingerprints were generated using the Zenblue software (Zeiss). For each species, the emission profile of individual pixels was taken from 6 areas of a FISH image and the average wavelength and intensity were saved. Mixed-culture images were spectrally unmixed using these fingerprints so that artificial fluorescence and bleed-through signals were minimised. For all experiments, both positive and negative controls were used. The negative control involved imaging a biofilm sample that had not been stained with a fluorescent probe. This helped identify false signals and autofluorescence. For the positive control, a universal EUB338 probe (Table 2.5) that binds to a conserved region of across bacterial phyla, was used. All permeabilisation steps were kept the same across both Gram + and Gram – species to reduce bias as signal was found to

be affected by the permeability step.

Table 2.5 All FISH probes used in this research project. Fluorophores were selected to minimise excitation overlap. The probe for *N. subflava* was designed using Snappene.

| Bacterial strain | Target | FISH Probe | Fluorophore | Reference |
|------------------------------------|-------------|--------------------------------------|-------------|---------------------------|
| <i>Streptococcus gordonii</i> DL1 | 16S rRNA V3 | CAC CCG TTC TTC TCT TAC A | Alexa 594 | (Thurnheer et al., 2001) |
| <i>Streptococcus mutans</i> UA159 | 16S rRNA V4 | ACT CCA GAC TTT CCT GAC | Alexa 488 | (Thurnheer et al., 2001) |
| <i>Actinomyces oris</i> MG1 | 16S rRNA V1 | CGG TTA TCC AGA AGA AGG G | Alexa 555 | (Thurnheer et al., 2004a) |
| <i>Neisseria subflava</i> DSM17610 | 16S rRNA V8 | AGT CCG GAT TGC ACT CTG CAA CTC G | Alexa 405 | Designed in this research |
| <i>Veillonella parvula</i> DSM2008 | 16S rRNA V3 | CTA ACT GTT CGC AAG AAG GC | Alexa 647 | (Sunde et al., 2003) |
| Universal | 16S rRNA | GCT GCC TCC CGT AGG AGT | Alexa 405 | (Amann et al., 1990) |

2.6.3 Live dead staining for imaging of biofilms

Live dead staining was used to assess the viability of the biofilm through microscopy. Biofilms were scraped off hydroxyapatite coupons (Biosurface technology, Bozeman, USA) and suspended in PBS (Thermo Fisher). Cells were centrifuged at 3,800 xg at 4°C and resuspended in 1mL of PBS (Thermo Fisher). Cells were stained according to the steps detailed in Section 2.5, were. Plates were incubated in the dark for 15 min. Biofilms were imaged using the Olympus BX60 fluorescence microscope using excitation/emission wavelengths of 480/500 (SYTO9) and 490/635 (PI). For all samples, multiple images were taken to get a better representation of the health of the overall biofilm.

2.7 CDC reactor invasion experiments

2.7.1 Reactor system setup

The invasion experiments were all conducted using CDC reactors (Biosurface Technologies, US). These were selected based on the ability to control important variables in the system, including flow rate, temperature and stirring speed. The vessels allowed for sufficient sampling opportunities of biofilms growing on hydroxyapatite disks, and planktonic culture. Several practice runs were conducted to assess the ability to maintain a sterile system and to practice sampling from the system. The reactors were always run in triplicate, with each reactor supplied with AFMC from its own carboy. A shared waste carboy was connected to all 3 reactors. A schematic of the reactor setup can be seen in Figure 2.2.

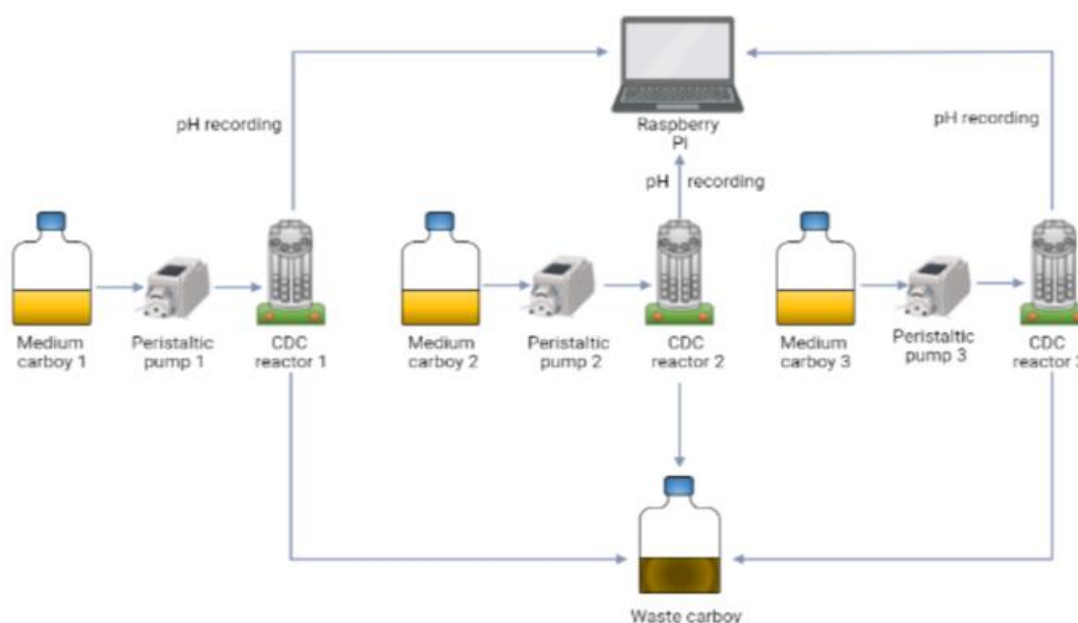


Figure 2.2 Schematic of CDC reactor setup. Each reactor, kept on a hot plate to maintain temperature, had its own medium carboy, containing 6 L of AFMC, fed at a flow rate of 0.4 mL min^{-1} . One port per vessel contained the pH probe, which continuously recorded the pH. The reactors were connected to a 20 L waste carboy. The flow of medium followed the arrows in the diagram, as did the flow of data from pH probes to the computer system and Raspberry Pi.

The CDC reactors contained 7 polypropylene rods per reactor (Biosurface Technologies), with each rod holding 3 hydroxyapatite coupons. An autoclavable pH probe was inserted into the eighth port, allowing for continuous pH readings to be taken. The pH probes were connected

to a Raspberry PI using a BNC cable (RS components, London, UK) and a tentacle device. All data logged on the Raspberry PI was processed through Atlas IoT software (Atlas, NY, USA).

Each CDC reactor was connected by 1 m of platinum-cured silicone tubing (Watson Marlow, Falmouth, UK) to a 10 L autoclavable carboy containing AFMC. A peristaltic pump was used to feed AFMC medium from a 10 L carboy into the reactor. An outflow tube connected each reactor to a shared 20 L waste carboy. The weir maintained the volume in the reactor at 350 mL. A sampling tube was connected to the top of the vessel which was connected to an air filter. All feed carboys, pumps and reactors were kept at the same height to prevent variable effects on the flow rate of AFMC (Figure 2.3).



Figure 2.3 Setup of the CDC reactors. Each CDC reactor, positioned on top of a magnetic stirrer hot plate, was connected to its own carboy containing 6 L of AFMC medium and fed using a peristaltic pump. All reactors were run over the course of 9 days.

2.7.2 Invasion experiments

All reactor components and hydroxyapatite coupons were washed with Cleanline bleach (Cleanline, Coventry, UK) and rinsed with distilled water prior to assembly. Hydroxyapatite coupons were inserted into the polypropylene rods and reactors filled with 300 mL of distilled water before autoclaving. All pH probes were calibrated using the appropriate pH 4, 7 and 10

solutions (Cole-Parmer, Illinois, USA) and one probe per reactor was inserted in the place of one of the eight rods. All tubing connected to the reactors and carboys was clamped and ends wrapped in aluminium foil. Carboys containing a magnetic stir bar were filled with 5.5 L of distilled water and autoclaved, along with tubing and reactors, at 121 °C for 15 min.

After the completion of the autoclave cycle, sterile media components with a total volume of 500 mL, were added to the carboys and mixed on a magnetic stirrer/hot plate for 3 h. This helped to cool the medium. The carboys were connected to the reactors and the autoclaved distilled water from within the reactors poured off via the weir to maintain sterility. 300 mL of medium was pumped into the reactors using the peristaltic pumps, ready for inoculation.

2.7.2 Inoculation strategy

All species were seeded with the same number of cells, 3.85×10^9 per CDC reactor. Glycerol stocks were centrifuged at 3,800 xg at 4 °C and resuspended in 2 mL of AFMC. These were pipetted into the CDC reactor through a coupon holder port under aseptic conditions. *A. oris* was seeded on day 1, with *S. gordonii*, *N. subflava* and *V. parvula* seeded on day 2 *S. mutans* was inoculated on day 3. The flow rate of 0.4 mL min^{-1} was set to reflect the flow rate of saliva *in vivo* (Iorgulescu, 2009). The bulk was observed for potential contamination on the day after each inoculation using a light microscope. This was done before the invasion experiments were continued. The reactors were run for 9 days and maintained at 37 °C using hot plates and thermal insulation wrapping.

2.7.3 Sampling from invasion experiments

An autoclaved, silicone sample inlet tube (Watson Marlow) was inserted into a sampling port of the reactor. The sterility of this was maintained by sampling in a biological safety cabinet, spraying with 70% ethanol and covering tube ends with autoclaved foil after sampling. Feeding of the reactors from the carboys was paused during sampling and tubes were clamped. 10 mL of culture medium was withdrawn using a syringe and ejected into a 15 mL Falcon tube. 5 mL of this culture was filtered using a 0.2 µm filter (Merck, Darmstadt, SA) into a separate Falcon tube so that the sterile medium could be used for substrate analysis and the rest used for qPCR analysis. The filtrate and remaining culture were stored at -20 °C until analysed. On days 3, 5, 7 and 10, hydroxyapatite coupons were extracted from the rods (Figure 2.4) and placed into 12 well microtiter plates. The coupons were covered in either 50% ethanol (for FISH) or

PBS (for qPCR analysis). Rods were placed back into the reactors. All sampling was done in sterile conditions, in a biological safety cabinet. Ports were sprayed with 70% ethanol (Thermo Fisher) and covered with autoclaved aluminium foil. Tubes were disconnected (during sampling of hydroxyapatite coupons) as far away from the reactor ports as possible, towards the waste carboy.

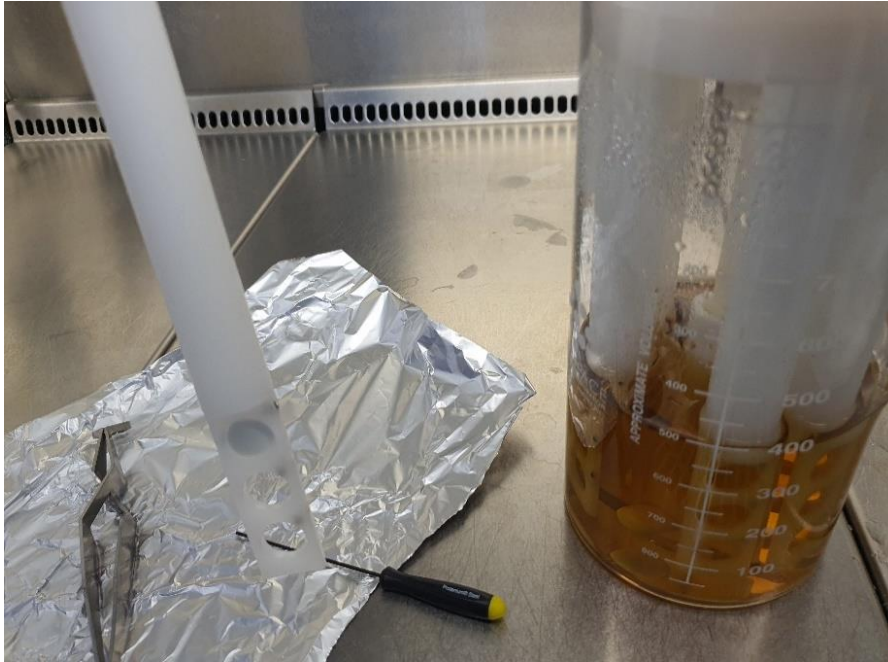


Figure 2.4 Sampling of coupons in the laminar flow hood. One coupon per analytical method was taken and placed in a microtiter plate, which was stored at -20 °C. Care was taken with sampling to minimize the risk of contamination.

2.8 *In silico* modelling of the synthetic community

The mathematical models in this research aimed to describe the behaviour of the synthetic community, including the growth of each species over time and the pH change of the medium. The development of the altered FMC medium (Section 2.3.2) was supported and validated by FBA, described in Section 2.8.1. To describe the phenomena occurring in the continuous stirred tank reactor (CSTR) and on the biofilm coupons, two different modelling approaches were used. A continuous 0-D mathematical model, based on ordinary differential equations (ODEs), was used to simulate the reactor bulk. A 2-D Individual-based Model (IbM) was used to model the biofilms formed on the coupons (Figure 2.5).

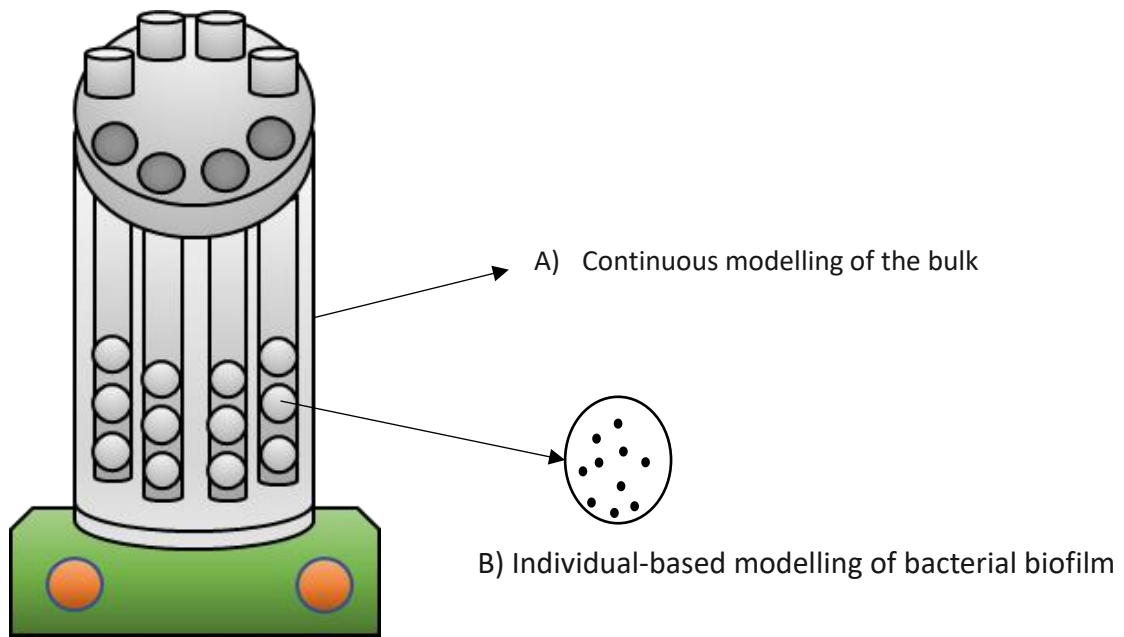


Figure 2.5 Two mathematical modelling approaches were used in this research to describe the behaviour of the synthetic community. A) The continuous 0-D model was used to simulate the planktonic bulk. B) The 2-D IBM was used to simulate the synthetic community bacterial biofilm.

2.8.1 Flux balance analysis

Flux balance analysis (FBA) was used to simulate the metabolism of the bacterial species through genome-scale reconstructions. This was used to help assist in the development and validation of AFMC (Appendix A), to support the growth of *A. oris* and *V. parvula*. KBase (The Departments of Energy Systems Biology Knowledgebase; <https://www.kbase.us>) was used for constructing draft metabolic models, using genomes for each species obtained from the NCBI database (<https://www.ncbi.nlm.nih.gov/>) and genome annotations (Table 2.1). Components of FMC (Terleckyj et al., 1975), proven experimentally to support the growth of *S. gordonii*, *S. mutans*, and *N. subflava*, were uploaded into KBase. Chemicals were added to the uploaded medium once at a time (in the order listed in Appendix A) and FBA was run to determine if biomass was generated from the simulations. Once FBA was completed for each species, the objective value was used to determine whether growth on AFMC was possible.

2.8.2 Stoichiometry considered for the bacterial species

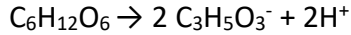
A simplified reaction for the catabolic and anabolic pathways for each of the bacterial species was proposed (eq 1a-1c). In dental biofilms, *S. gordonii*, *S. mutans*, and *A. oris* are mainly facultative anaerobes that consume glucose (carbon source and electron donor) in anaerobic conditions and produce lactic acid as the main product (Dame-Teixeira *et al.*, 2016; Lemos *et al.*, 2019; Loo *et al.*, 2000). *V. parvula* is an obligate anaerobe that consumes lactic acid (carbon source and electron donor), producing acetate and propionate (Ilie *et al.*, 2012; Seeliger *et al.*, 2002). *N. subflava* is an aerobic species that consumes glucose and has oxygen as the primary electron donor, producing acetate and formate (Bradshaw *et al.*, 1996a). This species was considered in the synthetic community as a scavenger for oxygen to protect the strict anaerobes, as previously reported for chemostat and biofilm experiments with dental biofilm species (Bradshaw *et al.*, 1996a). To respect *N. subflava* known stoichiometry (eq 1b) and to replicate the experimental micro-aeration conditions *in vitro*, in this research, a constant concentration of 1 mg L⁻¹ of oxygen inside the biofilm/reactor was considered. *N. subflava* as glucose sink and the oxygen consumption was not modelled.

For the anabolism, I used the general biomass formula CH_{1.8}O_{0.5}N_{0.2}, proposed by Roels (Roels, 1980.), using glucose and lactic acid, respectively as the carbon source and ammonia as the nitrogen source. The anabolic reactions were written with respect to 1 C-mole of biomass. The energy required for performing the anabolism was derived from catabolism, during which substrates were converted into lower-energy products, producing ATP.

The stoichiometric equations for each species were presented in equations 1 a-c: the catabolic reactions correspond to those reported by Ilie (Ilie *et al.*, 2012) and Seeliger (Seeliger *et al.*, 2002).

***S. gordonii*, *S. mutans* and *A. oris* – anaerobic glycolysis** (1a)

Catabolism:



Anabolism:

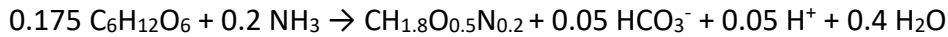


***N. subflava*– aerobic glucose respiration** (1b)

Catabolism:

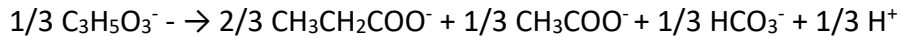


Anabolism:



***V. parvula* – anaerobic lactic acid fermentation** (1c)

Catabolism:



Anabolism:



The maximum theoretic growth yield (Y_{XS}) estimation accounted for the number of times the catabolic reaction needed to run to generate enough energy for biomass formation. It was the ratio between the free energy supplied by the catabolic pathway ΔG_{cat} , the energy that was required for the anabolic pathway ΔG_{ana} , and the energy that was dissipated by the bacterial species for maintenance ΔG_{dis} (eq. 2), as proposed by Heijnen and Kleerebezem (2010):

$$Y_{XS} = \frac{\Delta G_{cat}}{\Delta G_{ana} + \Delta G_{dis}} \quad (2)$$

The Gibbs free energy was computed for each catabolic and anabolic reaction using eq. 3, with the values for the chemical species free energy of formation listed in Appendix B.

$$\Delta G_r = \Delta G_r^0 + RT \frac{\prod_n [\text{Prod}]}{\prod_m [\text{React}]} \quad (3)$$

where: ΔG_r^0 (kJ mol⁻¹) represented the free energy of reaction in standard conditions (1 atm and 20 °C); [Prod] (mol L⁻¹), the concentration of the reaction products; [React] (mol L⁻¹), the concentration of reactants; R (kJ mol⁻¹·K⁻¹), the ideal gas constant; and T (K) the temperature. In eq. 2, the value used for the dissipation energy value was 200 kJ C·mol⁻¹, similar to the value used for glucose fermenters in anaerobic digestion studies (Buckel, 2021).

The inverse of the growth yield was used to derive the overall growth reaction, according to eq 4.

$$OVG = Ana + f_{cat} \cdot Cat \quad (4)$$

where *OVG*, *Ana* and *Cat* were the sets of stoichiometric coefficients corresponding to the overall growth reaction, anabolic and catabolic reactions, respectively (eq 1a-1c). f_{cat} was defined as proposed by Heijnen and Kleerebezem (2010):

$$f_{cat} = -\frac{1}{Y_{XS}} + \lambda_{ed} \quad (5)$$

where λ_{ED} was the stoichiometric coefficient of the electron donor. The stoichiometry for the synthetic community (eq 1a-c) is included in matrix form in Appendix C.

2.8.3 Growth kinetics for each bacterial species

The bacterial growth and substrate consumption was modelled with a mixed thermodynamic–empirical Monod approach, previously described in Gogulancea *et al.*, (2019). The growth kinetics were described by a traditional Monod calculation, and the bacterial yield was estimated using a thermodynamic approach (Section 2.8.2). Here, Monod kinetics were used

to model the growth kinetics of the bacteria, considering the growth based on only one limiting substrate. In eq.6, the growth rate (μ) for bacterial species was computed.

$$\mu = \mu_{\max} \frac{[S]}{K_s + [S]} - m \quad (6)$$

where, the growth rate (μ , h^{-1}) of each bacterial species considered the maximum specific growth rate of that microorganism (μ_{\max} , h^{-1}) on the limiting carbon source (S , mmol L^{-1}), the Monod substrate affinity constant (K_s , mmol L^{-1}) and the maintenance term (m , h^{-1}). The Monod substrate affinity constant (K_s , mmol L^{-1}) was equal to the substrate concentration at which $\mu = \frac{1}{2} \mu_{\max}$. The kinetic parameters were unique for each species and were measured experimentally. They were detailed for each species in Table 2.6. K_s was presented both in (mmol L^{-1}) and ($\text{g}\cdot\text{L}^{-1}$) as the concentrations of substrates were measured experimentally in ($\text{g}\cdot\text{L}^{-1}$) and the model results will be reported as such.

The maintenance term included in the bacterial cell mass balance in the lbM, considered the Gibbs free energy of dissociation and catabolism, defined by eq. 7:

$$m = \frac{m_G}{\Delta G_{\text{cat}}} \quad (7)$$

Where m_G was the maintenance energy, considered constant for all species and equal to 4.5 $\text{kJ C}\cdot\text{mol}^{-1}\text{h}^{-1}$ (Heijnen & Kleerebezem, 2010).

Table 2.6. The kinetic parameter for each bacterial species used in mathematical models were collected experimentally. *S. gordonii* had the highest maximum specific growth rate (μ_{\max}) of 0.492 h^{-1} , whilst *A. oris* had the lowest, 0.227 h^{-1} . *S. mutans* and *N. subflava* had the lowest substrate affinity constant, K_s (1.0 gL^{-1}).

| Bacterial species | Kinetic parameter | | | Carbon source |
|-------------------------------|------------------------------|----------------------------|------------------------|---------------|
| | $\mu_{\max} (\text{h}^{-1})$ | $K_s (\text{mmol L}^{-1})$ | $K_s (\text{gL}^{-1})$ | |
| <i>Streptococcus gordonii</i> | 0.492 | 6.60 | 1.88 | Glucose |
| <i>Streptococcus mutans</i> | 0.406 | 5.55 | 1.00 | Glucose |
| <i>Actinomyces oris</i> | 0.227 | 7.78 | 1.40 | Glucose |
| <i>Neisseria subflava</i> | 0.261 | 5.55 | 1.00 | Glucose |
| <i>Veillonella parvula</i> | 0.246 | 26.90 | 2.42 | Lactic acid |

The use of Monod kinetics assumed that each species only utilised one limiting substrate at a time, whereas species have complex metabolic pathways (Section 1.2.3) and can often use more than one carbon source to generate biomass. The growth rates in Table 2.6 were also derived from single-species experiments, therefore the use of Monod kinetics to model the mixed-species synthetic community with these parameters was a simplification of the more complex multispecies synthetic community. No explicit decay was considered in the modelling of the suspended culture using the 0-D continuous model. Here, the assumption was that the dead cells were accounted for and removed by the outlet flow at a flow rate of 0.4 mL min^{-1} .

I modelled cell decay in the biofilm using the lbM. If the maintenance term became larger than the growth term, I assumed that the bacteria entered a decay stage. The decay was modelled using linear kinetics, presented in eq (8):

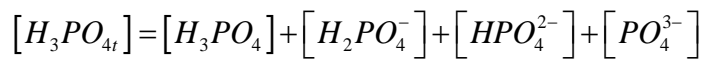
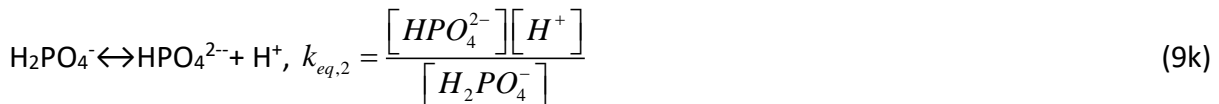
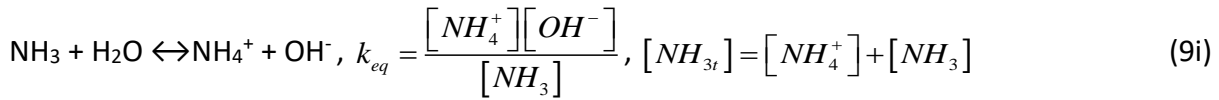
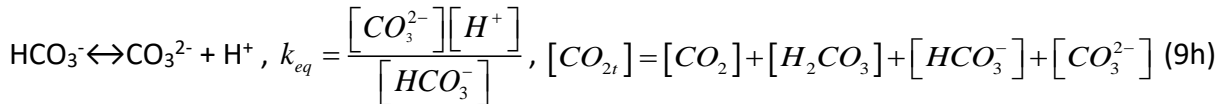
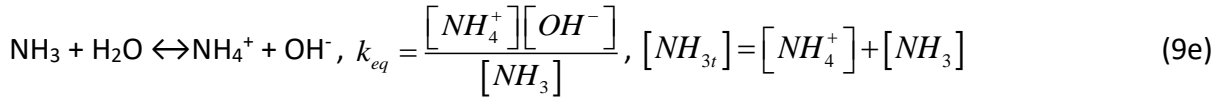
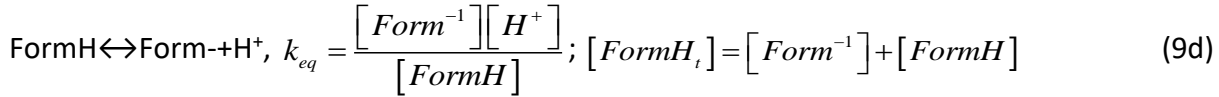
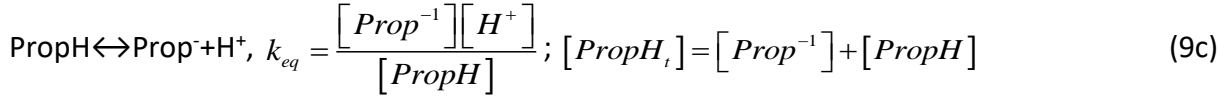
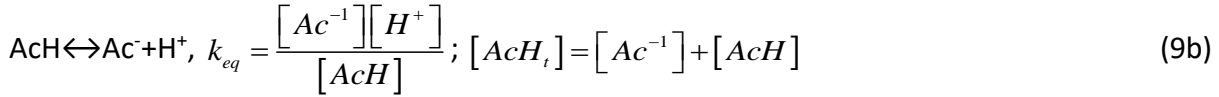
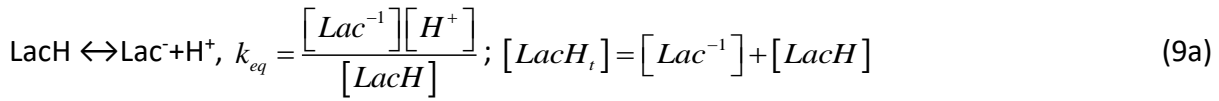
$$\mu = -k_d \quad (8)$$

where k_d was the decay coefficient, assumed to value of $4.2 \cdot 10^{-3} \text{ h}^{-1}$, similar to Head *et al.*, (Head *et al.*, 2014a).

2.8.4 pH influence on growth

The variation in pH is known to be one of the most important parameters affecting bacteria, including their growth. The pH affects enzyme activity within bacteria and the structural integrity of cells. The protonation of acids can trigger cytoplasmic acidification and collapse proton gradients, leading to cell death (Yin *et al.*, 2019). In the model, substrates were considered in one dissociated form *i.e.*, either lactic acid or lactate, not both, assuming bacteria could uptake only one form of a chemical. The concentrations and the availability of these chemical forms were affected by diffusion, mass transfer and the biological processes of the bacteria. The speciation of lactic acid affects *V. parvula* growth, as it can only utilize lactate for growth (Ilie *et al.*, 2012). Glucose, the primary carbon source for four of the species, does not undergo dissociation and therefore this did not have a direct impact on their growth. The energy balance for the catabolic and anabolic pathways for these species was, however, influenced by pH, which influenced the computed values of the growth yields.

I modelled the pH variation explicitly, considering the deprotonation and hydration reactions that occurred in the main chemical components of the system (organic acids, CO₂ and ammonia). The system was buffered using a phosphate buffer in the continuous model, to mimic the experimental system. Due to the computational burden, I used a carbonate buffer in the IbM, to minimize the number of soluble species and mass balance equations that were solved. The deprotonations were modelled as equilibrium equations. Both the deprotonation and hydration reactions were assumed to occur instantaneously (by comparison with the timescale of bacterial growth and diffusion reactions). The pH was computed at every time step by solving the mass and charge balances (Volcke *et al.*, 2005). The equations for the pH calculations were detailed below in eq 9 a-m:



I retrieved the equilibrium constant values from the literature, and these were listed in Appendix D. The concentration of all the species in the system of equations above was expressed as a function of the proton $[H^+]$ concentration and their respective equilibrium constant.

The solution was neutral (from the ionic standpoint), and the concentration of all negatively charged species was balanced by that of the positively charged species, as described in the charge balance equation (10):

$$[H^+] + [NH_4^+] = [Ac^-] + [Prop^-] + [Form^-] + [HCO_3^-] + [CO_3^{2-}] + [OH^-] \quad (10)$$

The concentrations of all species (function of proton concentration) can be replaced in the charge balance (equation 10) above. The equation was solved using the Newton method for non-linear equations and the pH was expressed using equation 11 below.

$$pH = -\log_{10} [H^+] \quad (11)$$

To consider the direct impact of pH on the bacterial species growth rate (Boisen *et al.*, 2021), I implemented a pH correction method to adjust the maximum specific growth rate of each species, as proposed by Rosso *et al.*, (1995), presented in eq 12.

$$\mu_{\max}(pH) = \mu_{\max,opt} \frac{(pH - pH_{\min})(pH - pH_{\max})}{(pH - pH_{\min})(pH - pH_{\max}) - (pH - pH_{opt})^2} \quad (12)$$

In eq. (8), I considered three different parameters: i) the pH at which μ_{\max} was optimal (pH_{opt}); ii) the pH above which no growth occurred (pH_{max}); and iii) the pH below which no growth occurred (pH_{min}). The pH boundaries were specific to each bacterial species, as species have different tolerances to acidic and alkaline conditions (Table 2.7). Although slightly lower than in other reports, the pH_{min} for *S. mutans* was proposed here based on the fact that this species can continue to grow in continuous cultures at pH values of 4.5–5.0, and it is known to continue to perform glycolysis and membrane proton transport at pH 2.5–3.0 (Baker *et al.*, 2017). Moreover, in studies with dental biofilm, the local pH fell regularly below 4.0 (Bradshaw

& Marsh, 1998) and *S. mutans* biofilm survived acid stress of pH 3.0 (Welin-Neilands & Svensäter, 2007).

Table 2.7 The boundaries for each of the bacteria species considered in the pH correction for species kinetic parameters. Each condition was specific to the species and now had a direct impact in bacteria kinetics within model simulations.

| Species | pH _{min} | pH _{opt} | pH _{max} | References |
|-------------------------------|-------------------|-------------------|-------------------|---|
| <i>Streptococcus gordonii</i> | 4.5 | 7.0 | 9.0 | (Castillo et al., 2000) |
| <i>Streptococcus mutans</i> | 4.0 | 6.0 | 9.0 | (Castillo et al., 2000; Bender et al., 1985) |
| <i>Actinomyces oris</i> | 5.3 | 7.0 | 9.0 | Proposed based on (Caous et al., 2013) |
| <i>Neisseria subflava</i> | 5.0 | 7.0 | 9.0 | Proposed based on (Tønjum & van Putten, 2017) |
| <i>Veillonella parvula</i> | 4.8 | 7.0 | 9.0 | Proposed based on (Head et al., 2017) |

2.8.5 Continuum stirred tank reactor (CSTR) model

The synthetic community growth in the suspended culture of the CDC was modelled as a 0-D continuous model. The continuous model allowed for the simulation of a homogenous mixed species system. It allowed for the comparison of the relative abundances in the liquid culture against those measured in the invasion experiments, whilst predicting substrate concentration/consumption, and pH in the bulk. The model assumed that the bulk was a homogenous mixture, at constant temperature of 37 °C.

The continuum model was comprised of 15 ordinary differential equations which represented the mass balances for the 10 chemical species included in the stoichiometry (Appendix B; Section 2.8.2 eq 1a-i) and the 5 bacterial species (eq. 13).

$$\frac{dS_i}{dt} = \sum \frac{1}{Y_{i,X_j S}} \mu_j X_j + \frac{1}{\tau} (S_{i,0} - S_i) \quad (13)$$

where S_i was the concentration of soluble species i (mol L^{-1}), $S_{i,0}$ was the inlet concentration to the bioreactor (mol L^{-1}), $Y_{i,X_j S}$ was the yield for the i -bacterial species growing on/producing the chemical species i (mol-X mol-S^{-1}), μ_j and X_j were the corresponding growth rate (h^{-1}) and concentration for bacterial species j (mol L^{-1}) and τ was the reactor residence time (h^{-1}).

$$\frac{dX_j}{dt} = \mu_j X_j + \frac{1}{\tau} (X_{j,0} - X_j) \quad (14)$$

where X_j was the concentration of bacterial species j (mol L^{-1}), $X_{j,0}$ was the inlet concentration of the bacterial species j (mol L^{-1} ; set to zero for all the species), μ_j was the growth rate (h^{-1}) of the species j and τ was the reactor residence time (h^{-1}).

For the continuous model, the synthetic community members were introduced in the simulation at the same times as in the inoculation procedure reported in Chapter 3. The order of inoculation was *A. oris* on day 1; *S. gordonii*, *N. subflava* and *V. parvula* on day 2; and *S. mutans* on day 3.

2.8.6 Implementation of the CSTR model

The 0-D continuum model was implemented in Matlab® and the system of 15 ordinary differential equations integrated with Runge Kutta numerical method (ode15s built in function). The code was added in Appendix E. The main file of the model was “MainStaggeredpH.m” which called all the subroutines. The model assembled the metabolic matrix of the selected species (through the function assemble.m) and read all simulation parameters (function ‘read_param.m’) from the Excel file “Repository.xlsx”. This file contained the kinetic parameters for the species, as well as the stoichiometry, thermodynamic parameters, and influent concentrations for the substrates.

For the continuous model, the synthetic community members were introduced in the simulation at the same times as in the inoculation procedure. This was *A. oris* on day 1; *S. gordonii*, *N. subflava* and *V. parvula* on day 2; and *S. mutans* on day 3. The continuous model outputted simulation results over 9 days. For all the soluble species' concentration and the biomass. The model computed and updated the pH values after every successful integration step. The results were plotted against the date from the *in vitro* experiments. For the bacterial species, the results were calculated as relative abundances, to be able to compare them with the data collected from the *in vitro* system, while for the substrates concentration and pH there was a direct comparison with the measured data.

2.8.7 Individual based model

The multispecies biofilm developed on the hydroxyapatite coupons in the CDC reactor was simulated with a 2-D individual based model (IbM). In the IbM, the bacterial cells were represented as discrete entities (particulate components of the model), while the chemical species involved in the biochemical reactions (Section 2.8.2 eq 1a-i) were soluble components which participated in diffusion-reaction processes, generating the field of concentration. The two-dimensional biofilm model was split in three subdomains (Figure 2.6). These were the biofilm itself growing at the bottom of the domain, the boundary layer, and the bulk liquid.

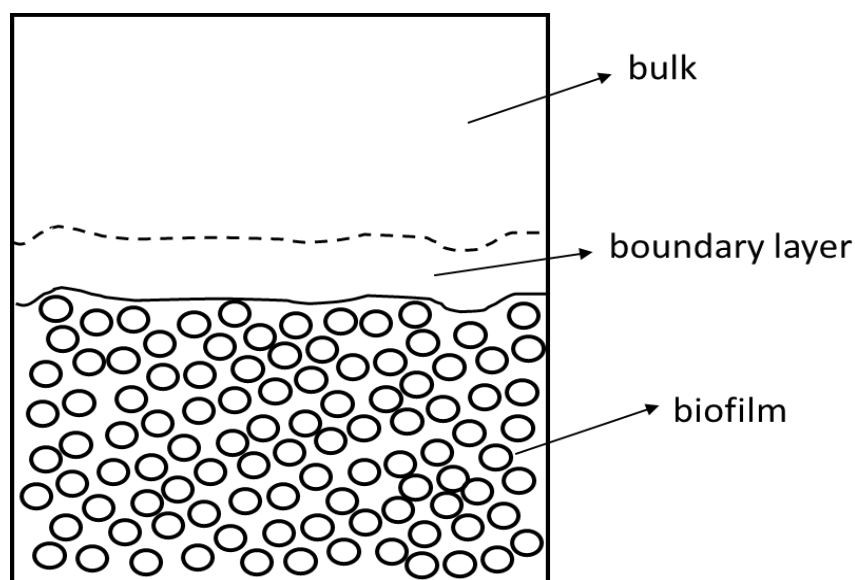


Figure 2.6. Schematic representation of the sub-domains included in the IbM. In the bulk and boundary layer sub-domains, there were only soluble components (i.e., glucose, lactic acid, acetate etc.), while in the biofilm sub-domains there was biomass (bacterial cell) and soluble components.

Bacterial cells were modelled as cylinders of constant height (1 μm), each bacterial agent having its own set of properties (radius, mass, set of kinetic parameters). The cells were placed in a 2-D computational domain, a square of 100 x 100 μm , where the bacterial biofilm was allowed to reach the maximum height of 80 μm . Bacterial cells above this height were removed from the computational domain, to replicate the detachment phenomena that occurred in the reactor biofilms. Each bacterial cell had its unique sets of spatial coordinates, specifying the position of its centre and its radius.

The bacterial cells had a maximum (division) radius of 2 μm , chosen to be in the same range reported by Head *et al.*, (2014). The initial seeding radius for all the cells was set at 90% of the division radius.

The lbM allowed for three possible behaviours of bacterial cells:

- a. Growth: if the growth requirement ($\mu_{max} \cdot \frac{S}{K_s + S}$) was higher than its maintenance requirement (m), the cell was allowed to grow, using the following mass balance equation

$$\frac{dX_j(x, y)}{dt} = \left(\mu_{max} \frac{S_i(x, y)}{K_s + S_i(x, y)} - m \right) X_j(x, y) \quad (15)$$

where μ_{max} (h^{-1}) was the maximum specific growth rate; K_s (mmol L^{-1}) was the substrate affinity constant; $S_{i(x,y)}$ was the limiting substrate concentration in the grid cell (x,y) ; m maintenance term calculated with eq 16; and $X_j(x, y)$ the concentration of biomass of species i in the grid cell (x,y) .

- b. Maintenance: if the growth requirement was equal to its maintenance requirement, the cell maintained its current mass

$$\frac{dX_i(x, y)}{dt} = 0 \quad (16)$$

- c. Decay: if the growth requirement was higher than the maintenance requirement, the cell entered the decay stage

$$\frac{dX_i(x, y)}{dt} = -k_d X_i(x, y) \quad (17)$$

where k_d was the decay coefficient, assumed to have the value of $4.2 \cdot 10^{-3} \text{ h}^{-1}$ similar to Head *et al.*, (2014).

As bacteria grew, they reached the maximum imposed radius and were divided into two individual cells, each containing between 45-55% of the initial parent cell mass. The cell mass was determined by a random number within the code. One of the daughter cells retained the position of the parent, while the other was placed adjacent to it, at a random angle. After each successful integration step, a division check was performed and the new numbers and positions of the bacterial cells were recorded. As cells may have overlapped following a division event, an overlap check was performed. Overlaps were resolved by pushing the existing neighbour cells until the maximum overlap between bacterial cells became lower than 10% (of their area). This process was traditionally called “shoving” and it was initially described by Kreft *et al.*, (Kreft *et al.*, 2001). During the decay stage, the cell shrunk and the biomass (with general formula $\text{CH}_{1.8}\text{O}_{0.5}\text{N}_{0.2}$) was transformed back into soluble components (the reverse of the anabolic reaction). When the radius of a bacterial cell became smaller than a threshold (10% of its radius following division), the cell was considered “dead” and removed from the biofilm.

In the biofilm sub-domain, it was assumed that the nutrients were transported only by diffusion, which was modelled using Fick’s second law. The mass balance equation for the solute i in the grid cell of the coordinates (x,y) was, therefore:

$$\frac{\partial S_i}{\partial t} = D_{eff} \left(\frac{\partial^2 S_i}{\partial x^2} + \frac{\partial^2 S_i}{\partial y^2} \right) + \sum r_i(x, y) \quad (18)$$

where S_i was the molar concentration of chemical species i , D_{eff} the effective diffusion of chemical species i , and $\sum r_i(x, y)$ was the net reaction term for the chemical species i in the grid cell (x,y) . The net reaction term represented the sum of the rates of all the processes in

which the soluble component i was involved, weighted by the yield factors corresponding to the particular bacterial cell type present in the grid cell (x,y) .

Table 2.8 Diffusion coefficients for the soluble components considered in the lbM. Nutrients were transported only by diffusion in the biofilm sub-domain, modelled using Fick's law.

| Soluble component | Diffusion coefficient (m ² h ⁻¹) | Reference |
|---------------------------|---|---------------------|
| Glucose | 3.06 · 10 ⁻⁶ | (Ilie et al., 2012) |
| Acetic acid/Acetate | 4.97 · 10 ⁻⁶ | |
| Lactic acid/Lactate | 4.72 · 10 ⁻⁶ | |
| Formic acid/ Formate | 6.62 · 10 ⁻⁶ | |
| Propionic acid/Propionate | 4.97 · 10 ⁻⁶ | |
| Ammonia | 5.90 · 10 ⁻⁶ | (Yaws, 2009) |
| Oxygen | 9.58 · 10 ⁻⁶ | |
| Carbon dioxide | 5.40 · 10 ⁻⁶ | |

In the biofilm subdomain, the diffusion coefficients of the solutes were affected by the presence of cells (which had a higher density than the bulk). Their values were adjusted with a diffusion factor proposed by Fan *et al.*, 1990 (Fan et al., 1989). This was further used in the lbM as proposed by Ofiteru *et al.*, 2014 (Ofițeru et al., 2014):

$$d_f(x, y) = 1 - \frac{0.43 \cdot X(x, y)^{0.92}}{11.19 + 0.27 \cdot X(x, y)^{0.99}} \quad (19)$$

On top of the biofilm, there was a 20 μm boundary layer, in which the entire diffusional resistance of the bulk liquid was concentrated. No chemical reactions occurred in the boundary layer, and the diffusion coefficients for the soluble species were the same as those reported for water, presented in Table 2.8. Therefore, the mass balance for the soluble components in these two sub-domains was also described by eq 18, but without the reaction

term. In the boundary layer, the diffusion factors $d_f(x, y)$ were equal to 1 (as $X(x, y) = 0$) and therefore the diffusion coefficients had the same value as reported in water.

In the bulk sub-domain, the diffusion coefficient was assumed to be several orders of magnitude (10^3) higher than in the boundary layer and the biofilm. This was to describe the perfectly mixed environment on the top of the biofilm, which had the same concentrations as the bulk liquid in the reactor. This assumption was previously used by Ofiteru *et al.*, 2014 (Ofiteru *et al.*, 2014). Modelling the bulk liquid of the reactor as perfectly mixed was in line with the assumption that the bulk was perfectly mixed (as CSTR) during the *in vitro* experiments.

The model assumed that the biofilm was placed inside a continuous reactor, whose behaviour was solely influenced by the biofilm, as presented originally in Picioreanu *et al.*, (2004)

The mass balance equations for the reactor were:

$$\frac{dS}{dt} = \frac{\sum_{i=1}^n r_{liq,i}}{V_{reactor}} + \frac{S_0 - S}{\tau} \quad (20)$$

where $\sum_{i=1}^n r_{liq,i}$ was the sum of all the reaction rates at which the soluble species were consumed or produced by each bacterial agent (i) located in the biofilm subdomain. The biofilm volume represented a small fraction of the bulk liquid volume (i.e. its characteristic length was assumed to be 100 times larger than a biofilm grid cell).

2.8.8 lbM implementation and solving algorithm

Individual based model (lbM) simulations were implemented and solved in Matlab® (Mathworks, Ca, USA) where it solved the mass balance equations for the soluble species and bacterial cells sequentially, as presented in Figure 2.7.

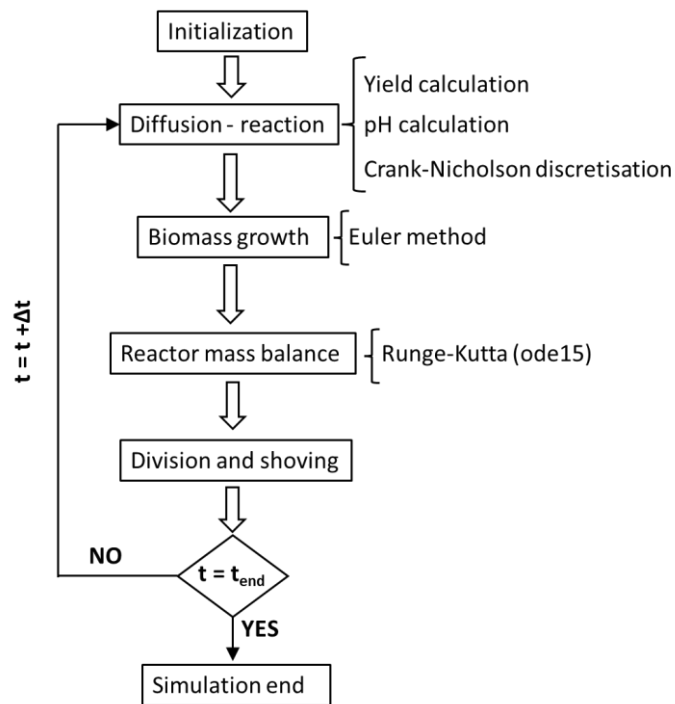


Figure 2.7 Workflow for solving the algorithm for the lbM and the interactions between the model's modules. Solving began with initialization (building the stoichiometric matrix, defining all soluble components concentrations, and bacterial cell placements at the bottom of the computational domain). This was followed by resolving the diffusion-reactions, biomass growth, mass balance for the reaction, division and decay and the mechanical interactions, including shoving.

The domain was first seeded with 46 bacterial cells, such that the entire first row of the computational domain was filled with bacterial cells, placed at an equal distance from each other and from the walls of the computational domain. The five species were seeded with the same initial number of agents, while the positions of the agents were randomly assigned. To solve the diffusion reaction equations for the soluble species, domain discretization was performed as follows: first, the height of the domain was computed, by adding the height of the boundary layer on top of the height of the biofilm. The computational domain was divided into grid cells, the length and height of the maximum division diameter for the bacterial cells

(2 μm). The pH was computed in every grid cell, using the current soluble species concentrations. The reaction rates for each soluble species were computed using the concentration of bacterial agents in each computational grid and the estimated growth yields.

To allow the decoupling of the system of equations for the bacterial and soluble species, I assumed that the diffusional processes were much faster than the biological processes (the concentration of the bacterial species was considered constant, while solving the mass balances for the chemical species) (Kreft et al., 2001). The partial differential equation system (PDE) described by equation 18, was transformed into a system of algebraic equations using the Crank-Nicholson discretisation method.

The boundary conditions were as follows:

- Dirichlet boundary condition at the top of the computational domain:
 $0 < x < \text{max_x}; y = \text{max_height}, S = S_0$
- The vertical domain walls have periodic boundary conditions
 $0 < y < \text{max_height}, x=0, x=\text{max_x}, S_i=S_j$
- No flow condition at the bottom of the computational domain
 $0 < x < \text{max_x}; y = 0, dS/dt = 0;$

The resulting system was solved iteratively using matrix left division and lower-upper (LU) decomposition. The time step for the diffusion calculations was set at 10^{-6} h. Following convergence, the soluble species concentrations were updated in every grid cell. The mass balance equations for the bacterial cells were solved: the system of ordinary differential equations (eq. 15) was solved using the backward Euler method and a time step of 15 min. The boundary conditions were re-calculated, using the reactor coupling to compute the top boundary conditions for the next time step. The last steps in the algorithm were the division checks, followed by resolving the overlap. After solving the reactor balance, the mass and radius of each bacterial agent were updated and the division and overlap check was performed. These steps were repeated until the total simulated time reached 9 days. The lbM simulations were initially run in triplicates, to verify the random division positioning and overlap resolve did not significantly impact the outcomes of the model. The average simulation time on a computer with 11th generation Intel® Core™ i7 @2.30GHz processor and

16GB RAM was 48h. The Matlab® files and a description of the main functions were included in Appendix E.

2.9 Statistical analysis

All experiments involved in Chapters 3 and 4 were repeated as biological triplicates containing technical triplicates. Plotted points were the average, with error bars representing the standard deviation from the mean. For all image analyses, including FISH and live-dead imaging, a minimum of three images were taken from the sample. Statistical analysis was completed using Prism (Graphpad, USA) to determine significant differences between the means of the two groups. T-tests were used to assess significant differences ($p < 0.05$) between flow cytometer cell viability. One-way analysis of variance (ANOVA) with Tukey post hoc tests (P value lower than 0.05) was used to observe differences between different species abundances from qPCR data. This was using Prism 9 statistical software (GraphPad, Inc., San Diego, CA, USA), with a significance of 5% used.

Chapter 3. Development of a synthetic microbial community model

3.1 Introduction

Caries develops when the commensal dental biofilm shifts to a cariogenic state (Marsh, 2006b). Understanding factors contributing towards caries progression, including overpopulation of acidogenic species e.g., *S. mutans*, is important in informing the development of safe oral care products e.g., toothpaste and mouthwash. These will help prevent the global health and economic impact of caries.

Characterising the factors that lead to the invasion of *S. mutans* into dental biofilms over time, and the effect on commensal species is challenging *in vivo*. This is due to the number of species in the oral environment and the rich chemical environment in the mouth. To understand the factors leading to *S. mutans* invasion *in vitro* requires a model biofilm, or synthetic community of bacteria, to represent dental biofilms. These oral synthetic communities help better understand changes to bacterial ecology *in vivo*, including metabolic interactions and the effects on the local environment, e.g., pH changes through acid production (Chatzigiannidou et al., 2020a). Microbial communities provide the advantage of simplifying a very complex system found *in vivo*, where there are often hundreds of species in a biofilm, which is difficult to work with on a lab scale. The use of these communities allows for the control of variables e.g. sugar concentration and analysis of the effect that these changes have on the community (Bengtsson-Palme, 2020). Selection of the species used in a synthetic community needs to balance being clinically relevant *in vivo*, in terms of function and abundance, whilst also being able to be cultured under the same conditions e.g., oxygen tolerances. Mono and dual-species models have been used extensively (Díaz-Garrido et al., 2020), but they do not resemble the complexity of dental biofilms due to considering a limited number of species. Therefore, many recent studies have employed defined synthetic communities containing numerous species to understand these interactions and more accurately model the *in vivo* environment (Thurnheer et al., 2004a; van Holm et al., 2022 ; Wang et al., 2011). Whilst these models are examples of work characterising dental biofilms by using complex commensal communities, there are a limited number of models used to characterise the transition of a commensal dental biofilm to a cariogenic-associated state in a defined environment. Once these synthetic communities have been established to appropriately represent the *in vivo* environment, they can be used

in computational modelling approaches (as done in Chapter 5). Synthetic communities can be used to understand drivers of cariogenic species invasion by simulating the activity of oral species in different conditions (Head et al., 2017). The simulation of these synthetic communities has shown to have better correspondence to experimental data when the kinetic parameters of each species were used to inform *the in silico* models (Rosso et al., 1995). Kinetic parameters include the maximum specific growth rates (μ_{max}) and substrate affinity constants (K_s). To collect these parameters and further study the bacterial communities experimentally, the environmental conditions needed to support growth must first be established. This includes an appropriate growth medium.

Chemically defined media (CDM) are often used in understanding bacterial behaviour, as they reduce the chemical complexity of the system. They allow for the quantification of the chemical compounds fed into the system, consumption and production by bacteria. CDM have been developed for oral species (Socransky et al., 1985) (Terleckyj, 1975), however, as bacteria have specific nutrition requirements, these do not support the growth of all oral species. CDM are useful when considering *in silico* strategies they allow for inputting of all chemical concentrations within the system, which are needed for growth simulation and pH balancing. They also allow the main carbon source/electron donor to be determined, which was needed in the mass balance equations of such mathematical models. The development of CDM can be directed by using flux balance analysis (FBA). This mathematical modelling approach allowed for the construction of bacterial metabolic models and the simulation of the potential growth of bacteria on a defined medium (Orth et al., 2010). FBA can show whether biomass production was possible on a given medium. This saves time by directing the selection of which chemicals are needed, rather than experimenting with individual substrates blindly. FBA has been used to show the nutritional requirements of *S. mutans* (Jijakli & Jensen, 2019). Once a CDM had been developed to support the growth of the synthetic community, experimentation can be conducted to understand species' behaviour and their effect on the local environment.

Bacteria are metabolically complex, showing different characteristics in a rich environment of different substrates (Afroz, 2016). *S. mutans* can utilise glucose and sucrose, but physically behave differently depending on which sugar was present. *S. mutans* produces exopolysaccharides from extracellular sucrose, which helps adhesion to surfaces, biofilm formation and microcolony development (Olivera, 2021). *S. mutans*, therefore, has properties

making it suited to the invasion of dental biofilms, especially in the presence of sucrose. This species was also resistant to acidic environments, due to its acid tolerance response (N Takahashi & Yamada, 1999). This helps *S. mutans* resist the bacterial stress of low pH environments, which contributes to this species thriving in carious lesions (Dinis et al., 2022). Characterising the behaviour of each species in a mixed-species biofilm is therefore critical in understanding the behaviour of the system in different conditions.

Characterising and quantifying a mixed microbial system, including the invasion of a species into a mixed-species biofilm, requires the use of optimised analytical tools that can help understand ecological changes. This includes qPCR, which can be used to quantify the absolute amount of each bacterial species, allowing changes to be tracked over time (Wang, 2021). However, qPCR does not allow for the composition of a mixed system to be visualised or give any spatial information. It can therefore be used in conjunction with other analytical tools, e.g., *fluorescence in situ hybridization* (FISH). When optimised for the bacteria studied, FISH can reveal the spatial characteristics and patterns lacking from cell quantification (Thurnheer et al., 2004b). The combination of qPCR and FISH provides a powerful analytical tool for characterising the changes in a mixed microbial community. Using qPCR only enumerates bacteria based on the DNA present within the community and FISH only provides information on the presence of the bacteria cells. It is important to determine the viability of the members of the community to understand cell stresses and species prevalence in the system, which change under different conditions. Flow cytometry and live/dead staining have been used to quantify the proportions of viable microorganisms in the system over time (Berney, 2007).

3.2 Aims and objectives

In this chapter, I aimed to select a synthetic community to represent the dental biofilm and develop a CDM supporting growth of the 5-oral species. I aimed to characterise the synthetic community of oral bacteria, including collecting μ_{max} and K_s , and develop methods needed to quantify *S. mutans* colonisation into the commensal biofilm. This was in preparation for the colonisation experiments in Chapter 4 and the *in silico* simulations in Chapter 5.

Objectives:

- 1) Select a representative cohort of oral species to comprise the synthetic community, including 4-commensal species and the cariogenic species *S. mutans*.
- 2) Develop a chemically defined medium, that supported the growth of all members of a 5-species synthetic community of oral bacteria. This medium was needed to support growth without the cells being significantly stressed.
- 3) Collect the kinetic parameters from the bacterial species needed to inform the *in silico* models. This included the maximum specific growth rates (μ_{max}) and the substrate utilisation constants (K_s).
- 4) Identify characteristics of the bacteria species, including substrate utilisation, growth at different pH and acid production.
- 5) Develop and refine the analytical techniques needed to investigate *S. mutans* colonisation into the synthetic biofilm. This included qPCR and FISH.
- 6) Establish an inoculation strategy, so that the whole synthetic community could grow in an *in vitro* system.

3.3 Results

3.3.1 Selection of a synthetic community of oral bacteria and *in vitro* growth model

Selecting oral species to comprise the synthetic community, used in both the *in vitro* and *in silico* models to represent the oral microbiome and specifically dental biofilms, was central to this research. With the oral microbiome consisting of over 700 species, it is difficult to represent with too few species, as this would not capture the complexity of the system and help characterise important inter-species interactions. Selecting too many species poses difficult challenges in terms of laboratory work and *in silico* computational demand. Furthermore, as many species have similar roles in dental biofilms e.g., *S. mutans* and *S. wiggsiae* are both species directly implicated in caries progress, it is important to recognise that justification for other oral species could have been made. The oral bacterial species chosen were *S. mutans* UA159, *S. gordonii* DL1, *A. oris* MG1, *Neisseria subflava* DSM17610 and *V. parvula* DSM2008. *S. mutans* was selected as the cariogenic species due to its well-known involvement in disease progression (as discussed in Section 1.2.4). A pre-formed commensal bacterial community, comprising the other 4 species, representing the dental biofilm, was exposed to *S. mutans*. These commensal bacteria were selected based on their reported abundance from taxonomic quantification studies in literature, known function in the oral microbiome and established inter-species interactions that play a role in dental caries. This includes the nitrate reduction and anti-cariogenic properties discussed in Section 1.2.4. The species were also used routinely in my research group (excluding *N. subflava*), which influenced my decision in selecting the community due to my research group characterising the behaviour of these oral species and their role in the oral microbiome. The justification for synthetic community selection was detailed in Table 3.1. This synthetic community was central to all laboratory work and mathematical simulations involved in this research.

Table 3.1 Selection of the synthetic community of oral bacteria, including names of strains, justification of selection and references. Species were selected based on the reported abundance *in vivo*, function and known interactions. *S. mutans* was the cariogenic species introduced into the 4-species community to characterise invasion.

| No. | Strain | Reasons for inclusion | References |
|-----|--|--|--|
| 1 | <i>Streptococcus gordonii</i> DL1 | <p>A pioneering colonizer of the oral microbiome, part of initiating dental biofilm development.</p> <p>Found in large abundances in dental biofilm and established relationship with other commensal bacteria e.g., <i>Actinomyces</i>.</p> <p>Produces hydrogen peroxide that has been shown to reduce the success of <i>S. mutans</i> in dental biofilms.</p> <p>Fully sequenced strain of <i>S. gordonii</i>, useful for primer design and any metabolic analysis.</p> | <p>(Rath et al., 2017)</p> <p>(Zhang & Senpuku, 2013; Xu et al., 2020)</p> <p>(Kreth et al., 2009)</p> <p>Accession number NC009785</p> |
| 2 | <i>Streptococcus mutans</i> UA159 | <p>Strong consensus on <i>S. mutans</i> being cariogenic and having a large role in caries progression due to acid production and tolerance.</p> <p>Paves way for secondary colonisers e.g., <i>Lactobacillus</i> spp. and <i>Candida</i> spp.</p> <p>Comprises only 2% of the initial <i>Streptococci</i> population, which increases in caries-related patients This makes it of interest when attempting to characterise the transition of a commensal dental biofilm to a caries-associated state/</p> <p>Fully sequenced strain of <i>S. mutans</i>, useful for primer design and any metabolic analysis.</p> | <p>(Chenicheri et al., 2017)</p> <p>(Matsui & Cvitkovitch, 2010a; Cavalcanti et al., 2017)</p> <p>(Fakhruddin et al., 2019)</p> <p>Accession number AE014133</p> |
| 3 | <i>Actinomyces oris</i> MG1 | <p>Among the most common early colonisers of freshly cleaned teeth and is found in high abundance.</p> | <p>(Li et al., 2004)</p> <p>(Mohammed et al., 2018)</p> <p>(Dame-Teixeira et al., 2016a)</p> |

| | | | |
|---|---|--|---|
| | | <p>Found to populate dental biofilms in all age groups and through different stages of caries, owing to acid production and high acid tolerance. In high abundance in early dental plaque formation.</p> <p>Observed in different morphologies, but evidence points towards the importance of interaction with other species in microcolonies for initial biofilm development e.g., <i>S. gordonii</i>.</p> | |
| 4 | <p><i>Neisseria subflava</i> DSM17610</p> | <p><i>Neisseria</i> is abundant in the oral microbiome, despite not being prevalent in many oral models.</p> <p>Shown to be able to reduce nitrate to nitrite and be one of the main species causing this in the oral environment. This may have relevant benefits e.g., blood pressure regulation.</p> <p>Consumption of oxygen contributes to a reduced oxygen environment and acts as a carbon sink to help anaerobic species.</p> <p>Aerobic nature meant the synthetic community successfully represented bacteria with different oxygen demands/tolerances as the case is <i>in vivo</i></p> | <p>(Liu et al., 2015)</p> <p>(Hyde et al., 2014;</p> <p>Petersson et al., 2009b)</p> <p>(Bradshaw et al., 1996)</p> <p>(Marangoni et al., 2020)</p> |
| 5 | <p><i>Veillonella parvula</i> DSM2008</p> | <p>Present in progression stages of dental biofilm formation and relatively high abundance in dental biofilm.</p> <p>Established interaction and protection of <i>S. mutans</i> during caries progression.</p> <p>Several positive effects on oral microbiome and beyond, including the metabolism of acid produced by species e.g., <i>S. mutans</i> as well as reduction of nitrate to nitrite.</p> <p>Fully sequenced strain of <i>V. parvula</i>, useful for primer design and any metabolic analysis.</p> | <p>(Crielaard et al., 2011b)</p> <p>(Luppens et al., 2008a)</p> <p>(Mashima et al., 2016a;</p> <p>Vanhatalo et al., 2018)</p> <p>Accession number NC 013520</p> |

An appropriate growth model was needed to study the invasion of *S. mutans* into the dental biofilm. The CDC bioreactor (Figure 3.1) was selected due to the advantages discussed in Section 1.3.3. This included providing a flow-through system that was amenable to the measurements of key parameters e.g., medium flow rate, different growth substrates and temperature control, whilst being able to grow multiple biofilms simultaneously.

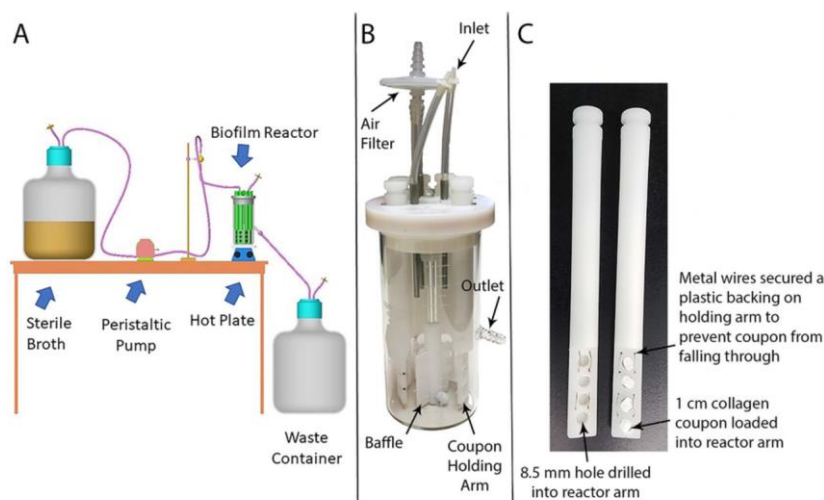


Figure 3.1 A CDC bioreactor setup, recently used for dental biofilm research (Miller et al., 2020). The CDC bioreactor allowed for constant flow-through of the medium under varying flow rates. Up to twenty-four coupons could be contained within, allowing for multiple biofilms to be formed at the same time. The reactor setup involved medium fed into the reactor using a peristaltic pump, media weirs out of the reactor into the waste carboy via the outlet port once the volume reaches 350 mL.

3.3.2 The development of a CDM to support the growth of the oral synthetic community

I aimed to develop a CDM that would support the growth of the synthetic community. This was to untangle the complexity of the chemical environment, better understand the nutritional demands of the bacterial species, and help inform the *in silico* approaches used in Chapter 5. First, I attempted to culture all 5 species on THYE + lactic acid medium, to gather preliminary information on the species, including morphology. I imaged all 5 species using Gram staining, done at the start and end of each experiment, to determine the shape of the cells and check the purity of the cultures. *S. gordonii* (Figure 3.2A) and *S. mutans* (Figure 3.2B) looked very similar down a microscope as they were both cocci, formed chains and were Gram-positive. This made them difficult to differentiate images using routine light microscopy techniques. *A. oris* (Figure 3.2C) was also Gram-positive, but cells had a distinct rod shape that often formed a “V” shaped pair. *N. subflava* (Figure 3.2D) and *V. parvula* (Figure 3.2E) looked

similar to each other, being Gram-negative cocci, however, *N. subflava* formed diplococci. I observed that *A. oris* cells tended to cluster together in liquid culture, relative to the other species. Similarities in morphology between pairs of species highlighted the need to use FISH to differentiate in later mixed-culture experiments.

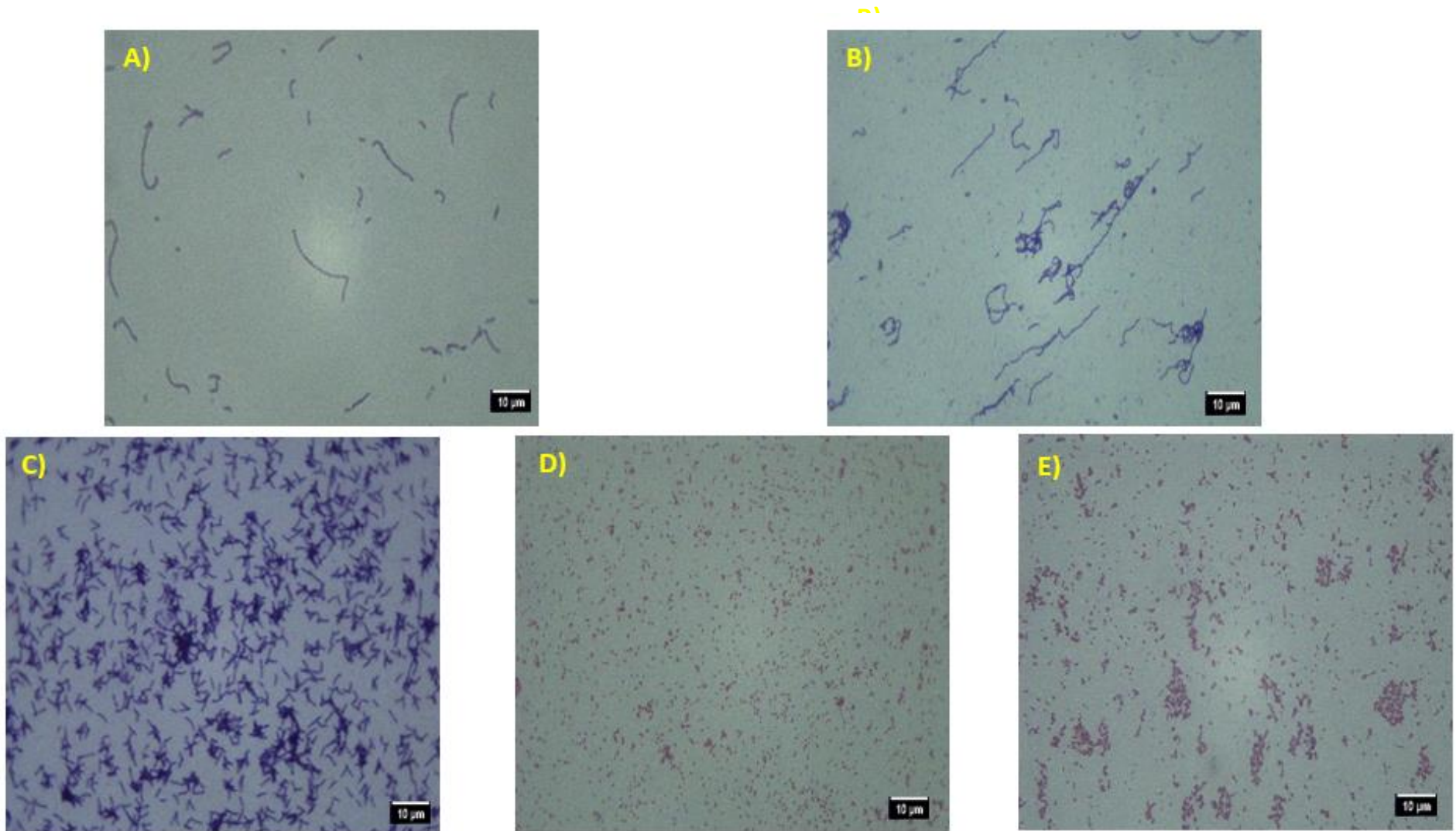


Figure 3.2 Imaging the members of the synthetic community on THYE + lactic acid medium, using a light microscope and Gram staining. *S. gordonii*, *S. mutans* and *A. oris* were Gram-positive and appeared purple. *N. subflava* and *V. parvula* were Gram-negative and appeared pink. All experiments were checked for contamination by confirming the presence of only one cell type A) *S. gordonii*, B) *S. mutans*, C) *A. oris*, D) *N. subflava*, E) *V. parvula*.

I attempted to grow the synthetic community on FMC medium, as described in Chapter 2.3.1. I recorded the optical density of each monoculture sample over 24 h. *S. gordonii*, *S. mutans* and *N. subflava* grew on FMC to high turbidity (Figure 3.3), with OD_{600nm} values of over 1.5 reached at 24 h for all. No signs of cell stress, e.g., bulging cells or un-uniform morphology, were observed when looking down the microscope. *A. oris* and *V. parvula* cultures were not able to grow to high turbidity, with OD_{600nm} after 24 h being below 0.2 for both species. This showed that FMC lacked the required nutrients to support these species.

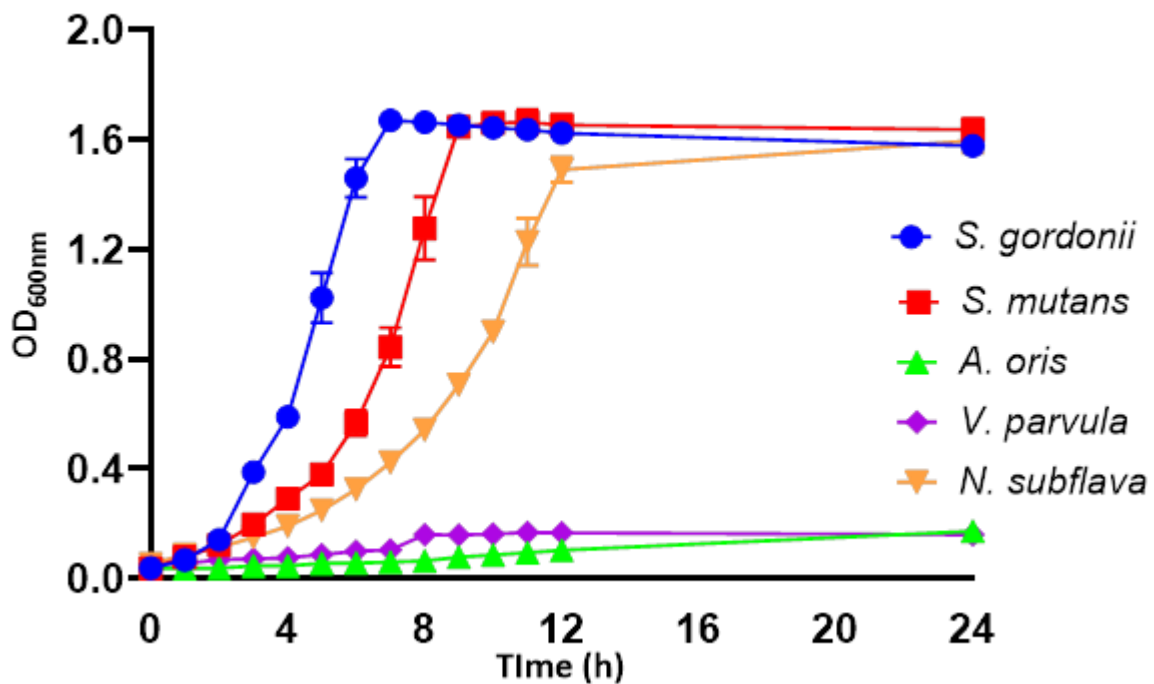


Figure 3.3 Growth curves of the oral bacteria over 24 h in FMC medium. *S. gordonii*, *S. mutans* and *N. subflava* grew on the medium, whilst *A. oris* and *V. parvula* failed to grow. Plotted points were the average OD_{600nm} values taken per h, over biological triplicates, with error bars representing the standard deviation from the mean. Each biological replicate contained technical triplicates (n=3).

To validate experimental approaches in the development of a CDM that would also support the growth of *A. oris* and *V. parvula*, I used Flux balance analysis (using KBase software). This was used in combination with what I found from the literature (see *V. parvula* use of lactic acid in Chapter 1). I constructed metabolic models of each species and used FBA to simulate whether biomass could be fully generated on my defined medium. My FBA showed that neither *A. oris* nor *V. parvula* could grow on FMC medium, with the objective value for biomass production both being 0. I was unable to get *A. oris* to generate biomass through these simulations, so I attempted to supplement with chemicals found in the literature. When I

included lactic acid and putrescine in the medium, I obtain a positive objective value of 3.63 for biomass generation of *V. parvula*, indicating that the species could grow on the medium. Simulations of the metabolic fluxes of *V. parvula* on this medium showed that lactic acid uptake contributed the most towards biomass production, with a flux of 60.90 (Figure 3.4). When I omitted lactic acid from FBA simulations, the objective value was 0 and there was no reaction output figure from KBase. This was because of the inability of *V. parvula* to generate biomass from a carbon source without the presence of lactic acid. The difference in simulated results with and without lactic acid confirmed that supplementation was necessary to support synthetic community growth.

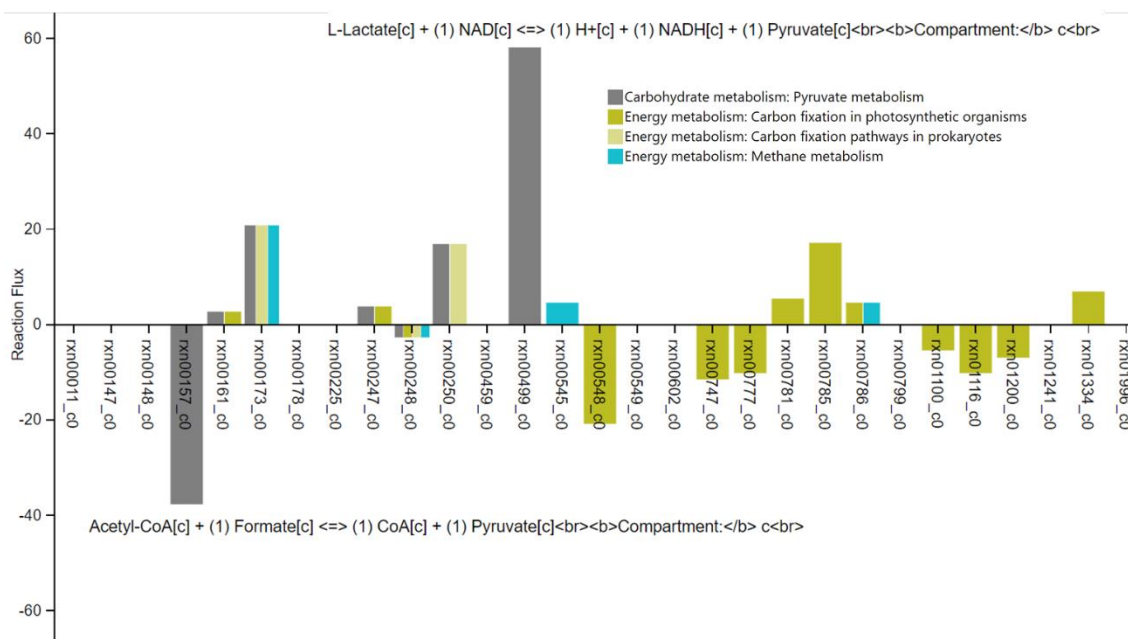


Figure 3.4 Reaction flux of *V. parvula* growth. Lactate uptake contributed significantly towards the objective value, with biomass being the desired function. FBA showed that growth was not supported on FMC medium, which did not contain lactate, but was attainable when lactate and putrescine were added to the medium. This figure was a snapshot from simulation results generated using AFMC in KBase, where no figure could be generated without lactic acid present .

The combined approach of literature and metabolic modelling helped formulate AFMC. I used AFMC to attempt to grow all 5 species of the synthetic community. The components of AFMC medium can be seen in Table 3.2

Table 3.2 Development of the AFMC medium to support the growth of the whole synthetic community. FMC medium was not able to do so, but with the addition of several chemicals, including cysteine, lactic acid and putrescine, the growth of all species was achieved. Each species was grown in biological triplicate to confirm the status of growth on the medium (n=3).

| No | Medium | <i>Species growth</i> ^a | | | | |
|----|---|------------------------------------|------------------|----------------|--------------------|-------------------|
| | | <i>S. gordonii</i> | <i>S. mutans</i> | <i>A. oris</i> | <i>N. subflava</i> | <i>V. parvula</i> |
| 1 | FMC | + | + | - | + | - |
| 2 | FMC + L-cysteine HCl 1 gL ⁻¹ Inositol 2 mgL ⁻¹ Thioctic acid 0.1 mgL ⁻¹ Oleic acid 2 mgL ⁻¹ Pimelic acid 0.1 mgL ⁻¹ | + | + | + | + | - |
| 3 | Medium from No. 2 + lactic acid (12.1 gL ⁻¹) | + | + | + | + | - |
| 4 | AFMC (Medium from No.3 + 1 mgL ⁻¹ putrescine) | + | + | + | + | + |

a. Growth was defined as reaching an OD_{600nm} of ≥0.5 after 24 h.

AFMC supported the growth of all synthetic community species (Figure 3.5) and supported multiple-generation subculturing (over 50 generations). All 5 species entered the stationary phase at different times, with *S. gordonii* reaching it the fastest after 6 h, but all reached it within 24 h of inoculation into fresh medium. *A. oris* and *V. parvula* reached OD_{600nm} values of 1.3 and 1.1 respectively, which they were not able to do on FMC. This showed that the combination of using FBA and literature research was effective in developing a chemically defined medium. AFMC was used for future experimentation.

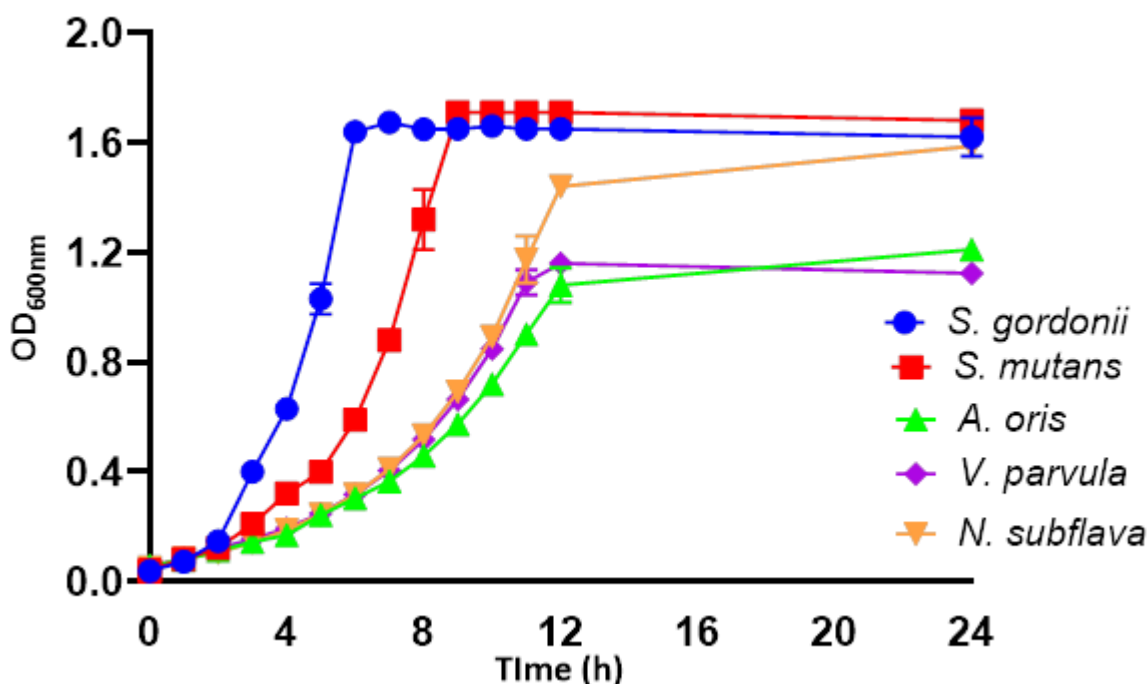


Figure 3.5 Growth curves of the oral bacteria over 24 h in AFMC medium. All synthetic community members were able to grow on this medium, all achieving an OD_{600nm} above 1.0. Plotted points were the average OD_{600nm} values over biological triplicates, with error bars representing the standard deviation from the mean. Each biological replicate contained technical triplicates (n=3).

3.3.3 Determining the kinetic parameters of the oral bacterial species

The maximum specific growth rate (μ_{max}) and substrate affinity constant (K_s) were determined for each bacterial species. This was so that the experimentally measured kinetic parameters could be used by the mathematical model to simulate growth of the synthetic community in Chapter 5. The μ_{max} values for each bacterium (Table 3.3) were calculated using the gradient of the exponential phase of growth. To determine K_s values, I grew each species, excluding *V. parvula*, in AFMC supplemented with lactic acid at a concentration of 12.1 gL⁻¹, and glucose at varying concentrations. I plotted the growth rates determined for

each species against the substrate concentration and K_s was equal to the substrate concentration at which $\mu = \frac{1}{2} \mu_{max}$. I grew *V. parvula* on AFMC supplemented with glucose at 20 gL⁻¹, but also with lactic acid at varying concentrations.

Table 3.3 μ_{max} and K_s values for all oral bacterial species. The μ_{max} values were taken from the average gradient of the exponential phase of growth (n=3). *S. gordonii* had the highest growth rate of 0.492 h⁻¹, whilst *A. oris* had the lowest growth rate of 0.227 h⁻¹. Substrate affinity constant values (K_s) for all species were determined by plotting the growth rate (μ) against their primary substrate concentration. The K_s value was equal to the substrate concentration at $\frac{1}{2} \mu_{max}$.

| | Species characteristics | | |
|-------------------------------|--------------------------------|---------------------------|---------------|
| | μ_{max} (h ⁻¹) | K_s (gL ⁻¹) | Carbon source |
| <i>Streptococcus gordonii</i> | 0.492 | 1.88 | Glucose |
| <i>Streptococcus mutans</i> | 0.406 | 1.00 | Glucose |
| <i>Actinomyces oris</i> | 0.227 | 1.40 | Glucose |
| <i>Neisseria subflava</i> | 0.261 | 1.00 | Glucose |
| <i>Veillonella parvula</i> | 0.246 | 2.42 | Lactic acid |

S. gordonii had the fastest growth rate of 0.492 h⁻¹, compared to the other species (p<0.005). *A. oris* was the slowest growing of the species, with a μ_{max} of 0.227 h⁻¹. For each of the four glucose-consuming species, μ_{max} was highest at 20 gL⁻¹ glucose and decreased at a higher glucose concentration (Figure 3.6). For *S. mutans*, the growth rate decreased from 0.406 h⁻¹ to 0.349 h⁻¹ when the glucose concentration increased from 20 gL⁻¹ to 30 gL⁻¹. *N. subflava* was able to grow without glucose, unlike *S. gordonii*, *S. mutans* and *A. oris*, showing that this species could grow by using other components of AFMC (data not shown). The lower the K_s value, the higher the affinity for the substrate and the greater the concentration needed to reach μ_{max} . *S. mutans* and *N. subflava* had the lowest K_s value of the glucose consumers, with a K_s of 1.00 gL⁻¹, whilst *A. oris* has the highest K_s value of 1.40 gL⁻¹.

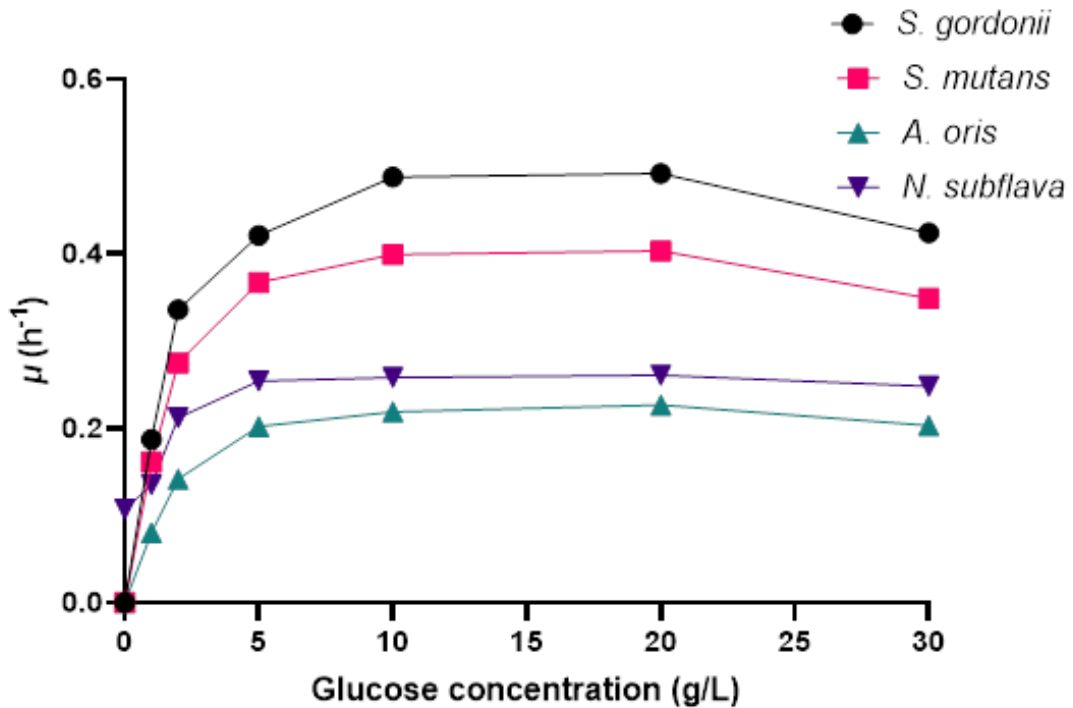


Figure 3.6 Substrate affinity constants (K_s), estimated from the substrate concentration at which $\mu = \frac{1}{2} \mu_{max}$. Plotted points were the μ_{max} for each species at different glucose concentrations. All species had their μ_{max} plateau and then decreased when the concentration increased above 20 gL⁻¹.

V. parvula was not able to grow without lactic acid. The growth rate plateaued at 12.1 gL⁻¹ lactic acid (Figure 3.7). The μ_{max} value decreased significantly, when the starting lactic acid concentration was reduced, dropping from 0.246 h⁻¹ at 12.1 gL⁻¹, to 0.216 h⁻¹ at 7.26 gL⁻¹. At 24.2 gL⁻¹ lactic acid, there was a slight drop, showing that saturation occurs between 1% and 2%. Overall, these results show that the growth rate of *V. parvula* was directly related to the lactic acid concentration of the medium. *V. parvula*, consuming lactic acid as a primary carbon source, had a higher K_s value (2.42 gL⁻¹) than any of the glucose consumers, therefore requiring higher quantities of lactic acid to grow compared to the amount of glucose needed for the other species. Based on these data, a glucose concentration of 2 gL⁻¹ and a lactic acid concentration of 2.42 gL⁻¹ were used in the substrate-limiting systems (Chapter 4).

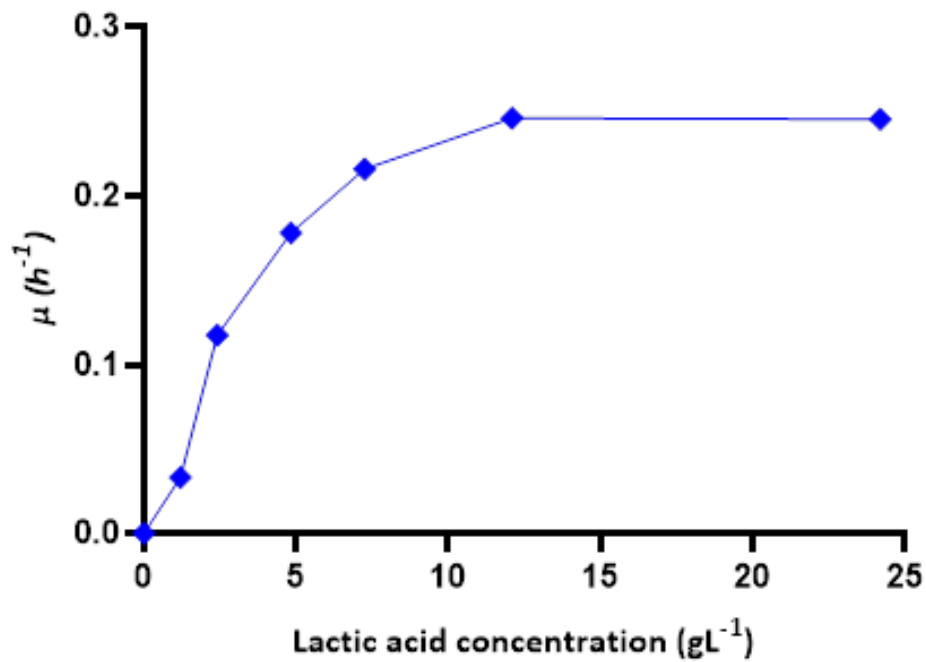


Figure 3.7 Substrate affinity constant (K_s) for *V. parvula*, estimated from the substrate concentration at which $\mu = \frac{1}{2} \mu_{max}$. Plotted points were the μ_{max} for *V. parvula* at different substrate concentrations. *V. parvula* did not grow in the absence of lactic acid and μ_{max} plateaued between a concentration of 12.1 gL⁻¹ to 24.2 gL⁻¹.

3.3.4 Substrate utilisation by the synthetic community

I grew each species on AFMC supplemented with either glucose or sucrose to confirm the substrate usage for the synthetic community members. I also observed any differences in characteristics of the species between growing on glucose or sucrose. I quantified growth and substrate concentration over 24 h. All species, excluding *V. parvula*, consumed glucose as they grew over time (Figures 3.8 a-e). The results showed that a starting glucose concentration of 20 gL⁻¹ was in excess of what was needed in the monoculture growth experiments, for all species. For *V. parvula*, it was confirmed that lactic acid was the carbon source consumed for growth (Figure 3.8e). Lactic acid was also in excess AFMC, as the concentration of lactic acid never dropped below 3.19 gL⁻¹. Glucose and sucrose levels remained the same, as they were not consumed by *V. parvula*. *V. parvula* was not affected by the presence or absence of these sugars. *N. subflava* grew without either glucose or sucrose in AFMC. *S. gordonii*, *S. mutans* and *A. oris*, however, did not grow without having either glucose or sucrose in the medium (data not shown).

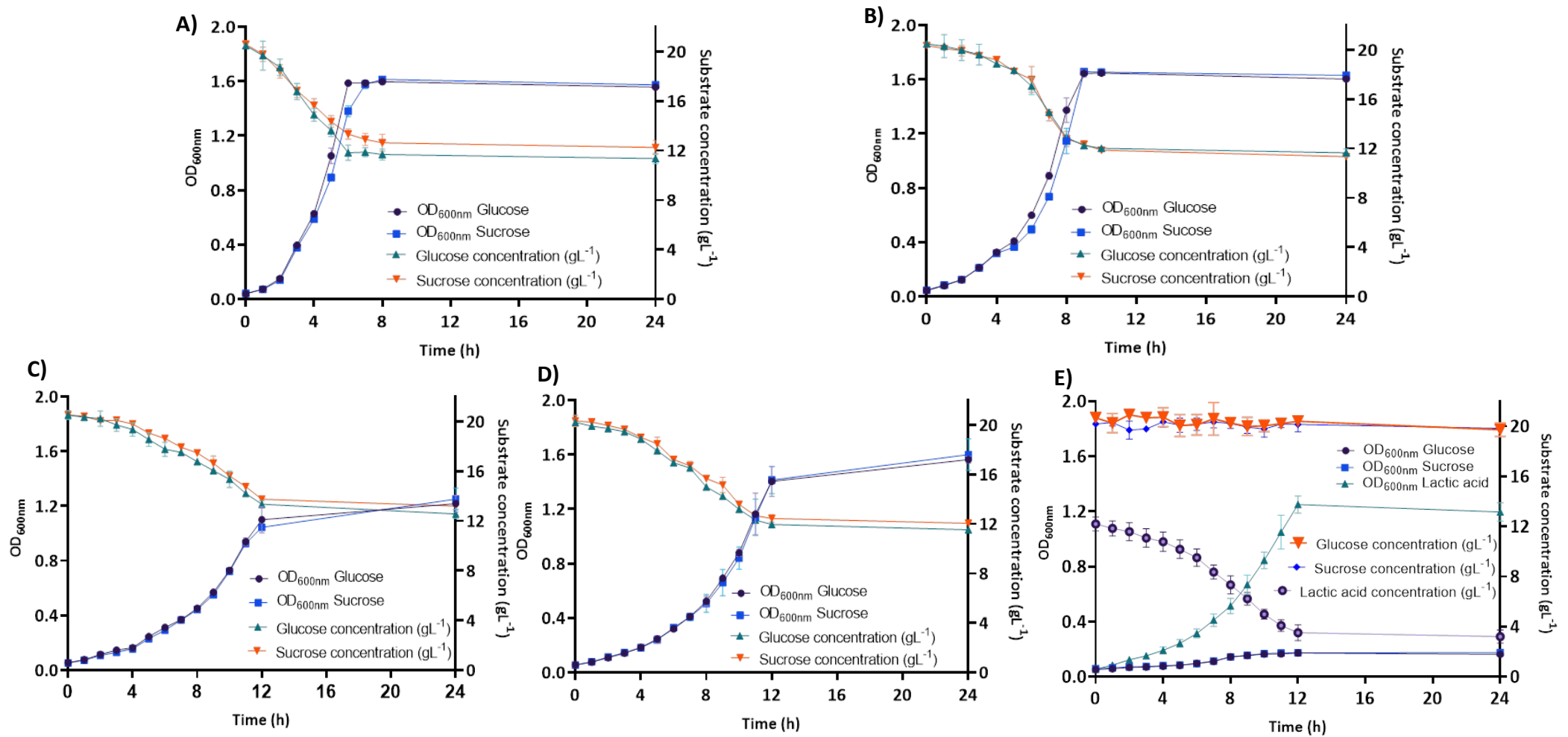


Figure 3.8 Growth and substrate utilisation of the synthetic community members over 24 h on AFMC supplemented with either glucose or sucrose. All species grew in the presence of glucose and sucrose. *V. parvula* was unable to consume these sugars but consumed lactic acid for growth. Data points represented the average OD_{600nm} or substrate concentration value across biological triplicates, all with three technical triplicates. Error bars represent the standard deviation from the mean (n=3). *S. gordonii* (A), *S. mutans* (B), *A. oris* (C) and *N. subflava* (D), *V. parvula* (E).

I examined the growth of the species on different sugars to determine any significant difference in behaviour. When grown in AFMC containing sucrose, *S. mutans* cells aggregated, with the amount of aggregation noticeably different depending on the quantity of the sugar (Figure 3.9). With either glucose or fructose present in the absence of sucrose, there was no aggregation of *S. mutans*. No other species exhibited this behaviour.

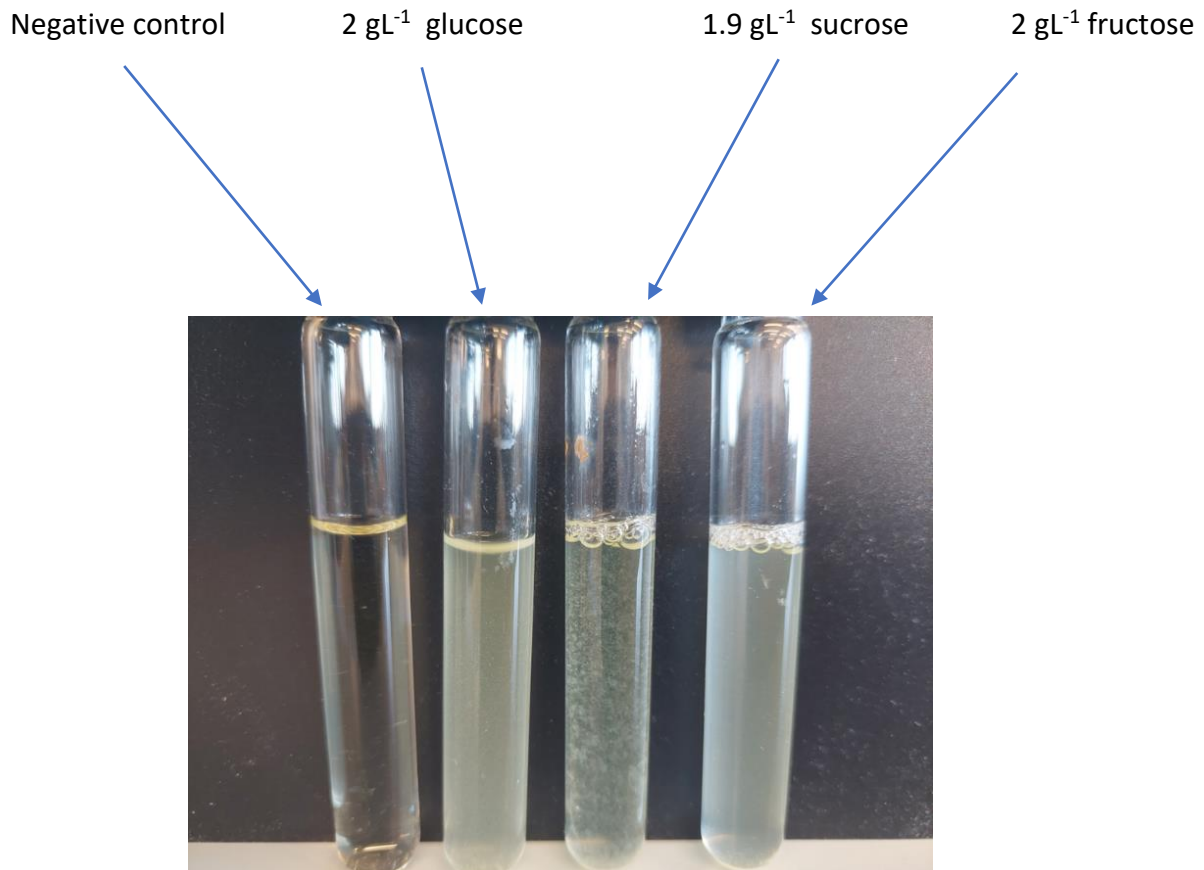


Figure 3.9 Growth of *S. mutans* on AFMC supplemented with glucose, sucrose, or fructose. *S. mutans* behaved differently depending on the carbon source used. Whilst capable of growing on glucose sucrose or fructose, *S. mutans* exhibited the unique attribute of aggregating together when grown on sucrose. This was not observed from any of the other species members or on any of the other sugars.

I used calorimetry to observe if any difference in metabolic activity was detected between the 5 oral species on the different sugars. The species were grown on AFMC supplemented with either glucose or sucrose in monoculture, inside vials. The calorimeter recorded heat generation from the cultures. *N. subflava* showed a significantly greater thermal output on glucose than on sucrose, reaching a peak of 82 μ W on glucose, compared to 58 μ W on sucrose (Figure 3.10). *S. gordonii* and *A. oris* (not shown) showed no difference in metabolic activity, regardless of whether the species were grown on glucose or sucrose. *N. subflava* also produced far more energy than any of the other species ($p < 0.005$), likely due to this species

undergoing aerobic respiration, a far more energy-efficient method of growth compared to anaerobic respiration. *V. parvula* was not able to grow in these experiments, likely due to the oxygen presence in the vials of the experiments. *S. mutans* produced a greater amount of energy on sucrose (48 μ W), than on glucose (40 μ W).

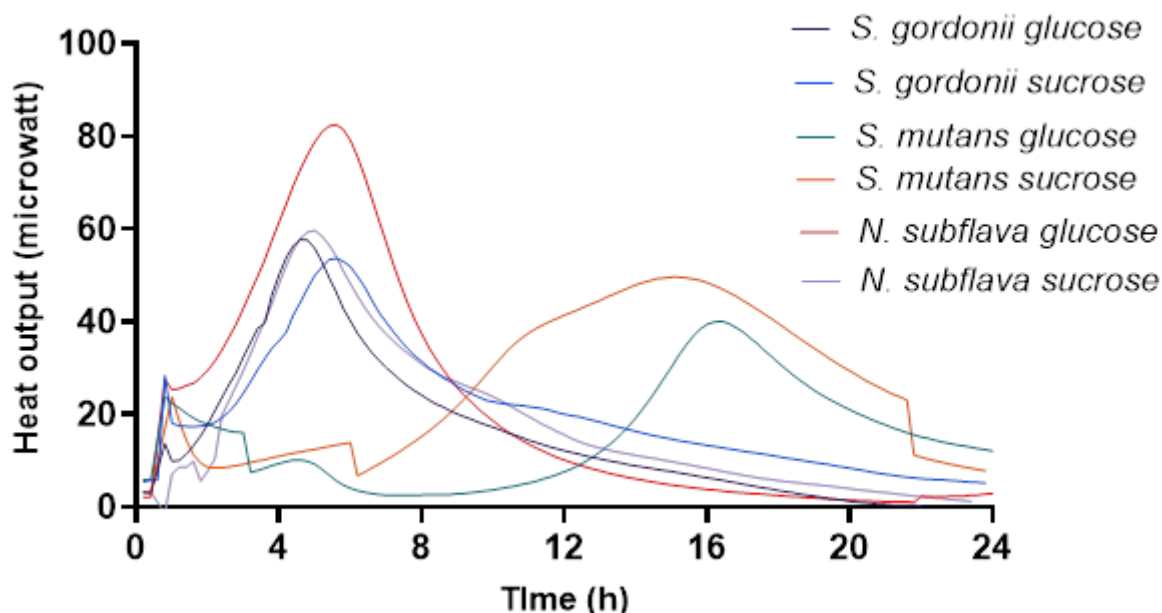


Figure 3.10 Heat output from *S. gordonii*, *S. mutans* and *N. subflava* on glucose and sucrose over 24 h recorded using a microcalorimeter. *N. subflava* produced a significant amount of heat on glucose compared to sucrose, whilst *S. gordonii* had a similar amount of heat produced regardless of the substrate. All experiments were conducted in biological triplicate containing technical triplicates (n=3).

3.3.5 Growth of oral species and acid production at different pH

Acid production by bacterial species has a significant impact on caries progression, where demineralisation occurs around a pH of 5.5 and below. The yield of bacterial growth also differs depending on the pH of the local environment. I investigated the ability of each species to grow to high turbidity in acidic environments, and the pH variation of AFMC resulting from the growth of each species. This was to help identify species' ability to thrive in acidic environments, often seen in caries, and their potential contribution to demineralisation *in vivo*, by way of understanding how the species impact the pH of their environment. Furthermore, understanding their contribution to pH change would help explain any pH changes seen in the invasion experiments (Chapter 4). Species were grown in monoculture and data collected after 48 h.

All 5 synthetic community species were affected by the starting pH of the medium. *S. mutans* grew far better than the other species at an initial pH of 6 (Figure 3.11) ($p < 0.05$), with an OD_{600nm} of 1.14 reached. *S. mutans* was the only species to grow at a pH of 5.3, all others did not grow significantly from their starting optical densities (OD_{600nm} values below 0.1). For all species, the optimal pH for growth from those tested was determined to be pH 7. These findings demonstrated that *S. mutans* grew significantly better in a more acidic condition than the other species and indicated that once the mixed-culture environment decreases below 5.5, the majority of the synthetic community members would struggle to grow.

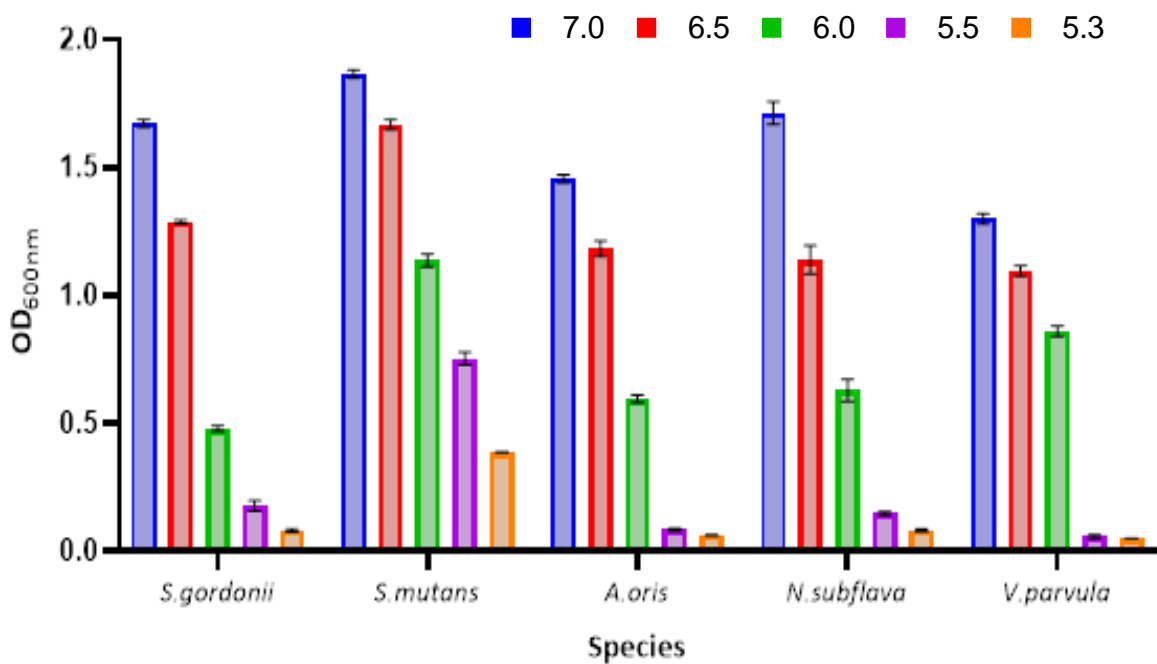


Figure 3.11 Maximum OD_{600nm} of the synthetic community members at different initial pH over 48 h on AFMC medium. *S. mutans* grew significantly better at lower starting pH, compared to the other species in the synthetic community. Data plotted was taken after 48 h and was the average across biological triplicates, with error bars representing the standard deviation from the mean ($n=3$).

I measured the pH after 48 h of growth of each species in AFMC, at different starting pH levels. I observed that all species produced significant amount of acid by the time they have reached stationary phase. *S. mutans* was the most acid producing species, lowering the pH from 7 to 4.94 (Figure 3.12), compared to *V. parvula* which lowered the pH the least to 5.98. As the starting pH lowered, for all species, the pH changed from the initial pH by a smaller amount. This was due to less growth being observed once the pH fell below the optimal condition of

pH 7. By a pH of 5.3, the end pH was similar to the starting pH as all species struggled to grow, therefore producing minimal acid from fermentation.

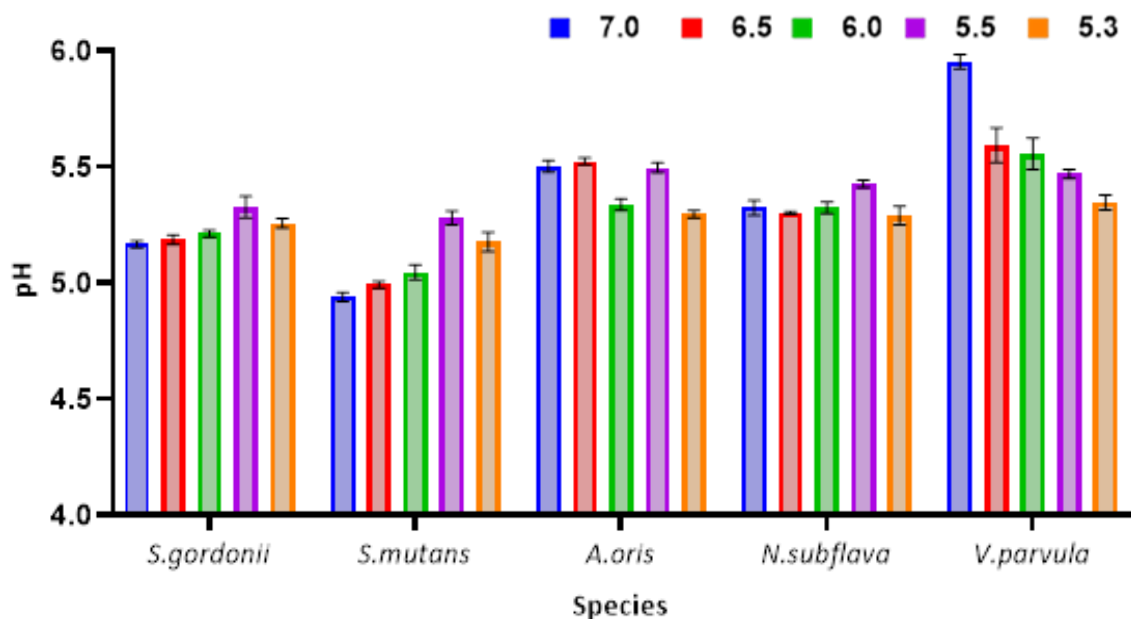


Figure 3.12 The final pH of the AFMC medium after 48 h of growth for each species of oral bacteria. *S. mutans* was the most acid-producing species, whilst *V. parvula* was the least acid-producing. Data represented the average pH across triplicate experiments, with error bars representing the standard deviation from the mean (n=3).

3.3.6 Synthetic community visualisation through fluorescence in situ hybridization

I developed an optimised FISH method to visualise members of the synthetic community. This was because it was difficult to differentiate between synthetic community species using light microscopy, as there were bacteria with similar cell morphologies i.e., both *S. gordonii* and *S. mutans* form cocci chains. I selected 5 different fluorophores that were as far spread on the wavelength spectrum as possible (Figure 3.13) to minimise the overlap of fluorescent emission. However, with the chosen fluorophores, there was still spectral overlap. In Figure 3.13, the excitation of each fluorophore was represented by the dashed lines, and the emission peaks by the solid peaks. The emission spectra of Alexa 594 bled into that of Alexa 647 and so some of the signal would have been picked up by the detector. The excitation of Alexa 594 was also close to the emission of Alexa 555.

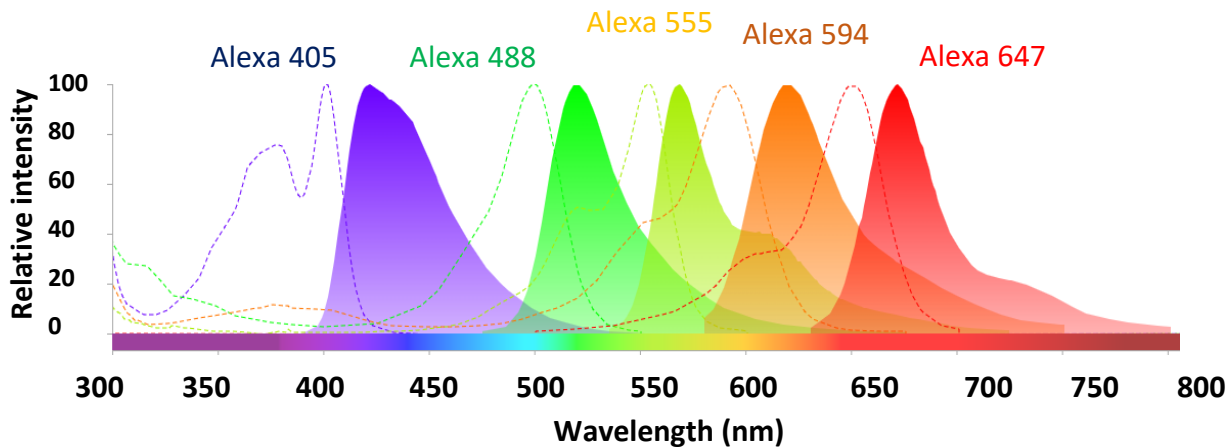


Figure 3.13 Fluorophores selected to optimise minimal overlap. I used Spectra viewer (ThermoFisher) as a tool to represent excitation (dashed lines) and emission (solid lines) of all peaks for the 5 fluorophores. These 5 fluorophores were selected to conjugate to the FISH probes used in this research (Alexa 405= *N. subflava*, Alexa 488= *S. mutans*, Alexa 555= *A. oris*, Alexa 594 = *S. gordonii*, and Alexa 647 = *V. parvula*).

Each bacterium was hybridized using the same conditions so that I could make the transition to hybridize all of them in a mixed sample. I refined the experimental conditions so that optimal images could be taken. This included optimising the hybridization steps and wash steps to significantly reduce background noise (Figure 3.14). The Alexa 555 fluorophore, used to image *A. oris*, resulted in significant background fluorescence before optimisation, which was reduced by optimising the hybridization temperature, including a short hybridization period at room temperature, and then using a series of wash steps. This had a drastic effect on the amount of autofluorescence, which would have been even greater in a mixed-species system, where more than one fluorophore was employed.

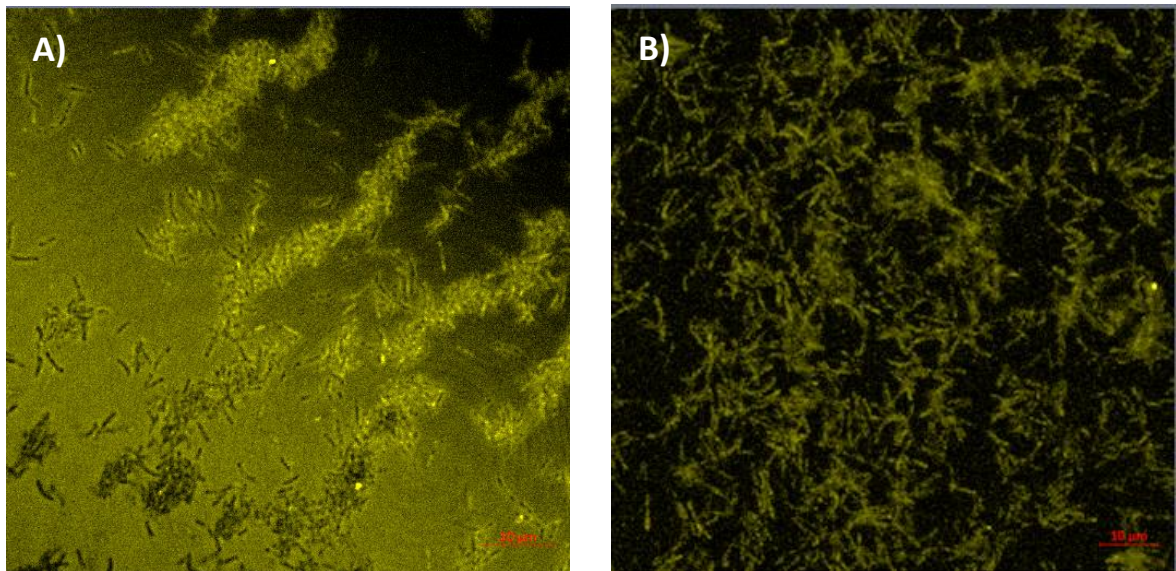


Figure 3.14 *A. oris* planktonic cells visualised using FISH. (A). Without the improved washing cycle steps and hybridization step at room temperature I observed a large amount of background noise and autofluorescence. (B) Optimising the protocol led to a significant reduction in background noise. Images were taken in a minimum of triplicates, with representative images used.

Initially, I grew each species planktonically in monoculture using THYE + lactic acid medium (as described in Chapter 2). I was able to image all species in planktonic culture using FISH. I imaged areas of low density so that I could observe the cell structure. For example, in Figure 3.15A, *S. mutans* could be seen forming cocci chain structures and *A. oris* with a distinct rod shape (Figure 3.15C). Each fluorophore emitted light at different intensities with Alexa 594, used for *S. gordonii*, emitting a weak signal. This was improved by adjusting the gain to equalise the signal.

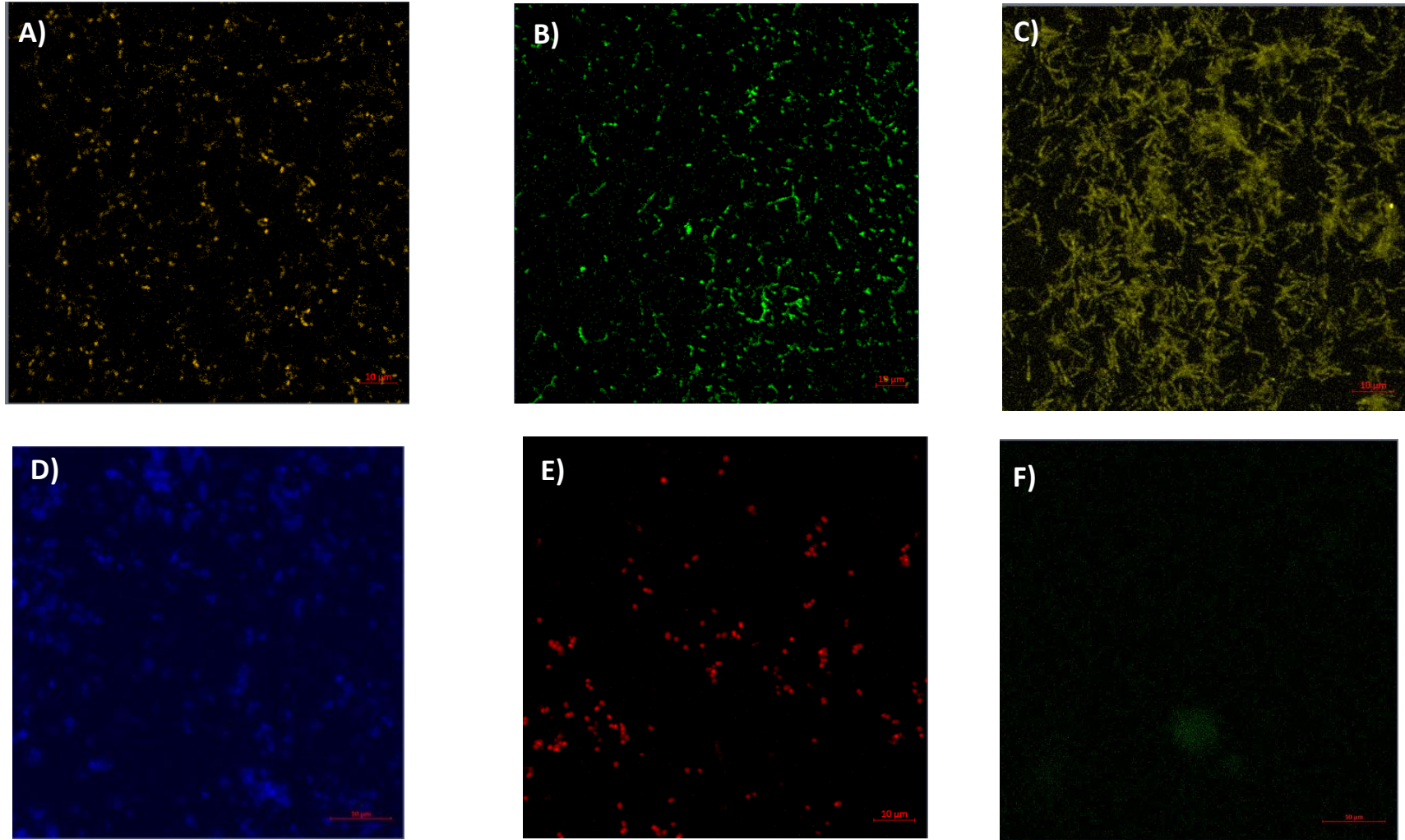


Figure 3.15 Members of the synthetic community visualised as monoculture planktonic cells using FISH. I imaged each species after 24 h and identified their structure. Positive controls using EUB338a (not shown) and negative controls using non-species-specific primers were used in all FISH experiments. A) *S. gordonii*, B) *S. mutans*, C) *A. oris*, D) *N. subflava*, E) *V. parvula* F) Negative control.

Once all species had been imaged in monoculture as planktonic cells, I visualised each species as mono-species biofilms of different maturities. Each biofilm was cultured initially in THYE + lactic acid medium on glass coverslips, contained within 6-well plates. Once I was able to do this, I visualised each biofilm grown in AFMC on hydroxyapatite disks placed within 6-well plates (Figure 3.16). These were the desired conditions within the CDC reactor system (Chapter 4). I was able to visualise each species. It was evident that individual cells could be observed, but also the structure formed by the biofilms. *A. oris* cells in a biofilm preferentially grew densely together in structures (Figure 3.16C), whereas *N. subflava* (Figure 3.16D) and *V. parvula* (Figure 3.16E) cells disperse over the surface more. *S. gordonii* (Figure 3.16A) and *S. mutans* (Figure 3.16B) formed chains of cocci and grew to very high cell densities.

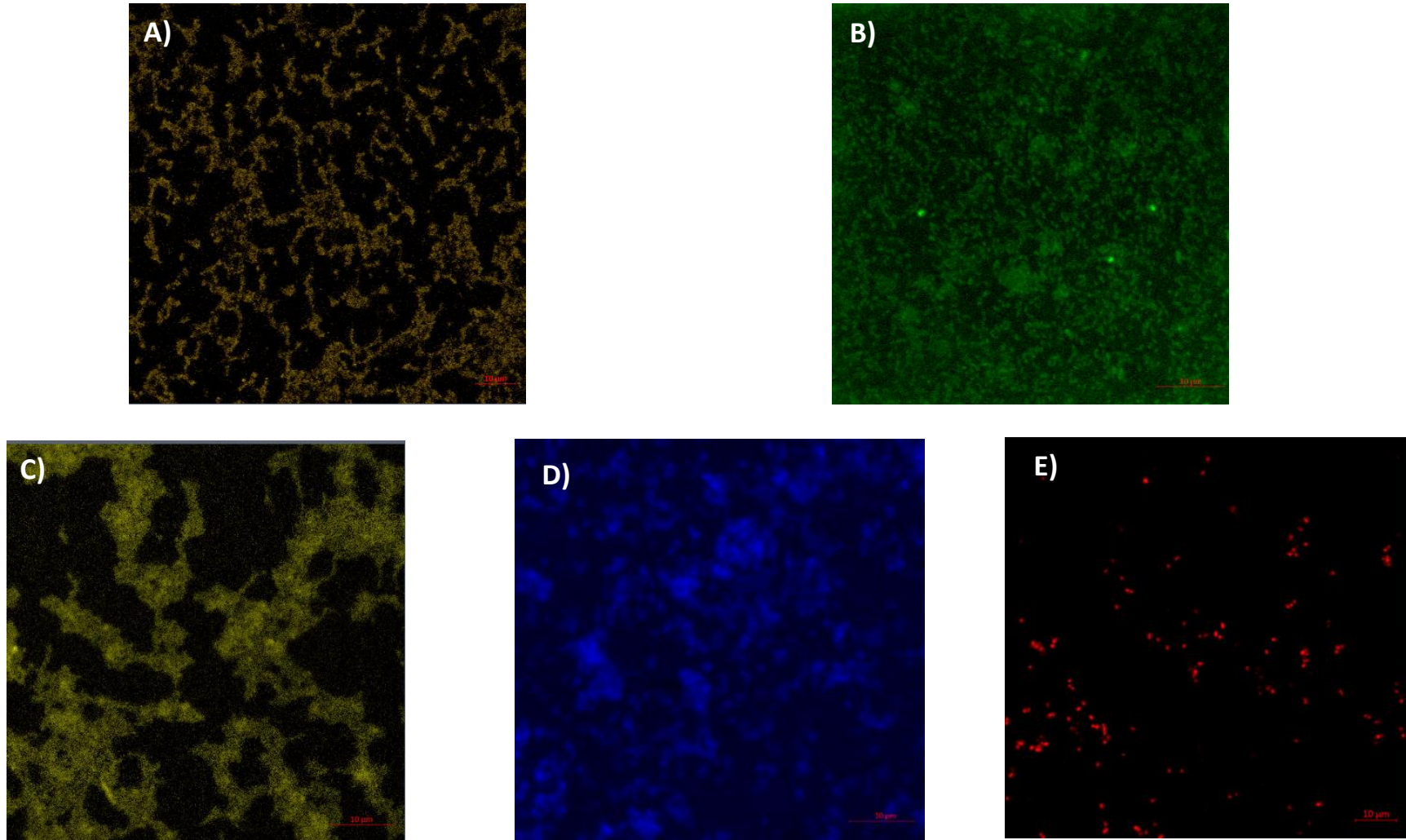


Figure 3.16 Members of the synthetic community visualised as monoculture biofilms using FISH. I grew each biofilm anaerobically, excluding *N. subflava*, which was grown aerobically, on hydroxyapatite disks for 24 h before imaging. Species were grown on AFMC. The images shown were representative samples of numerous tests. A) *S. gordonii*, B) *S. mutans*, C) *A. oris*, D) *N. subflava*, E) *V. parvula*

Once I was able to image all biofilms separately, I attempted to image mixed species biofilms in different combinations to test whether they could be enumerated together. I attempted this with *S. gordonii* and *S. mutans*, as they looked very similar without fluorescent imaging (Figure 3.17A), as both formed chains of cocci cells, so it was important to be able to differentiate them. By using species-specific probes, they could be separated in the same image from the same sample (Figure 3.17B). Here, both species were grown together for 24 h after being inoculated at the same time.

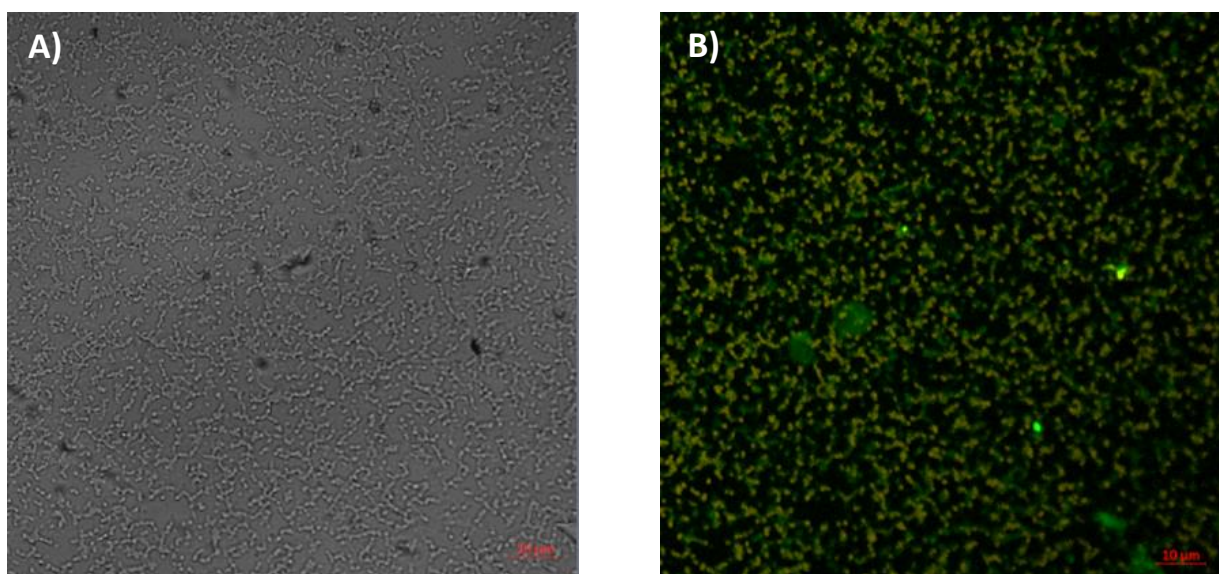


Figure 3.17 Visualising *S. gordonii* (orange) and *S. mutans* (green) in a mixed-species biofilm using confocal microscopy. (A) When the sample was viewed using bright field and no fluorescence, both were difficult to differentiate due to forming chains of cocci cells. B) The use of fluorescent staining as part of FISH allowed for separating them in a mixed-species environment

The final aim was to image all 5 species in the same biofilm. I encountered significant overlap in the emission/excitation of the fluorophores, despite them being selected to be as far away on the spectrum as possible. I reduced the overlap in spectra by employing spectral fingerprinting for each of the 5 fluorophore-species combinations (Figure 3.18A). This involved recording several emission signals from mono-culture samples for each species biofilm and using the profile to create a “fingerprint”. The fingerprint showed what emission should be for the species and what was autofluorescence or coming from a different channel. With this approach, there was a possibility of not recording the full fluorescent signal of the sample, but it provided a more accurate signal received from the bacteria and significantly reduced bleed

over from other channels. In the mixed-species biofilm, *A. oris* was grown first (inoculation strategy discussed in 3.2.7), with *S. gordonii*, *N. subflava* and *V. parvula* brought in 24 h later. *S. mutans* was inoculated after 48 h. All 5 fluorophores could be seen, demonstrating that it was possible to grow a biofilm including the whole synthetic community (Figure 3.18B). No specific spatial pattern was observed. Using spectral fingerprinting on the mixed-species biofilms reduced background fluorescence and overlap of emission spectra, although this was not eliminated completely. The Alexa 405 dye conjugated probe, hybridized to *N. subflava*, still contributed to bleed-through and over-saturation.

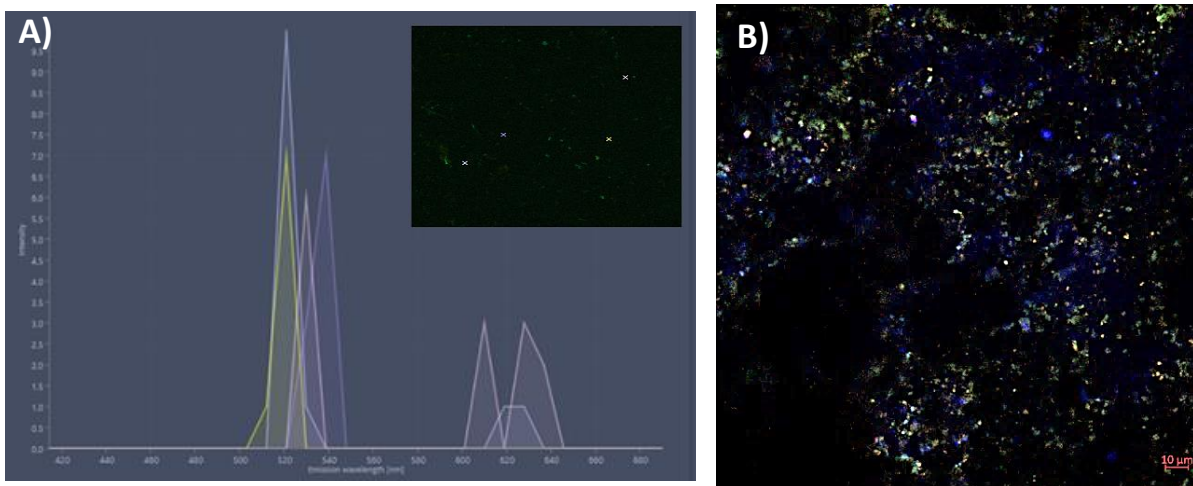


Figure 3.18 Imaging the 5 species synthetic community biofilm using FISH, aided by spectral fingerprinting. A) I took multiple signals from cells in a mono-culture biofilm for each species (shown here for *S. mutans*) and averaged the emissions to create a spectral fingerprint file. The peaks represent emission from individual cells. This was used to help filter overlapping fluorescent emissions and reduce autofluorescence. B) I was able to visualise all 5 synthetic community members in AFMC medium on hydroxyapatite disks.

3.3.7 Development of a qPCR method to quantify bacterial species

I used qPCR to quantify each bacterial species in my synthetic community. I needed to develop the assay before progressing with the *in vitro* model, as tracking the change in abundance of each species, particularly *S. mutans*, was vital in characterising invasion into the synthetic community biofilm.

I extracted genomic DNA (gDNA) from each species and amplified species-specific regions of the 23s rRNA gene for synthetic community member using the primers and probes in Chapter 2. I ran the PCR products on a 1% agarose gel (Figure 3.19) to check that the correct targets had been amplified. These fragments corresponded to the desired sizes and produced strong bands within this region, confirming the amplification of the region of interest. The presence of a strong band confirmed sufficient quality of DNA fragments.

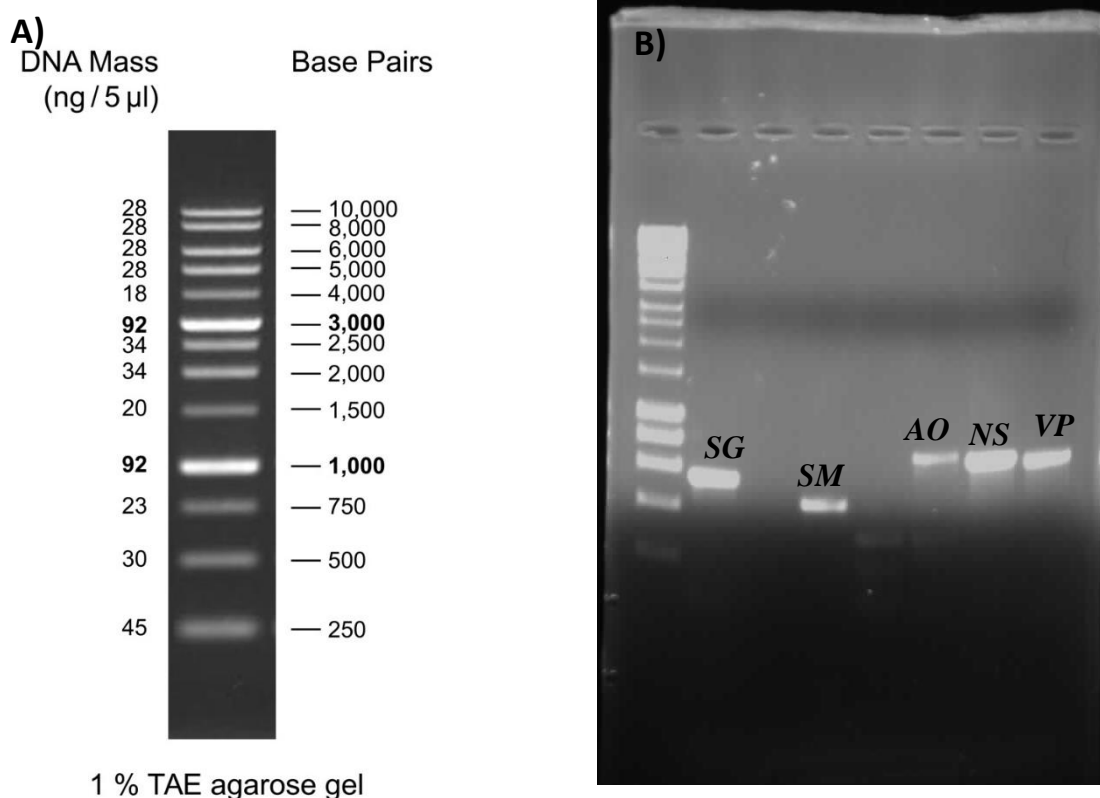


Figure 3.19 Amplification of gDNA targets using designed cloning primers. A) I ran the targets using gel electrophoresis on a 1% TAE gel, with 1kb HyperLadder™. B) The PCR products for each species were compared against the ladder to determine the correct size (Expected target size *S. gordonii* (SG)= 552 bp, *S. mutans* (SM)=313 bp, *A. oris* (AO) =692 bp, *N. subflava* (NS) =679 bp, *V. parvula* (VP) = 672 bp).

I cloned each of these targets into *E. coli* using the TOPO™ TA cloning kit (Invitrogen, MA, USA). I extracted bacterial plasmids from each species using the QIAprep Spin Miniprep plasmid kit (Qiagen, Hilden, Germany). I confirmed the insertion of the region of interest by sending samples for sequencing, using the Mix2seq sequencing kit (Eurofins, Luxembourg). I ran these on a gel to confirm the presence of the fragment within the TOPO™ plasmid. I extracted the plasmid DNA (pDNA) from *E. coli* for each species. The quality of each plasmid, sufficient concentration and degree of DNA contamination were all confirmed using

NanoDrop™ and gel electrophoresis (Figure 3.20). The 260/280 ratios were all between 1.80-2.00, confirming that the plasmid DNA was of acceptable quality (Figure 3.20).

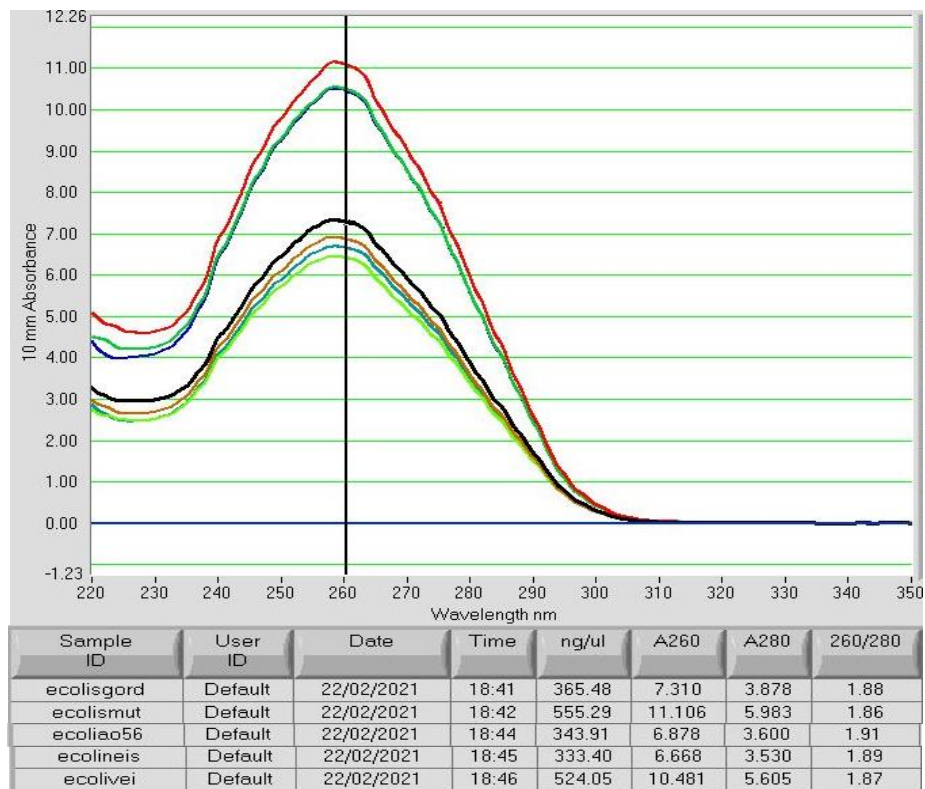


Figure 3.20 Analysis of pDNA species extracts post-cloning using the NanoDrop™. 260/280 ratios were between 1.80-2.00 indicating suitable quality. Concentrations of each plasmid ranged from 333-555 ng/uL.

I quantified each *E. Coli* plasmid extract using the PicoGreen™ assay kits (Thermo Fisher, MA, USA). I generated a standard curve (Figure 3.21) so that I could accurately quantify the exact amount of DNA in each sample, as the method was more accurate than using the NanoDrop™. This was necessary for generating the standard curves needed in my qPCR assay. The quantity of each of the plasmids differed from the concentrations on the NanoDrop™, which also picks up other obstacles in the light path other than DNA. I, therefore, used the concentrations determined by PicoGreen™ (Thermo Fisher, MA, USA) for my qPCR standard curves.

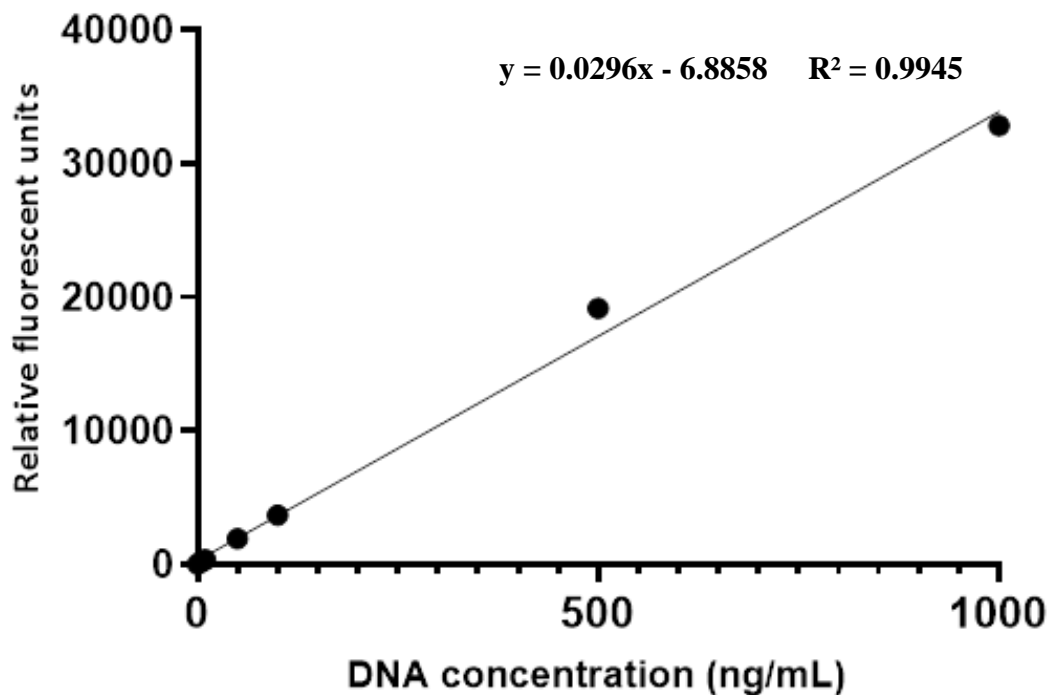


Figure 3.21 Standard curve generated using the PicoGreen™ assay kit (Thermo Fisher, MA, USA). This was used to accurately quantify the concentration of each plasmid standard, to be used in qPCR. The R^2 value of the curve was 0.9945.

It was necessary to confirm a working protocol for qPCR quantification of the oral species before use in the invasion experiments in Chapter 4. First, I generated a standard curve for each bacterial species' pDNA. To do this, I amplified serial dilutions between 10^{-2} - 10^{-8} of the known pDNA standards using species-specific primers. I confirmed that the primer/probe set efficiencies for each species were between 90-100%, deemed acceptable by the MIQE guidelines (Bustin et al., 2009). I ran these products on a gel to confirm the correct size of the target. I used these standard curves for all future qPCR quantification experiments. I grew biofilms on glass coupons in monoculture and extracted DNA as described in Chapter 2. After amplifying the gDNA of my species, I ran each product on a gel to confirm that the amplified region from each standard corresponded to the desired target (Figure 3.22A). These were confirmed to be of the expected size when run on a gel. Once I had confirmed the amplification of gDNA for each species from monoculture biofilms, I multiplexed the reaction to make the experiment more time and cost-efficient, cutting down the analysis from 5 samples to 2. This was necessary as a significant number of samples were generated for the invasion experiments. I amplified mixed species pDNA standard extracts in a multiplex setup, *S.*

gordonii, *A. oris* and *V. parvula* in one sample, with *S. mutans* and *N. subflava* in the other. Once this was confirmed to work, I amplified gDNA from planktonic cells of each species, using multiplex qPCR (Figure 3.22B), to validate that this method could be used on bacterial samples, as needed for *in vitro* samples in Chapter 4.

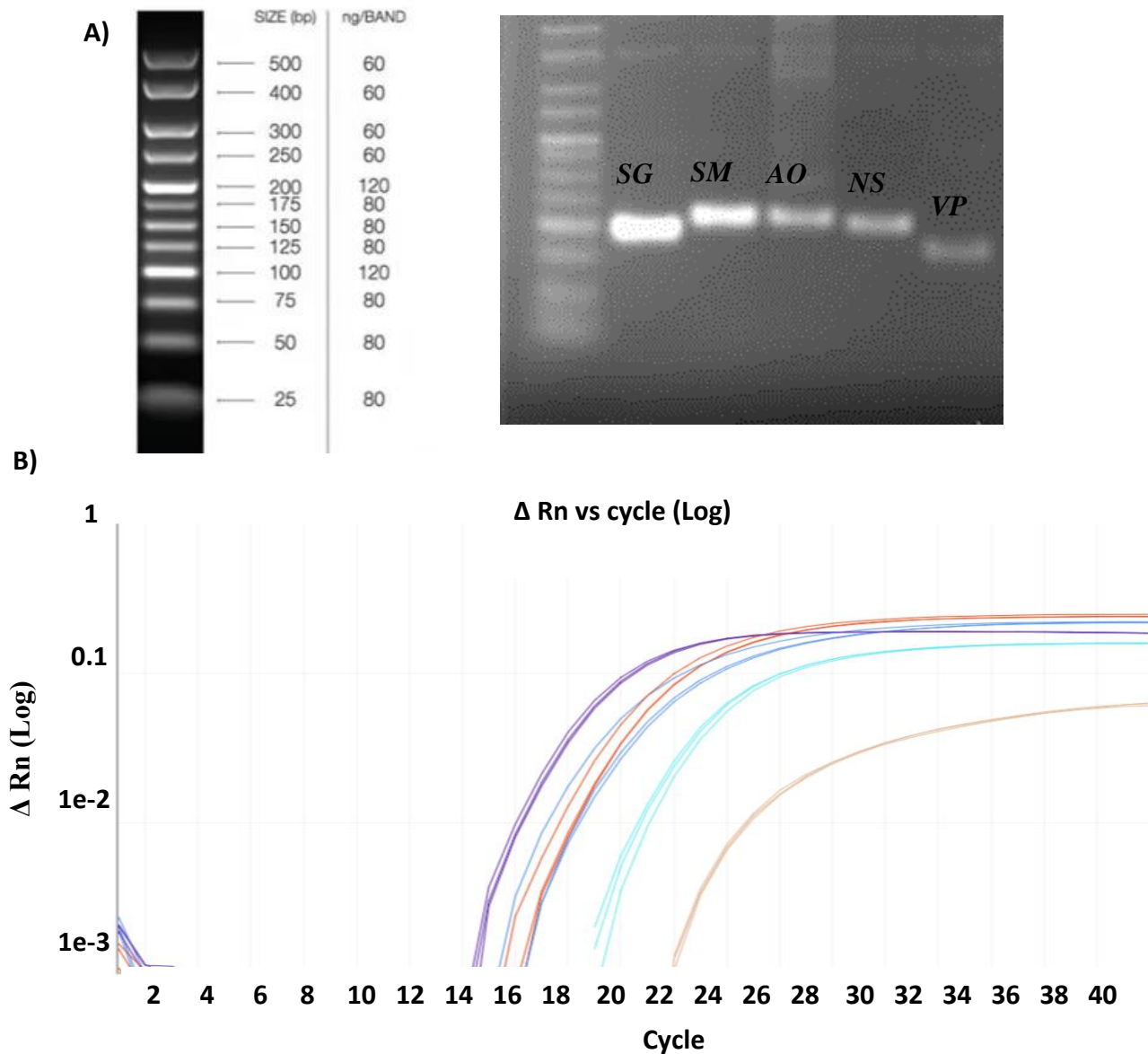


Figure 3.22 Amplification of genomic DNA from each species using multiplex qPCR (A). Samples were amplified in triplicate and the product was run on an agarose gel to confirm the correct size of the amplified product (Expected target size *S. gordonii* (SG)= 102 bp, *S. mutans* (SM)=111 bp, *A. oris* (AO) = 153 bp, *N. subflava* (NS) =110 bp, *V. parvula* (VP) = 88 bp). (B) Multiplex qPCR was used to amplify gDNA from a mixed species sample (Colour of amplification plot line *S. gordonii* = purple, *S. mutans* = orange, *A. oris* = yellow, *N. subflava* = dark blue, *V. parvula* = light blue).

3.3.8 Using qPCR and FISH to develop inoculation strategy

I conducted test runs of the CDC reactors to establish the early colonisers in a mixed-species biofilm. The synthetic dental biofilms were to consist of *S. gordonii*, *A. oris*, *N. subflava* and *V. parvula*. Biofilms were grown on hydroxyapatite disks and fed using AFMC medium. I used FISH and qPCR to test for the growth of these species.

After forming biofilms with the four species inoculated at different times, I determined that *A. oris* struggled to establish a mixed-species biofilm when grown with the *Streptococci*. One such test involved the inoculation of *S. mutans* and *A. oris* at the same time. *A. oris* was not detectable by FISH after 24 h (Figure 3.23A). *A. oris* has the slowest growth rate, therefore was likely to have been out-competed. When I grew a 24 h *A. oris* biofilm and then introduced *S. mutans*, both *A. oris* and *S. mutans* formed a mixed-species biofilm (Figure 3.23B). This showed that the inoculation order was very important and *A. oris* was not well suited to growing at the same time as competing species. Rather, I needed to grow *A. oris* first when attempting to establish the synthetic community biofilm. *S. mutans* must be inoculated last as I am studying the invasion of *S. mutans* into the pre-formed biofilm. When I inoculated *A. oris* first, *S. gordonii*, *N. subflava* and *V. parvula* after 24 h, and *S. mutans* 24 h later, I was able to establish the growth of a mixed species biofilm containing the whole synthetic community (Figure 3.18B).

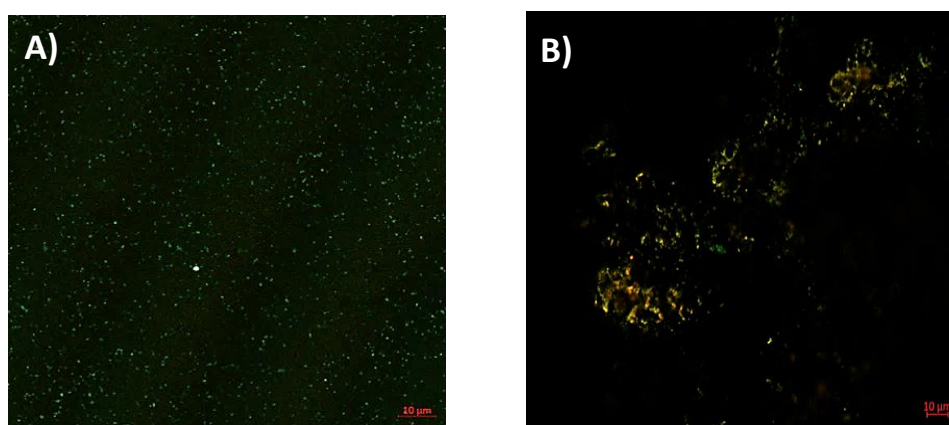


Figure 3.23 (A) Visualising *A. oris* and *S. mutans* mixed-species biofilms grown anaerobically on AFMC. When both were inoculated at the same time, *A. oris* (red) struggled to grow after 24 h. When inoculated 24 h before *S. mutans* (green), both species were established in a 48-h biofilm (B). Overlapping signals where cells grew in the same region resulted in yellow colours. This image was a maximum projection image of a z-stack.

To confirm that it was possible to enumerate all species in the synthetic community biofilm, I used qPCR to quantify the absolute cell number of each species. I grew mixed species biofilms for 72 h on AFMC in the CDC reactor, using the inoculation strategy in 3.3.8, and amplified the extracted gDNA from samples. Each CDC reactor was inoculated with 3.85×10^9 cells per species. I obtained amplification for all species (Figure 3.24). The absolute number of cells quantified per species accounted for the copy number (number of times the amplified region of genetical material repeats in the species genome). In this instance, *S. gordonii* was the most abundant species, with 3.93×10^8 cells cm^{-1} . *A. oris* was the least abundant of the synthetic community, with a cell concentration of 1.13×10^5 cells cm^{-1} , despite being inoculated first.

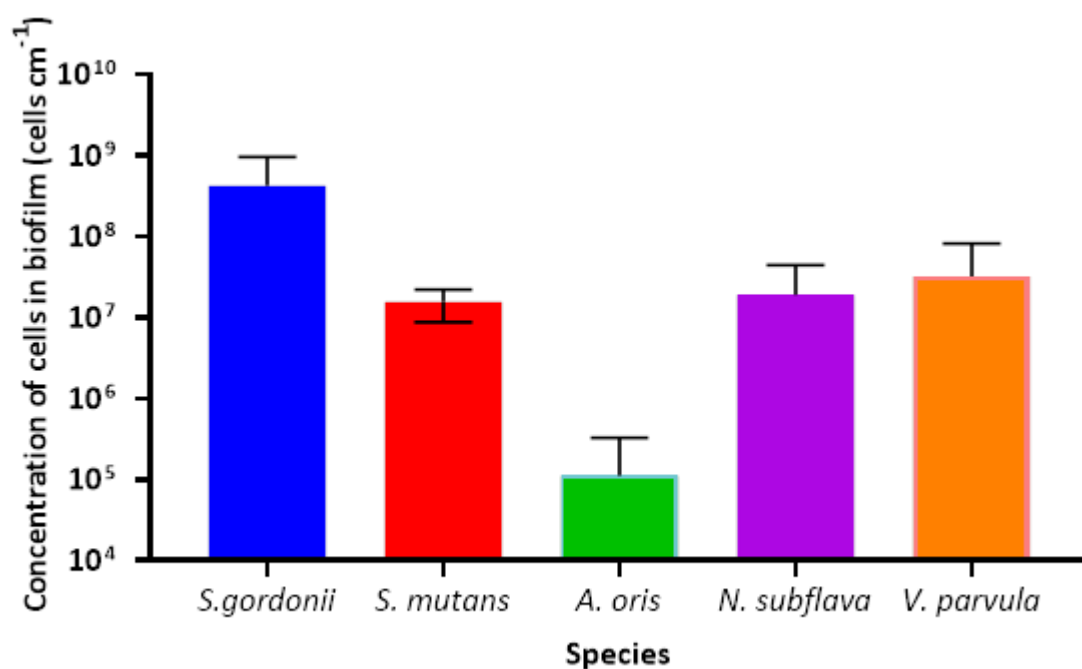


Figure 3.24. The cell concentration per 72 h biofilm was quantified using multiplex qPCR to confirm an appropriate inoculation strategy. All species were established within the biofilm, with *S. gordonii* being the most abundant. Plotted data points were the average across triplicates, with error bars representing the standard deviation from the mean.

These results confirmed an inoculation strategy whereby all species could grow together in a synthetic community biofilm for the *in vitro* system (Table 3.4). This strategy was used in future experiments using the *in vitro* system in Chapter 4.

Table 3.4 Inoculation strategy to be used for the *in vitro* experiments. I decided upon this based on roles *in vivo*, growth rate and observing their ability to establish in a mixed-species biofilm using FISH and qPCR.

| Inoculation strategy | |
|----------------------|--|
| Day | Species |
| 0 | <i>Actinomyces oris</i> |
| 1 | <i>Streptococcus gordonii</i> <i>Neisseria subflava</i> <i>Veillonella Parvula</i> |
| 2 | <i>Streptococcus mutans</i> |

3.4 Discussion

I have successfully developed a biofilm model for studying the invasion of *S. mutans* into a pre-existing 4-species early coloniser biofilm. A key step was the development of a chemically defined medium, termed AFMC, that supported the growth of all 5 species. I have obtained the kinetic parameters of the species on AFMC medium, which will be used to inform the *in silico* modelling approaches for species growth simulation in Chapter 5. Finally, I have developed key tools in assessing mixed-species biofilms and species invasion into a microbial community, including FISH and qPCR.

I selected a synthetic community of oral bacteria comprised of *S. mutans* and several early colonisers, that are known to be abundant in dental biofilms. *S. gordonii* (Salli & Ouwehand, 2015), *S. mutans* (Zhou et al., 2018) *A. oris* (Luo et al., 2022), *N. subflava* (Bradshaw & Marsh, 1998a) and *V. parvula* (Mashima & Nakazawa, 2015a), have all been used in previous models to characterise dental biofilms. There have also been models that have used a combination of these commensal species and *S. mutans* within the same model (Chatzigiannidou et al., 2020b). Despite a significant number of synthetic communities assembled for dental biofilm research, there has not been one used to track the transition of a commensal dental biofilm to a cariogenic state, in a defined environment, using an *in vitro-in silico* combinatorial approach. This unique 5-species community allowed me to track the invasion of *S. mutans*

over time, quantifying the abundance of each species, and the effect on substrate concentration *in vitro* (Chapter 4). It also allowed me to simulate the abundances, substrate and pH impact *in silico* (Chapter 5), with the *in silico* models informed by synthetic community kinetic parameters collected experimentally in this chapter, and validated by the reactor results in Chapter 4.

I developed AFMC by advancing a previously assembled chemically defined medium (Terleckyj et al., 1975) to support the growth of this synthetic community. There were other CDM produced for oral species, (Socransky et al., 1985), but FMC was chosen due to it supporting the oral *Streptococci* used in this research and having been previously used by my research group. Despite FMC being rich in nutrients, the chemical demand of oral bacteria is complex and diverse, therefore explaining why growth was not successful for the whole synthetic community. This was evident by the omission of putrescine from AFMC not allowing for the growth of *V. parvula*, which is known to be an important component of the cell wall (Gronow et al., 2010a). Upon formulation, I was able to use AFMC as the foundation for all the characterisation experiments in this Chapter and invasion experiments in Chapter 4. The advantages of having a CDM were apparent through the experiments in this Chapter. I was able to input AFMC into the metabolic modelling to show me fluxes for each species, which helped me finalise the AFMC. I was also able to determine more about my species by using AFMC, including substrate usage. Developing AFMC allowed me to grow the synthetic community in a defined environment in the *in vitro* colonisation experiments and study the influence of one parameter at a time (Chapter 4). It also underpinned the defined stoichiometry and kinetics used *in silico* in Chapter 5. The use of FBA (using KBase) was a useful tool in validating experiments in the development of AFM. The metabolic analysis confirmed that both putrescine and lactic acid were needed for *V. parvula* growth. FBA helped determine which chemicals were missing from the medium, as was cross-referencing other chemically defined media for the other species. Further work with KBase would be useful in directing the development of a minimal medium, as has been done for *S. mutans* (Mazumdar et al., 2009b). This would have saved preparation time and cost over using a medium as rich as AFMC. The use of FBA should be used further to characterise the synthetic community. This will help better understand factors that contribute towards *S. mutans* invasion and the effect of the synthetic community on the local environment i.e., acid production (beyond lactic acid) that contribute towards pH decrease. Approaches have already been developed using

constraint-based FBA, that can predict metabolic fluxes, community growth rates and fractional biomass abundance within microbial communities (Khandelwal et al., 2013).

My growth curves and K_s experiments showed that the species have very different growth profiles but consume similar substrates. For example, *S. gordonii* has a growth rate over double that of *A. oris*, at 0.492 h^{-1} vs 0.227 h^{-1} . The superior growth rate of oral *Streptococci* has been observed before (Beckers, 1982). *S. gordonii* and *A. oris* both consume glucose as a primary carbon source, as do *S. mutans* and *N. subflava*. The preference for glucose as a carbon source for oral species, e.g., *Streptococci*, is well known (Willenborg & Goethe, 2016a). My results showed that there would be competition for glucose in a mixed system as all species consumed glucose, excluding *V. parvula*, although *N. subflava* was able to grow without glucose present. The *Streptococci* would have a competitive advantage due to how fast they grow. My substrate experiments showed that *S. mutans* grew differently when grown on sucrose, with the cells aggregating together. This was a phenomenon that has been seen before (H. Zhang et al., 2022). I, therefore, expected that *S. mutans* would have a competitive advantage when I ran my *in vitro* experiments using sucrose, compared to one using glucose, in Chapter 4. This meant, when evaluating colonisation in the sucrose-fed reactor system, nutrient availability and growth rate were not the only factors to be considered. *V. parvula*, despite having one of the lower growth rates, has an advantage over the other species in that it consumes lactic acid for growth, not glucose, therefore not having the same competition for the primary carbon source. This is already a well-known characteristic of *V. parvula* (Periasamy & Kolenbrander, 2010). Also, the production of lactic acid by oral species, as seen in literature with *S. mutans* (Baker et al., 2017b) suggested *V. parvula* could grow on the by-products of the other community members from fermentation which would help in providing a growth nutrient.

I have also shown the synthetic community species were impacted differently by acidic conditions, by observing their decrease in maximum $\text{OD}_{600\text{nm}}$ reached, at different starting pH of AFMC. I observed they have different acid production levels on AFMC. This was very important for several reasons. As a cariogenic biofilm develops *in vivo*, the environment becomes more acidic. Species that have shown a higher acid tolerance were more likely to thrive than those that struggle at a low pH. My experiments showed that *S. mutans* grew better at a low pH compared to the other species. *S. mutans* reached an $\text{OD}_{600\text{nm}}$ of 0.755 at a pH of 5.5, whereas the next highest $\text{OD}_{600\text{nm}}$ reached was by *S. gordonii* at 0.176. *S. mutans*

has been seen previously to have an acid adaptation response. This species can alkalinize the cytoplasm to reduce cell stress (Baker et al., 2017a) and has a lower optimal pH for F-ATPase, which is responsible for generating ATP. F-ATPase is also upregulated in acidic conditions for *S. mutans* (Kuhnert et al., 2004). This could explain why *S. mutans* grew to a higher OD_{600nm} in Section 3.3.5. *S. mutans* exhibits further acid tolerance as a biofilm (McNeill & Hamilton, 2003a) and was therefore likely to thrive in the synthetic community biofilm in an acidic system, compared to the other oral species. Whilst *V. parvula* grew to a higher OD_{600nm} than the other synthetic community members (excluding *S. mutans*), it still struggled at pH of 5.5 and 5. This is despite previous studies finding that *V. parvula* is resistant to low pH environments and has been found in a high abundance within carious sites at pH 5.5 and below (Do et al., 2015). The finding in this study, that the histidine biosynthetic pathway was elevated in low pH-caries regions, suggests that histidine could have provided a greater intracellular buffering capacity for this species in saliva.

It was very important to understand the contribution of each species to the pH of the environment. This is because teeth will demineralise when exposed to excess acids produced by bacteria, past a certain pH. Whilst the pH resulting in demineralisation varies depending on factors such as the calcium and phosphate ion concentration, it occurs at pH of around 5.5 (Dawes, 2003.). My results showed that all species produce a large amount of acid, as indicated by the drop in pH of the growth medium. *S. mutans* dropped the pH the most, down to 4.94 from a starting pH of 7. *V. parvula* was the least acid-producing species. This is not surprising as *V. parvula* consumes lactic acid to produce weaker acids, namely propionic acid, and formic acid (Prasetianto Wicaksono et al., 2020). The reduction in pH of AFMC resulting from the growth of *V. parvula* was surprising but could be due to the carbon dioxide fixation (Zhou et al., 2021b). Overall, this data explained why *S. mutans* is implicated in caries, as it is adapted to grow at a low pH, significantly contributes to a low pH environment through acid production and would produce an environment for the growth of aciduric species. The drop in pH also demonstrated that the buffering capacity of the medium could not balance the pH against the amount of acid produced by the species. This is despite the AFMC being rich in phosphate buffers, which is effective at buffering between a pH 5.8-8 (Ganesh et al., 2017).

The development of qPCR and FISH helped to better define species characteristics in Chapter 4, including the inability of *A. oris* to establish in a mixed-species biofilm which has been seen previously (Jakubovics et al., 2008) This allowed me to confirm their enumeration within the

biofilm in Chapter 4. Having so many fluorophores did present the challenge of overlapping excitation and emission wavelengths but obtaining spectral fingerprint profiles for each species helped reduce the impact that this had. However, there was still bleed-through of the Alexa 405 blue dye, attached to *N. subflava*, limiting FISH as a quantitative tool in its current form. This showed that given more time, further optimisations, such as that done by Valm et al., (2012) are necessary to make the most out of this technique.

The development of a qPCR protocol was key in tracking the colonisation of *S. mutans* and the abundance of the commensal species over time in Chapter 4. The quantitative data provided by qPCR was essential in comparing to *in silico* simulations in Chapter 5 and has been lacking in other oral models (Thurnheer et al., 2004b). It took numerous stages to be able to quantify species using multiplex qPCR, from primer design and cloning in amplified targets, to altering the qPCR run parameters. Being able to multiplex was very helpful as I needed to sample from the biofilms and the planktonic bulk from three reactors on multiple sampling occasions. This technique made the method far more manageable. One disadvantage of this qPCR method is that it does not show the viability of the samples from the reactors, as it only quantifies DNA. I, therefore, needed to use live/dead analysis using flow cytometry at the end of my reactor run in Chapter 4. This showed how viable the system was. The use of this method in this research did not differentiate viability between species but identified the conditions in the synthetic community biofilms thrived in.

By using FISH and qPCR, I was able to establish an inoculation strategy suitable for the invasion experiments (Chapter 4). Through imaging using FISH, I demonstrated that *A. oris* formed a robust biofilm, it struggled to establish itself in a mixed-species biofilm if it is inoculated at the same time as a faster-growing species, such as *S. mutans*. *A. oris* had the least number of cells in the synthetic community biofilm after 72 h of growth on the hydroxyapatite coupon, despite being inoculated first, as seen in Section 3.3.8, showing that *A. oris* needs to be introduced first. This was likely due to *A. oris* having much lower growth rates whilst competing for glucose. *A. oris* has been known to struggle in mixed-species systems, where the production of hydrogen peroxide by species i.e., *S. gordonii* can significantly reduce the ability of *A. oris* (*A. naeslundii*) to grow, with cell numbers found to be >90% lower in mixed culture vs monoculture after 24 h (Jakubovics et al., 2008). It is justifiable to introduce *A. oris* first as it was a known early coloniser of freshly cleaned teeth *in vivo* (Palmer et al., 2003). The results

showed the importance of techniques e.g., qPCR and FISH in determining inoculation strategies for mixed-species biofilms.

Having developed the tools to establish and monitor the development of mixed-species biofilms, the next section of work (Chapter 4) aimed to investigate the impact of different carbohydrate concentrations on *S. mutans* invasion and the effect of the synthetic community growth on the local environment, including pH.

Chapter 4. *In vitro* modelling approaches to characterise the invasion of *Streptococcus mutans* into an oral commensal community

4.1 Introduction

The invasion and overpopulation of *Streptococcus mutans* into dental biofilms has been associated with the progression of caries and increased risk of cavities (Nomura et al., 2020). This is directly related to environmental conditions. *S. mutans* is well adapted to high-sugar, low-pH environments (Baker et al., 2017a), particularly when a large amount of sucrose is present. This shifts the composition of the oral microbiota (Angarita-Díaz et al., 2022). *S. mutans* utilises sucrose to produce intracellular and extracellular polysaccharides that give it a competitive advantage in biofilm formation (Costa Oliveira et al., 2021b). The dominance of *S. mutans* in dental biofilms has been associated with the presence of other caries-related species within the biofilm, that thrive in a low-pH environment (van Ruyven et al., 2000) (Lamont et al., 2018). For these reasons, the development of models to characterise *S. mutans* invasion in the dental biofilm is of great importance, particularly as caries is a global burden on billions of people (Kassebaum et al., 2017).

Acid production by oral bacteria alters the pH of the oral environment, which favours aciduric species and can change the microbial composition within dental biofilms. By-products of sugar fermentation by oral bacteria, including lactic acid, can drive the composition of the oral microbiota towards lactic acid-consuming bacteria i.e., *V. parvula* (Mashima et al., 2016). *V. parvula* protects cariogenic species e.g., *S. mutans*, through catalase activity that reduces the antibacterial effects of hydrogen peroxide, produced by commensal microbes such as *S. gordonii* (Liu et al., 2020, Zhou et al., 2017). Overall, this demonstrates that substrate availability is important in understanding the microbial composition of dental biofilms. It is also important to characterise what conditions contribute to the invasion and prevalence of cariogenic species in the oral microbiota, including *S. mutans*. These factors *in vivo*, which can be understood through *in vitro* modelling approaches, are necessary for understanding what protection and environment is needed for commensal species and preventing the overpopulation of caries-contributing species.

Synthetic communities have been used to study dental biofilm growth and *S. mutans* invasion. Mono and dual-species models have been used extensively to better understand what factors

may influence this colonisation (Díaz-Garrido et al., 2020). These do not efficiently explore the complex interaction between species and are too simple to represent the oral microbiome, which consists of over 700 species (Kilian et al., 2016). More complex communities have been developed to represent the dental biofilm, including the use of 14 species systems, to test the probiotic effect of glycerol in a mixed-species biofilm (van Holm et al., 2022).

Growth models used to study these synthetic communities include closed systems i.e., microtiter plates. This provides a low-cost model, which has been used to grow *S. mutans* and *P. gingivalis*, and to test the antimicrobial effect of chlorohexidine. CSTR reactor systems have been used that enable control of operating variables in a way that is not possible with closed models. This includes setting the flow rate of media fed into the model to mirror that of salivary flow. One CSTR model recently used for dental biofilm research was the CDC reactor. This has been used to test the adhesion of *S. mutans* in dental biofilms developed on orthodontic brackets (Park et al., 2022). The CDC reactor has been used by An (2022), to successfully grow, maintain and test the reproducibility of diverse oral microbiota. This was operated under conditions mimicking the oral environment, including using a flow rate of medium at 0.5 mL min^{-1} , similar to that of saliva, and using hydroxyapatite disks, mimicking the enamel surface. These models employed complex media. The use of a CDM can simplify the chemical environment (Fontana et al., 2000) (Edlund et al., 2013), and helps test dental biofilm activity and invasion whilst changing one parameter at a time.

Collecting data from these mixed-species models requires the refinement of molecular and microscopic techniques. The use of qPCR is beneficial in quantifying the change in the abundance of species in dental biofilms, including the prevalence of *S. mutans* (Suzuki et al., 2005). Imaging complex mixed-species biofilms, to identify bacterial species prevalence and provide structural information, can be challenging. The implementation of *fluorescence in situ hybridization* (FISH), refined further for multi-species analysis, helped circumvent these issues (Thurnheer et al., 2004). This, however, did not give information on the viability of bacterial cells, which can vary significantly depending on environmental factors, including pH (Lund et al., 2014). To assess this, the live:dead ratio of dental biofilm cells can be quantified using flow cytometry (Grainha et al., 2020).

The use of *in vitro* oral models allows for validating *in silico* modelling approaches, by testing invasion in mixed-species biofilm, and comparing the experimental data with the simulation

results. Furthermore, *in silico* models are cost and time efficient in directing the *in vitro* experimental approaches before they are carried out (Herzog et al., 2017). This means that mixed modelling approaches can be used to better understand the factors underpinning *S. mutans* invasion of dental biofilms, without the invasive and ethical implications associated with animal and human models (Levy, 2012).

4.2 Aims and objectives

In this Chapter, I aimed to characterise the factors underpinning *S. mutans* invasion of a 4-species, commensal community of oral bacteria. I also aim to understand how these factors affected the early colonisers within the dental biofilm. I aimed to develop an *in vitro* CSTR reactor model to quantify the invasion of *S. mutans* into a commensal dental biofilm, and the effect on the local environment i.e., pH change, over time. The 5-species synthetic community was grown on AFMC in a defined system, where variables i.e., temperature and flow rate were controlled to reflect the *in vivo* environment. Different glucose and lactic acid concentrations, as well as sucrose, were tested to evaluate their influence on invasion.

- 1) Characterise the effect of synthetic community growth in the reactor on the local environment. Invasion experiments were tested at varying glucose and lactic acid concentrations, as well as on sucrose. This included quantifying the turbidity of the bulk, substrate consumption/production and pH.
- 2) At these substrate concentrations, quantify *S. mutans* invasion into the commensal biofilm and bulk, over time using qPCR. This included quantifying the change in early coloniser species abundance.
- 3) Observe any spatial-temporal patterns within the synthetic community biofilm and confirm species presence using FISH.
- 4) Ascertain how decreasing the glucose and lactic acid concentrations affect the viability of the synthetic community biofilm using flow cytometry.

4.3 Results

4.3.1 Description of *in vitro* invasion experiments

I quantified the invasion of *S. mutans* into the 4-species oral community, in both high and low glucose/lactic acid environments, to understand the influence of the chemical environment on invasion. The glucose and lactic acid concentrations used were selected based on the experiments in Chapter 3. After these experiments, I tested *S. mutans* invasion on AFC supplemented with sucrose, rather than glucose. This was to determine if the competitive advantage that *S. mutans* has when grown on sucrose, including EPS production and increased adhesion (H. Zhang et al., 2022; Kreth et al., 2008), restored the ability of *S. mutans* to dominate the synthetic community biofilm at low substrate concentrations. The substrate concentrations used in each reactor experiment were detailed along with the starting pH of the bulk, in Table 4.1.

Table 4.1 Reactor experiment conditions used in this Chapter. Experiments 1 (high glucose, high lactic acid) and 2 (high glucose, intermediate lactic acid) were at high glucose concentrations. Reactor experiments 3 (low glucose, high lactic acid) and 4 (low glucose, low lactic acid) were at low glucose concentrations. Reactor 5 (low sucrose, low lactic acid) contained sucrose instead of glucose. The lactic acid concentrations were high in experiments 1 and 3, intermediate in run 2 and low in runs 4 and 5. The starting pH was similar across all simulation runs.

| | Glucose concentration (gL ⁻¹) | Lactic acid concentration (gL ⁻¹) | Sucrose concentration (gL ⁻¹) | Starting pH |
|-------------------------|---|---|---|-------------|
| Reactor experiment 1 | 21.85 | 11.61 | - | 6.92 |
| Reactor experiment 2 | 21.30 | 6.28 | - | 6.82 |
| Reactor experiment 3 | 2.09 | 12.46 | - | 6.94 |
| Reactor experiment 4 | 1.98 | 2.61 | - | 6.93 |
| Reactor experiment 5 | - | 2.60 | 1.92 | 7.0 |

I operated the CDC *in vitro* model under parameters that mimicked the oral environment. This included using a flow rate of 0.4 mL min⁻¹ resembling the flow of saliva (Iorgulescu, 2009), and using hydroxyapatite coupons as a growth substrate to mimic the enamel surface (Habibah et al., 2022). The temperature of the reactors was maintained at 37 °C, similar to that of the oral environment (Sund-Levander et al., 2002), using a hot plate and insulation. Each reactor was inoculated with 3.85 x10⁹ cells per species. The only species present within the first 24 h was *A. oris*. *S. gordonii*, *N. subflava* and *V. parvula* were added 24 h later, with *S. mutans* added at 48 h. FISH and qPCR were used to quantify species abundance change over the course of the 9-day experiment. The effect on the local environment, including the change in pH of the bulk, was examined. Furthermore, the viability of the synthetic community at the end of the experiment was quantified using flow cytometry. An overview of the experimental design was detailed in Figure 4.1.

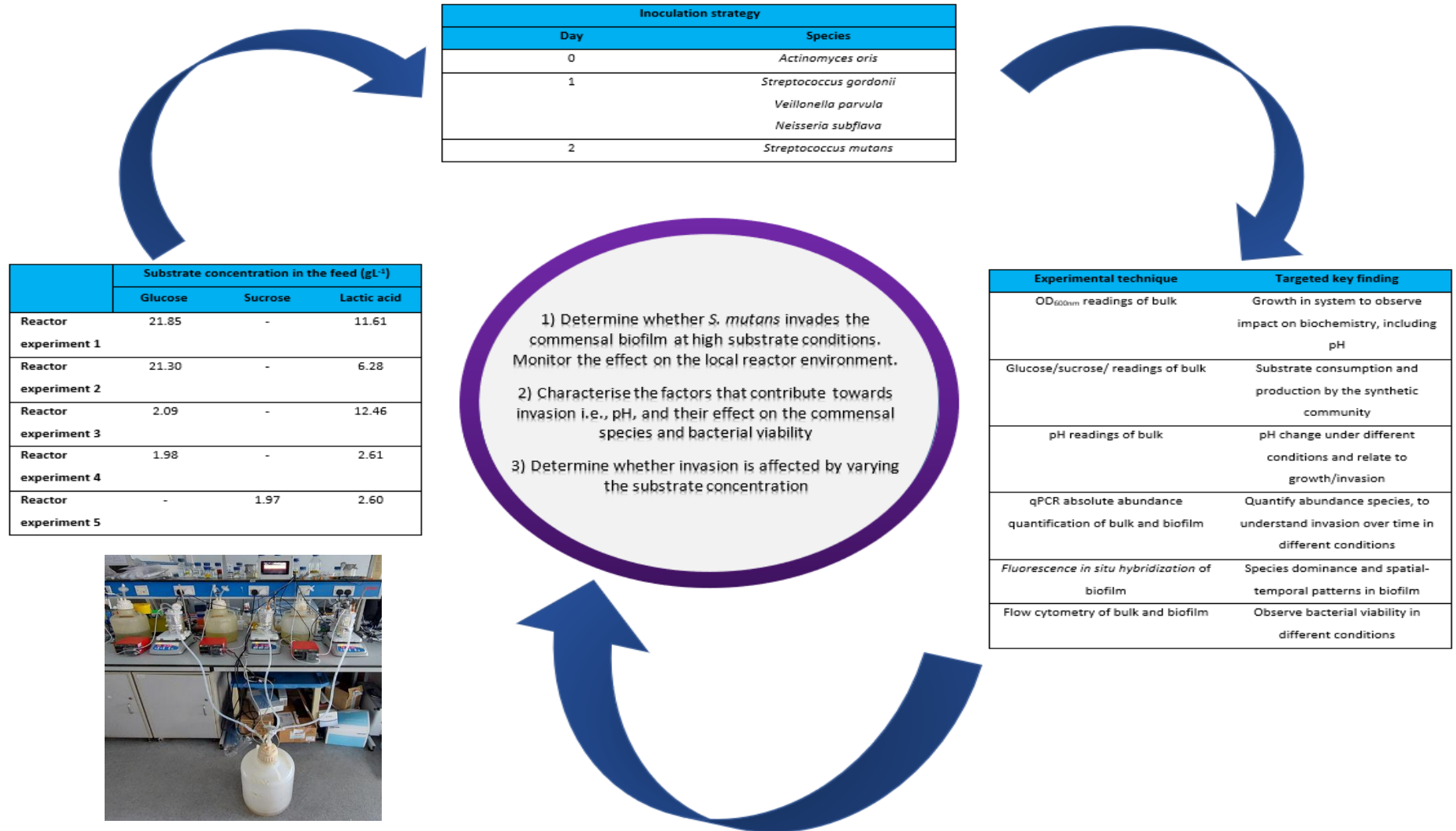


Figure 4.1 Overview of the reactor strategy and goals of this Chapter. The glucose and lactic acid concentrations were varied in AFM. *S. mutans* invasion, using the same inoculation strategy for all runs, was analysed using techniques i.e., qPCR and FISH. The end goal was to characterise *S. mutans* invasion into the commensal dental biofilm and understand the factors that drive this.

4.3.2 Observing turbidity of the reactor bulk over time

I measured the turbidity of the reactor bulk over 9 days. A decrease in optical density over time would have indicated that planktonic growth, was less than the amount of biomass washed out of the system. The bacterial turbidity was compared across experiments to understand the effect of glucose and lactic acid concentration on growth. In reactor experiment 1 (high glucose, high lactic acid), an OD_{600nm} of 1.3 was reached after day 1 (Figure 4.2), attributed to *A. oris* growth. On day 2, a peak OD_{600nm} of 1.57 was reached. Throughout the rest of the nine-day experiment, the OD_{600nm} dropped significantly and reached a low of 0.73 by day 9. The largest drop in OD_{600nm} was observed between days 3 and 5, where the OD_{600nm} dropped from 1.29 to 0.92.

For reactor experiment 2 (high glucose, intermediate lactic acid), a lower OD_{600nm} of 0.9 on day 1 was recorded. For this experiment, the maximum OD_{600nm} was also reached on day 2. This value of 1.60, was similar to that reached at the higher lactic acid concentration (1.57). For reactor experiment 2, the OD_{600nm} also dropped over time. There was a decrease between days 2 and 5, from 1.60 to 0.73. There was a steady decline down to day 9, where the lowest OD_{600nm} of 0.58 was recorded.

For reactor experiment 3 (low glucose, high lactic acid), the decrease in glucose concentration had a significant effect on the turbidity of the bulk. Here, an OD_{600nm} of 1.35 was reached after day 1 and a peak OD_{600nm} of 1.63 on day 2. This was similar to the two previous experiments (1.57 and 1.60 respectively). However, at the lower glucose concentration, the OD_{600nm} remained high throughout the remainder of the experiment. By day 9, the OD_{600nm} was 1.48, over twice as high as the OD_{600nm} reached at the higher glucose concentration experiments. This indicated that the bacterial growth was higher at the lower glucose concentration than at the higher glucose concentration, most likely due to the higher pH resulting in less cell stress (Figure 4.5).

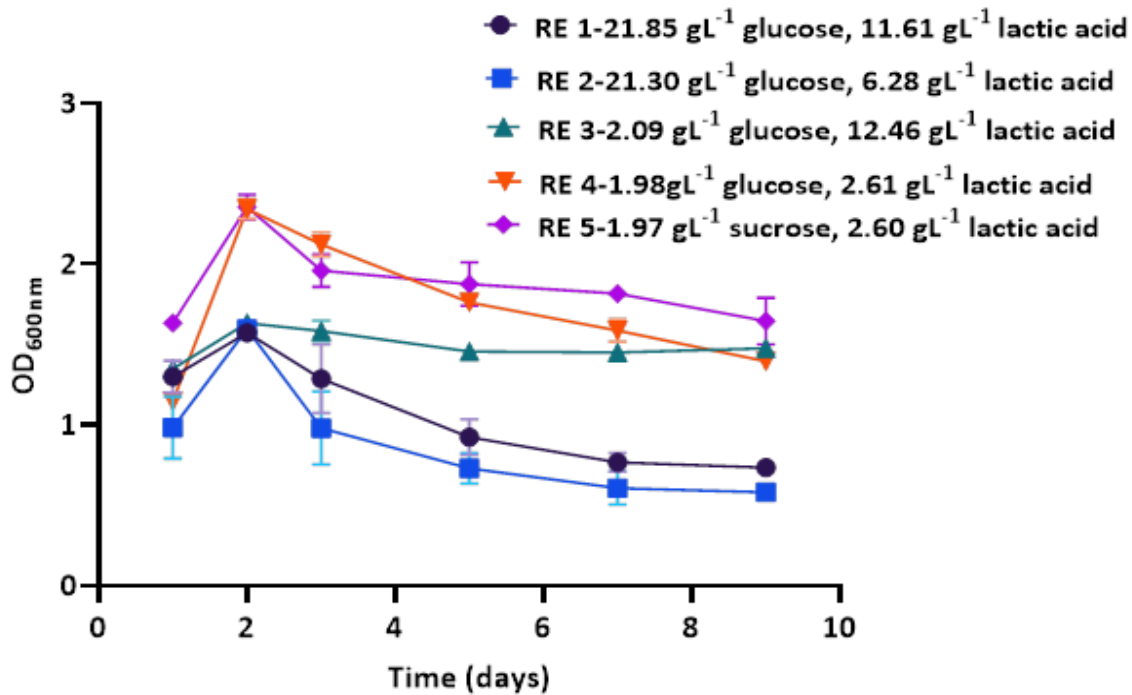


Figure 4.2. The OD_{600nm} readings were recorded over 9 days for the reactor experiments (RE). The OD_{600nm} reached a peak on day 2 for all conditions. It dropped significantly at high glucose concentrations (RE 1 and 2) but stayed at high levels at low glucose/sucrose levels (RE 3,4 and 5). Plotted data points were the mean of three CDC reactor conditions and the error bars represented the standard deviation from the mean.

For reactor experiment 4 (low glucose, low lactic acid), lowering both the glucose and lactic acid concentration led to significantly higher turbidity of the bulk, compared to the high glucose experiments. The OD_{600nm} reached 1.15 after day 1, and a high of 2.34 after day 2. This was higher than any OD_{600nm} recorded from reactor runs where AFMC contained glucose. There was a significant decrease in OD_{600nm} between days 2 and 5, from 2.34 to 1.76. The OD_{600nm} decreased to 1.40 on day 9. This was still higher than the high glucose experiments and similar to that of reactor experiment 3 (low glucose, high lactic acid).

In reactor experiment 5 (low sucrose, low lactic acid), the *in vitro* system was run on AFMC containing sucrose rather than glucose. The OD_{600nm} increased from 1.63 on day 1, to 2.36 on day 2. This was the highest OD_{600nm} reached across all experiments and meant that for all experiments, the peak OD_{600nm} was reached on day 2. The OD_{600nm} decreased from 2.36 on day 2, to 1.88 on day 9. The OD_{600nm} then decreased over time down to 1.65 by day 9. This was the highest OD_{600nm} recorded on day 9 for any experiment. A summary of OD_{600nm} readings across the experiments can be seen in Table 4.2.

Table 4.2 A summary of the OD_{600nm} readings across all reactor experiments. High turbidities were reached across all conditions, but the OD_{600nm} dropped from day 2 onwards, particularly for the high glucose conditions (reactor experiments 1 and 2). All values were the mean across readings from three CDC reactor runs, with standard deviations from the mean also detailed.

| | Reactor experiment 1 | Reactor experiment 2 | Reactor experiment 3 | Reactor experiment 4 | Reactor experiment 5 |
|--|----------------------------|----------------------------|----------------------------|----------------------------|----------------------------|
| Day 2-Highest OD _{600nm} reached | 1.57 ± 0.05 | 1.60 ± 0.03 | 1.63 ± 0.04 | 2.34 ± 0.06 | 2.36 ± 0.08 |
| Day 9- Final day OD _{600nm} | 0.73 ± 0.02 | 0.58 ± 0.03 | 1.48 ± 0.02 | 1.40 ± 0.05 | 1.65 ± 0.15 |

4.3.3 Quantifying the glucose and sucrose concentration of the reactor bulk over time

I aimed to understand the ability of *S. mutans* to invade the synthetic community biofilm under different glucose concentrations. This included determining the difference in invasion between a glucose-rich environment and one where this carbon source was limited. Furthermore, I was interested in whether this invasion was more effective when the carbon source was switched from glucose to sucrose, where *S. mutans* has previously been shown to have a competitive advantage over other species (see Chapter 1). In reactor experiment 1 (high glucose, high lactic acid), glucose was consumed in the first 24 h, decreasing from 21.85 gL⁻¹ to 15.15 gL⁻¹ on day 1 (Figure 4.3) when only *A. oris* was inoculated. The glucose concentration decreased to 5.73 gL⁻¹ on day 2. The lowest glucose concentration recorded for this experiment was 3.93 gL⁻¹ on day 3, 24 h after the introduction of *S. mutans*. The glucose concentration then increased over time, reaching 9.02 gL⁻¹ on day 9. This showed that the glucose concentration for this experiment was in excess at all times in the samples recorded.

I observed a similar pattern in the glucose concentration of the bulk for reactor experiment 2 (high glucose, intermediate lactic acid). Here, levels dropped to 14.36 gL⁻¹ on day 1, then down to a low of 5.21 gL⁻¹ on day 2. The concentration increased over time to 10.93 gL⁻¹ on day 9. This showed that whilst the synthetic community used a significant amount of glucose,

particularly in the first 48 h of the invasion experiment, the glucose concentration was still in excess. There was a drop in biomass (Figure 4.2) from day 3 onwards, leading to less glucose consumption. This explained why there was an increase in glucose concentration over time, as AFMC was still fed into the system.

In reactor experiment 3 (low glucose, high lactic acid), glucose became a limiting substrate. The glucose concentration dropped to 0.143 gL^{-1} on day 1. The concentration dropped to 0.078 gL^{-1} on day 2 and remained below 0.1 gL^{-1} for the remainder of the 9-day experiment. This showed that the glucose being supplied to the reactors was depleted by the synthetic community. This also occurred in reactor experiment 4 (low glucose, low lactic acid). The starting glucose concentration of 1.984 gL^{-1} dropped to 0.983 gL^{-1} on day 1, then down to 0.073 gL^{-1} by day 2. The glucose concentration in this experiment also remained below 0.1 gL^{-1} for the remainder of the experiment, with a final concentration of 0.04 gL^{-1} .

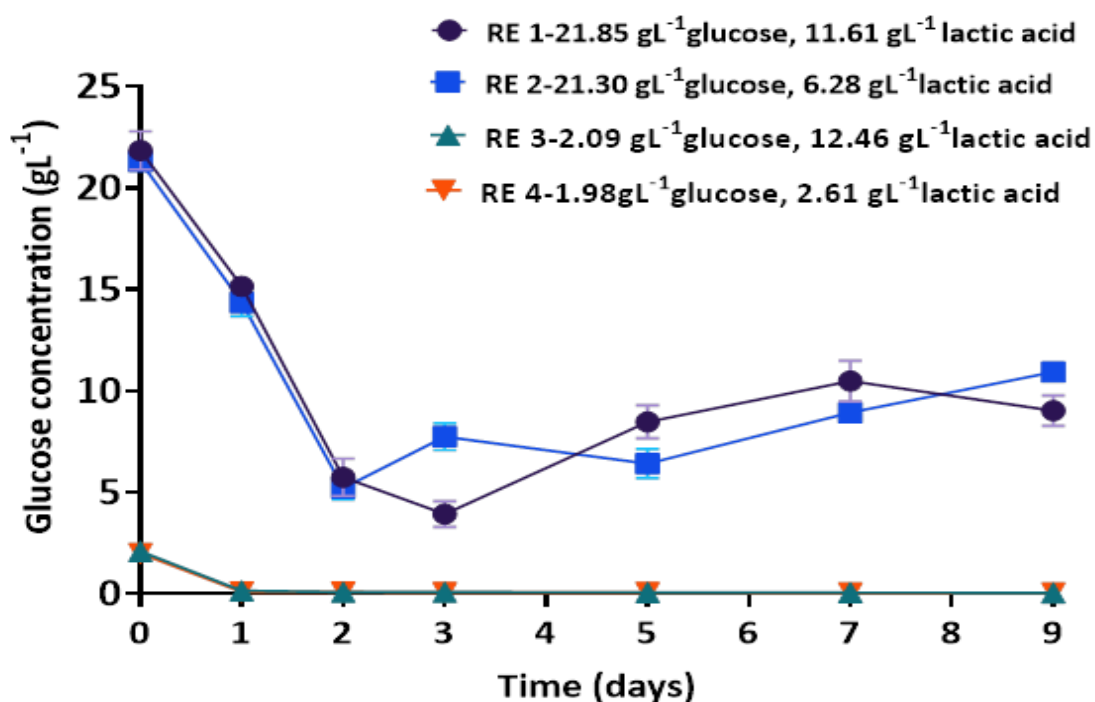


Figure 4.3 The change in glucose concentration in the reactor bulk over time for all reactor experiments (RE). The substrate concentration was in excess for RE 1 (high glucose, high lactic acid) and RE 2 (high glucose, intermediate lactic acid), but depleted for the rest. In all cases, the concentration dropped significantly within the first 48 h. All plotted points were the average of triplicate reactor readings, and the error bars represented the standard deviation from the mean.

In reactor experiment 5 (low sucrose, low lactic acid), the sucrose concentration for the fifth reactor concentration was at 1.92 gL⁻¹, chosen to give a similar carbon source concentration to the runs with low glucose. The sucrose concentration dropped to 0.097 gL⁻¹ by day 1 and stayed below 0.1 gL⁻¹ for the remainder of the experiment. The sucrose concentration was therefore also a limiting carbon source in this environment. A summary of the carbon source concentrations can be seen in Table 4.3.

Table 4.3. A summary of the glucose concentrations across all reactor experiments. Glucose was in excess in reactor experiments 1 (high glucose, high lactic acid) and 2 (high glucose, intermediate lactic acid). It was depleted by the synthetic community by day 2 for reactor experiments 3 (low glucose, high lactic acid) and 4 (low glucose, low lactic acid). The values were the mean across readings from three CDC reactor runs, with standard deviations from the mean detailed.

| | Reactor experiment 1 | Reactor experiment 2 | Reactor experiment 3 | Reactor experiment 4 |
|---|---------------------------------|---------------------------------|---------------------------------|---------------------------------|
| Day 0- Starting glucose concentration | 21.85 ± 0.94 | 21.30 ± 0.41 | 2.09 ± 0.18 | 1.98 ± 0.04 |
| Day 9- Final glucose concentration | 9.02 ± 0.76 | 10.93 ± 0.43 | 0.04 ± 0.01 | 0.04 ± 0.01 |

4.3.4 Quantifying the lactic acid concentration of the reactor bulk over time

I quantified the concentration of lactic acid in the reactor bulk under the different conditions tested in the *in vitro* model. It was important to quantify change over time as lactic acid is produced in abundance by oral species, including the *Streptococci* in this study (See Chapter 1,). Furthermore, it is the primary substrate consumed by *V. parvula*. Therefore, monitoring its concentration in the bulk gave an indication of the balance between production from *Streptococci* and consumption by *V. parvula*. I compared this against the species relative abundance.

In reactor experiment 1 (high glucose, high lactic acid) the lactic acid concentration dropped significantly from 11.61 gL⁻¹ to 3.47 gL⁻¹ after 24 h (Figure 4.4). For the remainder of the experiment, the lactic acid concentration ranged between 4.03 gL⁻¹ recorded on day 2 and 3.97 gL⁻¹ on day 9. The lactic acid concentration was therefore in excess during this reactor experiment.

In reactor experiment 2 (high glucose, intermediate lactic acid), there was a significant difference in the resulting lactic acid concentration. The lactic acid concentration dropped after 24 h, from 6.8 gL⁻¹ to 4.72 gL⁻¹, but subsequently increased over time. On day 2, the concentration increased to 8.79 gL⁻¹ and remained stable up until day 7, when the concentration recorded was 8.64 gL⁻¹. The lactic acid concentration increased to 10.31 gL⁻¹ on day 9. This was the highest concentration of lactic acid recorded for this experiment. It was also more than double the concentration recorded at the end of reactor experiment 1 (high glucose, high lactic acid), where the lactic acid concentration was 3.97 gL⁻¹. This was despite the starting concentration of lactic acid for reactor experiment 2 (high glucose, intermediate lactic acid) being half that of the previous experiment.

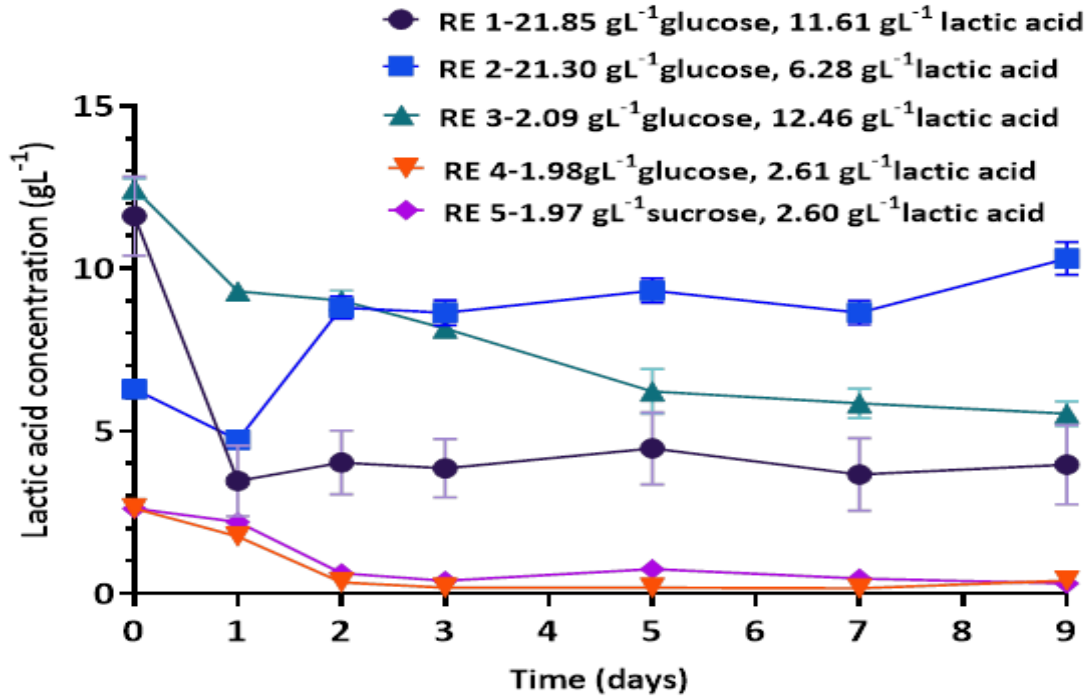


Figure 4.4 The change in lactic acid concentration in the reactor bulk over time for all reactor experiments (RE). The substrate concentration was in excess for RE 1 (high glucose, high lactic acid), RE 2 (high glucose, intermediate lactic acid) and RE 3 (low glucose, high lactic acid). The lactic acid concentration was depleted by day 2 for RE 4 (low glucose, low lactic acid) and RE 5 (low sucrose, low lactic acid). All plotted points were the average of triplicate reactor readings, and the error bars represented the standard deviation from the mean.

In reactor experiment 3 (low glucose, high lactic acid), the lactic acid concentration decreased from 12.46 gL⁻¹ to 9.30 gL⁻¹ on day 1. The lactic acid continued to decrease throughout the remainder of the experiment. On day 3, the lactic acid concentration was 9.12 gL⁻¹. This decreased over time to 5.53 gL⁻¹ by day 9, the end of the experiment.

In reactor experiment 4 (low glucose, low lactic acid), the lactic acid concentration decreased to 2.21 gL⁻¹ after day 1 and further to 0.63 gL⁻¹ by day 3. This was the lowest lactic acid concentration recorded on day 3 for any of the conditions tested. Lactic acid levels dropped further until day 7, where the concentration was 0.16 gL⁻¹. This was the lowest concentration measured on any day for any experiment. The lactic acid concentration increased back up to 0.40 gL⁻¹ on day 9 of the *in vitro* experiment for this condition.

In reactor experiment 5 (low sucrose, low lactic acid), lactic acid became a limiting nutrient. The lactic acid concentration dropped to 2.21 gL⁻¹ on day 2 and decreased significantly by day 2, to 0.63 gL⁻¹. The concentration recorded was 0.39 gL⁻¹ by day 4, before increasing to 0.75 gL⁻¹ by day 5. The lactic acid levels dropped until the end of the experiment until day 9, where the concentration measured was at 0.31 gL⁻¹. This was the lowest value recorded on day 9 compared to all of the other reactor experiments tested (Table 4.4).

Table 4.4. A summary of the lactic acid concentrations across all reactor experiments. Lactic acid was in excess in reactor experiments 1 (high glucose, high lactic acid), 2 (high glucose, intermediate lactic acid) and 3 (low glucose, high lactic acid). It was depleted by the synthetic community by day 2 for reactor experiments 4 (low glucose, low lactic acid) and 5 (low sucrose, low lactic acid). All values were the mean across readings from three CDC reactor runs.

| | Reactor experiment 1 | Reactor experiment 2 | Reactor experiment 3 | Reactor experiment 4 | Reactor experiment 5 |
|---|----------------------------|----------------------------|----------------------------|----------------------------|----------------------------|
| Day 0- Starting lactic acid concentration | 11.61 ± 1.22 | 6.28 ± 0.29 | 12.46 ± 0.32 | 2.61 ± 0.09 | 2.60 ± 0.09 |
| Day 9- Final lactic acid concentration | 3.97 ± 1.23 | 10.31 ± 0.51 | 5.53 ± 0.39 | 0.41 ± 0.02 | 0.31 ± 0.01 |

4.3.5 Quantifying changes in the pH of the reactor bulk over time

The pH is a key contributor to tooth demineralisation *in vivo*. Monitoring the pH in the reactor bulk indicated the acid production resulting from synthetic community growth. Furthermore, pH was recorded to understand its influence on invasion and species growth. The pH in the reactor dropped significantly in reactor experiment 1 (high glucose, high lactic acid). On day 1, when only *A. oris* was present, the pH decreased from 6.92 to 5.64 (Figure 4.5). The pH dropped further by day 2, down to 5.19. The pH increased back up to 5.90 by day 3, 24 h after *S. mutans* was added. The pH dropped to 5.20 on day 4 and stayed constant between 5.20-5.30 throughout the remainder of the experiment, as *S. mutans* dominated the bulk. The pH, therefore, stayed below the critical value of 5.5 for most of the experiment.

A similar pattern in the pH of the bulk was observed in reactor experiment 2 (high glucose, intermediate lactic acid). The pH dropped by day 1, from 6.82 to 6.14. This was, however, higher than the pH at the elevated lactic acid concentration. The pH dropped further to 5.23 by day 2, the lowest reached during this experiment. The pH increased to 5.91 on day 4, before dropping down throughout the rest of the experiment. The pH by the end of the experiment was 5.35. This meant that the pH for both the high glucose reactor experiments was low and similar, despite the change in lactic acid concentration.

There was a higher pH recorded in reactor experiment 3 (low glucose, high lactic acid), compared to reactor experiment 1 (high glucose, high lactic acid). The pH dropped from 6.92 to 5.90 by day 1. The acid produced was an outcome of *A. oris* fermentation of glucose. The pH dropped further to 5.60 by day 2. This was the lowest pH reached during this experiment, which was significantly higher than the pH of 5.19 and 5.23 reached at the higher glucose concentrations. The pH increases over time to 5.90 by day 5 and stayed between 5.90-6.00 throughout the remainder of the rest of the experiment.

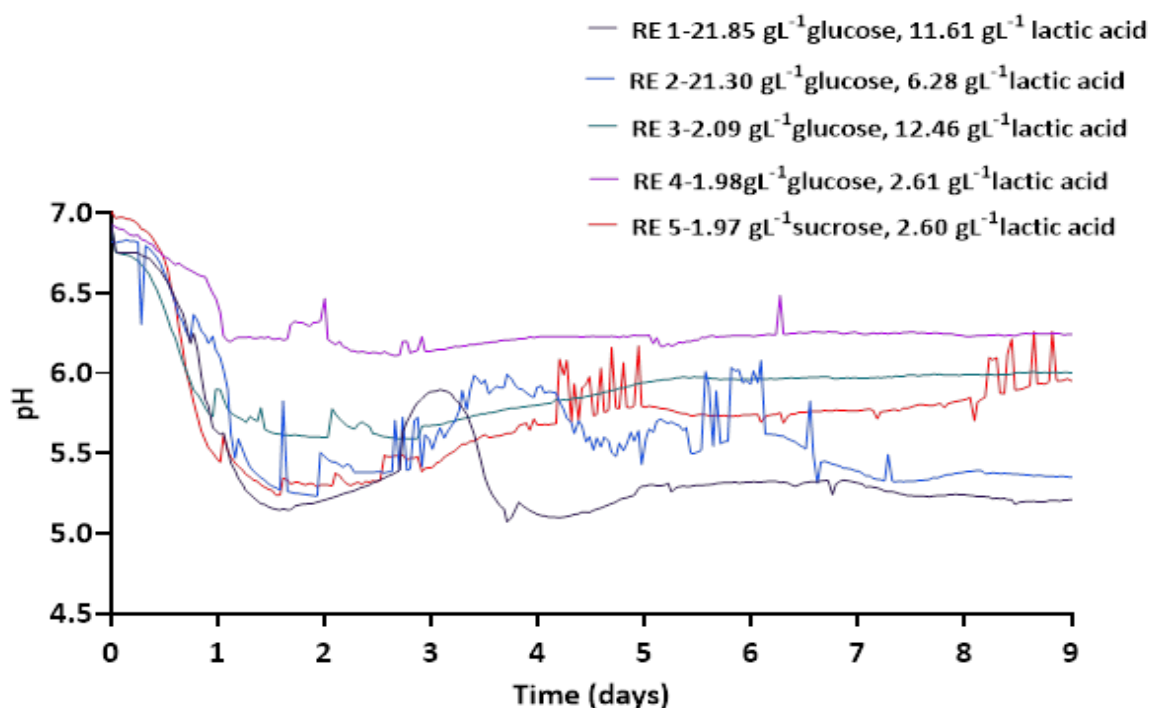


Figure 4.5 The pH variation in the CDC reactor bulk for each condition of the reactor experiments (RE). In all cases, the pH dropped, with the decrease being greater at the high glucose and sucrose conditions. The lowest pH was recorded for RE 1 (high glucose, high lactic acid), with a pH reached on day 9. Readings were plotted every hour through the 9-day experiment.

For reactor experiment 4 (low glucose, low lactic acid), the lactic acid decrease in the feed led to a higher pH of the reactor bulk. Here, the pH dropped to 6.47 on day 1. The pH decreased to 6.32 on day 2, before *S. mutans* was inoculated into the rest of the system. For the remainder of the 9-day experiment, the pH stayed constant between 6.15-6.25. This was the highest pH that was reached of all the conditions tested in the invasion experiments.

In reactor experiment 5 (low sucrose, low lactic acid), there was a significant pH drop in the reactor bulk. Here, the pH dropped to 5.48 by day 1. The pH dropped further to 5.30 on day 2. This pH was significantly lower than that reached at the low glucose concentrations and similar to those at the high glucose concentrations. The pH increased significantly over time. By the end of the experiment, the pH was 5.97, which was higher than that for reactor experiments 1 (high glucose, high lactic acid) and 2 (high glucose, intermediate lactic acid), but lower than the low glucose concentrations in experiments 3 (low glucose, high lactic acid) and 4 (low glucose, low lactic acid).

A summary of the pH readings taken across all experiments can be seen in Table 4.5. It was clear that the starting substrate concentration has a significant impact on the pH recorded from the reactor bulk. At the high glucose concentrations and the sucrose concentration, there was a drop in pH of over 1.5 units from the starting pH to the lowest levels and at least 1.0 by the end of the experiments, showing a significant amount of acid production by the synthetic community. The most acidic runs (experiments 1 and 2) also led to the lowest OD_{600nm} values, demonstrating that pH negatively impacted growth.

Table 4.5 The pH recording across the 9-day reactor experiments for all conditions. The pH dropped across all conditions tested. The lowest pH reached by the end of the run was for reactor experiment 1 (high glucose, high lactic acid), whilst the highest pH recorded was for reactor experiment 4 (low glucose, low lactic acid). Recordings were averaged across 2 reactors whilst

| | Reactor experiment 1 | Reactor experiment 2 | Reactor experiment 3 | Reactor experiment 4 | Reactor experiment 5 |
|-----------------------|----------------------------|----------------------------|----------------------------|----------------------------|----------------------------|
| Day 0- Starting pH | 6.92 | 6.82 | 6.92 | 6.93 | 7.00 |
| Day 2- Lowest pH | 5.23 | 6.14 | 5.60 | 6.32 | 5.30 |
| Day 9- End pH | 5.20 | 5.35 | 6.00 | 6.24 | 5.97 |

4.3.6 Quantifying the relative abundance of the synthetic community species in the reactor bulk

I quantified the abundance of each oral bacterial species, within the reactor planktonic bulk, over the course of the 9-day experiment. This was done for each reactor experiment to determine the impact of substrate concentration on *S. mutans* invasion, and on the commensal species, over time. The abundance of each species was measured using qPCR with species-specific primers. To facilitate absolute quantification, templated DNA for each species was amplified and cloned into a pTOPO2.1 vector and purified plasmid was quantified with PicoGreen™.

In reactor experiment 1 (high glucose, high lactic acid), *S. gordonii*, *A. oris*, *N. subflava* and *V. parvula* were all able to establish in the bulk by day 2 (Figure 4.6). Here, *S. gordonii* was the most abundant species, with 2.86×10^{12} cells L⁻¹. There were 3.08×10^8 *A. oris* cells, the least on this day despite being inoculated into the system 24 h before the other species. By day 3, *S. gordonii* was still the most abundant species, with 1.60×10^{12} cells L⁻¹, however *S. mutans* had established within the system with 9.78×10^{11} cells L⁻¹. By the end of the 9-day experiment, *S. mutans* had dominated the planktonic bulk, increasing in cell concentration over time to 3.60×10^{12} cells L⁻¹. *S. gordonii* was the second most abundant species by day 9, although reduced in cell concentration to 2.47×10^{10} cells L⁻¹, as also occurred for *A. oris*, which had a cell concentration of 5.60×10^8 cells L⁻¹ on day 9. *N. subflava* decreased in cell concentration, from 2.59×10^{11} on day 2, to 1.83×10^9 by day 9). This also occurred for *V. parvula*, with a cell concentration of 1.74×10^{11} cells L⁻¹ on day 2, and 6.98×10^8 cells L⁻¹ on day 9.

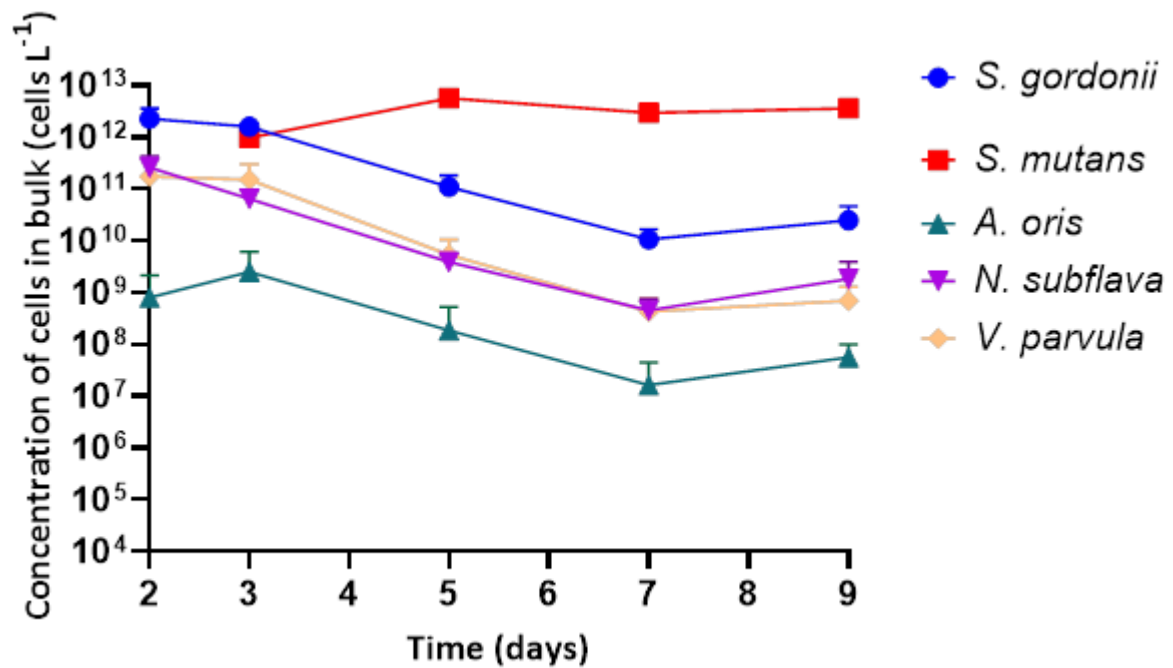


Figure 4.6. Relative abundance of each synthetic community member in the reactor bulk for reactor experiment 1 (high glucose, high lactic acid). *S. mutans* (red) dominated the bulk from day 5 onwards, whilst the other species reduced in number over time. Each point represented the average of triplicate values from three CDC reactor systems. Error bars represent the standard deviation from the mean.

In reactor experiment 2 (high glucose, intermediate lactic acid), *S. gordonii* dominated the number of cells on day 2, with 2.03×10^{13} cells L⁻¹ (Figure 4.7). Again, *A. oris* was the least abundant species in the system on day 2, with 3.08×10^{10} cells L⁻¹. By day 3, the cell concentration for *S. gordonii* was 7.32×10^{12} cells. There were 3.98×10^{12} cells L⁻¹ on day 9. *S. mutans* dominated the bulk by day 9, as with reactor experiment 1 (high glucose, high lactic acid), with 1.43×10^{13} cells L⁻¹. *S. gordonii* had reduced in cell concentration to 4.43×10^{10} cells L⁻¹ by day 9. There were 8.08×10^8 *A. oris* cells L⁻¹ by day 9. *N. subflava* had reduced in cell concentration from 1.50×10^{12} cells L⁻¹ on day 2, to 5.25×10^8 cells L⁻¹ by day 9. *V. parvula* was the least abundant species by day 9 in this experiment, with 5.86×10^8 cells L⁻¹. This was a reduction from day 2, where 2.59×10^{11} cells L⁻¹ were measured. These results showed that in both experiments where the glucose concentration was high, *S. mutans* dominated the bulk, with over 99% of the cells number by day 9. The other species reduced in cell concentration over time, with *A. oris* struggling to grow in this mixed-culture system, despite being the first species inoculated into the reactor.

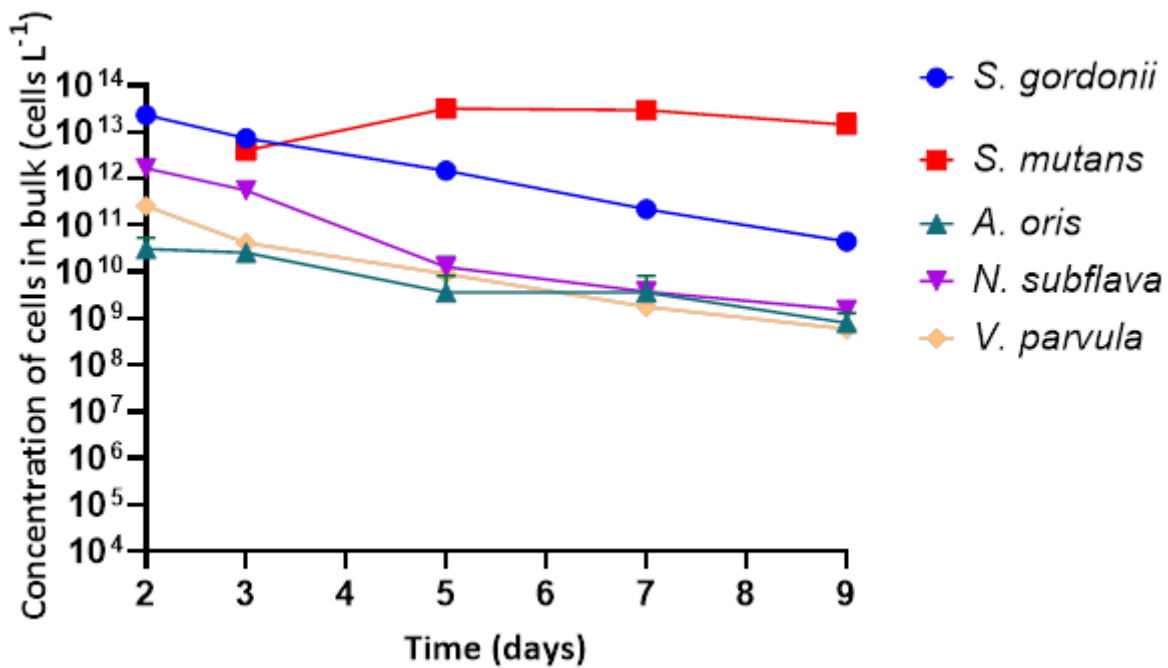


Figure 4.7. Relative abundance of each synthetic community member in the reactor bulk for reactor experiment 2 (high glucose, intermediate lactic acid). Patterns in species abundance were similar for reactor condition 1 (high glucose, high lactic acid). *S. mutans* (red) dominated the bulk from day 5 onwards, whilst the other species reduced in number over time. Each point represented the average of triplicate values from three CDC reactor systems. Error bars represent the standard deviation from the mean.

In reactor experiment 3 (low glucose, high lactic acid), the lower glucose concentration significantly impacted the abundance of the synthetic community in the reactor bulk. *S. gordonii* was the most abundant species on day 2, with 5.37×10^{11} cells L⁻¹ (Figure 4.8). Here, *N. subflava* was the least abundant species with 7.64×10^4 cells L⁻¹. On Day 3, *S. mutans* was the most abundant species, despite only being in the system for 24 h, with 3.20×10^{11} cells L⁻¹. *V. parvula* was the least abundant species on day 3, with 5.35×10^{11} cells L⁻¹. By day 9, *S. mutans* was the most abundant species, with 8.72×10^{12} cells L⁻¹. *V. parvula* had increased significantly in cell concentration to 5.03×10^{12} cells L⁻¹, the second most abundant in the synthetic community. *A. oris* had decreased in cell concentration, from 8.95×10^{10} cells L⁻¹ on day 2, to 1.03×10^{10} cells L⁻¹ on day 9. *S. gordonii* had also reduced in cell concentration to 8.44×10^9 cells L⁻¹ by day 9. *N. subflava* was the least abundant species by day 9, with 7.00×10^7 cells L⁻¹. This showed that in reactor experiment 3 (low glucose, high lactic acid), *S. mutans* and *V. parvula* dominated the planktonic bulk, with the relative abundance by day 9 being 63.40% and 36.46% respectively.

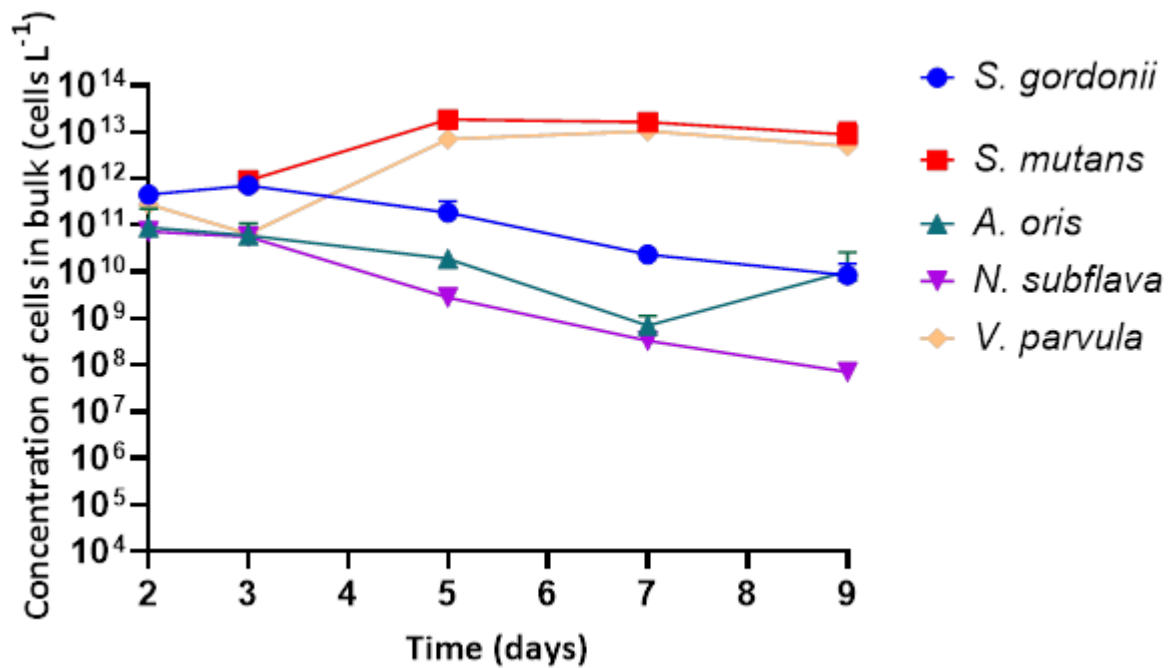


Figure 4.8. Relative abundance of each synthetic community member in the reactor bulk for reactor experiment 3 (low glucose, high lactic acid). *S. mutans* (red) and *V. parvula* (yellow) dominated the bulk by the end of the experiment. *N. subflava* (purple) in particular struggled to grow, reducing in number over time. Each point represented the average of triplicate values from three CDC reactor systems. Error bars represented the standard deviation from the mean.

In reactor experiment 4 (low glucose, low lactic acid) *N. subflava* was the most abundant species after day 2, with 8.30×10^{12} cells L⁻¹ (Figure 4.9). *A. oris* was the least abundant species in the reactor bulk, with 1.12×10^{10} cells L⁻¹. By day 3, *N. subflava* had remained the most abundant species, with 5.12×10^{12} cells L⁻¹, and *S. mutans* had become the second most abundant, with 3.26×10^{12} cells L⁻¹. By day 9, *S. mutans* was the most abundant species, with a cell concentration of 1.29×10^{13} cells L⁻¹. *V. parvula* was the second most abundant species at 6.84×10^{12} cells L⁻¹. This was an increase from 1.86×10^{12} cells L⁻¹ on day 2. *S. gordonii* had reduced in cell concentration, from 3.06×10^{12} cells L⁻¹ on day 2, to 1.12×10^{11} cells L⁻¹ on day 9. The abundance of *N. subflava* was 8.35×10^8 cells L⁻¹ on day 9, this was a 4-log reduction compared to day 2 than on day 2. *A. oris* was the least abundant species by the end of the experiment, with 1.69×10^9 cells L⁻¹.

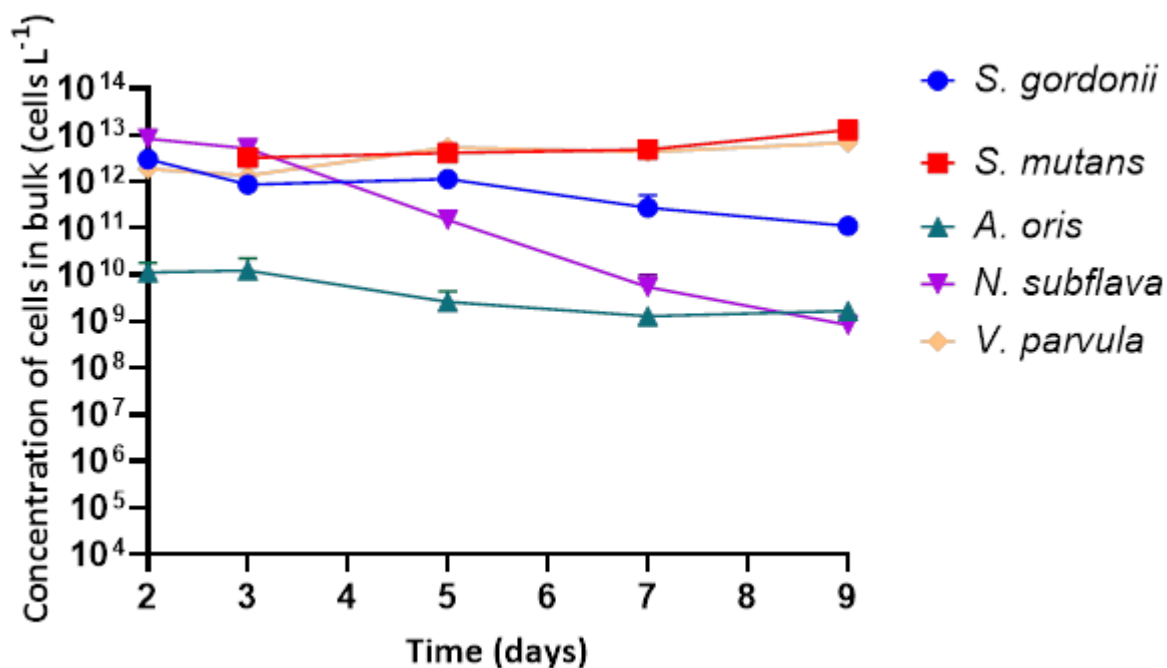


Figure 4.9. Relative abundance of each synthetic community member in the reactor bulk for reactor experiment 4 (low glucose, low lactic acid). Patterns in species abundance were similar for reactor condition 3. *S. mutans* (red) and *V. parvula* (yellow) dominated the bulk by day 9, whilst *S. gordonii* (blue) and *N. subflava* (purple) reduced in number over time. Each point represented the average of triplicate values from three CDC reactor systems. Error bars represented the standard deviation from the mean.

In reactor experiment 5 (low sucrose, low lactic acid), the use of sucrose in AFMC instead of glucose resulted in *S. gordonii* still being the most abundant species on day 2 with 2.92×10^{12} cells L⁻¹ (Figure 4.10). *A. oris* was the least abundant species with 8.78×10^{10} cells L⁻¹. This meant that *A. oris* was the least abundant species on day 2 across all reactor experiments. By day 3, *V. parvula* had become the most abundant species with 1.78×10^{12} cells L⁻¹. The second most abundant species on day 3 was *S. mutans*, with 1.55×10^{12} cells L⁻¹. *A. oris* was the least abundant species with 1.03×10^{11} cells L⁻¹. By day 9, *S. mutans* had become the most abundant species in the reactor bulk, with 1.56×10^{13} cells L⁻¹. *V. parvula* was the second most abundant species, with 6.81×10^{12} cells L⁻¹. This meant that *S. mutans* and *V. parvula* dominated the planktonic bulk in all low glucose/sucrose conditions (reactor experiments 3-5), even when the lactic acid concentrations had been reduced. *S. gordonii* had reduced in cell concentration to 3.00×10^{11} cells L⁻¹ on day 9. *A. oris* had also reduced in cell concentration to 4.49×10^9 cells L⁻¹ by day 9. *N. subflava* was the least abundant species in the synthetic community on day 9. The cell concentration had reduced to 2.02×10^9 cells L⁻¹ on day 9, down from 3.09×10^{11} cells L⁻¹ on day 2.

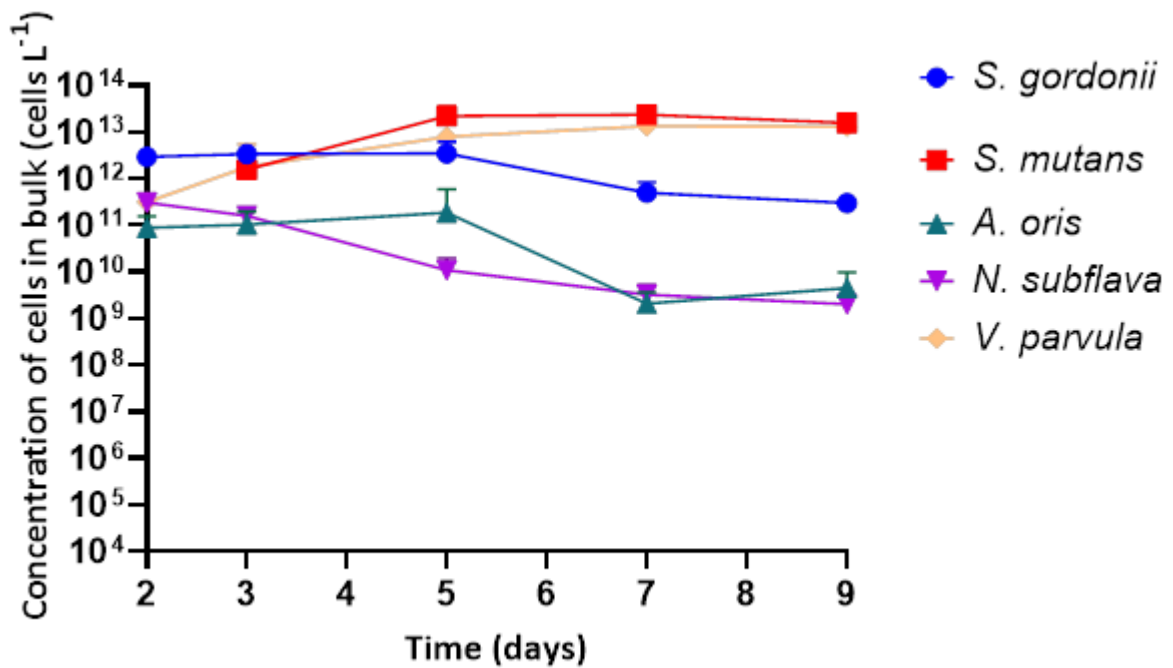


Figure 4.10. Relative abundance of each synthetic community member in the reactor bulk for reactor experiment 5 (low sucrose, low lactic acid). Patterns in species abundance was similar for reactor conditions 3 (low glucose, high lactic acid) and 4 (low glucose, low lactic acid). *S. mutans* (red) and *V. parvula* (yellow) dominated the bulk by day 9, whilst *S. gordonii* (blue), *A. oris* (green) and *N. subflava* (purple) reduced in number over time. Each point represented the average of triplicate values from three CDC reactor systems. Error bars represented the standard deviation from the mean.

4.3.7 Quantifying the relative abundance of the synthetic community species in biofilms

I quantified the abundance of each oral bacterial species in the synthetic community biofilm. This was necessary to understand the microbial composition of the biofilm and to what extent *S. mutans* was able to invade/dominate the biofilm. These invasion experiments were done with different substrate concentrations in the AFMC medium to better understand the drivers behind *S. mutans* invasion into dental biofilms *in vivo*. Here, qPCR was also used with species-specific primers to quantify cell concentration over 9 days. The cell concentrations in these sections were those collected from each hydroxyapatite coupon, factoring in a total of 21 coupons within the reactor. Biofilms were observed to have grown on the coupon holders but were not taken into consideration within qPCR sampling.

In reactor experiment 1 (high glucose, high lactic acid), *S. gordonii* was the most abundant species on day 2 with a cell concentration of 4.48×10^8 cells cm⁻¹ (Figure 4.11). There were 5.44×10^7 cells cm⁻¹ for *N. subflava* on day 2. *A. oris* was the least abundant species, with a cell

concentration of 3.06×10^5 cells cm^{-1} , despite being introduced into the reactor first. On day 3, *S. gordonii* remained the most abundant species, with 2.23×10^9 cells cm^{-1} . *S. mutans* was the second most abundant species, with a cell concentration of 5.42×10^8 cells cm^{-1} . *A. oris* remained the least abundant species in the biofilm on day 3, with 1.52×10^6 cells cm^{-1} . By the end of the 9 days, *S. mutans* had dominated the biofilm, increasing in number to 1.57×10^{11} cells cm^{-1} . *S. gordonii* was the second most abundant, with 6.79×10^8 cells cm^{-1} . *A. oris* also increased in cell concentration to 2.21×10^7 cells cm^{-1} but was still the least abundant species by day 9. For *N. subflava*, there were 4.88×10^7 cells cm^{-1} on day 9. *V. parvula* had increased in cell concentration over time, from 1.77×10^7 cells cm^{-1} on day 2, to 1.16×10^8 cells cm^{-1} on day 9. The dominance of *S. mutans* in the biofilm and the relatively low cell concentration of *A. oris* was similar to the patterns seen in the planktonic phase of reactor experiment 1 (high glucose, high lactic acid) (Figure 4.5).

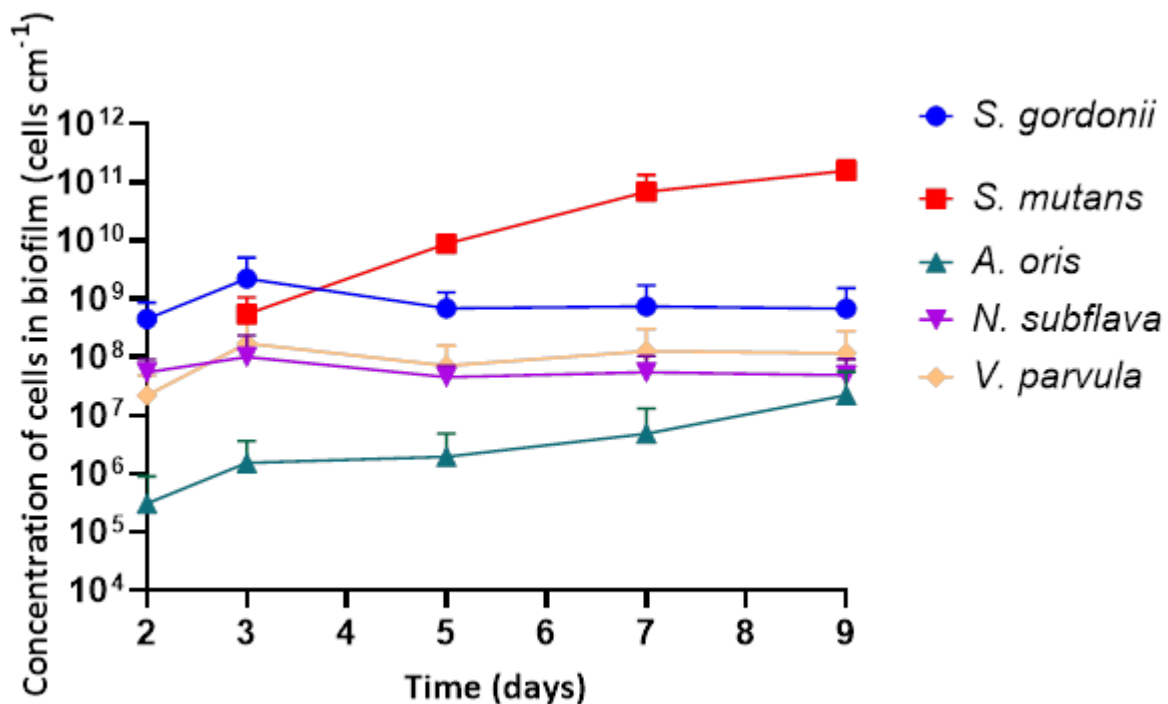


Figure 4.11. Relative abundance of each species in the synthetic community for reactor experiment 1 (high glucose, high lactic acid). *S. mutans* (red) dominated the bulk from day 5 onwards. *A. oris* (green) increased in cell concentration over time. Each point represented the average of triplicate values from three CDC reactor systems. Error bars represented the standard deviation from the mean.

In reactor experiment 2 (high glucose, intermediate lactic acid) *S. gordonii* was the most abundant species within the biofilm on day 2, with 4.87×10^9 cells cm^{-1} (Figure 4.12). There were 7.16×10^8 cells cm^{-1} of *N. subflava* on day 2, and 3.36×10^7 cells cm^{-1} for *V. parvula*. *A. oris* was the least abundant species with 2.34×10^7 cells cm^{-1} . *S. gordonii* was also the most abundant species on day 3, with 6.98×10^9 cells cm^{-1} whilst *S. mutans* was the second most abundant species with 1.82×10^9 cells cm^{-1} . By day 9, *S. mutans* had dominated the biofilm, with a cell concentration increasing over time to 1.62×10^{12} cells cm^{-1} . The number of *S. mutans* cells was significantly higher than in any of the other reactor experiments ($p < 0.05$). *S. gordonii* was the second most abundant species, increasing to 5.59×10^9 cells cm^{-1} on day 9. *A. oris* had increased in cell concentration from day 3, with a cell concentration of 8.98×10^8 cells cm^{-1} . On day 9, there were 4.17×10^8 cells cm^{-1} for *N. subflava*, and 7.54×10^7 cells cm^{-1} for *V. parvula*. This meant that *V. parvula* was the least abundant species in the synthetic community biofilm by day 9.

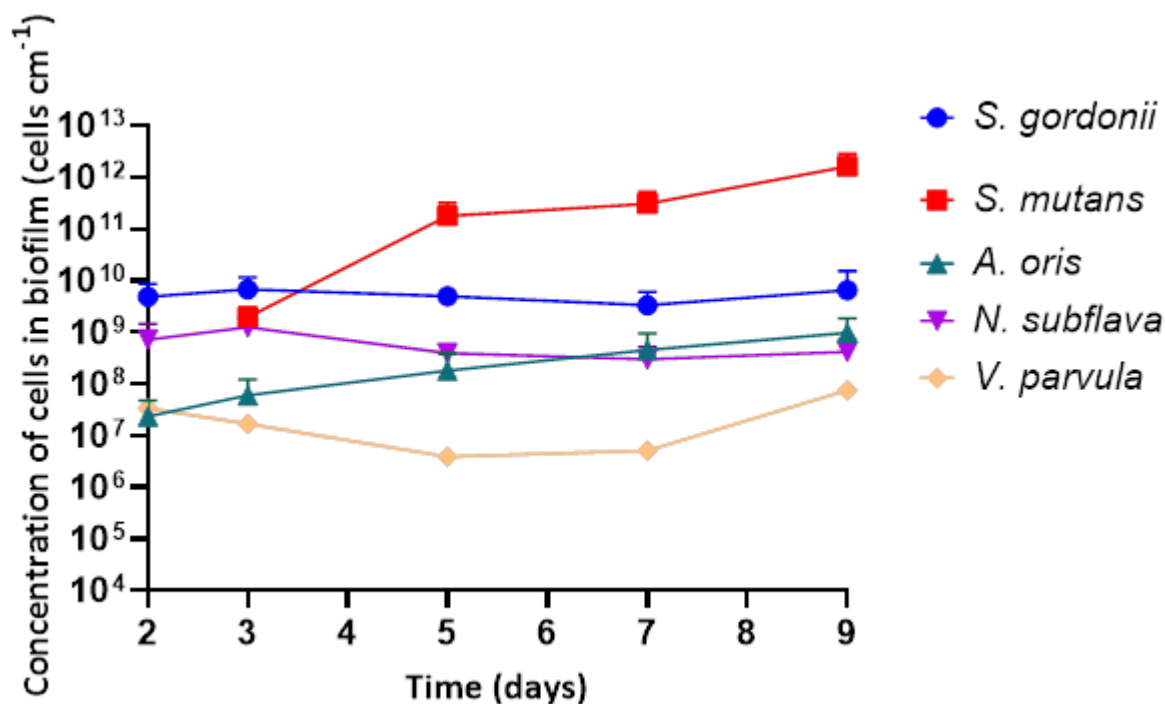


Figure 4.12. Relative abundance of each species in the synthetic community for reactor experiment 2 (high glucose, intermediate lactic acid). *S. mutans* (red) dominated the bulk from day 5 onwards. *A. oris* (green) increased in cell concentration over time. *V. parvula* (yellow) was the least abundant species but did increase in cell concentration. Each point represented the average of triplicate values from three CDC reactor systems. Error bars represent the standard deviation from the mean.

In reactor experiment 3 (low glucose, high lactic acid), *V. parvula* was the most abundant species on day 2, with 2.14×10^8 cells cm^{-1} (Figure 4.13). *A. oris* was by far the least abundant species in this experiment, where there were only 1.37×10^5 cells cm^{-1} measured. By day 3, *V. parvula* remained the most abundant species in the biofilm, with 7.19×10^8 cells cm^{-1} . *S. mutans* was the second most abundant species, with 1.76×10^8 cells cm^{-1} . By day 9, *V. parvula* had continued to dominate the synthetic community biofilm, comprising 2.16×10^{11} cells cm^{-1} . *S. gordonii* was the second most abundant species, with a cell concentration of 1.13×10^{10} cells cm^{-1} . This was an increase from day 2, where there were 1.16×10^8 cells cm^{-1} . *S. mutans* had also increased in cell concentration, with 8.27×10^9 cells cm^{-1} by day 9. *N. subflava* had increased in cells cm^{-1} , from 5.89×10^7 cells cm^{-1} on day 2, to 1.88×10^8 cells cm^{-1} on day 9. Whilst *A. oris* remained by far the least abundant species in the synthetic community biofilm on day 9, it still increased over time, with 7.57×10^6 cells cm^{-1} recorded on day 9. Overall, this showed that all species increased in number over time, and that *V. parvula* dominated the synthetic community biofilm in a low glucose, high lactic acid environment. The number of *V. parvula* cells in the biofilm was significantly higher than in any of the other reactor experiments ($p < 0.05$).

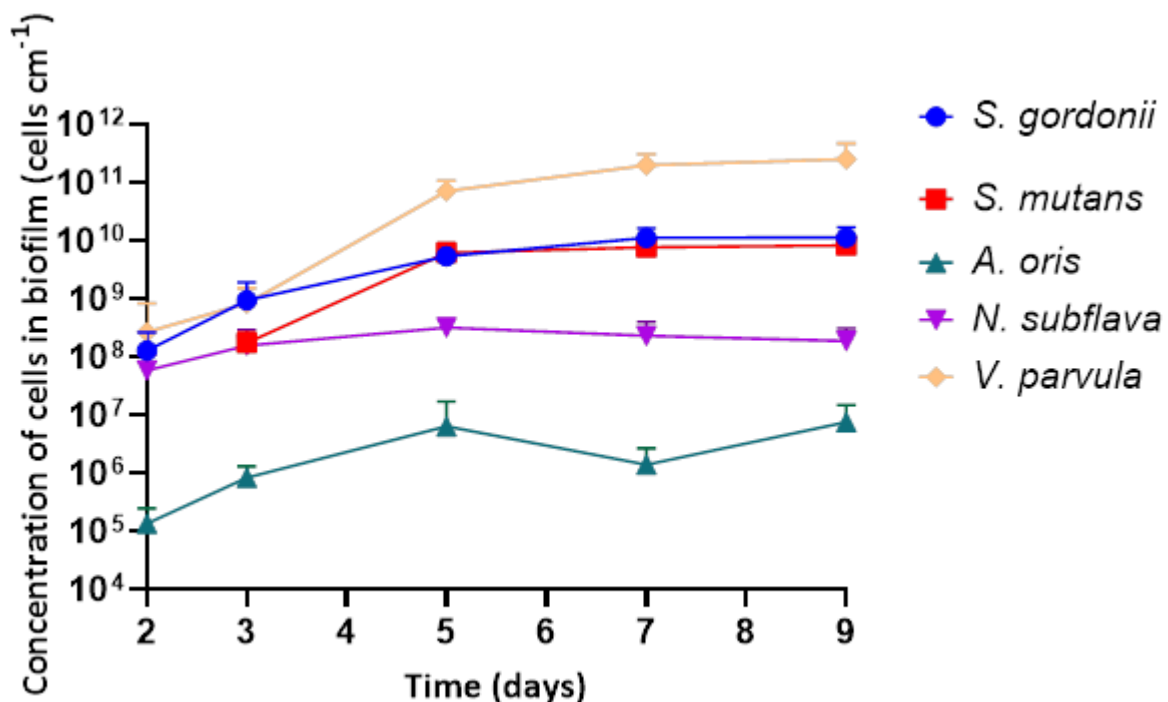


Figure 4.13. Relative abundance of each species in the synthetic community for reactor experiment 3 (low glucose, high lactic acid). *V. parvula* dominated the bulk from day 5 onwards. *S. gordonii* (blue) and *S. mutans* (red) were in similar abundances in the biofilm by day 9. *A. oris* (green) increased in cell concentration over time but was the least abundant species. Each point represented the average of triplicate values from three CDC reactor systems. Error bars represent the standard deviation from the mean.

In reactor experiment 4 (low glucose, low lactic acid), *N. subflava* was the most abundant species on day 2, with 1.13×10^9 cells cm^{-1} . *A. oris* was the least abundant species with 5.10×10^7 cells cm^{-1} (Figure 4.14). *N. subflava* was still the most abundant species on day 3, with 5.36×10^8 cells cm^{-1} . *S. mutans* was the second most abundant species, with 3.69×10^8 cells cm^{-1} . *A. oris* remained the least abundant species with 7.12×10^7 cells cm^{-1} . By day 9, *V. parvula* was the most abundant species, with the cell concentration increasing to 1.06×10^{10} cells cm^{-1} . *S. gordonii* was the second most abundant species, with the cell concentration increasing from 7.03×10^8 cells cm^{-1} on day 2, to 4.18×10^9 cells cm^{-1} on day 9. *S. mutans* cell concentration also increased, with a count of 3.71×10^9 cells cm^{-1} on day 9. The cell concentration for *N. subflava* was 7.60×10^8 cells cm^{-1} on day 9. *A. oris* remained the least abundant species in the synthetic community biofilm on day 9, with the cell concentration decreasing to 3.35×10^7 cells cm^{-1} on day 9. This meant that *V. parvula* still dominated the synthetic community, despite a reduction in lactic acid concentration, but in both experiments, *S. mutans* was able to invade and establish itself in the biofilm. Overall, there was a more balanced abundance between species, due to a higher pH, lower glucose concentration and lower lactic acid concentration preventing *S. mutans* or *V. parvula* from dominating the synthetic community.

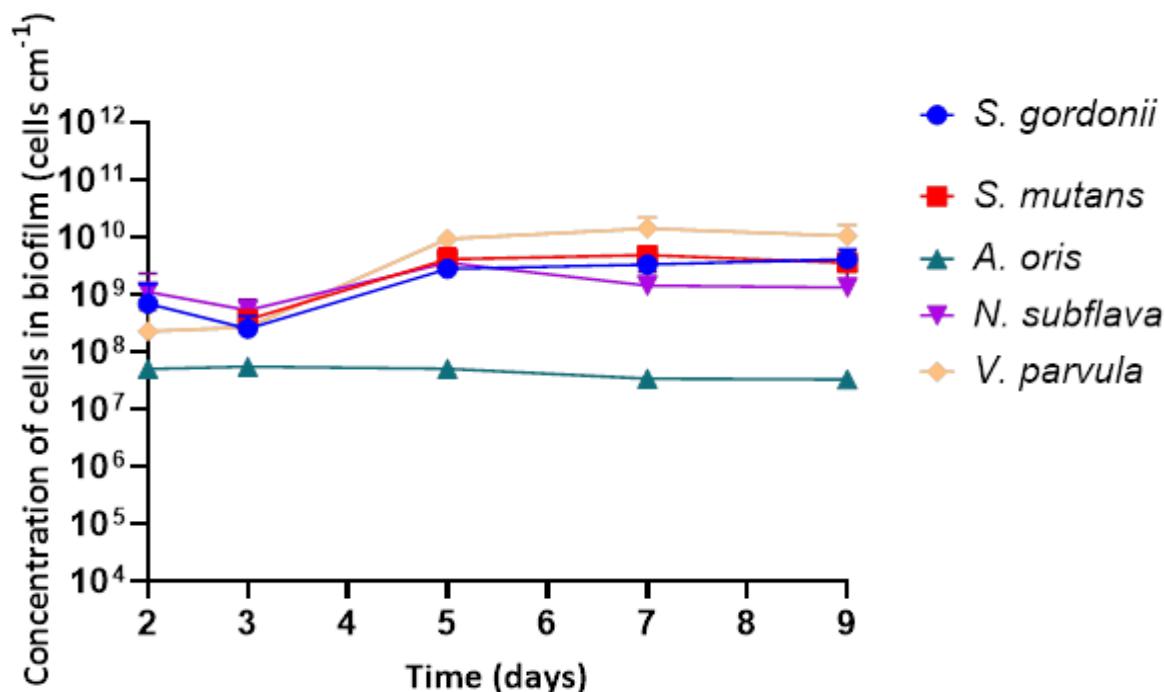


Figure 4.14. Relative abundance of each species in the synthetic community for reactor experiment 4 (low glucose, low lactic acid). *V. parvula* (yellow) was the most abundant species by day 9. *A. oris* (green) was the least abundant species. Each point represented the average of triplicate values from three CDC reactor systems. Error bars represent the standard deviation from the mean.

In reactor experiment 5 (low sucrose, low lactic acid), *N. subflava* became the most abundant species on day 2, with a cell concentration of 1.59×10^8 cells cm^{-1} . *A. oris* was the least abundant species, with 5.10×10^7 cells cm^{-1} (Figure 4.15). This meant that *A. oris* was the least abundant species in the synthetic community biofilm on day 2 across all experiments, despite being introduced into the reactor system first. By day 3, *S. mutans* had become the most abundant species, with a cell concentration of 1.36×10^9 cells cm^{-1} . There were 1.13×10^9 cells cm^{-1} for *S. gordonii* on day 3. *A. oris* was again the least abundant, decreasing in cell concentration to 2.85×10^6 cells cm^{-1} . By day 9, *V. parvula* was the most abundant species in the biofilm, increasing from 3.09×10^7 cells cm^{-1} on day 2, to 7.64×10^{10} cells cm^{-1} on day 9. *S. mutans* was the second most abundant species, increasing over time to 2.68×10^{10} cells cm^{-1} on day 9. The cell concentration on day 9 for *S. gordonii* was 5.57×10^9 cells cm^{-1} , and for *N. subflava* it was 2.21×10^8 cells cm^{-1} . *A. oris* was the least abundant synthetic community member on day 9, with 2.47×10^7 cells cm^{-1} . This meant that changing the carbon source to sucrose led to an increase in cell concentration for all synthetic community species, with *V. parvula* still the most abundant species at the low substrate concentration. *S. mutans*, however, was the second most dominant species in the presence of sucrose, overtaking *S. gordonii*, when compared to reactor experiment 4.

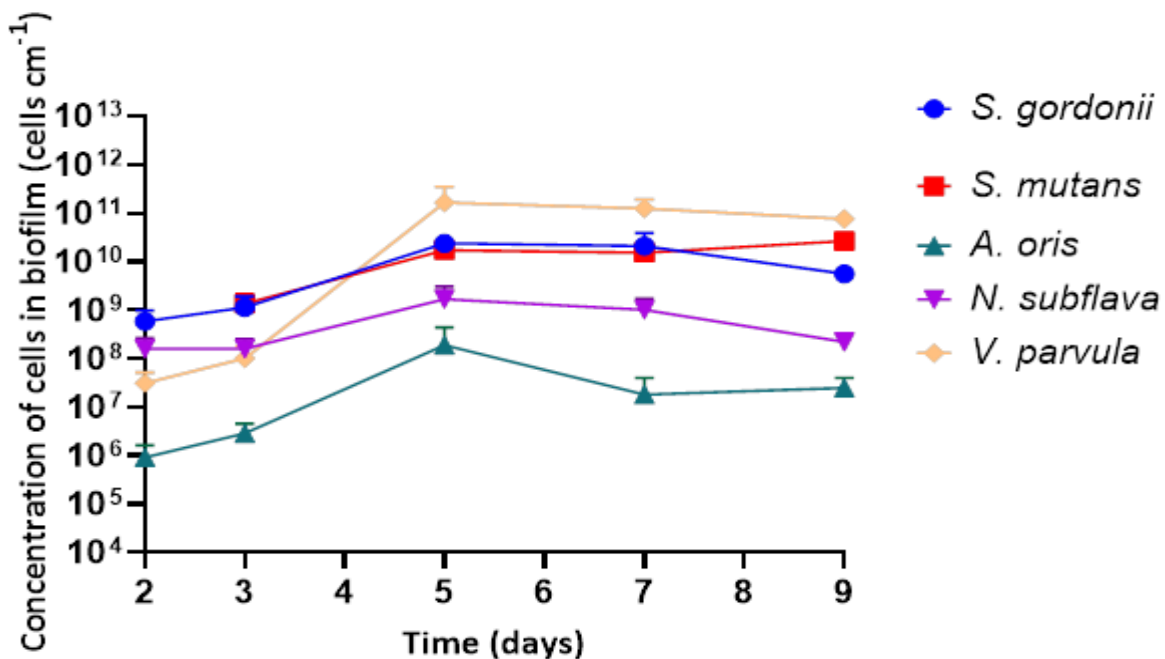


Figure 4.15. Relative abundance of each species in the synthetic community for reactor experiment 5 (low sucrose, low lactic acid). *V. parvula* (yellow) was the most abundant species by day 9. *S. mutans* (red) overtook *S. gordonii* (blue) as the second most abundant species when compared to condition 4 (low glucose, low lactic acid). Each point represented the average of triplicate values from three CDC reactor systems. Error bars represent the standard deviation from the mean.

4.3.8 Imaging the synthetic community biofilm using fluorescence in situ hybridization

I used FISH to visualise the dental biofilm growing on the hydroxyapatite coupons in the CDC reactor. This was to identify that the species had all been established and to determine any qualitative shift in species prevalence over time or between reactor experiments. Furthermore, FISH was used to try to determine any structural pattern shifts of the synthetic community biofilm resulting from substrate change. Here, FISH was used to qualitatively validate qPCR results, rather than being used to quantify bacterial abundance within the biofilm. I used spectral fingerprinting to reduce any false signal and bleed of fluorescence from one channel into another (See Chapter 3).

In reactor experiment 1 (high glucose, high lactic acid) at day 2 (Figure 4.16A), I observed that the biofilm formed was immature and primarily comprised of *S. gordonii* (grey), as was also seen in the qPCR abundance data (Figures 4.11-4.15). *N. subflava* (blue) and *V. parvula* (red) were also observed in this biofilm. It was difficult to identify the signal from *A. oris*. On day 3 (Figure 4.16B), *S. mutans* (green) had already started to colonise the biofilm and appeared to be the most abundant species. Over time, *S. mutans* dominated the biofilm, and by day 9 (Figure 4.16E) the FISH images were primarily showing green fluorescence. The biofilms appeared to become greater in bacterial number over time. No structural changes were identified throughout the experiment, but a greater amount of autofluorescence and bleed-through from the blue channel appeared as the biofilm matured.

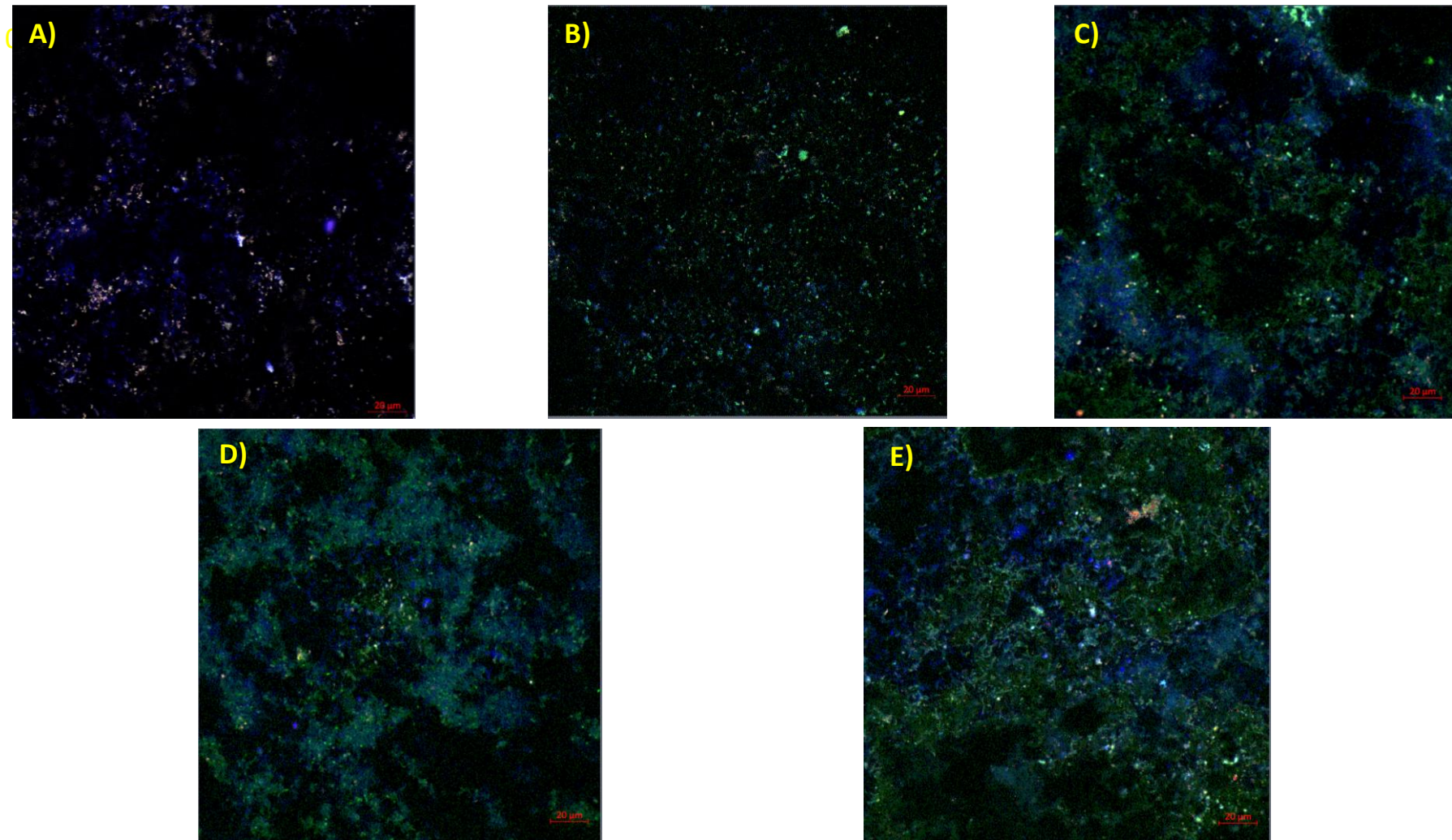


Figure 4.16. Imaging of the synthetic community biofilm over time for reactor experiment 1 (high glucose, high lactic acid) using fluorescence in situ hybridization (FISH). *S. gordonii* was the most visible species on day 2, but by day 3, *S. mutans* had already invaded the biofilm. *S. mutans* dominated the biofilm over time, whilst the presence of other species declined. Images were taken using the LSM 880 confocal microscope with spectral fingerprinting used to minimise fluorophore overlap. Images were representative of multiple images taken per biofilm. Colour- *S. gordonii* (grey), *S. mutans* (green), *A. oris* (yellow), *N. subflava* (blue) *V. parvula* (red). Day- 2 (A), 3 (B), 5 (C), 7 (D), 9 (E).

I compared FISH images on day 9 across reactor experiments to identify any structural differences and species presence change as a result of substrate concentration change. *S. mutans* dominated the biofilm in reactor experiment 1 (high glucose, high lactic acid) (Figure 4.17 A) by the end of the experiment. This was evident by the green chain cocci cells seen in the image. There was a signal recorded from *S. gordonii* (grey) within the biofilm, but far less than there were in previous days of this reactor experiment (images not shown). This was also seen in reactor experiment 2 (high glucose, intermediate lactic acid) (Figure 4.17 B), showing that *S. mutans* dominated the synthetic community at high glucose concentrations. The presence of the other species was not as prevalent as it had been earlier in the experiment (not shown), and there was no observable signal of *N. subflava* (blue) within this biofilm.

In reactor experiment 3 (low glucose, high lactic acid), where the glucose had been reduced, *S. mutans* was still seen to have invaded the biofilm (Figure 4.17 C). There was a significant amount of green signal observed. At this lower glucose concentration, there was far more signal from *V. parvula*, which appeared orange in areas where both green and red signals were recorded. There was very little signal observed from *A. oris* (yellow) or *N. subflava* (blue). For reactor experiment 4 (low glucose, low lactic acid) (Figure 4.17 D), there was still a significant level of *S. mutans*, but more *V. parvula* could be seen. There was also more *A. oris* (yellow) and *N. subflava* present, indicating a more balanced composition of the synthetic community species than in the high sugar experiments. In reactor experiment 5 (low sucrose, low lactic acid), *S. mutans* formed large islands of cells, rather than spread out chains (4.17 E). This morphology was more prominent than in the other experiments. *V. parvula* (red) was also present, although as with experiments 3 (low glucose, high lactic acid) and 4 (low glucose, low lactic acid), there was much less signal than expected when compared to the qPCR results. There was more bleed-through of the Alexa 405 (blue) into other channels and from autofluorescence, therefore I used background bleeding reduction for this fluorophore. Figure 4.17F was a positive control used during imaging to stain all bacterial cells using a universal EUB338 probe.

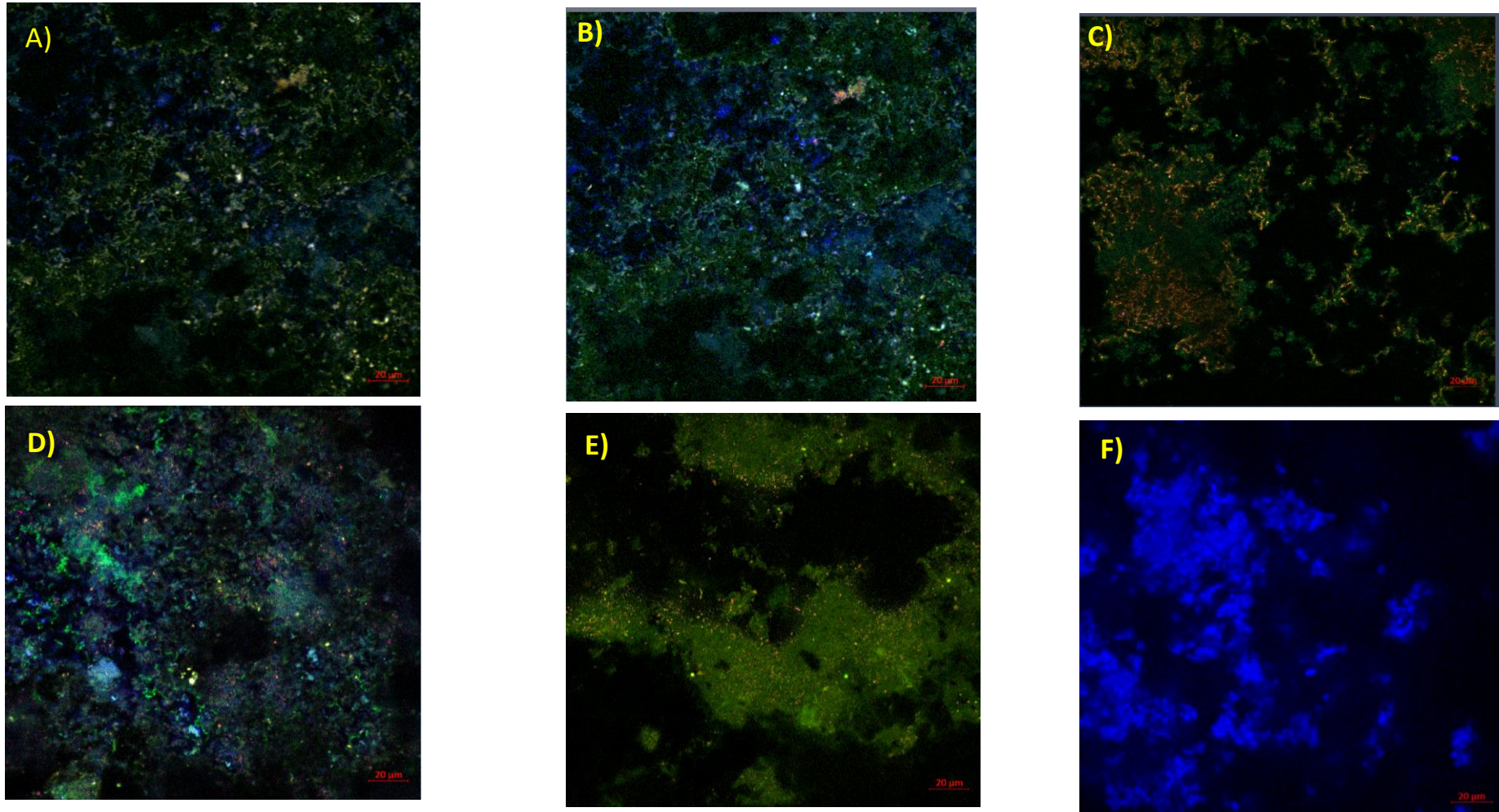


Figure 4.17. Imaging of the synthetic community biofilm over time for each reactor condition using FISH. *S. mutans* invaded the biofilm in all conditions by day 9. It dominated the biofilm, with a signal difficult to identify from other species in reactor experiments 1 (high glucose, high lactic acid) and 2 (high glucose, intermediate lactic acid). *V. parvula* was more prominent in reactor experiment 3 (low glucose, high lactic acid), 4 (low glucose, low lactic acid) and 5 (low sucrose, low lactic acid). Images were taken using the LSM 880 confocal microscope with spectral fingerprinting used to minimise fluorophore overlap. Images were representative of multiple images taken per biofilm. Colour- *S. gordonii* (grey), *S. mutans* (green), *A. oris* (yellow), *N. subflava* (blue) *V. parvula* (red). Reactor condition- 1 (A), 2 (B), 3 (C), 4 (D), 5 (E), F=positive control.

4.3.9 Assessing the viability of bacteria within the reactor system

I assessed the viability of the synthetic community at the end of the 9-day invasion experiments. This was done by using flow cytometry and live-dead staining to quantify the number of live and dead cells, within the bulk and biofilms. I did this across all experiments, to see how altering the substrate concentrations, the resulting pH, species rank abundance etc, affected the viability of the system. In reactor experiment 1 (high glucose, high lactic acid), there were 3.40×10^{10} dead cells in the bulk, accounting for 57.35% of the overall planktonic cell number (Figure 4.18). There were 2.53×10^{10} live cells in the bulk, accounting for 42.65 % of the overall planktonic cells. In the biofilm, there were 5.52×10^8 dead cells, equalling 24.97% of the overall number of cells. There were an overall cell number of 6.15×10^{10} cells. Overall, this showed that there were a significant number of dead cells in the system, particularly in the bulk when compared to the biofilm ($p < 0.05$), and that most of the cells in the system were accounted for by the planktonic phase.

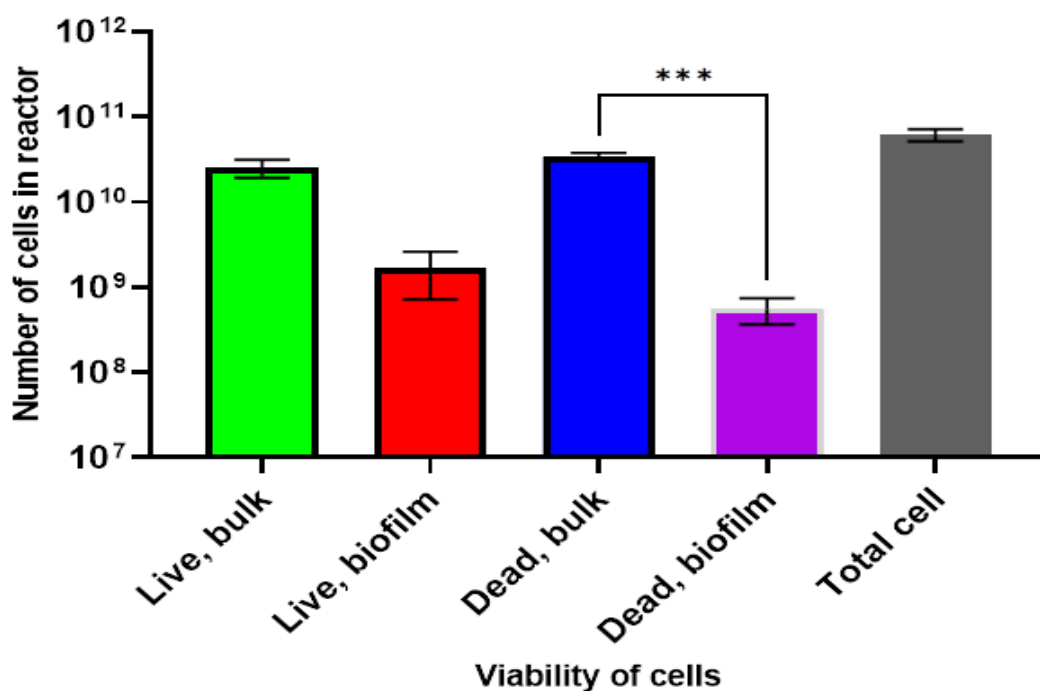


Figure 4.18 Viability of the synthetic community in both the reactor bulk and biofilm for reactor experiment 1 (high glucose, high lactic acid). There were a significant number of dead cells in the bulk (blue) and biofilm (purple) in this condition. Numbers were counted and gated using the Attune NxT flow cytometer, with the average of triplicate samples across three reactors taken. The error bars represented the standard deviation from the mean. Asterix indicated a significant difference between dead cells in the bulk and biofilm ($p < 0.05$).

In reactor experiment 2 (high glucose, intermediate lactic acid), the percentage of dead cells in the reactor bulk dropped significantly to 24.92 %, at a cell number of 2.63×10^{10} (Figure 4.19). The number of live cells in the bulk was 7.92×10^{10} , accounting for 76.55% of the bulk. In the biofilm, there were 3.14×10^8 dead cells, equating to 23.45% of the biofilm cell number. The other 76.55%, equalling 1.02×10^9 cells, were live. This indicates that the system, particularly the bulk, had a higher viability at the lower lactic acid concentrations, although there were still a significant number of dead cells in both the bulk and biofilm. The overall cell number was 1.07×10^{11} cells. The results from reactor experiments 1 (high glucose, high lactic acid) and 2 (high glucose, intermediate lactic acid), demonstrate that the low pH as a result of high glucose concentration, led to cell stress, particularly in the bulk.

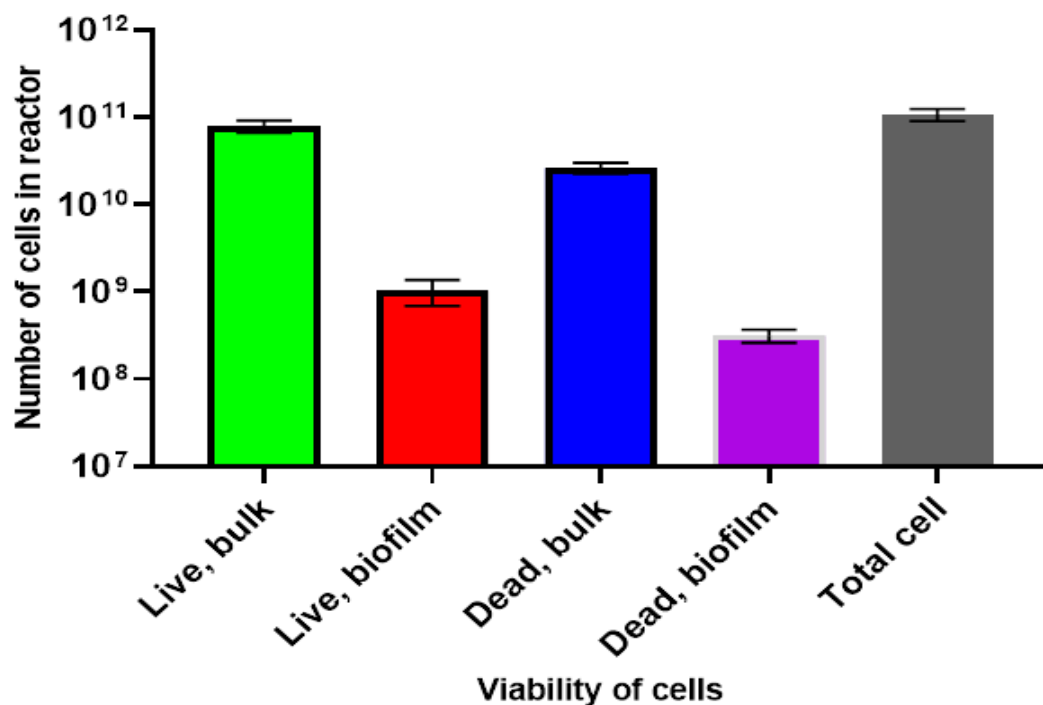


Figure 4.19 Viability of the synthetic community in both the reactor bulk and biofilm for reactor experiment 2 (high glucose, intermediate lactic acid). Similar to reactor experiment 1 (high glucose, high lactic acid), there were a significant number of dead cells in the bulk (blue) and biofilm (purple) in this condition. Numbers were counted and gated using the Attune NxT flow cytometer, with the average of triplicate samples across three reactors taken. The error bars represented the standard deviation from the mean.

In reactor experiment 3 (low glucose, high lactic acid), there were 1.69×10^9 dead cells in the bulk of the reactor, accounting for 5.78% of the overall cell number (Figure 4.20). There were 4.38×10^{10} live cells, which was 94.22% of the overall cell number. In the biofilm, there were 1.35×10^8 dead cells, accounting for 3.72% of the biofilm cell number. The other 96.28% of the biofilm cell number, at 2.21×10^9 cells, were live. The overall cell number was 4.78×10^{10} . These results show that the viability of both the synthetic community biofilm and bulk was significantly higher at the low glucose (and higher pH) concentration than at the high glucose (lower pH) concentration.

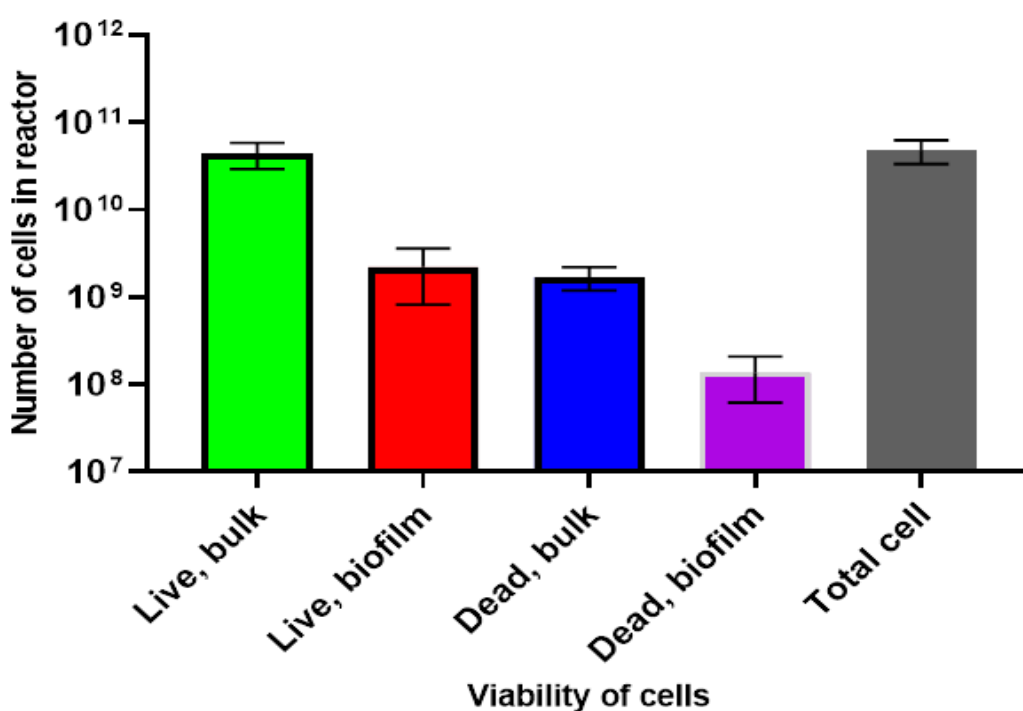


Figure 4.20 Viability of the synthetic community in both the reactor bulk and biofilm for reactor experiment 3 (low glucose, high lactic acid). The percentage of live cells in both the bulk (green) and the biofilm (red) were significantly higher than at the high glucose conditions. Numbers were counted and gated using the NxT flow cytometer, with the average of triplicate samples across three reactors taken. The error bars represented the standard deviation from the mean.

For reactor experiment 4 (low glucose, low lactic acid), where there was a low concentration of both glucose and lactic acid in the AFMC medium, the viability of the system was reduced from reactor experiment 3. There were 3.62×10^{10} dead cells in the bulk (Figure 4.21), which represented 23.26% of the total number of cells in the planktonic phase. There were 1.22×10^{11} live cells, which accounted for 77% of the bulk. In the synthetic community biofilm, there were 4.62×10^8 dead cells, which was 10.05% of the total biofilm cell number. There were 4.13×10^9 live cells in the biofilm, which was 89.95%. The total cell number of the reactor was 1.62×10^{11} .

$\times 10^{11}$ cells. The viability of both the biofilm and bulk were lower than for reactor 3 (low glucose, high lactic acid). This was possibly due to a lactic acid limitation leading to cell stress for *V. parvula*, the most abundant species during this reactor experiment. The viability of both the bulk and biofilm was higher than in reactor experiment 1 (high glucose, high lactic acid). The planktonic phase viability was similar to experiment 2 (high glucose, intermediate lactic acid), whilst the percentage of dead cells in the synthetic community biofilm was less than half.

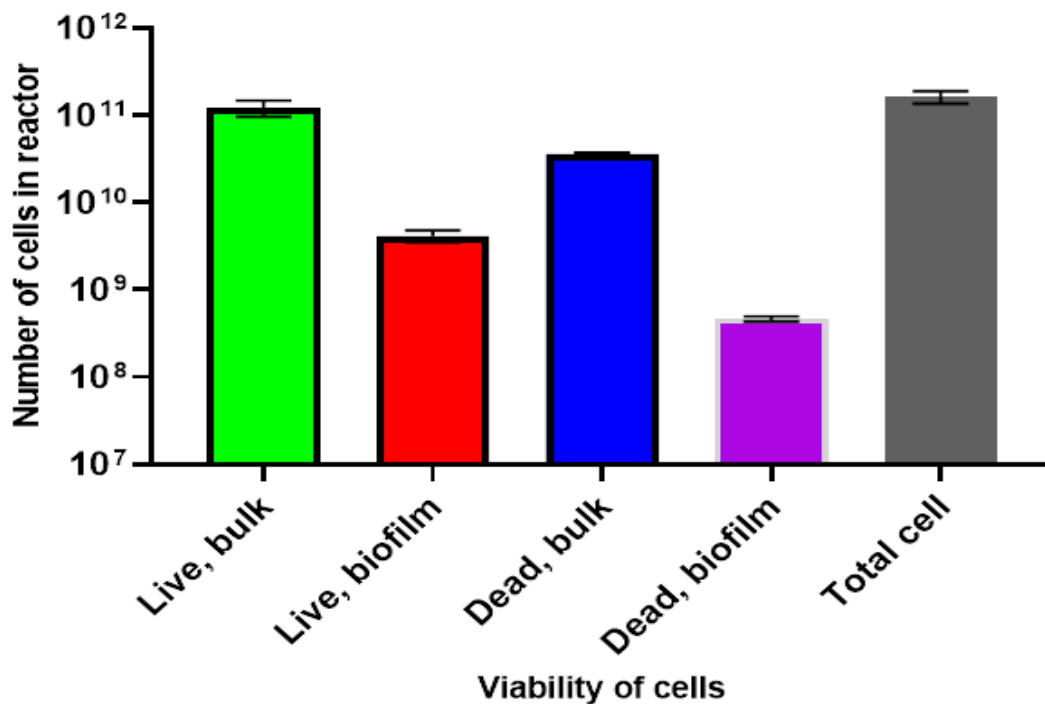


Figure 4.21 Viability of the synthetic community in both the reactor bulk and biofilm for reactor experiment 4 (low glucose, low lactic acid). Similar to reactor experiment 3 (low glucose, high lactic acid), the system had higher viability compared to the high glucose conditions. Most of the cells in the biofilm were live (red), although there were significantly more dead cells in the bulk (blue) than in reactor condition 3 (low glucose, high lactic acid). Numbers were counted and gated using the NxT flow cytometer, with the average of triplicate samples across three reactors taken. The error bars represented the standard deviation from the mean.

In reactor experiment 5 (low sucrose, low lactic acid), the viability of the system after 9 days for both the bulk and the biofilm was high. There were 4.01×10^9 dead cells in the bulk (Figure 4.22), accounting for 4.59% of the total cell number. There were 8.34×10^{10} live cells in the bulk, accounting for 95.41% of the total cell number in the planktonic phase of the model. In the synthetic community biofilm, there were 3.35×10^8 dead cells after 9 days. This was 9.64%

of the total biofilm cell number. There were 3.14×10^9 live cells in the biofilm, accounting for 90.36% of the total biofilm cell number. The overall number of cells in the reactor was 9.09×10^{10} cells. These results show that the viability of the planktonic phase was greater when the synthetic community was grown on sucrose, than in any experiment tested using glucose in AFMC ($p < 0.05$). This could be because *S. mutans* had better tolerance to the acidic conditions in the bulk when grown on sucrose due to an ATR and EPS formation (see Chapter 1). Furthermore, this was the only experiment where the viability was greater for the bulk than it was for the biofilm. The viability of the biofilm remained high also, second only to reactor experiment 3 (low glucose, high lactic acid).

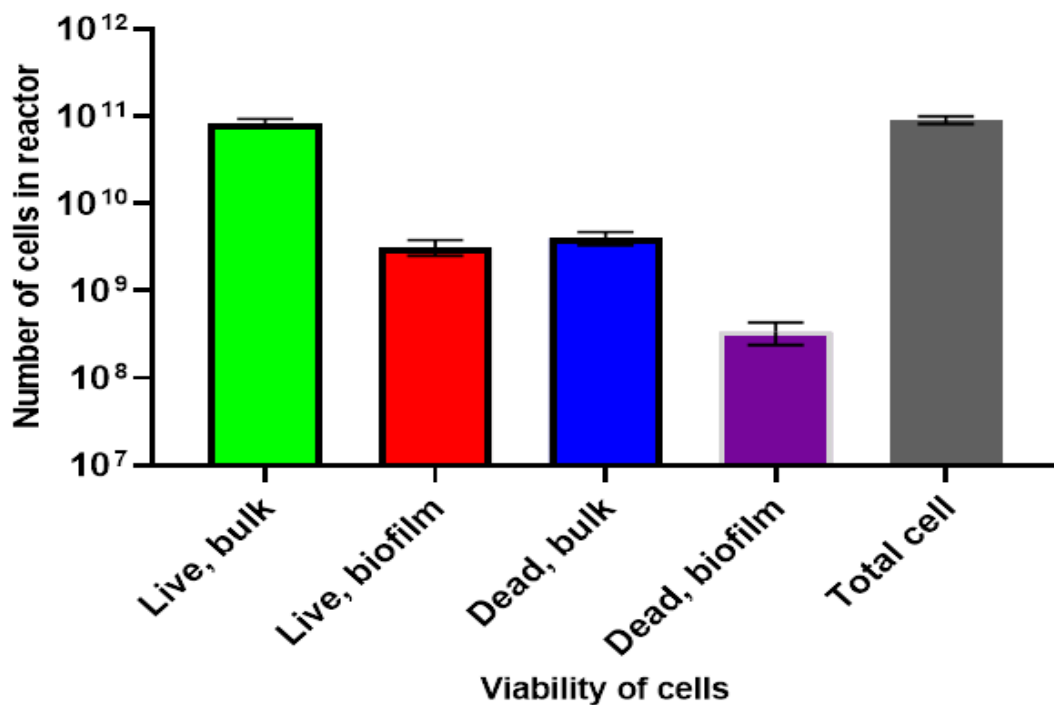


Figure 4.22 Viability of the synthetic community in both the reactor bulk and biofilm for reactor experiment 5 (low sucrose, low lactic acid). Most of the cells in the biofilm were live (red), and there was a greater percentage of live cells in the reactor bulk (green) than in any other condition. Numbers were counted and gated using the NxT flow cytometer, with the average of triplicate samples across three reactors taken. The error bars represent the standard deviation from the mean.

4.4 Discussion

In this Chapter, I aimed to use my defined *in vitro* model to investigate factors underpinning *S. mutans* invasion into a commensal community of oral bacteria, and how those factors and invasion affected the early colonisers. My results demonstrated that a high glucose concentration led to *S. mutans* dominating the planktonic phase at a high glucose concentration, regardless of the lactic acid concentrations tested, and resulted in a large pH drop in the bulk. The higher glucose concentration also led to a decrease in the abundance of the commensal species over time. At the lower glucose and high lactic acid concentration, *V. parvula* dominated the biofilm at high lactic acid concentrations, with a more balanced species abundance observed when the lactic acid concentration was also lowered. Switching to sucrose from glucose increased the abundance of *S. mutans* in the biofilm, although *V. parvula* was still the most dominant species. Using flow cytometry, I also observed that the viability of the biofilm increased significantly at low glucose concentration experiments compared to high glucose concentrations.

I quantified the pH of the reactor bulk over time under different substrate concentrations. There was a significant drop in pH, across all experiments, as the synthetic community developed. This was not surprising as these species, especially the oral *Streptococci*, are known to produce significant amounts of acids (e.g., lactic acid) as they ferment sugars (Dashper & Reynolds, 2000). The pH dropped within the first 24 h across all experiments, where *A. oris* is known to produce acids from the fermentation of glucose (Könönen & Wade, 2015). The pH dropped to a low of 5.23 at reactor experiment 1 (high glucose, high lactic acid) on day 2, where there was an excess of glucose. A similar drop in pH *in vivo* would likely cause tooth demineralisation (Dawes, 2003). This decrease from pH 7 to 5.3 was significant, as pH is a log scale and so this meant there was 100 times more H⁺ present. The reduction in glucose concentration conditions during experiments 3 (low glucose, high lactic acid) and 4 (low glucose, low lactic acid), led to a much higher pH at the end of the experiment. This can be explained by a shift of the bacterial abundance away from *S. mutans* and towards *V. parvula*, which is known to consume lactic acid to produce weaker acids, rather than ferment sugars to produce strong acids (Palmer et al., 2006). Whilst the pH on day 9 was similar for glucose and sucrose, there was a much lower pH by day 3 compared to glucose. The production of more acid from bacteria grown on sucrose has been observed before. It is also known to cause a shift towards aciduric species (Matsui & Cvitkovitch, 2010b). The *in vitro* model, therefore,

replicated *in vivo* findings that the fermentation of sucrose is more acid-contributing than glucose.

Significant growth was observed in the reactor bulk by measuring the optical density. This was expected as the species reached high OD_{600nm} values in monoculture (Chapter 3). The significant drop in OD_{600nm} over time during reactor experiments 1 (high glucose, high lactic acid) and 2 (high glucose, intermediate lactic acid), where there was a high glucose concentration, was likely due to the low pH of the reactor bulk, caused by fermentation of glucose by the oral species (excluding *V. parvula*). It is known that a low pH causes cell stress and creates a suboptimal environment for growth. This can lead to cell death. (Guan & Liu, 2020b). This also explained why decreasing the substrate concentrations in reactor experiments 3 (low glucose, high lactic acid), 4 (low glucose, low lactic acid), and 5 (low sucrose, low lactic acid), led to a higher end OD_{600nm} value at day 9, as it resulted in higher pH of the bulk, therefore less cell stress. Whilst there was still a high lactic acid concentration in reactor experiment 3 (low glucose, high lactic acid), consumption of lactic acid by *V. parvula* did not contribute as much to an acidic environment, as it was breaking this acid down into weaker acids, specifically propionic acid and formic acid (Seeliger et al., 2002.)

I intended to study the invasion of *S. mutans* into the pre-formed dental biofilm in both a glucose-rich and glucose-limiting system. My results showed that reactor experiments 1 (high glucose, high lactic acid) and 2 (high glucose, intermediate lactic acid) contained an excess of glucose, whilst experiments 3 (low glucose, high lactic acid) and 4 (low glucose, low lactic acid) were glucose limiting. The significant amount of glucose consumed, as seen in Figure 4.3, can be explained by the substrate utilisation experiments in Chapter 3, where 4 of the species consume a large amount of glucose in monoculture. In this Chapter, the bacteria were in mixed-culture, therefore glucose consumption could be different from the monoculture experiments in Chapter 3. This is because species were competing for the same substrate and behave differently in a mixed-species environment (Elias & Banin, 2012). The glucose consumption can be attributed to the known findings that glucose is used as a preferential carbon source by oral species, particularly the *Streptococci* (Willenborg & Goethe, 2016b). This explained why the glucose concentration depleted so quickly, especially as *S. gordonii* dominated the bulk by day 2 and *A. oris*, the species that grew in the first 24 h, also uses glucose for growth (Norimatsu et al., 2015).

I quantified the lactic acid concentration in the reactor bulk to understand the potential impact on pH. Also, to understand the balance between lactic acid producers i.e., *Streptococci*, which played an important role in the acidification of the environment, as shown by the significant pH decrease, and the lactic acid consumer *V. parvula*. The oral *Streptococci* are known to produce significant amounts of lactic acid in sugar-rich, oxygen-limiting environments (Willenborg & Goethe, 2016c), which explained the lactic acid increase seen in reactor experiment 2 (high glucose, intermediate lactic acid). Especially, as the qPCR results here show that *S. mutans* dominated this system. The significant drop in lactic acid seen within the first 24 h in reactor experiment 1 (high glucose, high lactic acid) was surprising as *A. oris*, the only species present, consumed glucose as a primary substrate according to results in Chapter 3 and literature (N. Takahashi & Yamada, 1999). One explanation is that whilst *A. oris* is known to produce lactic acid in an anaerobic environment, it has also been shown to utilise lactic acid in oxygen-rich environments (van der Hoeven & van den Kieboom, 1990; N. Takahashi & Yamada, 1999), and there is likely to be more oxygen present in the first day of the invasion experiment. This was because *N. subflava* is an aerobe and would have consumed oxygen within the reactor when it was inoculated on day 2. The lactic acid concentration decrease seen in reactor experiments 3 (low glucose, high lactic acid), 4 (low glucose, high lactic acid) and 5 (low sucrose, low lactic acid) can be explained by *V. parvula* dominance. This species has been shown to consume lactic acid from the substrate consumption experiments in Chapter 3 and what was known in the literature (Gronow et al., 2010b). Overall, I have observed from these results that lactic acid concentrations made a difference in the synthetic community biofilm composition, as seen by the drop in relative abundance of *V. parvula* between reactor experiments 3 (low glucose, high lactic acid) and 4 (low glucose, low lactic acid), from 91.60% to 54.81% respectively.

The dominance of *S. mutans* in the bulk of reactor experiments 1 (high glucose, high lactic acid) and 2 (high glucose, intermediate lactic acid), as seen in the qPCR results, was likely due to the significant pH drop and the ability of *S. mutans* to adapt to this harsh environment. This is more likely to be a contributing factor than direct substrate availability or growth rates. This is because both *S. gordonii* and *N. subflava* grew to high turbidity on excess glucose, and *S. gordonii* had a faster growth rate than *S. mutans* (Chapter 3), yet *S. mutans* still dominated. *S. mutans* is well known to be able to cope with acidic conditions (Baker et al., 2017) which gave it a competitive advantage over other synthetic community species. The decrease in the

relative abundance of the other bacteria was likely to be down to the pH drop, where acidic conditions are known to lead to cell stress (Guan & Liu, 2020c). The excess of glucose and lactic acid in reactor experiments 1 and 2, compared to experiments 3 and 4, lead to greater growth and therefore a lower pH. *V. parvula* increases significantly in abundance in reactor experiments 3, 4, and 5, explained by the fact that it consumes lactic acid (Mashima & Nakazawa, 2015b) rather than glucose and sucrose like the other species do, so it is not competing for the same nutrients. In all experiments, *N. subflava* decreases in abundance over time. This is likely due to the oxygen limitation in the reactors, with *N. subflava* generally requiring oxygen for growth. It has been observed that some *Neisseria* species can grow in oxygen-limiting systems by reducing nitrate (Rock et al., 2007), so further work could be done to see if supplementing with nitrate would help *N. subflava* establish better in this reactor model.

The dominance of species in the *in vitro* model biofilm correlates well with those seen in the reactor bulk for experiments 1 and 2. The *S. mutans* dominance, accounting for 99% of cell number occurred in both the biofilm and planktonic. This *S. mutans* dominance, in the reactor experiments with the lowest pH, is likely to be due to the competitive advantage of *S. mutans* in acidic environments, seen in Chapter 3, as well as literature (Matsui & Cvitkovitch, 2010b). In reactor experiment 3 there were significant differences in species abundance between the biofilm and the bulk, where *V. parvula* comprised 91% of the biofilm, but only 36.46% of the planktonic phase, while *S. mutans* comprised 63.40% of the bulk in reactor 3, but only 3.51% of the biofilm. This could be explained by the greater availability of glucose in the planktonic bulk than in the biofilm, where *S. mutans* may not have a sufficient amount of glucose. The excess lactic acid seen in Figure 4.4 showed that lactic acid was likely in abundance for *V. parvula* to grow. The difference in nutrient availability between the bulk and the biofilm can affect species growth (Reddersen et al., 2021). Changing the carbon source from glucose to sucrose in reactor experiment 5 (low sucrose, low lactic acid) led to a greater ratio of *S. mutans* to *S. gordonii* in the biofilm. *S. mutans* was not able to dominate the biofilm, with *V. parvula* comprising 70.12% abundance. This contradicts findings in the literature, where sucrose gives *S. mutans* a competitive advantage *in vivo* and *in vitro* due to EPS production and attachment (Costa Oliveira et al., 2021b; van der Hoeven et al., 1985; Tanzer et al., 2012). One explanation for this could be the limited concentration of sucrose testing, leading to a limited substrate source. *S. gordonii*, *A. oris* and *N. subflava* all consumed sucrose in Chapter 3, likely reducing

the amount of sucrose available to *S. mutans* even further. This could be tested in future work by increasing the sucrose concentration supplemented in AFMC. Whilst low lactic acid concentration was fed in this experiment, *V. parvula* faces less competition for this substrate and consumes lactic acid produced by the other species (Dashper & Reynolds, 1996.).

The use of FISH proved useful in imaging the synthetic community species. The dominance of *S. mutans* was confirmed through FISH in these images, particularly at the high glucose concentrations, but the prevalence of *V. parvula* at the lower sugar concentrations, as seen in the qPCR results, was not as evident. This meant that the technique was only in partial agreement with what was seen with the qPCR. The structural difference seen on sucrose, where large islands of *S. mutans* were seen in the FISH images for reactor experiment 5 (low sucrose, low lactic acid), was also observed by Kreth (2002). Using spectral fingerprinting and optimising steps seen in Chapter 3 helped reduce autofluorescence, background noise, and bleed-through from emission channels. This did not reduce all of this though, and in particular there was bleed-through of the Alexa 405 blue dye, attached to *N. subflava*, indicating far more of this species than what was quantified in the qPCR. These concerns limit FISH as a quantitative tool in its current form. There has been extensive work done in other labs, notably from Borisey's group (2012), which developed a "CLASI-FISH" approach, including the use of refined spectral fingerprinting and attaching two fluorescent probes to each species, to accurately image 15 taxa (Valm et al., 2012). This showed that it is possible to use FISH more effectively, given more time to refine the technique. Furthermore, there have been recent techniques that improve on using basic fingerprinting to circumvent the issues regarding spectrally overlapping fluorophores (Seo et al., 2022).

The significant difference in viability between the high glucose concentrations (reactor experiments 1 and 2) and low concentrations of sugar (reactor experiments 3,4 and 5) was likely to do with the stress of the high pH in those experiments. This can affect the viability of synthetic community members, as seen with *S. gordonii* (N Takahashi & Yamada, 1999). The viability of the planktonic phase at day 9 for reactor experiment 1 being only 42.64% shows how stressed a mixed culture can become as the pH drops to approximately 5.2. Not only is it well known that biofilms are more resistant to such stresses (Singh et al., 2017; Lories et al., 2020; Lee et al., 2014a; Rath et al., 2021), but there is research done showing that mixed-species biofilms show unique resilience not seen in mono-species biofilms or mixed-species planktonic cultures due to community level interactions (Lee et al., 2014b). Biofilm

quantification with qPCR and flow cytometry only accounted for growth on hydroxyapatite coupons, despite biofilm also having been observed to grow on the coupon holders. This meant that cell counting only approximated that in the system. Future work to quantify the viability changing over time would help correlate this with the pH of the bulk.

The synthetic community species established in a biofilm in all cases, but with *N. subflava* struggling in an environment that was oxygen-depleted, future work should consider controlling oxygen or at least feeding in a nitrate source, as the nitrate reduction by *N. subflava* (Prasetianto Wicaksono et al., 2020; Rock et al., 2007) would help it fare better in the synthetic community. The numerous sampling opportunities provided by the CDC reactor (21 in total), were very useful considering the abundance of techniques used in this section. The ability to control as many variables and sample as many biofilms is not something that would have been possible in more simple *in vitro* devices e.g., microtiter plates. Development of this model helped inform on the conditions needed to protect commensal species, such as lowering sugar concentration to prevent a significant pH drop. The ability to change one parameter at a time i.e., sugar concentration, was possible by using AFMC. Other models, using the CDC reactor to grow dental biofilms on a rich medium, did not offer the same control and simplification of the chemical environment (Rudney et al., 2012). Finally, the ability to replace a coupon holder in the CDC reactor allowed the continuous recording of pH. This allowed me to determine that a significant pH drop led to *S. mutans* dominance from day 5 onwards in the CDC reactors the experiments with low pH (high glucose), and *V. parvula* dominance at the higher pH (low glucose) conditions. This benefit has also been used in other CDC reactor models when characterising dental biofilms (An et al., 2022).

The model has the potential to inform safe product development by testing the use of antimicrobial actives on *S. mutans* invasion. Having developed the *in vitro* model and understood the invasion into the biofilm under different conditions, the next section of work (Chapter 5) aimed to develop an *in silico* model to simulate *S. mutans* invasion and biofilm growth. The results from the *in vitro* model were compared to the results of the *in silico* model. The significant impact of pH on *S. mutans* invasion, and the commensal species, seen in this Chapter, provided evidence that pH considerations need to be made during *in silico* simulations. This was made more necessary by the results in Chapter 3, which demonstrate that the synthetic community species were all impacted differently by low pH conditions, with *S. mutans* having a competitive advantage.

Chapter 5- *In silico* modelling approaches to characterise the invasion of *Streptococcus mutans* into an oral commensal community

5.1 Introduction

It is important to characterise the transition of a health-associated dental biofilm, to one overpopulated by acidogenic species. This includes the invasion and activity of cariogenic species e.g., *S. mutans*, which is implicated in caries prevalence and progression (Nanda et al., 2015). The abundance of bacteria and the numerous interspecies interactions in the mouth, where over 750 bacterial species have been identified (Chen *et al.*, 2010; Verma *et al.*, 2018), leads to challenges in disentangling the *in vivo* complexity. It is necessary to do so to understand the factors that contribute towards caries.

Mathematical models are recognized to play a key role in characterising biofilms, and they have significantly contributed to the advancement of the field (Dzianach *et al.*, 2019). There are limited reports of *in silico* models being used in dental biofilm research (Dzianach *et al.*, 2019). The groundwork was set by the pioneering work of Dibdin and Reece (Dibdin, 1990; Dibdin & Reece, 1984), who developed 1-D and 2-D continuous models, to calculate the pH profiles in the dental biofilm. These models were pioneering in the application of mathematical modelling in dental biofilm research. Early continuous models did not differentiate between species, nor consider their interactions. The study by Wimpenny *et al.*, (1997) focused on the diffusion of substrates within dental biofilms, rather than the role of individual bacteria. More recent models have better captured the complex interactions between species, including simulating lactic acid production/consumption, to understand their function in dental biofilms. This includes the work by Ilie *et al.*, (2012). This continuous model considered four microbial species (aciduric *Streptococcus*; non-aciduric *Streptococcus*, *Actinomyces* and *Veillonella*), and several metabolic processes of these bacteria, including anaerobic glucose fermentation and lactate fermentation. The model hypothesised, and confirmed, that *Veillonella* had a protective effect against demineralisation, as it consumed the lactic acid produced by aciduric *Streptococcus*. However, recent experimental results contradict this finding and suggested that *Veillonella* may participate in the development of caries through increased EPS production of *S. mutans* and reducing the inhibitory effect of lactic acid buildup (Liu *et al.*, 2020). This showed that oral species can play varying functions within the dental biofilm, both beneficiary and detrimental. These contradictions between *in*

silico and *in vitro* models emphasise the need for validation of the *in silico* models with *in vivo/in vitro* experiments.

The use of Individual-based models (IbM) has allowed for the studying of bacterial species on an individual agent basis in dental biofilm research. This is important as each bacterial cell has a biological, physical, and chemical impact on surrounding cells and the environment (and vice versa). IbM enables the characterising of these influences. Whilst limited in number, these types of models have shown promise in characterising dental biofilms. One such model was that developed by Head *et al.*, (Head *et al.*, 2014a). This model considered a dental biofilm formed by two competing types of acidogenic bacteria, with one being aciduric and therefore pathogenic. The two types of bacteria competed for space, but not for glucose, as there was no mass transfer limitation considered for this substrate in the model. Bacteria only interacted through acid production. This limitation of the model was later relaxed in their follow-up paper (Head *et al.*, 2017), where glucose diffusion in the biofilm was considered. Head (Head *et al.*, 2017) recommended that simulation models required validation with *in vitro* experiments, to better understand species behaviour i.e., substrate usage. A limitation of this study was the consideration of only two types of bacteria, which does not suitably represent the dental biofilm as well as the study by Ilie *et al.*, (Ilie *et al.*, 2012). As the dental biofilm responsible for demineralisation is surrounded by bacterial load in the saliva, both continuous modelling of planktonic cells and IbM modelling of biofilms are useful tools in combination. This would help better the known influence of saliva on biofilms and its role in caries progression (Belstrøm *et al.*, 2014; Rusu *et al.*, 2022).

Studies utilising mixed *in vitro* and *in silico* approaches, to understand dental biofilm activity in caries, are limited. Rath *et al.*, (2017) analysed *S. gordonii* biofilms by combining *in vitro* and *in silico* modelling strategies to predict dental biofilm formation. However, this model only considered a mono-species biofilm, so does not capture the complexity of dental biofilms, and the validation of the model was only based on the biofilm height. Even two species systems, such as that by Martin *et al.*, (Martin *et al.*, 2017) used to observe the interactions between *P. gingivalis* and *S. gordonii*, do not capture the complexity of dental biofilms in the mouth due to a lack of species considered. This model also did not consider a flow rate similar to that in the oral environment. This is important to mimic, as salivary flow directly affects dental biofilm formation (Sotozono *et al.*, 2021).

An important environmental impact on bacteria within dental biofilms is the pH. The fermentation of sugars by bacteria produces acids e.g., lactic acid decreases the pH in dental biofilms. This decrease in pH is conserved in microenvironments for several hours (Schlafer *et al.*, 2011). This leads to bacterial cell stress, including compromising the structural integrity of cell membranes (Guan & Liu, 2020a). Species have different optimum pH levels for growth, and gradients found within carious lesions have led to differing species abundance. This includes a high abundance of *Lactobacilli* in low pH ranges of 5.5-6.0. Species such as *S. mutans* have shown an acid tolerance response allowing them to thrive in low pH environments often associated *in vivo* with caries sites, relative to other species (McNeill & Hamilton, 2003b). This acid tolerance has been shown to be greater in biofilms than in planktonic cells (Boisen *et al.*, 2021b). With the importance of pH in the relationship of dental biofilms and caries progression, and the variation of behaviour between species at different pH, it becomes evident that this needs to be considered during simulation to understand dental biofilm behaviour *in vivo*. Whilst models have considered pH in the bacterial growth kinetics to characterise biofilms (1995), this application has been limited in dental biofilm research.

It is desirable to use *in silico* models, considering representative, multispecies communities, as a tool in dental biofilm research and caries development. This should also consider the direct impact of pH on species kinetics. By using a combination of *in vitro* and *in silico* approaches, including the use of a CDM, the influence of factors i.e., sugar concentration, on *S. mutans* invasion and commensal species growth, can be tested one parameter at a time. This includes the effect of sugar concentration on pH, species growth, and the transition of a healthy biofilm to a cariogenic-associated state. These *in silico* models should be informed with experimental work, including species-specific kinetic parameters i.e., maximum specific growth rate (μ_{max}) and (K_s). This has previously resulted in models better reflecting *in vivo* and *in vivo* data, compared to those that do not consider species-specific kinetic parameters (1995).

5.2 Aims and objectives

In this chapter, I aimed to characterise the factors driving *S. mutans* into a pre-formed, 4 species oral commensal community. I also aimed to quantify the resulting effect on the local environment i.e., pH change, and the effect on the commensal bacterial community, to understand the transition of a commensal microbiome to a caries-associated one. To do this, I aimed to model the synthetic community bulk using continuous modelling, and the synthetic community biofilm using IbM. Simulations were run under the same glucose and lactic acid concentrations as those tested in the *in vitro* model. This allowed for the direct connection and comparison between simulations and experimental data, which was facilitated by the experimental use of AFM. This underpinned the defined species stoichiometry. The models were also informed by experimentally collected kinetic parameters, μ_{max} and K_s . The models were used with and without direct pH consideration in the bacterial growth kinetics, to understand the effect of pH on simulating invasion beyond chemical speciation.

Objectives:

- 1) Simulate the substrate concentration and pH profile of the bulk, using continuum modelling, as the synthetic community grew over 216 h.
- 2) Simulate the relative abundance of the synthetic community species in the bulk at the same glucose and lactic acid concentrations tested in Chapter 4.
- 3) Use the individual-based model to simulate the pH and substrate concentrations of the synthetic community biofilm.
- 4) Simulate the invasion of *S. mutans* into the 4-species commensal dental biofilm, using the 2-D IbM.
- 5) Investigate the effect of different seeding strategies, on invasion and species abundance. This included simulating *S. mutans* invasion when cells were seeded clustered bacteria by species and comparing invasion to when seeding mirrored the same inoculation strategy implemented in the *in vitro* experiments.

5.3 Results

5.3.1 Description of *in silico* modelling experiments

The invasion of *S. mutans* into a 4-species commensal oral community. was simulated concurrently with the glucose/lactic acid concentrations and pH change. A 0-D continuum model was used to simulate these in the bulk, whilst a 2-D IbM was used to simulate the synthetic community biofilm. The substrate concentrations in AFMC and starting pH were identical to the experiments in Chapter 4, so that simulation and experimental results could be compared. These conditions were detailed in Table 5.1

Table 5.1 Simulation conditions mirrored those of the reactor experiments in Chapter 4. Reactor experiments 1 (high glucose, high lactic acid) and 2 (high glucose, intermediate lactic acid), were at high glucose concentrations. Reactor experiments 3 (low glucose, high lactic acid) and 4 (low glucose, low lactic acid) were at low glucose concentrations. The lactic acid concentrations were intermediate in reactor experiment 3 and low in reactor experiment 4. The starting pH was similar across all simulation runs.

| | Glucose concentration (gL ⁻¹) | Lactic acid concentration (gL ⁻¹) | Starting pH |
|-------------------------|--|--|-------------|
| Reactor experiment 1 | 21.85 | 11.61 | 6.92 |
| Reactor experiment 2 | 21.30 | 6.28 | 6.82 |
| Reactor experiment 3 | 2.09 | 12.46 | 6.94 |
| Reactor experiment 4 | 1.98 | 2.61 | 6.93 |

The continuous model simulations of the bulk in Section 5.3.2A-D followed the same seeding strategy as the experiments in Chapter 4. The order of inoculation was *A. oris* on day 1; *S. gordonii*, *N. subflava* and *V. parvula* on day 2; and *S. mutans* on day 3. For IbM simulations of the biofilm in 5.3.4A-C, the domain was first seeded with 46 bacterial cells, such that the entire first row of the computational domain was filled with bacterial cells, placed at an equal distance from each other and from the walls of the computational domain. The five species

were seeded with the same initial number of agents, while the positions of the agents were randomly assigned.

The flow rate was kept the same as the *in vitro* experiments, at 0.4 mL min^{-1} , to mirror that of saliva (Iorgulescu, 2009), as was the temperature at $37 \text{ }^\circ\text{C}$ (Sund-Levander et al., 2002). The results of the simulations were plotted against experimental data from Chapter 4. A simplified stoichiometry (see Chapter 2) was proposed, where the facultative anaerobes *S. gordonii*, *S. mutans* and *A. oris* fermented glucose, producing lactic acid. The obligate anaerobe *V. parvula* consumed lactic acid as the primary carbon source and electron donor, producing acetate and propionate. Acetate, formate and propionate contributed to the pH calculation, being considered as soluble species as part of the species stoichiometry, mass and charge balances (see Chapter 2). Initially, pH was not considered directly in bacteria kinetics, only in chemical speciation. I then considered the pH corrections into μ_{max} , as done by Rosso (Rosso et al., 1995). This involved considering three pH species-specific parameters (see Chapter 2). The pH for optimal growth (pH_{opt}), the pH above which no growth occurred (pH_{max}), and the pH below which no growth occurred (pH_{min}). The aerobe *N. subflava* consumed glucose and had oxygen as the primary electron donor, producing acetate and formate (Bradshaw & Marsh, 1998b). These chemical components were considered in the mass balance according to the stoichiometry of each species (Chapter 2). *N. subflava* was considered in the synthetic community as a scavenger for oxygen, to protect the strict anaerobes, as reported in chemostat experiments modelling dental biofilm species (Bradshaw et al., 1996). A constant oxygen concentration of 1 mg L^{-1} was assumed in the reactor and within the biofilms. This was to satisfy the stoichiometry of *N. subflava* and replicate the experimental micro-aeration conditions.

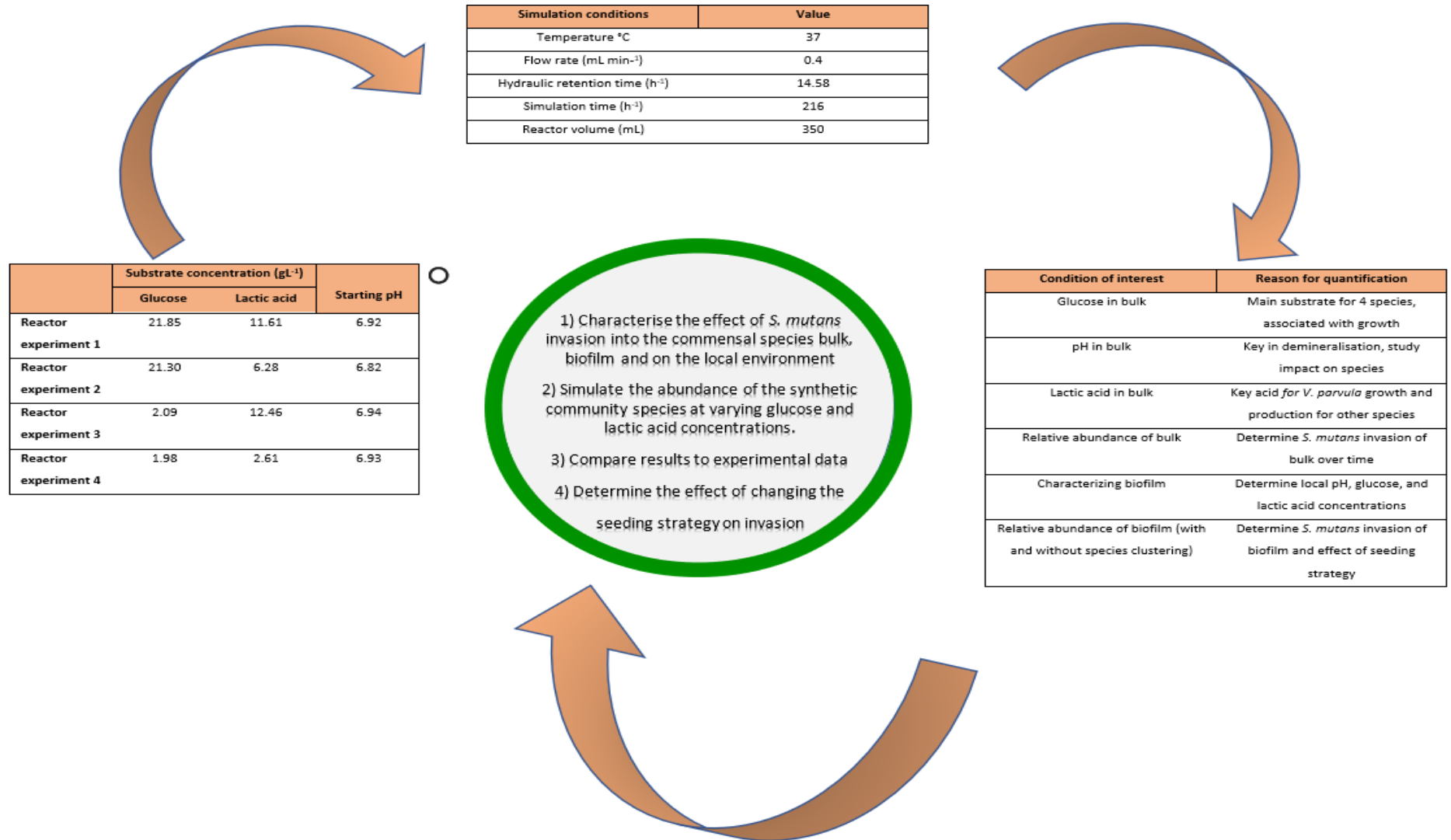


Figure 5.1 Overview of the *in silico* strategy and goals of this chapter to characterise *S. mutans* invasion. Starting substrate concentrations and pH mirrored *in vitro* conditions. Variables i.e., flow rate and temperature, were used to resemble the *in vivo* environment. Simulations were run over 216 h.

5.3.2A The glucose concentration of the reactor bulk

Glucose was the primary substrate consumed by all species of the synthetic community, excluding *V. parvula*. Fermentation of glucose produces biomass, resulting in waste products i.e. lactic acid, propionate, formate and acetate (see stoichiometry Chapter 2). Lactic acid was the main substrate consumed by *V. parvula*. The glucose, lactic acid pH and species abundance were simulated at the same time using continuum modelling.

The glucose concentration of the bulk was simulated concurrently with biomass production. This was to understand the sugar consumption of the synthetic community and its relation to biomass development. The simulation results, both with and without pH consideration in bacterial growth kinetics, were presented in Figure 5.2. The glucose concentration in all simulations decreased over time as biomass grew. The simulated glucose concentration was almost identical in reactor experiment 1 (high glucose, high lactic acid) (Figure 5.2A) and 2 (high glucose, intermediate lactic acid) (Figure 5.2B), which was not the case in the experimental data. The model did agree with experimental data that glucose decreased significantly in concentration over 48 h, followed by an increase until the end of the experiment. Agreement between *in silico* results and the experimental data improved when pH considerations were implemented. Without pH in growth kinetics, the simulated glucose concentration in reactor experiments 1 (high glucose, high lactic acid) and 2 (high glucose, intermediate lactic acid) did not change up until 50 h, and then depleted rapidly. This was not the case in the experimental data, where the glucose concentration decreased from the start of the experiment. The increase in glucose concentration in the experimental data from 72h onwards, was because glucose was still being fed into the reactor whilst biomass decreased, leading to less glucose consumption. In reactor experiments 3 (low glucose, high lactic acid) (Figure 5.2C) and 4 (low glucose, low lactic acid) (Figure 5.2D), the glucose concentration was depleted in the first ~72 h, but did not start decreasing until ~50 h, which was not the case in the experimental data. When the effect of pH on bacteria growth kinetics was considered, the simulations agreed better with the experimental data. There was an excess of glucose by the end of the reactor experiments for reactor experiment 1 (high glucose, high lactic acid) and 2 (high glucose, intermediate lactic acid) for simulations and experimental data. The simulated concentrations dropped steadily between ~50 h and ~120 h. There was a rapid decrease over ~48 h in the experimental data. For reactor experiments 3 (low glucose, high lactic acid) and

4 (low lactic acid), the simulations showed that the glucose was fully consumed in simulations, although a significant decrease in concentration was seen after 50 h in simulation, as opposed to over the first 24 h in the experimental data.

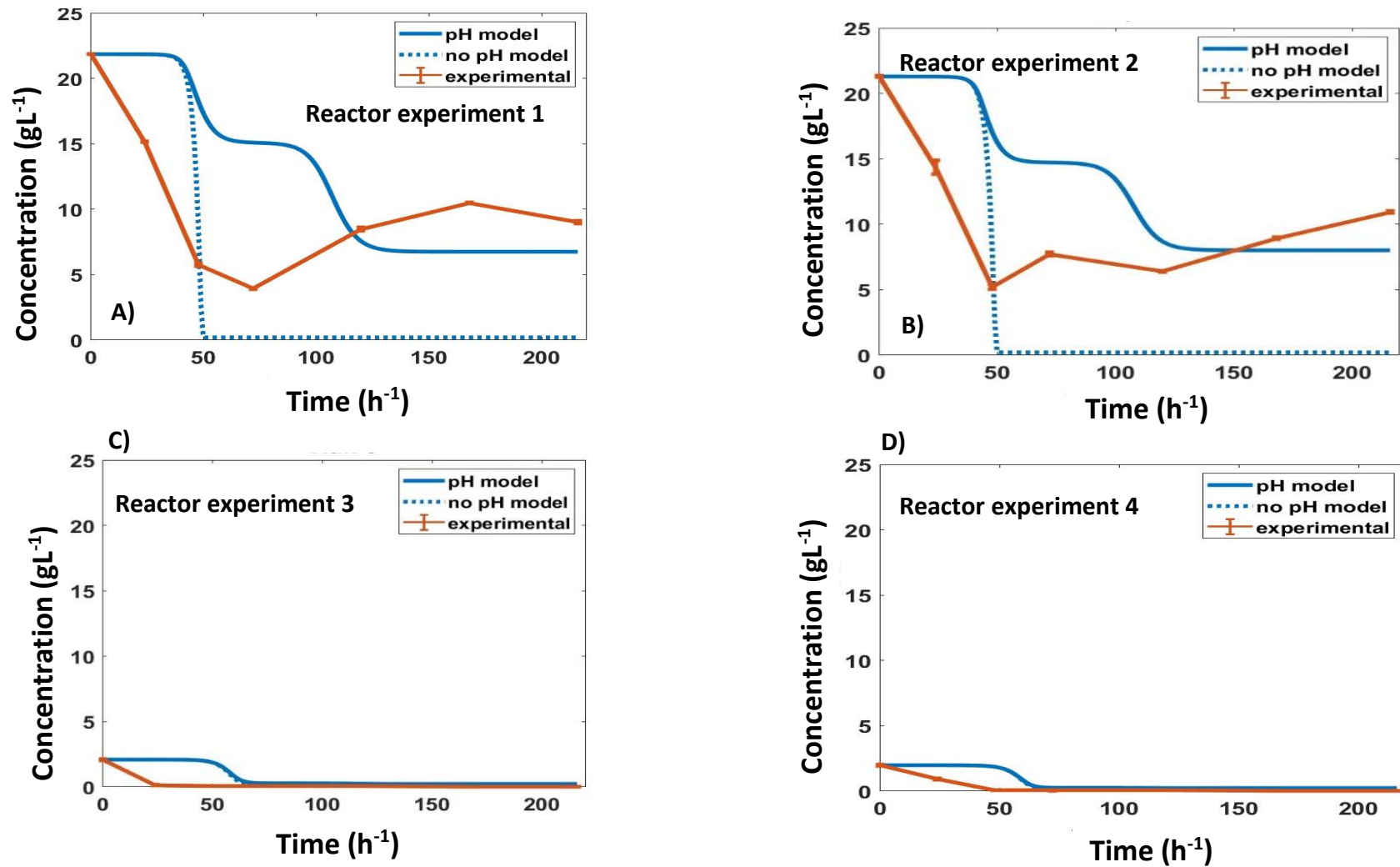


Figure 5.2 Glucose concentrations with and without pH influence on the growth rate of synthetic community members. A) Reactor experiment 1 (high glucose, high lactic acid), B) Reactor experiment 2 (high glucose, intermediate lactic acid), C) Reactor experiment 3 (low glucose, high lactic acid) and D) Reactor experiment 4 (low glucose, low lactic acid). Plots included experimental data (orange), simulation without pH consideration (blue dotted line) and with pH consideration (blue solid line).

5.3.2B The lactic acid concentration of the reactor bulk

Lactic acid was the main by-product of glucose fermentation for all species excluding *V. parvula*, which used it for biomass growth. The lactic acid concentration of the bulk was simulated concurrently with species growth, glucose, and pH. This helped describe lactic acid production/consumption of the synthetic community. This was important as *in vivo* lactic acid is a significant contributor to pH lowering, which leads to demineralisation (Dashper & Reynolds, 1996.). Simulating lactic acid concentration allowed for a better understanding of species growth, as a result of substrate availability in the case of *V. parvula*.

There were still discrepancies between the simulations and experimental data, despite pH corrections being implemented. For reactor experiment 1 (high glucose, high lactic acid) (Figure 5.3A) in simulations, the lactic acid concentration increased at ~50 h, but was depleted by ~100 h when pH was not considered. In the experimental data, the lactic acid dropped over 24 h and then remained similar throughout the experiment. When pH was considered in kinetics in simulations, the lactic acid increased over time. This was as the species grew and *S. mutans* dominated the simulations. In the stoichiometry (see Chapter 2) *S. mutans* produces lactic acid as it grows. The simulation results for reactor experiments 1 (high glucose, high lactic acid) and 2 (high glucose, intermediate lactic acid) (Figure 5.3B) were identical. In the experimental data for reactor experiment 2 (high glucose, intermediate lactic acid), there was still a lactic acid drop over 24 h, but the lactic acid concentration then increased over time, as it did in the simulations. In reactor experiment 3 (high glucose, high lactic acid) (Figure 5.3C), the lactic acid concentration remained constant until ~50 h, increased slightly and dropped to 0 by ~120 h. This contrasted with the experimental data, which showed the lactic acid concentration steadily decreasing over time. The simulation results for reactor experiment 4 (low glucose, low lactic acid) (Figure 5.3D) showed the lactic acid depleted completely with and without pH correction, with pH correction leading to depletion faster at ~100 vs 120 h. This decrease agreed with the experimental data, although this happened much sooner at around 50 h in the experiment. The discrepancy between simulations and experimental data for reactor experiments 1 (high glucose, high lactic acid) and 2 (high glucose intermediate lactic acid), could be explained by the simplified stoichiometry for the bacterial species. This considered that *S. gordonii*, *S. mutans* and *A. oris* produced lactic acid, leading to an increase during simulations from they were introduced on day 2. The consumption of lactic acid over time in both the experimental data and simulations

for reactor experiments 3 (low glucose, high lactic acid) and 4 (low glucose, low lactic acid), could be explained by *V. parvula* dominance, as this species consumed lactic acid for growth.

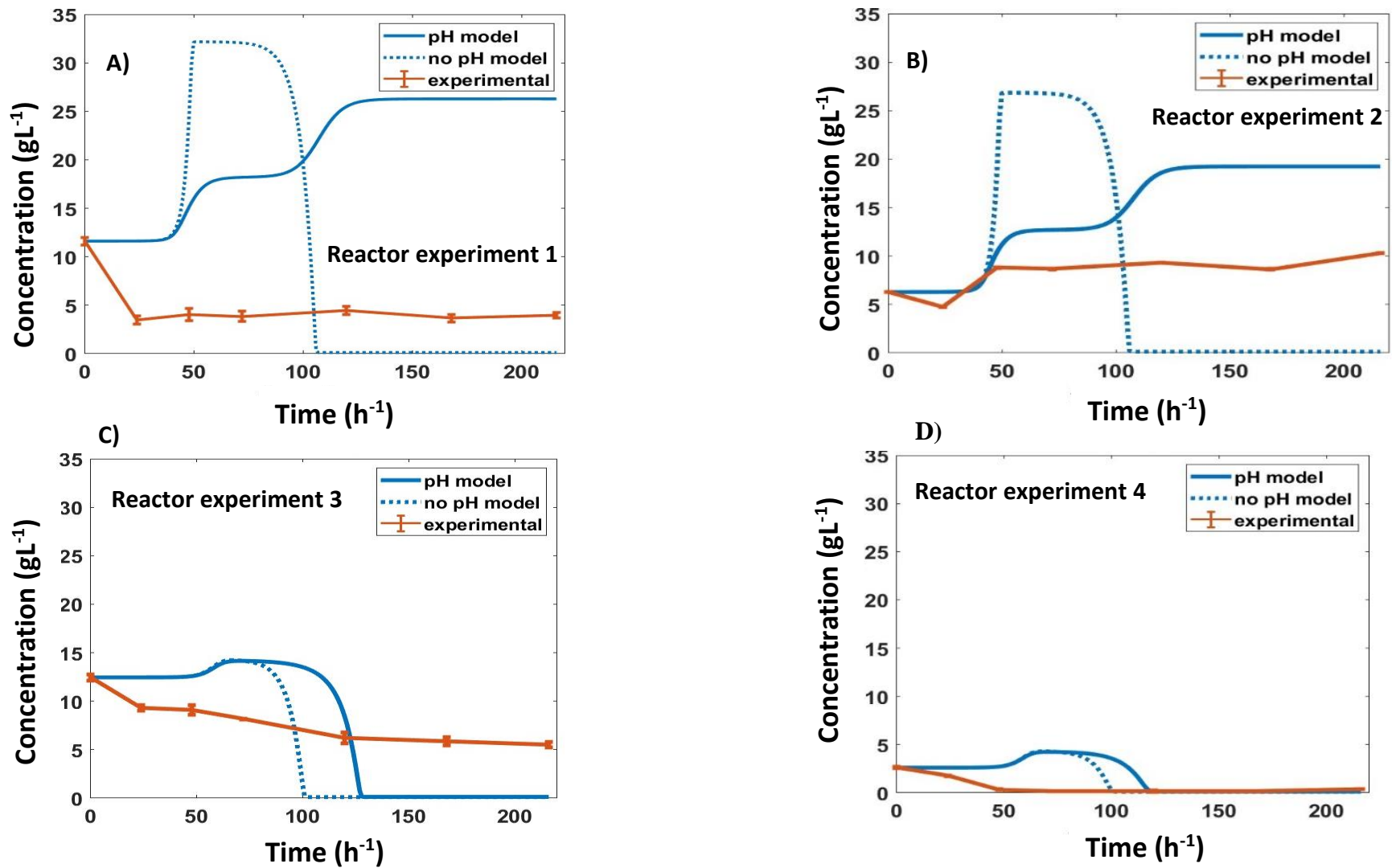


Figure 5.3 Lactic acid concentrations with and without pH influence on the growth rate of synthetic community members. A) Reactor experiment (high glucose, high lactic acid), B) Reactor experiment 2 (high glucose, intermediate lactic acid), C) Reactor experiment 3 (low glucose, high lactic acid) and D) Reactor experiment 4 (low glucose, low lactic acid). Plots included experimental data (orange), simulation without pH consideration (blue dotted line) and with pH consideration (blue solid line).

5.3.2C The pH of the reactor bulk

The pH is an important driver of cariogenic dental biofilm development and its role in enamel demineralisation (see Chapter 1). Furthermore, the experimental data in Chapter 4 indicated that pH was a primary driver of *S. mutans* invasion.

The pH of the reactor bulk decreased across all simulations, regardless of whether pH corrections were implemented in bacterial kinetics. In all cases, the simulated pH was lower than the values recorded in experimental data. For reactor experiment 1 (high glucose, high lactic acid) (Figure 5.4A), the pH dropped to ~4 within 50 h, before increasing back up to 5 by ~100 h. The pH remained constant throughout the rest of the experiment. With pH corrections implemented, the pH also dropped over the first 40 h, to a pH of ~4.7. The pH continues to drop to ~4.2 at 120 h and remained constant until 216 h. The pH of the reactor bulk in the experimental data never reached as low as 5. The simulated pH levels of the bulk for reactor experiment 2 (high glucose, intermediate lactic acid) (Figure 5.4B) were identical to those in reactor experiment 1 (high glucose, high lactic acid), so initial lactic acid concentration did not influence pH.

Simulations for reactor experiment 3 (low glucose, high lactic acid) (Figure 5.4C) demonstrated that the pH patterns were very similar, with a lower pH in reactor experiment 3 (high glucose, high lactic acid) than in reactor experiment 4 (low glucose, low lactic acid) (Figure 5.4D). In both simulations, the pH remained high until ~50 h, then dropped to ~5.7 in reactor experiment 3, and pH 6 in reactor experiment 4 (low glucose, low lactic acid). The pH increased back up further to ~6.30 in reactor experiment 3 at 130 h, before staying constant until the end of the experiment. In reactor experiment 4 (low glucose, low lactic acid) there was not a drastic change in pH between ~50-200 h. The pH simulations show a higher pH for reactor experiments 3 (low glucose, high lactic acid) and 4 (low glucose, low lactic acid), compared to 1 (high glucose, high lactic acid) and 2 (high glucose, intermediate lactic acid). This was likely due to the dominance of *V. parvula* in the bulk. *V. parvula* produces less acid than the *S. mutans*, which dominated the bulk in reactor experiments 1 (high glucose, high lactic acid) and 2 (high glucose, intermediate lactic acid). The lower pH in simulations for reactor experiments 3 (low glucose, high lactic acid) and 4 (low glucose, low lactic acid) were in agreement with the experimental results.

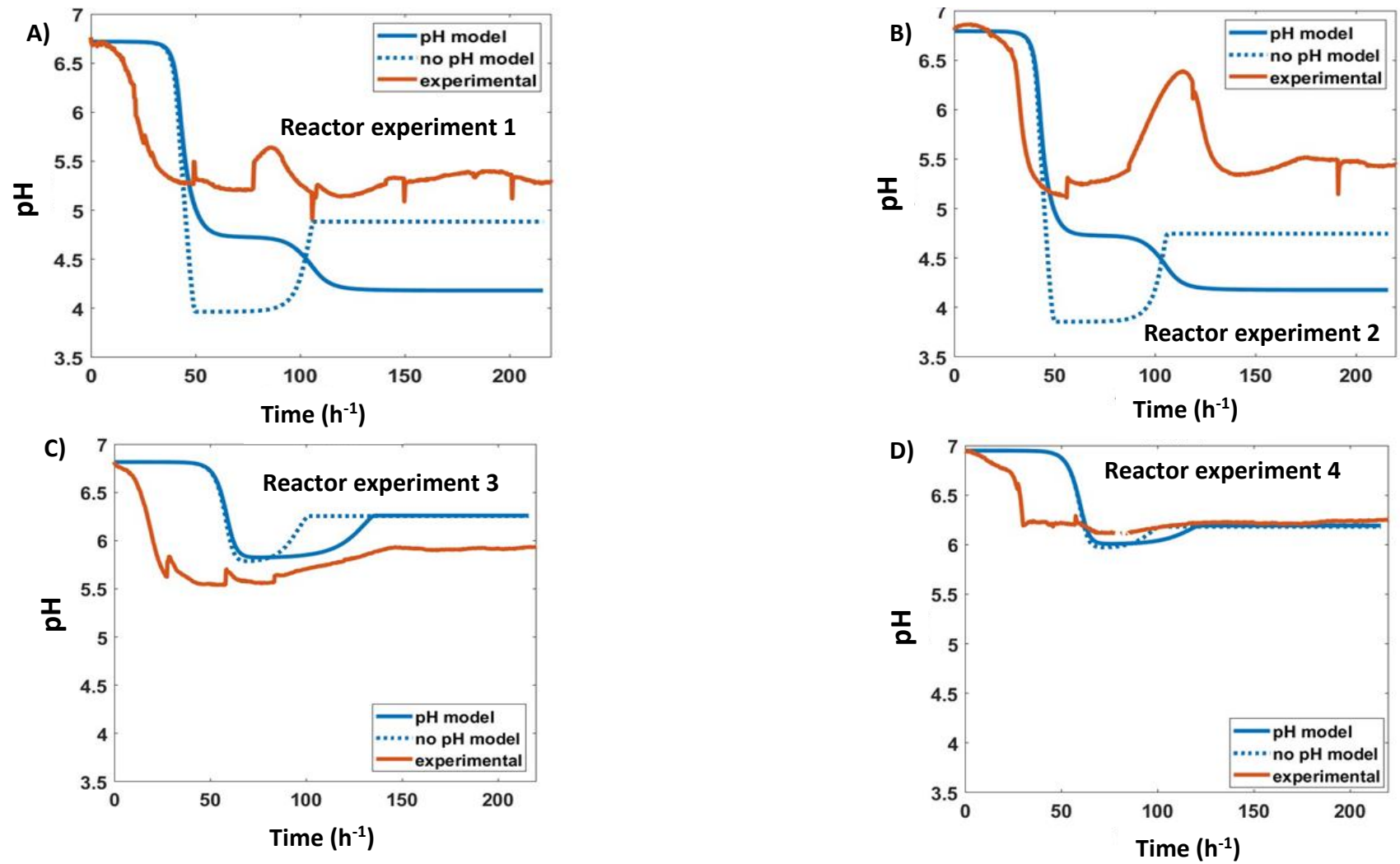


Figure 5.4 The pH of the bulk with and without pH influence on the growth rate of synthetic community members. A) Reactor experiment 1 (high glucose, high lactic acid), B) Reactor experiment 2 (high glucose, intermediate lactic acid), C) Reactor experiment 3 (low glucose, high lactic acid) and D) Reactor experiment 4 (low glucose, low lactic acid). Plots included experimental data (orange), simulation without pH consideration (blue dotted line) and with pH consideration (blue solid line).

5.3.2D Species relative abundance in the bulk

The species relative abundance of the bulk was simulated concurrently with the glucose, lactic acid and pH. This was to determine the invasion of *S. mutans* into the commensal bulk, and the community composition, at varying glucose and lactic acid concentrations. I used the simulated pH, glucose and lactic acid results to understand their influence on *S. mutans* invasion. I compared these relative abundances to those from experimental data to determine if simulations reflected the experiments.

There was a large discrepancy between the simulation results and the experimental data when pH was not considered in bacterial kinetics. For simulations of reactor experiment 1 (high glucose, high lactic acid) (Figure 5.5A), *S. gordonii* initially dominated the bulk between 24 h and 50 h, before dropping in abundance until ~100 h and staying constant. *V. parvula* dominated the bulk from 70 h onwards, increasing up to ~90% abundance by ~100 h. The abundance did not change until the end of the experiment. The simulation results were the same for reactor experiment 2 (high glucose, intermediate lactic acid) (Figure 5.5B). In these simulations, *S. mutans* did not dominate the synthetic community bulk. These results differed significantly from the experimental data. Simulations and experiments corroborated that *S. gordonii* dominated the first 24 h in the bulk in reactor experiments 1 (high glucose, high lactic acid) and 2 (high glucose, intermediate lactic acid). In the experiments, *S. mutans* dominated the bulk, constituting over 99% of the relative abundance by the end of the experiment. *S. gordonii* had the fastest growth rate (see Chapter 3) which explained why it dominated the first 24 h of simulation in reactor experiments 1 (high glucose, high lactic acid) and 2 (high glucose, intermediate lactic acid). The decrease in abundance of *S. gordonii* and the inability of *S. mutans* to invade the bulk can be explained by the depletion of glucose in the system by ~50 h, whilst there was still lactic acid present for *V. parvula* to grow on. Simulations of reactor experiments 3 (low glucose, high lactic acid) (Figure 5.5C) and 4 (low glucose, low lactic acid) (Figure 5.5D) were similar, with a slight decrease in *S. gordonii* at the low glucose concentrations and an increase in *V. parvula* abundance. This showed that altering the glucose concentration in the simulations was not enough in simulating the synthetic community growth patterns seen in the experiments, regarding the invasion and dominance of *S. mutans*. In all simulations without pH consideration, *A. oris* and *N. subflava* struggled to grow over time.

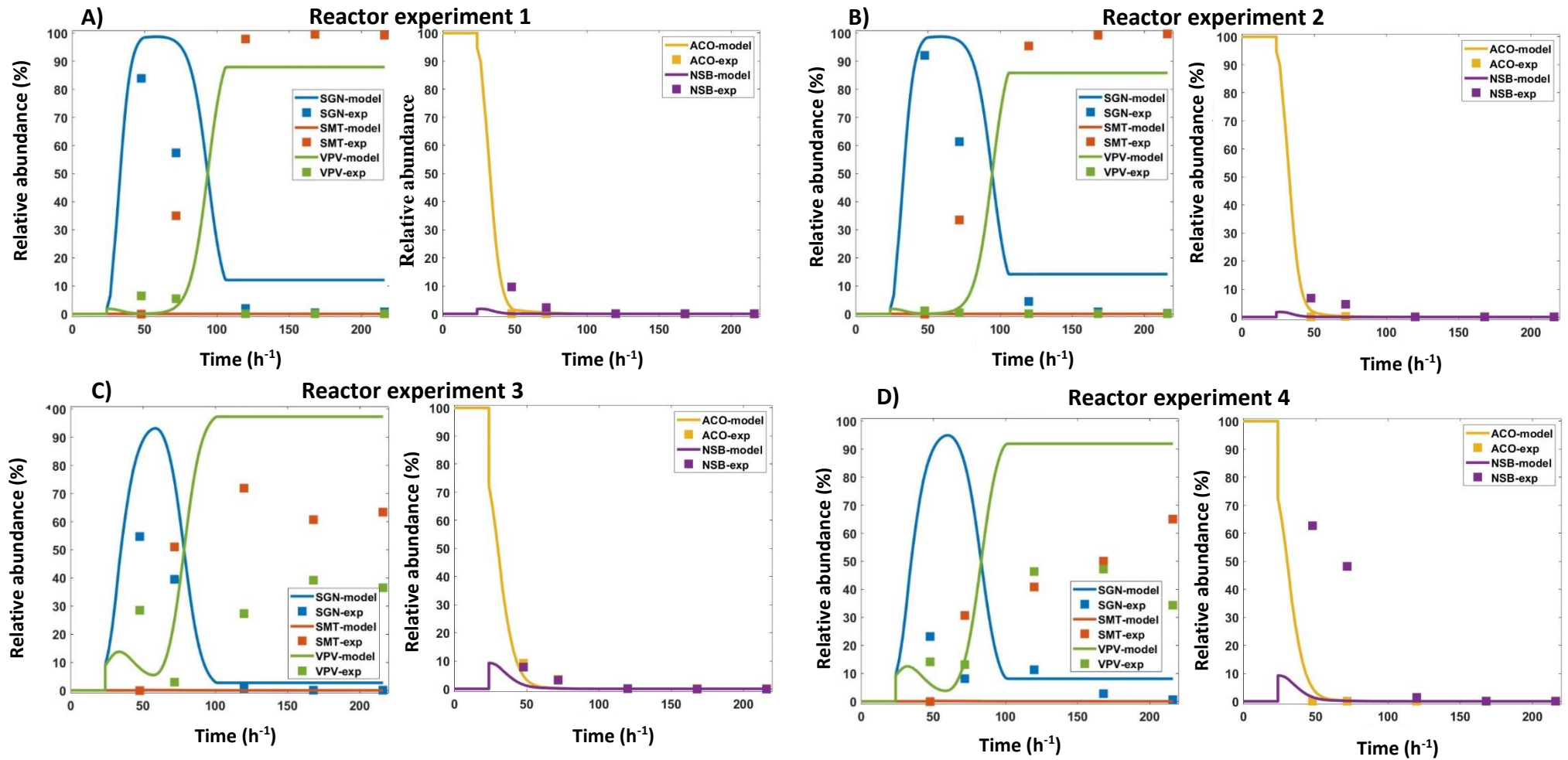


Figure 5.5 Relative abundance of *S. gordonii* (SGN), *S. mutans* (SMT), *V. parvula* (VPV), *A. oris* (ACO), and *N. subflava* (NSB) in the bulk. Model results did not consider pH in growth rates. A) Reactor experiment 1 (high glucose, high lactic acid), B) Reactor experiment 2 (high glucose, intermediate lactic acid), C) Reactor experiment 3 (low glucose, high lactic acid) and D) Reactor experiment 4 (low glucose, low lactic acid).

Considering pH effect on the bacterial kinetics at high glucose concentrations improved the agreement between simulations and experiments for species relative abundance. In simulations for reactor experiment 1 (high glucose, high lactic acid (Figure 5.6A), *S. mutans* dominated the bulk, reaching near 100% abundance by ~120 h. The species dominated the bulk for the remainder of the experiment. The pH consideration in growth kinetics led to difference from simulations without pH corrections, as it considered *S. mutans* ability to thrive in a low pH environment. *S. gordonii* dominated the first 24 h of simulation, as it did in the simulation not considering pH corrections, and in the reactor bulk, decreased in abundance. When considering pH, *S. gordonii* reached ~0% abundance at 216 h, whilst without considering pH, the abundance remained at ~15%. The simulations for reactor experiment 2 (high glucose, intermediate lactic acid) (Figure 5.6B) were identical to reactor experiment 1 (high glucose, high lactic acid), demonstrating that lactic acid did not affect simulation results at either of the high glucose concentrations.

The rank abundance results for simulation of reactor experiments 3 (low glucose, high lactic acid) (Figure 5.6C) and 4 (low glucose, low lactic acid) (Figure 5.6D), were identical to each other. This showed that lactic acid reduction did not significantly hinder the ability of *V. parvula* to dominate the bulk. As with all other simulations, *S. gordonii* dominated the bulk in the first 50 h. In the experimental data, *S. gordonii* abundance at 48 h was 54.61% in reactor experiment 3 (low glucose, high lactic acid), and 23.10 % in reactor experiment 4 (low glucose, low lactic acid), so the models did not agree. This species decreased in abundance down to ~0 in simulations by ~120 h for reactor experiment 3 (low glucose, high lactic acid) and 10% in reactor experiment 4 (low glucose, low lactic acid). Similar to the simulations not factoring pH, *V. parvula* dominated the bulk in reactor experiments 3 (low glucose, high lactic acid) and 4 (low glucose, low lactic acid), comprising ~90% of the bulk by the end of the simulation. During these simulations, glucose was limiting (Figure 5.3 C/D) which led to reduced growth of the species not including *V. parvula*. Lactic acid availability allowed *V. parvula* to dominate the system, as it did in the experimental data. These results showed that pH consideration made an impact, by allowing *S. mutans* to thrive better relative to the other species in the low pH (Figure 5.4 A/B) environment. As it did in the experimental data, *A. oris* and *N. subflava* struggled to grow in simulations at low pH.

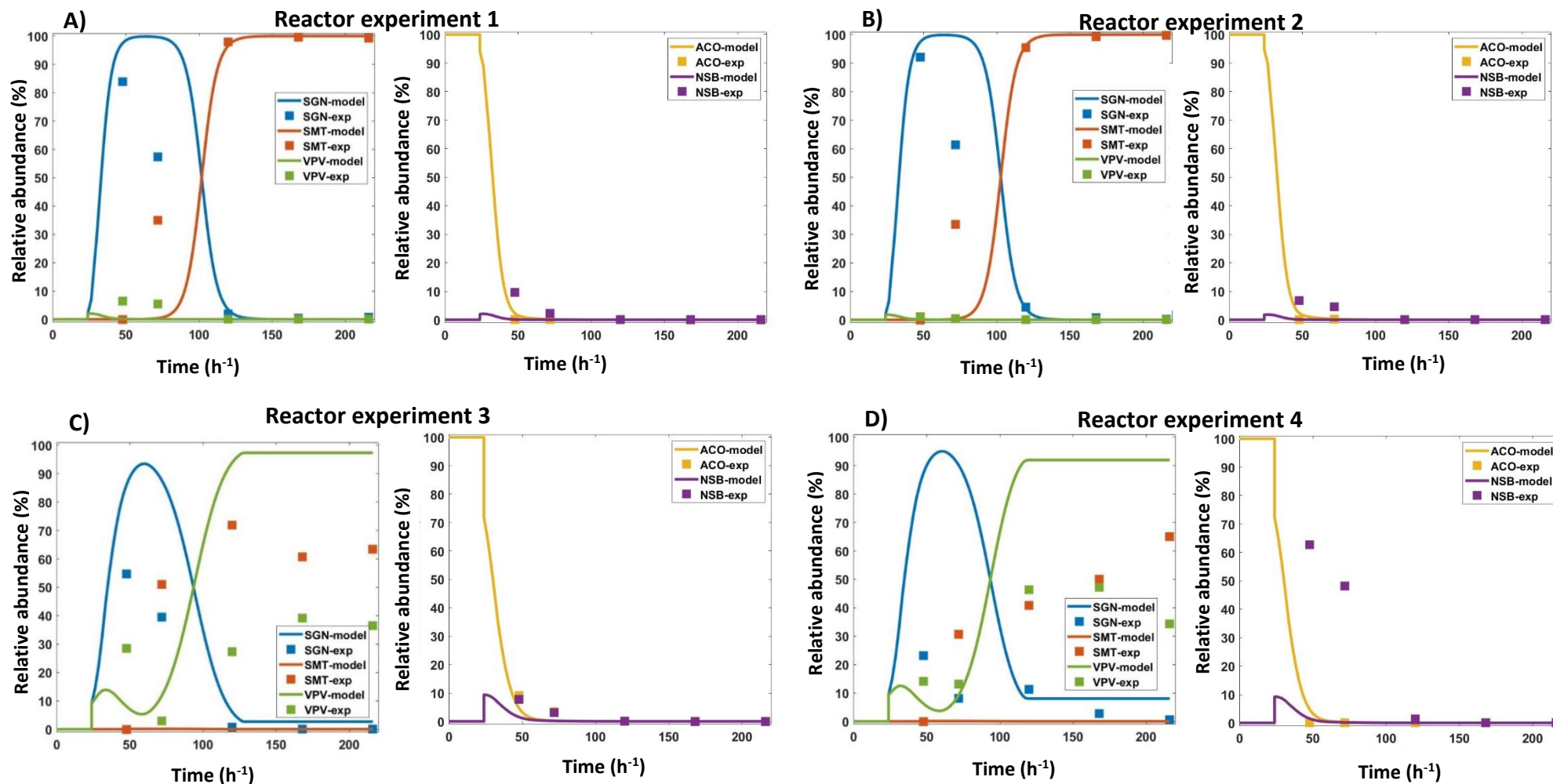


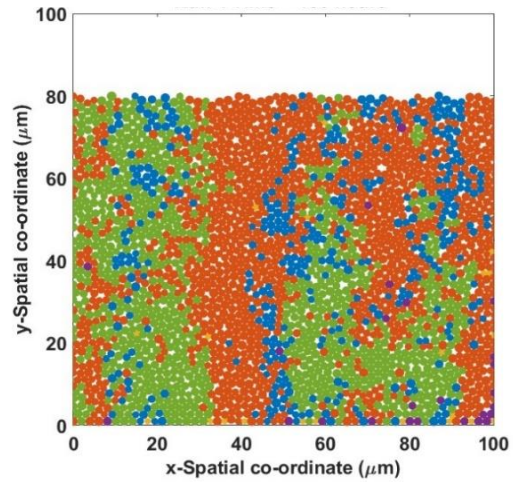
Figure 5.6 Relative abundance of *S. gordonii* (SGN), *S. mutans* (SMT), *V. parvula* (VPV), *A. oris* (ACO), and *N. subflava* (NSB) in the bulk. Model results considered pH in growth rates. A) Reactor experiment 1 (high glucose, high lactic acid), B) Reactor experiment 2 (high glucose, intermediate lactic acid), C) Reactor experiment 3 (low glucose, high lactic acid) and D) Reactor experiment 4 (low glucose, low lactic acid).

5.3.3A The pH and substrate concentrations of the synthetic biofilm

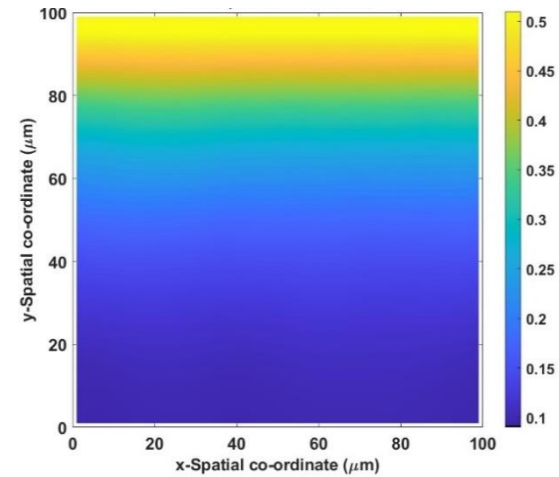
I used an individual-based model to characterise *S. mutans* invasion into the dental biofilm and the growth of the other commensal species, at different glucose and substrate concentrations. I also investigated the pH, which was difficult to do in the reactor, to understand biofilm behaviour and the local effect of species growth. These were all part of the same simulation. Biofilm growth was considered inside a 100 x 100 μm computational space with a maximum biofilm height of 80 μm , representing the growth of the synthetic community biofilm on the hydroxyapatite disks. An equal number of particles for each species was randomly distributed at the base of the computational domain in a monolayer at the start of the simulation.

A snapshot of the biofilm was taken at 100 h for reactor experiment 4 (low glucose, low lactic acid) to demonstrate growth within the domain (Figure 5.7A) in reactor experiment 4 (low glucose, low lactic acid). *S. mutans* (orange) and *V. parvula* (green) dominated the biofilm, with *S. gordonii* (blue) populating the biofilm. *A. oris* (yellow) and *N. subflava* (purple) struggled to grow within the biofilm, as they did in the experimental data. A snapshot of the glucose concentration (Figure 5.7B) showed that glucose was consumed within the biofilm, with a low concentration at the bottom and a gradient, with no consumption at the top boundary where biomass was not generated. All species, excluding *V. parvula*, were responsible for glucose consumption according to their stoichiometry. This was the inverse of the pattern seen with lactic acid. Here, lactic acid concentration was greatest at the bottom of the biofilm (Figure 5.7C), as those species produced lactic acid when fermenting glucose. *V. parvula* consumed lactic acid in its stoichiometry. Finally, the pH dropped significantly (Figure 5.7D). This drop in pH can be explained by the growth of the biofilm, consuming glucose, and producing lactic acid in the process, with the acid production decreasing the pH. A spatial variation in pH was observed within the biofilm as opposed to the homogenous bulk, which influenced the species relative abundance.

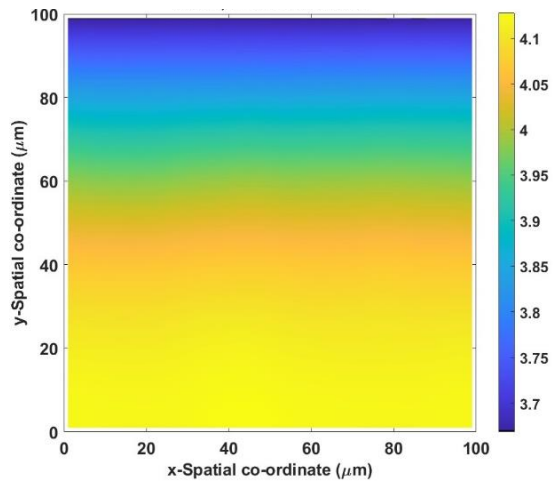
A) Reactor experiment 4, Biomass, Run time = 100



B) Reactor experiment 4, Glucose, Run time = 100 h



C) Reactor experiment 4, Lactic acid, Run time = 100 h



D) Reactor experiment 4, pH, Run time = 100 h

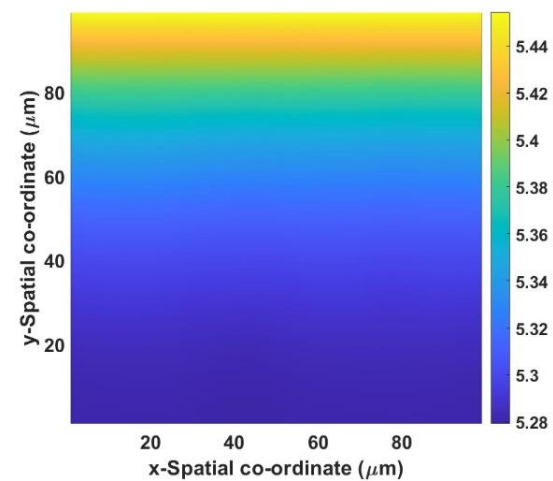


Figure 5.7 Representation of a biofilm (A) and its corresponding glucose (B), lactic acid concentration (C), and pH profiles (D). The snapshot corresponded to reactor experiment 4 (low glucose, low lactic acid) and simulation time of 100 h. Panel A: blue - *S.gordonii*; red - *S.mutans*; green - *V. parvula*; yellow – *A. oris*; magenta – *N. subflava*.

5.3.3B The relative abundance of bacterial species in the synthetic biofilm

Simulating the relative abundance of the biofilm helped describe how the species grew on high and low glucose/lactic acid concentrations over time. The species were seeded with the same number of cells to begin with, which were randomly distributed, and growth was simulated over 216 h, with starting conditions matching those of the *in vitro* experiments in Chapter 4.

In simulations of reactor experiment 1 (high glucose, high lactic acid) (Figure 5.8A) without pH correction, *S. gordonii* dominated the biofilm, ranging from 50-70 % abundance. This did not agree with the experimental data, where *S. gordonii* had a species abundance of 29.80% after 48 h, but then decreased to 3.51 % by 216 h. An explanation for *S. gordonii* dominance in simulations could be due to the superior growth rate (see Chapter 3). *S. mutans* was the second most abundant species in the simulation, ranging between 15-30%. This did not reflect the results from the experimental data, where *S. mutans* dominated the reactor biofilm, constituting over 99% of the abundance by 216 h. The simulation results for reactor experiment 2 (high glucose, intermediate lactic acid) (Figure 5.8B) were similar to that of reactor experiment 1 (high glucose, high lactic acid), and therefore also did not represent the experimental data. This again showed *S. gordonii* being the most abundant species in simulations, but *S. mutans* dominated the biofilm in experimental data. The model simulated that *A. oris*, *N. subflava* and *V. parvula* struggled to grow within the synthetic community biofilm, with none of the 3 species ever reaching a relative abundance of over 15%. This also occurred in the experimental data.

The simulation results from reactor experiments 3 (low glucose, high lactic acid) (Figure 5.8C) and 4 (low glucose, low lactic acid) (Figure 5.8D) corroborated more with the experimental results. Simulations showed *V. parvula* dominated the biofilm at these low glucose concentrations. This was also the case in the experimental data. Furthermore, the simulated abundance for *V. parvula* decreased between reactor experiments 3 (low glucose, high lactic acid) and 4 (low glucose, low lactic acid), as it did in the experimental data. This was likely due to the lactic acid concentration decrease. The relative abundance of *S. mutans* was similar in reactor experiments 3 (low glucose, high lactic acid) and 4 (low glucose, low lactic acid), whereas, in the experimental data, the abundance increased from 3.51% at 216h in reactor experiment 3 (low glucose, high lactic acid), to 19.29 % in experiment 4 (low glucose, low lactic

acid). For simulations of reactor experiments 3 (low glucose, high lactic acid) and 4 (low glucose, low lactic acid), *A. oris* and *N. subflava* struggled to grow, as they did in the experimental data. Overall, these results demonstrated that without pH corrections in species growth rates, the simulations struggled to simulate the invasion and dominance of *S. mutans* into the biofilm at high glucose concentrations, as was the case in the experimental data.

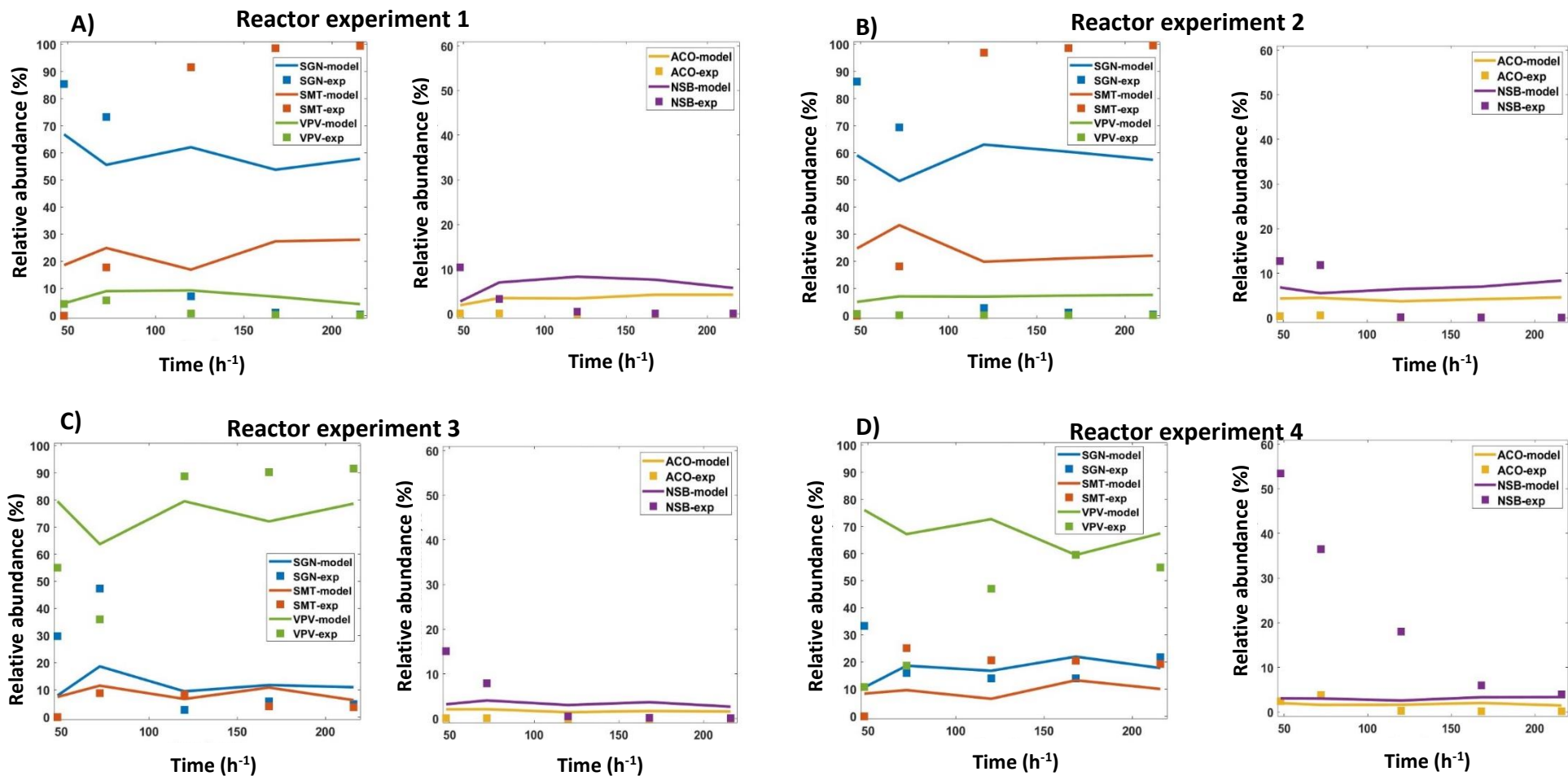


Figure 5.8 Relative abundance of *S. gordonii* (SGN), *S. mutans* (SMT), *V. parvula* (VPV), *A. oris* (ACO), and *N. subflava* (NSB) in the biofilm. Model results without pH correction for growth rates and experimental data. A) Reactor experiment 1 (high glucose, high lactic acid), B) Reactor experiment 2 (high glucose, intermediate lactic acid), C) Reactor experiment 3 (low glucose, high lactic acid) and D) Reactor experiment 4 (low glucose, low lactic acid). Simulation results were presented from 48 h, corresponding with the first experimental point. At 0 h, the five species had equal relative abundance.

When considering pH correction for the bacterial growth rates, the simulations of reactor experiment 1 (high glucose, high lactic acid) (Figure 5.9A) and 2 (high glucose, intermediate lactic acid) (Figure 5.9B) were identical. Both resulted in *S. mutans* dominating at high glucose concentrations, with all other species struggling to grow. This matched the results from experimental data. The identical nature of simulations for reactor experiments 1 (high glucose, high lactic acid) and 2 (high glucose, intermediate lactic acid) demonstrated that lactic acid concentration did not affect the dominance of *S. mutans* in simulation. This was also the case in the experimental data.

Simulation results for reactor experiment 3 (low glucose, high lactic acid) (Figure 5.9C) better resembled the experimental data. *V. parvula* dominated simulation at low glucose concentration, ranging between 50-70% abundance. This was lower than the experimental data, where the abundance was 91.60% at 216 h, but corroborated that the abundance was far higher than any other species. The simulation showed that *S. mutans* struggled to grow in simulations, despite the pH correction. This was similar to the experimental data. The abundance decreased from ~30% at 48 h, to 10% at 216 h in simulations. In the experimental data, the abundance in all samples taken was below 9%. *S. gordonii* was the second most abundant in simulations for reactor experiment 3 (low glucose, high lactic acid), with the abundance ranging between 10-20%. *A. oris* and *N. subflava* struggled to grow in this simulation. In simulations of reactor experiment 4 (low glucose, low lactic acid) (Figure 5.9D), *S. mutans* struggled to dominate the biofilm, making up ~10% abundance. *S. gordonii* abundance decreased over time, from ~30% at 48 h, to ~15% at 216 h. This was similar to experimental data, where the abundance decreased from 33.34% at 48h, to 21.72% at 216 h. In this simulation, *V. parvula* was the most dominant species, with an abundance of ~60% by 216 h. The decrease in lactic acid concentration decreased the abundance of *V. parvula*, in both simulations and experimental data, between reactor experiments 3 (low glucose, high lactic acid) and 4 (low glucose, low lactic acid). The abundance of *V. parvula* in simulations and experimental data were almost identical to each other when pH corrections were implemented. Overall, these simulations showed that considering pH was important when comparing the simulation results to the reactor results, particularly the dominance of *S. mutans* at high glucose concentrations and the dominance of *V. parvula* at low glucose concentrations.

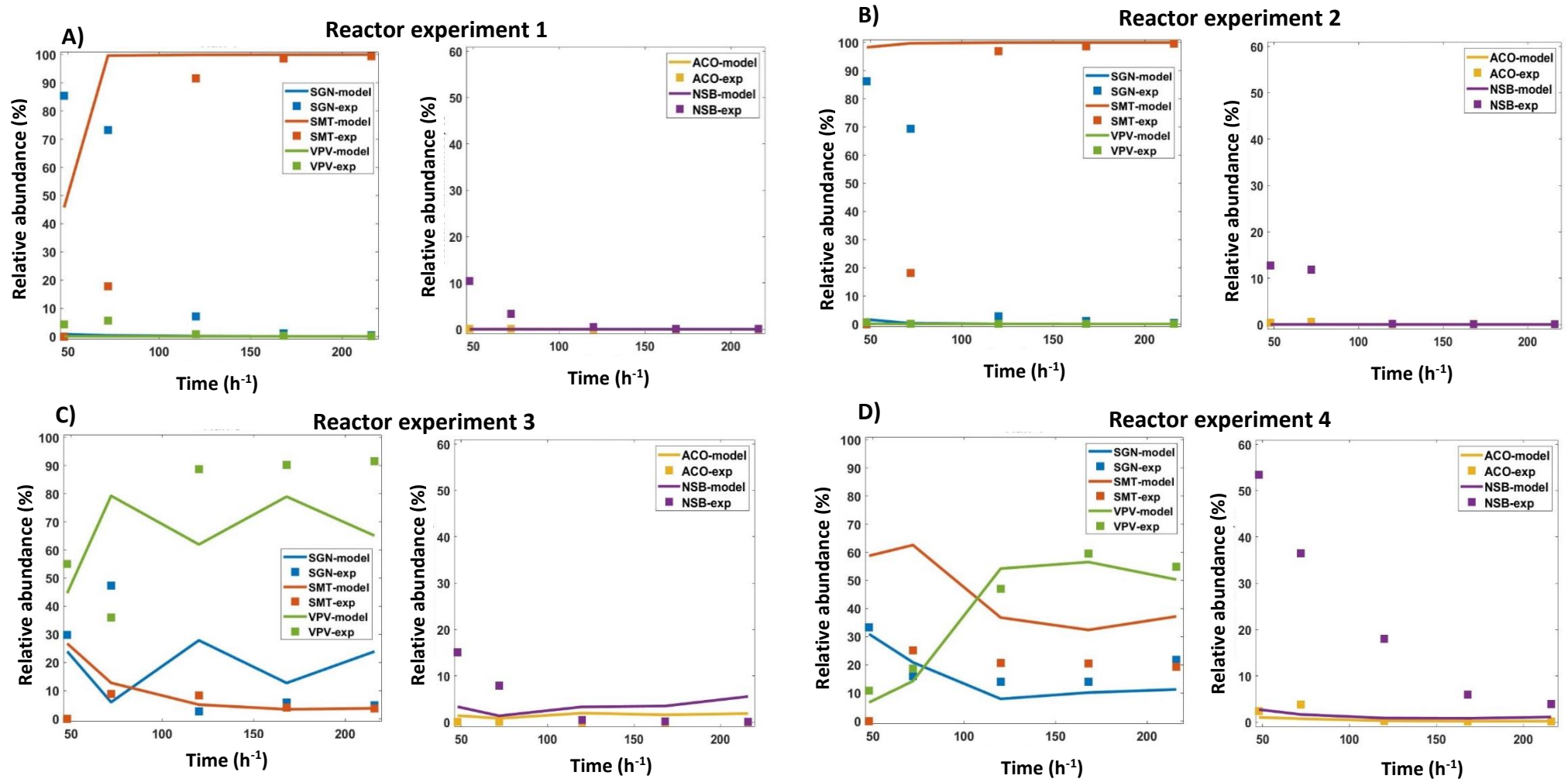


Figure 5.9 Relative abundance of *S. gordonii* (SGN), *S. mutans* (SMT), *V. parvula* (VPV), *A. oris* (ACO), and *N. subflava* (NSB) in the biofilm. Model results considered pH in growth rates. A) Reactor experiment 1 (high glucose, high lactic acid), B) Reactor experiment 2 (high glucose, intermediate lactic acid), C) Reactor experiment 3 (low glucose, high lactic acid) and D) Reactor experiment 4 (low glucose, low lactic acid). Results were presented from 48 h, corresponding with the first experimental point measured.

5.3.4 Influence of bacterial seeding on species relative abundance in the community biofilm

The simulations in 5.3.3A-C considered an equal number of individuals for each of the 5 species, in the seeding of the dental biofilm. These were randomly distributed at the base of the computational domain. I investigated the effect of initial seeding distribution on *S. mutans* invasion, and on the abundance of the commensal species, at the same conditions tested in the experimental data (Chapter 4). This was done by i) clustering the initial individuals by species type, and ii) altering the initial number of individuals to match the relative abundances, quantified from the biofilms on the hydroxyapatite coupons using qPCR. This was on the second day of the experimental data. In this instance, this was to mimic the invasion of *S. mutans* into the biofilms, as it was inoculated into the reactor on day 2. All simulations were performed considering pH correction in species growth rates.

Clustering the initial individuals by species did not significantly change the final rank abundance of the synthetic community members, compared to random distribution. *S. mutans* dominated the biofilm in the simulation of reactor experiment 1 (high glucose, high lactic acid) (Figure 5.10A), with a relative abundance of almost 100% by 72 h. *S. mutans* continued this dominance throughout the rest of the simulation, whilst all other species struggled to grow. In reactor experiment 2 (high glucose, intermediate lactic acid) (Figure 5.10B) *S. mutans* also dominated the biofilm, although in this instance, by 48 h. This dominance was seen in the experimental data, but the abundance did not reach above 90% until 120 h. Clustering the initial seeding did not affect rank abundance at low glucose concentrations, where *V. parvula* also dominated simulations for both reactor experiment 3 (low glucose, high lactic acid) (Figure 5.10C) and 4 (low glucose, low lactic acid) (Figure 5.10D). A difference was observed in the simulated abundance of *V. parvula* in reactor experiment 3 (low glucose, intermediate lactic acid) when cells were clustered, compared to randomly distributed. The abundance increased over time, from ~45% to 70%, similar to experimental data. In Section 5.3.3B, the abundance ranged from 60-80% throughout the remainder of the experiment. Clustering the cells also led to an almost identical trend between the simulation of reactor experiment 4 (low glucose, low lactic acid), and the experimental data. Only at 168 h did the values between the simulation and experiments differ.

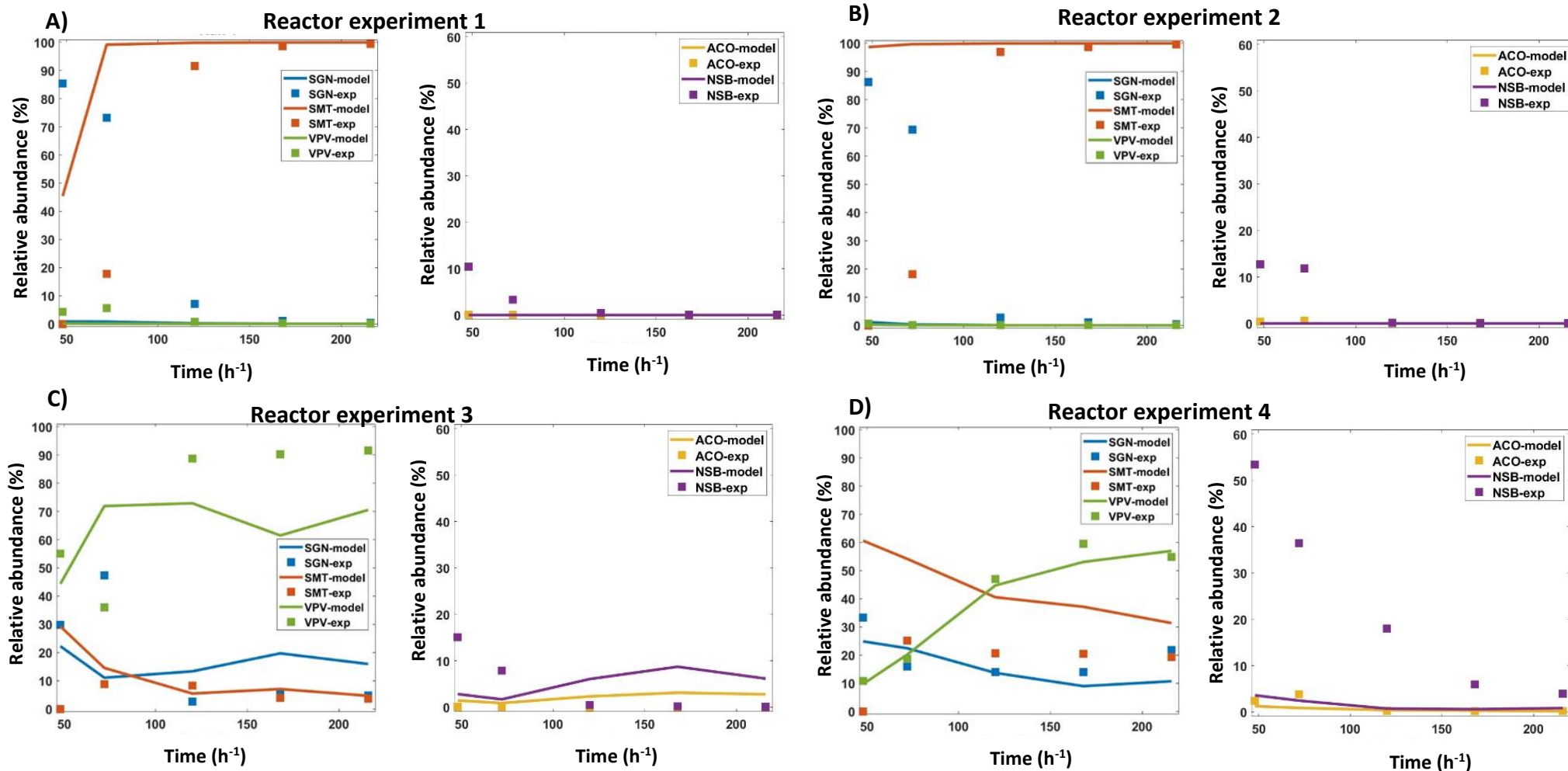


Figure 5.10 Relative abundance of each synthetic community member simulated in the biofilm, plotted with abundances from experimental data. The results consider pH correction for growth rates, with seeding of cells clustered by species. Simulation results are presented from 48h to correspond with the first experimental points measured. A) Reactor experiment 1 (high glucose, high lactic acid), B) Reactor experiment 2 (high glucose, intermediate lactic acid), C) Reactor experiment 3 (low glucose, high lactic acid) and D) Reactor experiment 4 (low glucose, low lactic acid).

Changing the seeding strategy to match that of the experiments in Chapter 4, also led to *S. mutans* dominating the biofilm in simulations of reactor experiment 1 (high glucose, high lactic acid) (Figure 5.11A). This was even if the starting density was one individual. The relative abundance in simulations reached ~90% after 120 h, so took longer to dominate the biofilm than when clustering species. Regardless of seeding, all other species struggled to grow. The growth pattern of *S. mutans* more closely resembled the experimental data, when following a similar seeding strategy. The trend in simulations of *S. mutans* growth was similar in reactor experiments 1 (high glucose, high lactic acid) and 2 (high glucose, intermediate lactic acid) (Figure 5.11B). This demonstrated that decreasing lactic acid at high glucose concentrations did not affect invasion. In simulations of reactor experiment 3 (low glucose, high lactic acid), *V. parvula* still dominated the biofilm abundance (Figure 5.11C) but more closely resembled the experimental data. The abundance in simulations was ~85% and was 91.60 % in the experimental data. For *S. gordonii*, the simulated abundance was ~50% after 72 h (Figure 5.11C), closer to the value of 47.37% recorded from the experimental data, compared to clustering. The simulated abundance of *S. gordonii* decreased between 72 h and 120 h, similar to the experimental data. All other species struggled to grow. In simulations of reactor experiment 4 (low glucose, low lactic acid) (Figure 5.11D), *V. parvula* was still the most abundant species, with an abundance of ~55%, similar to the random distribution simulation value and the experimental data abundance of 54.87%. *S. mutans*, *A. oris* and *N. subflava* struggled to grow, although there was more growth in simulation for *S. gordonii* compared to when the cell seeding was clustered. After 72 h, the abundance in simulations of *S. gordonii* was ~75%, far higher than the experimental data or the simulations from cell clustering.

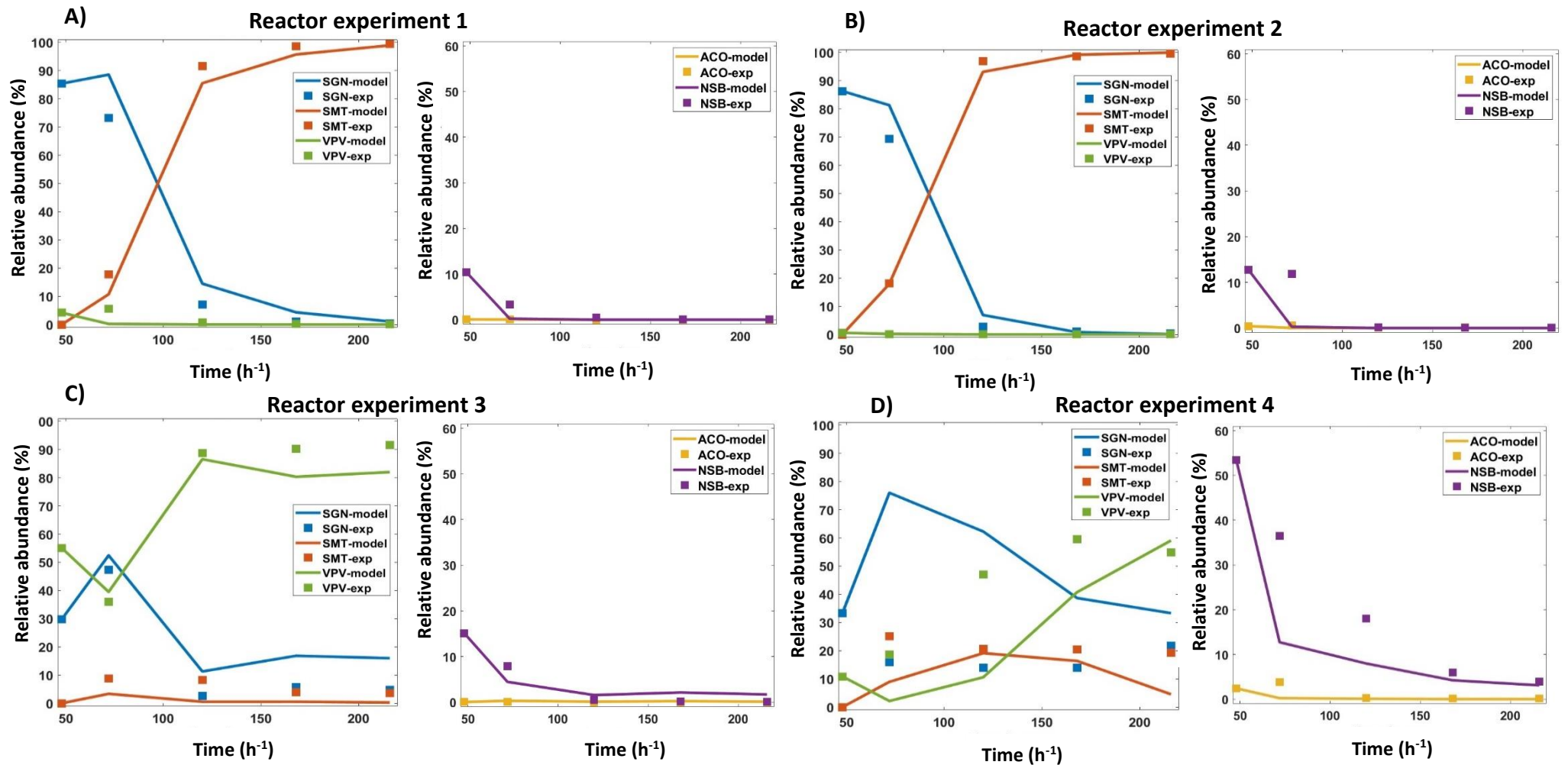


Figure 5.11 Relative abundance of each synthetic community member simulated in the biofilm, plotted with abundances experimental data. The results consider pH correction for growth rates, with seeding matching the reactor strategy. Simulation results are presented from 48h to correspond with the first experimental points measured. A) Reactor experiment 1 (high glucose, high lactic acid), B) Reactor experiment 2 (high glucose, intermediate lactic acid), C) Reactor experiment 3 (low glucose, high lactic acid) and D) Reactor experiment 4 (low glucose, low lactic acid).

5.4 Discussion

In this Chapter, I aimed to use both continuum and IbM modelling approaches to simulate the invasion of *S. mutans* into a pre-formed oral commensal community. I aimed to compare findings to the experimental data in Chapter 4 and determine factors that increased influenced *S. mutans* invasion, including factoring in pH to bacterial growth kinetics and testing the clustering of species upon initial seeding. Considering pH was important due to it having a known profound effect on bacterial growth (Guan & Liu, 2020a), as validated by findings in Chapter 3. My results show that pH consideration was important in modelling *S. mutans* invasion. When considering the pH correction for the growth rates, simulations showed *S. mutans* dominance at high glucose concentrations, whilst *V. parvula* dominated at low glucose concentrations. This was the case for both the bulk and biofilm, and the modelling results agreed with the experimental data. I also observed that whilst clustering cells during initial seeding still led to the same invasion patterns as random distribution, it did influence species abundance in the biofilm, including an increase in abundance for *S. gordonii*.

The simulated glucose concentration in the bulk demonstrated that the substrate decreased over time as the biomass grew, in all simulations. Simulation results agreed better with reactor findings when pH was considered. The consumption of glucose by these species, to produce biomass, is known. *S. gordonii*, *S. mutans*, *A. oris* and *N. subflava* all consumed glucose for biomass production (Dame-Teixeira et al., 2016b; Solsi et al., 2020; Decker et al., 2014). This explained the large amount of glucose consumed during simulations of reactor experiments 1 (high glucose, high lactic acid) and 2 (high glucose, intermediate lactic acid), as *S. mutans* dominated the simulation, which would require a large amount for growth. The glucose consumption was also demonstrated by my results in Chapter 3. The lower glucose concentrations in reactor experiments 3 (low glucose high lactic acid), and 4 (low glucose, low lactic acid) also led to the inability of *S. mutans* to dominate. The limiting nutrient here likely led to less growth, as glucose concentration has shown to correlate to species growth in literature (Dutra De Oliveira et al., 2016). The decrease in glucose concentration was also seen in the biofilm as biomass generation led to consumption. Modelling substrate concentration by the IbM was beneficial in understanding the characteristics of the dental biofilm, as this is difficult to measure *in vitro*, and was not done in Chapter 4.

The pH decreased across all simulations as biomass grew. This was also the case with experimental data and was expected, as these species produced acid. This explained why the greatest decrease in both the biofilm and the bulk was seen in simulations of reactor experiments 1 (high glucose, high lactic acid) and 2 (high glucose, intermediate lactic acid), as *S. mutans*, the most abundant species according to simulation results, is very acidogenic (Bedoya-Correa et al., 2021). The pH decrease mirrored the lactic acid production (Figure 5.3a-d), as lactic acid is known to be one of the main acids produced in fermentation (Egland et al., 2004). The higher pH in simulations where *V. parvula* dominated, can be explained by this species consuming lactic acid to produce weaker acids (Zhou et al., 2021c). These corroborated with the experimental data in Chapter 4. Even at low glucose concentrations, there was still a drop in pH of the bulk and the biofilm. The lbM was able to simulate the local pH in the biofilm, difficult to do experimentally and not done during the experiments in Chapter 4. This is one example where the lbM can help predict characteristics of biofilm further than that accomplished in the reactor system. The pH corrections in species growth rates showed to have a significant effect on the modelling of *S. mutans* invasion at higher glucose concentrations. This led to better agreement of the pH, glucose, and lactic acid concentrations when compared with experimental results. The optimum pH defined for *S. mutans* also had a significant effect on its ability to invade the oral community. In one simulation (data not shown), changing the pH_{opt} parameter in the pH correction to 7, rather than 6 and starting the relative abundance on day 2, resulting in *S. mutans* failing to invade the biofilm. In the absence of a more detailed representation of the metabolic process for species beyond anabolic and catabolic reactions, the pH correction for growth rates was a representation of the acid tolerance response in bacteria. The lower pH_{min} of *S. mutans* represented the known ATR response (Matsui & Cvitkovitch, 2010b), giving it a competitive advantage at low pH over the other synthetic community species. The sensitivity to the pH_{opt} , pH_{min} and pH_{max} in the pH corrections, do limit the predictive capacity of the models to the quality of the experimental data informing the model. The integration of pH here differed from other models, e.g., that by Head (Head et al., 2014b) who used inhibition terms with the same value for aciduric and non-aciduric species. I implemented a more realistic representation of biofilm development better reflecting the localised pH variation in the biofilm, particularly compared to models that do not consider the pH influence or chemical speciation (Rath et al., 2017; Ilie et al., 2012; Martin et al., 2017). In my model, acetate was part of the pH calculation and catabolism for *N. subflava* and *V. parvula*. Future work could

focus on quantifying this in the *in vitro* reactor and comparing to simulated concentrations using the continuous model and IbM.

I have observed that *S. mutans* dominated simulations led to an increase in lactic acid, which can be explained by the known lactic acid production from this species (Guo et al., 2013). The reduction in lactic acid when *V. parvula* dominated i.e., reactor experiments 3 (low glucose, high lactic acid) and 4 (low glucose, low lactic acid), can be explained by lactic acid metabolism (Luppens et al., 2008b). The production and consumption dynamics in the synthetic community underlined the importance of quantifying this acid. This is evident in the IbM concentration simulations showing an inverse pattern with glucose concentration as *V. parvula* had opposite metabolism with *S. mutans* in terms of lactic acid production/consumption, leading to the known synergism *in vivo* (Abram et al., 2022). To better understand the acid profile of the synthetic community would require measuring the products of lactic acid consumption by *V. parvula*, known to include propionate and formate (Seeliger et al., 2002).

The continuous model allowed control of the environment that could be varied independently. This was done with the glucose and lactic acid concentration. The continuous model demonstrated that *S. mutans* dominated at high glucose concentrations when pH was considered in kinetics. The acid tolerance response (N Takahashi & Yamada, 1999) was likely responsible for the discrepancy when pH was not considered. Simulation patterns then corroborated with reactor results on ranked relative abundance similarity, showing the usefulness of the continuous model. It was difficult to directly compare results with literature due to the unique combination of species in this synthetic community, substrate conditions and medium as well as simulation time. The liquid phase considered here was important as the bulk constituted most of the biomass in the system, and *in vivo* salivary microbiome and composition is important in the oral microbiome overall and impact on health (Lyng Pedersen & Belstrøm, 2019b). To an extent, this was reflected in the simulation results and the experimental work. The rank abundance of species within the biofilm and bulk were identical across all simulations and experimental work. I can therefore consider that the bulk plays the role of saliva (also mirroring the flow rate) and is a source for biofilm formation and replenishment of bacteria. Furthermore, simulation results indicated that shifts in the dental biofilm result from pH generated from carbohydrate fermentation rather than carbohydrate availability (Bradshaw & Marsh, 1998a). A limitation of the bulk simulations was that whilst

the homogenous assumption matches that of the CSTR, this is not the case *in vivo* (Proctor et al., 2018). Simulations did consider the average salivary flow rate to help represent that in the mouth. Another limitation was not considering the impact of the biofilm on the bulk, which has been remarked by Wimpenny *et al.*, (Wimpenny & Colasanti, 1997). This explained the lack of a clear steady state in the experimental data, as seen in the simulations, leading to a discrepancy between the two modelling approaches.

The simulation of the lbM showed similar rank abundances to both the bulk simulations, produced by the continuum model, and the experimental data in Chapter 4. The pH correction in species growth rates was also needed to simulate *S. mutans* invasion. The pH is vital in representing the *in vivo* dental biofilm as species were known to react differently to pH (Senneby et al., 2017a). It is therefore an advantage to represent the pH gradients in the biofilm which also occurs *in vivo* (Schlafer et al., 2011) and has a varying effect on caries development and demineralisation, often acting as a biomarker (Kalhan et al., 2019). The simulation of the biofilm allowed for yield variation as a function of the glucose and lactic acid concentration, differentiating itself from other models that keep yields constant (Head et al., 2014b). Yield calculations based on stoichiometry and local concentration are important in biofilm modelling as it links thermodynamics and environmental conditions to microbial growth (Gogulancea et al., 2019b). This better reflects the different conditions bacteria face in heterogeneous biofilms. The consideration of the defined stoichiometry for each species allowed for studying microbial composition over time and for comparison with experimental data. Not modelling the transition between aerobic and anaerobic metabolism is a limitation, but the inclusion of *N. subflava* as part of the synthetic community, acting as a sink for the oxygen concentration, helped offset this. This occurs naturally in the mouth, where both aerobes and anaerobes were present (Arweiler & Netuschil, 2016), with aerobes helping protect anaerobes in biofilms from oxygen-related stress (Bradshaw et al., 1996). A difficulty in comparing biofilm simulations to those in the reactor was the lack of consideration for the impact of the bulk on the biofilm. The biofilm also lacks aspects of interspecies interactions and the impact of EPS which is a known important part of biofilm development, support and protection for the species involved (Cugini et al., 2019). To improve on this would need the translation to a 3D model as done by Gogulancea *et al.*, (2019). This would allow for better research into phenomena such as the effect of sucrose pulsing on polymer production, which is influential in *S. mutans* invasion (Matsumoto-Nakano, 2018).

Clustering cells by species type and altering the initial number of cells to match those of the reactor, still led to *S. mutans* dominating high glucose and *V. parvula* dominating low glucose conditions. Bacterial species have interspecies interactions that help them thrive in dental biofilms. One such example is the *S. mutans*-*V. parvula* interaction, where *S. mutans* produces lactic acid for *V. parvula* to consume, which itself protects *S. mutans* from oxidative stress (Liu et al., 2020). Understanding these relationships better would require further implementation of mechanical and chemical interspecies interactions within the model. Whilst there was no significant change in rank abundance, a better correlation between the simulated abundance of *S. mutans* in reactor experiment 1 (high glucose, high lactic acid) to those from the experimental data, showed that matching the seeding strategy led to more agreement. This was also the case for *V. parvula* abundance in reactor experiment 3 (low glucose, high lactic acid). Overall, the results showed that the effect of pH and substrate concentration far outweigh bacterial positioning for the conditions tested.

The model has contributed to the overall knowledge of biofilm behaviour, including the glucose, lactic acid, pH, and species abundance changes under different substrate concentrations. The model has the potential to inform safe product development by simulating the invasion of disease-associated bacterial species, and the effect on health-related microbiomes, under different conditions. Two potential uses of the IbM are the simulation of antibiotic resistance and probiotic integration in the dental biofilm. Antibiotic resistance characteristics of biofilms are of interest as the bacterial cells within dental biofilms are far more resistant to antibacterial compounds (Høiby et al., 2010). This model can predict the diffusion of such actives into the biofilm over time. Probiotic research has been of interest in dental biofilm research, including the studying the antibacterial activity of *Lactobacillus* species against oral *Streptococci*, including *S. mutans*, which was determined to be pH-dependant (Wasfi et al., 2018; Lee & Kim, 2014). This model is suitable for simulating the integration of probiotic species into the dental biofilm. The simulations could also help inform *in vitro* experimental strategies, including the testing of antimicrobial actives, in a cost and time-efficient manner. As shown here, it was important to consider pH corrections for bacterial kinetics and further work is needed to improve the correlation of results to that *in vivo* and *in vitro*. This includes better defining the impact of pH on the growth of these species. Combining *in vitro* and *in silico* modelling approaches showed promise in characterising the dental biofilm and invasion. The use of a CDM allowed for studying the influence of one

parameter at a time. Informing simulations with species-specific kinetic parameters, collected in Chapter 3 and validating simulations with *in vitro* data from Chapter 4, helped better understand factors that may contribute towards oral dysbiosis *in vivo*. Further work to improve this model should include incorporating the appropriate kinetic parameters, including pH-specific growth rates, and considering mechanical interactions between species as part of a 3-D modelling approach.

Chapter 6. Conclusions

6.1 General discussion

I successfully developed *in vitro* and *in silico* models for characterising the invasion of *S. mutans* into a pre-existing, 4-species early coloniser biofilm. This allowed me to understand factors leading to the commensal community transitioning to a disease-associated state, and the impact on the local environment, including pH change, and the production/utilisation of glucose and lactic acid.

The research in Chapter 3 was essential in laying the foundation for the *in vitro* modelling in Chapter 4, and the *in silico* modelling in Chapter 5. A key step was the development of a chemically defined medium (AFMC) that supported the growth of all 5 species. This helped untangle the complexity of the chemical environment. AFMC supported the growth of all species, which was not the case for *A. oris* and *V. parvula* on FMC (Terleckyj *et al.*, 1975). It is well understood that bacteria have different abilities to grow in acidic conditions (Svensäter *et al.*, 1997), and my research in Chapter 3 showed this, confirming that *S. mutans* was the best adapted of my species to acidic environments. Finally, the development of the techniques in Chapter 3 proved necessary for collecting the information in Chapter 4 regarding invasion, allowing me to quantify the bacterial abundance and track *S. mutans* invasion over time using qPCR. The development of a multispecies FISH protocol allowed me to confirm presence of the species within the synthetic community biofilm in Chapter 4. It also helped identify the spatial-temporal differences when the community was grown on AFMC supplemented with sucrose, which was the formation of dense microcolonies, known from previous work (Kreth *et al.*, 2008). This was not observed when the community was grown on AFC supplemented with glucose. Whilst I optimised FISH to be able to visualise all 5 species, more needs to be done to refine this technique, and to reduce the bleed through from fluorescence channels.

This development of a multiplex qPCR protocol allowed me to quantify, *S. mutans* invasion and abundance change over time. Quantifying the abundance of the commensal species also allowed me to understand the impact that substrate concentrations, and the resulting pH, had on the commensal species. I was able to determine *S. mutans* dominance and the reduction in commensal species abundance at high glucose/low pH conditions due to qPCR. Collecting the kinetic parameters (μ_{max} and K_s) for my species, was essential for informing the *in silico*

model, as the medium developed was novel and so these kinetic parameters on AFMC had not been reported.

The development of the *in vitro* model was essential in studying the invasion of *S. mutans* at varying glucose/lactic acid conditions, as well as on sucrose. The CDC reactors allowed for controlling the temperature, flow rate and growth material (hydroxyapatite) of the coupons, which all helped more closely mimic the *in vivo* environment, compared to *other in vitro* systems (Ammann *et al.*, 2012; Roberts *et al.*, 2002.). The model improved on previous work by characterising the transition of a commensal biofilm, to a cariogenic-associated one, in a defined environment. This was possible due to the use of the synthetic community and CDM. Complex oral communities have been used in the past (Thurnheer *et al.*, 2004b; Ammann *et al.*, 2012a), but without the combined use of the CDM and quantifying species composition over time using qPCR. My results showed *S. mutans* dominance at high glucose concentrations, in a low pH environment. My *in vitro* model was able to show the change in abundance over time of this species and the commensals, and the glucose and lactic acid concentration variance during this period using the defined AFMC. The use of the CDM allowed for testing invasion with one variable changed at a time, which helped demonstrate the effect of substrate concentration on shifts in species abundance. The nature of the synthetic medium meant that variance between runs was less than would have been the case with using an animal-derived medium. The use of flow cytometry for live-dead testing at the end of the experiment was also useful to test the viability of the synthetic community. This was an important aspect of the transition to a disease-associated state. The drop in viability at low pH, which is known to occur *in vivo* (Senneby *et al.*, 2017b), demonstrated that this should be used alongside qPCR to understand the effect of substrate concentration and the resulting pH on biofilm health.

The use of Monod kinetics in the modelling of the synthetic community included several assumptions and limitations. Using Monod only considered one limiting substrate, whereas bacteria can use more than one at the same time. There are models that can consider two limiting substrates at the same time, including that by Bertolazzi *et al.*, (2005). I decided on the Monod-thermodynamic approach as I needed to consider one main carbon and energy source to define the stoichiometry considered for the species with the use of a chemically defined medium. The Monod-thermodynamic approach was therefore suitable in this instance, whereas models such as the Logistic model, is substrate independent and has been

reported to have a poor fit for predicting growth rates (Muloiwa et al., 2020). The use of Monod kinetics in this form, considering single-species growth rates, is also a simplification. Competition for nutrients in a multi-species environment and antagonistic interactions (See 1.2.3) are likely to reduce growth rates compared to single-species cultures. Future work should improve upon these limitations by observing the growth rates of each synthetic community member in the mixed-culture environment that occurs within the *in vitro* reactor systems.

I demonstrated in Chapter 5 the importance of considering pH in bacterial kinetics, to model the invasion of *S. mutans* into an dental biofilm, as seen in Chapter 4. I was able to simulate invasion in both the bulk, using a 0-D continuum model, and the biofilm using a 2-D model. These pH corrections have been shown to improve model fitting previously (Rosso *et al.*, 1995), but this has not been done in dental biofilm simulations. The use of pH corrections was vital in correctly simulating *S. mutans* invasion in a high glucose/low pH environment. The inability to simulate this without pH corrections in bacterial kinetics demonstrated how important it was to consider pH in kinetics, as well as substrate speciation, which has not been done in other dental biofilm models (Head *et al.*, 2017; Ilie *et al.*, 2012). The known impact that pH has on bacterial growth rates (Ratzke & Gore, 2018), also underlines that this aspect of the model is key to characterising dental biofilm activity that may occur *in vivo*. My findings that *S. mutans* dominated the biofilm at high glucose/low pH conditions, and the dominance of *V. parvula* at low glucose concentrations, corroborated with *in vitro* findings in Chapter 4. I also demonstrated that bacterial seeding led to minor changes in species abundance (Chapter 5), including an increase in growth of *S. gordonii* if species were clustered together. The IbM was able to simulate the local pH of the biofilm, something that is difficult to measure experimentally without invasive methods. The drop in glucose concentration simulated by both models was also seen *in vitro* and was expected due to the consumption of glucose by 4 of the species. The lactic acid increase observed was also expected as species i.e., *S. gordonii* and *S. mutans* produce lactic acid (Dashper & Reynolds, 1996.). There were limitations with this model, including not modelling the mechanical interactions of the species and assuming a constant concentration of oxygen at 1 mg L⁻¹. The use of *N. subflava* as a carbon sink, to reduce oxygen concentration and protect anaerobic species, helped offset the limitation of not modelling the transition between aerobic and anaerobic metabolism.

It is evident that there are limitations to both the *in vitro* and *in silico* models. The assumptions made within the *in vitro* model, including the use of single-species growth rates rather than those taken from a mixed-species environment, limit the ability of the model to more accurately model mixed-biofilm growth *in vivo*. Furthermore, the assumption in the *in silico* model, including not self-determining the pH boundaries used in pH correction for species kinetic parameter, do reduce the ability to accurately simulate *S. mutans* invasion. Finally, I did not use the analytical techniques from synthetic community samples as efficiently as possible due to time constraints. The use of FISH could have been used quantitatively to compare against the qPCR results if the technique had been further optimised. Whilst live-dead quantification was used to understand the general viability of the biofilms under each condition, use at different time points would have allowed for the understanding of the viability change over time as a result of the pH as part of caries-associated biofilm development. Future work should address such issues and are detailed in Section 6.2. The key findings from this research are summarised in Table 6.1.

Table 6.1 Summary of key findings and applications from each results chapter. Characterising the synthetic community species and refining analytical techniques, allowed for the *in vitro* and *in silico* models to characterise *S. mutans* invasion as high and low glucose/lactic acid concentrations.

| Chapter | Key findings/achievements | Progress from previous findings | Application of findings |
|---------|--|---|---|
| 3 | <ul style="list-style-type: none"> i) Development of AFMC ii) Kinetic parameters for synthetic community species iii) Substrate profile and acid tolerance of species iv) Development and refinement of analytical techniques and inoculation strategy | <ul style="list-style-type: none"> i) FMC did not support the growth of <i>A. oris</i> or <i>V. parvula</i> ii) There are no μ_{max} or K_s values for species grown on AFMC as the medium was produced in this research iii) Direct comparison of synthetic community species acid tolerance iv) Methods such as FISH had to be refined for my synthetic community | <ul style="list-style-type: none"> i) AFMC supported a more varied oral species community. Allowed for untangling of the complex chemical environment <i>in vitro</i> and testing of one variable at a time. ii) Inform the <i>in silico</i> modelling simulations and inoculation strategy iii) Understood species growth in different acidic environments in a mixed-culture environment later in Chapter 4 iv) Technique development for characterising invasion <i>in vitro</i> quantitatively and imaging biofilm. |

| | | | |
|-----------------|---|--|--|
| <p>4</p> | <ul style="list-style-type: none"> i) Development of a <i>defined in vitro</i> model for testing invasion. ii) Significant pH drop and viability drop at high glucose concentrations. iii) <i>S. mutans</i> dominated at high glucose concentrations, and commensals suffered. <i>V. parvula</i> dominated at low glucose concentrations. There was a more balanced community at low substrate concentrations, with <i>V. parvula</i> most abundant. | <ul style="list-style-type: none"> i) Lack of models that track the progress of a complex, commensal consortium to a cariogenic-associated one in a defined environment. ii) <i>S. mutans</i> ability to thrive at low pH validated by the model. iii) Successfully established complex commensal community on a defined medium in a growth model. Understood and quantified factors that led to <i>S. mutans</i> invasion. | <ul style="list-style-type: none"> i) The model can be used to test antimicrobial actives, probiotics, and to validate <i>in silico</i> model. ii) Agreement with <i>in vivo</i> findings validated the use of the <i>in vitro</i> model in characterising factors that contribute towards dysbiosis <i>in vivo</i>. iii) Ability to establish a synthetic community of multiple oxygen preferences and nutritional requirements promising in testing other species communities. Inform necessary conditions to prevent cariogenic species dominance and protect commensal species. |
| <p>5</p> | <ul style="list-style-type: none"> i) The pH consideration in bacterial kinetics were needed to predict invasion. ii) <i>S. mutans</i> dominated at high glucose concentrations and | <ul style="list-style-type: none"> i) Demonstrated the importance of considering pH corrections in bacterial kinetics, and substrate | <ul style="list-style-type: none"> i) The model can be used to test probiotic uptake into the biofilm and antimicrobial effect on species ii) Species activity better mimics <i>in vivo</i> and <i>in vitro</i> systems with corrections, |

| | | | |
|--|---|---|--|
| | <p>commensals suffered. <i>V. parvula</i> dominated at low glucose concentrations. There was a more balanced community at low substrate concentrations with <i>V. parvula</i> most abundant</p> <p>iii) Decrease in pH of biofilm and increase in lactic acid simulated using IbM.</p> <p>iv) Clustering cells leads to similar dominance of <i>S. mutans</i> at high glucose and <i>V. parvula</i> at low glucose, with both values closer to <i>in vitro</i> data, but <i>S. gordonii</i> growth increased.</p> | <p>.speciation, to correctly simulate invasion</p> <p>ii) Findings with pH correction mirrors that of <i>in vitro</i> model, showing that the model can simulate invasion.</p> <p>iii) IbM able to simulate biofilm activity that is difficult to determine experimentally</p> <p>iv) Showed that substrate concentration and pH were greater factors in invasion than bacterial positioning in this model.</p> | <p>so can be used to predict invasion and effect on healthy microbiome through commensal species.</p> <p>iii) Local pH and substrate simulations of biofilm allow for testing effect of compounds within biofilm i.e., diffusion. Important as species within a biofilm are more resistant to chemicals than planktonic cells.</p> <p>iv) Demonstrated testing of seeding strategies in species invasion. This can be considered for the integration of probiotic species in antimicrobial active development.</p> |
|--|---|---|--|

6.2 Future work

The models developed at the core of this research can characterise dental biofilms, inform microbial risk assessment and the development of safe products. The mixed *in vitro-in silico* approach could be used in the following ways:

1) Testing of antimicrobial actives/probiotics on dental biofilms and intervention studies

The antimicrobial-resistant properties of bacteria within biofilms leads to difficulties in the treatment of biofilm-related disease. The IBM could be used to simulate the exposure of dental biofilms to oral care products such as fluoride-based treatments, to see how bacteria respond to treatment. The IBM can simulate the diffusion of chemicals throughout the biofilm, to understand the access of chemicals to cells within deep layers of the structure. The use of the CDM allows for changing one variable at a time, so the effect of antimicrobials can be simulated under different conditions and strengths, by addition to AFMC. The *in vitro* model can be used to grow the synthetic community in planktonic and biofilm forms, whilst being exposed to these antimicrobials, to test their effect on the synthetic community in the different phenotypes. This can be tested through addition to AFMC for continuous exposure, or addition to the reactors at times reflecting treatment plans. Furthermore, the rate of exposure to the synthetic community in the reactor can be altered by changing the flow rate of AFMC. Through using the analytical tools i.e., FISH and qPCR, species abundance change can be quantified over time and any resulting structural changes to the biofilm can be understood. The *in vitro* data could then be used to validate the *in silico* models. Probiotic uptake into the synthetic community could also be tested. The exposure of the community to *Lactobacillus* species or other bacteria that have beneficial benefits to treat disease-associated states could be tested. Monitoring the resulting effects of pre/probiotics on the local environment i.e., substrate concentration, pH, and species abundance, can be quantified. Furthermore, intervention studies could be carried out by exposing the synthetic community to pulses of sucrose and other sugars during the reactor experiments. This would allow for the mimicking of eating that occurs *in vivo*, where dental biofilms are exposed to sugar. The resulting effect on the synthetic community over time could then be quantified similar to what has been done in this research. Such study would require the clearance of sugars from the bulk to prevent saturation with sugar, without exposing the synthetic community to shear force that can influence results.

The use of the *in vitro* and *in silico* models in intervention studies and to test antimicrobial actives, will help the development of novel oral hygiene products. This is because oral microbiota compositional changes can be quantified without the use of invasive, *in vivo* studies. By exposing these compounds in a defined environment to a synthetic community, products that are desired to protect a commensal biofilm, can be tested for their ability to preserve early colonisers. Furthermore, novel oral hygiene products can be tested at different concentration to understand minimum inhibitory concentrations for cariogenic species i.e., *S. mutans*. The *in silico* model should be used to direct the *in vitro* concentrations tested, by simulating the diffusion and perturbation of different product concentrations before running the experiments. This would be cost and time effective.

2) Characterising the invasion of an altered synthetic community of oral bacteria

The synthetic community that was selected as part of this research was relevant to dental biofilm and caries research, in terms of reported *in vivo* abundance, species role and function (Chapters 1 and 3). A variety of different species have been selected in oral research, and those species can be used instead of, or in addition to, the bacteria in this work. Using more species would further mirror the complexity of the dental biofilm. This would require adapting AFMC to support the growth of additional species. One example would be the integration of *S. wiggsiae*, which is associated with many cases of childhood caries and could be tested for invasion instead of *S. mutans*. It would also be possible to contain both species and test the competition of cariogenic species into a commensal biofilm. The bacteria selected should be appropriate to the disease of interest, for example, *P. gingivalis* could be chosen if gingivitis was the subject of interest, rather than caries. Any species used should be characterised similarly to what has been done here in Chapter 3. This includes collecting the kinetic parameters to inform the *in silico* model, define the carbohydrate utilisation and understand the pH profile of each species. As pH correction in growth rates was essential in the simulation of *S. mutans*, the pH optimum values for all species should also be determined, to improve simulation work. The invasion of *S. mutans* into the synthetic community could also be tested under different conditions. The use of the CDM allows for changing one chemical variable at a time in both *in vitro* and simulation testing. AFMC could be altered i.e., completely remove lactic acid to see if *V. parvula* still grows or increase the buffering capacity so there is not as big a pH drop. The ability of *S. mutans* to invade can be quantified using qPCR.

3) Investigating interspecies interactions and the effect of different substrates

Interspecies interactions are important in biofilm structure, function, and activity. This includes the production of lactic acid by the *S. gordonii*, *S. mutans*, and *A. oris*, and consumption by *V. parvula*. These interactions could be investigated further, where mechanical interactions and the role of EPS production could be included in the *lbM*, which could be built in 3D to better characterise dental biofilms. *V. parvula* dominated the synthetic community biofilm at low sucrose concentrations in Chapter 4. Testing if higher concentrations of sucrose lead to dominance by *S. mutans* will be better understood if *lbM* models the potential EPS production. Metabolic modelling approaches could also be used to better understand bacterial metabolism and interactions between species. FBA would allow for understanding metabolite sharing between species and help inform on the antagonistic effects of species on the commensal biofilm i.e., reduction in *A. oris* growth seen in Chapter 4 simply down to low pH, or the production of hydrogen peroxide by *S. gordonii*. As both *N. subflava* and *V. parvula* are capable of denitrification and this has shown to be capable of denitrifying nitrate to nitrite, and then to nitrogen, which has shown to help regulate blood pressure, this could also be investigated in the future. Supplementing AFMC with nitrate and quantifying the nitrite and nitrogen after the growth of the synthetic community will help understand if this process occurs in this synthetic community.

4) Refining the models by reducing assumptions and limitations

Models in biofilm research are subject to several assumptions that limit the characterisation of the *in vivo* environment. The flexibility of parameter control that the CDC reactor provided, including matching flow rate to saliva flow in the mouth, helped offset some of these assumptions. There are, however, more that need to be considered to improve the use of the models. Oxygen is known to have a large effect on oral species in dental biofilms. Within the synthetic community is a range of oxygen requirements: aerobes (*N. subflava*); facultative anaerobes (*S. gordonii*, *S. mutans* and *A. oris*); obligate anaerobes (*V. parvula*). *N. subflava* would not have grown in a completely anaerobic environment on AFMC. The *in silico* model simulations considered a constant oxygen concentration of 1 mg L⁻¹ so that *N. subflava* would grow, to respect its stoichiometry and replicate the experimental micro-aeration conditions. *N. subflava* is a scavenger of oxygen, so the inclusion of this species protects obligate anaerobes. To this end, oxygen could be monitored continuously in the reactor bulk by

replacing a hydroxyapatite coupon holder with an oxygen probe, as was done with the pH probe. This would allow for correlating oxygen concentration/consumption over time with species abundance to understand the effect on invasion. The downside is the foregoing of biofilms samples, which are required if numerous analytical techniques are used. Therefore, I decided to forego the use of a dissolved oxygen probe and focused on the importance of continuously monitoring the pH. It is also possible to test the reactor anaerobically by either purging reactor with nitrogen, using reducing agents, or purchasing the anaerobic CDC reactor. This was not done for this research as there is oxygen present in dental biofilms and therefore this would not have been as representative. The stoichiometry of the species is also a simplification of bacterial metabolism. Currently, the only VFA considered from the fermentation of glucose was lactic acid, but there are other acids produced by species e.g., *S. gordonii*. Currently, acetate, propionate and formate are considered in pH calculations and the catabolism of *N. subflava* and *V. parvula*. Quantifying these during the *in vitro* system, simulation production with the *in silico* models and comparing the results from the models, would help better explain the contribution of species to pH and metabolite exchange. The use of FBA would help understand acid production by the species in the synthetic community.

- 5) Rigorous statistical analysis to determine model agreement and experimental variability.

I was able to directly compare values of substrate concentration and species absolute abundance between the *in vitro* and *in silico* models. It is important to assess the agreement between these models which could be done with further regression analysis. The use of MANOVA could be done to quantify how close the values from the *in silico* simulations are for species abundance, substrate concentration and pH, to those from the *in vitro* experiments. A correlation coefficient between the models and the effect of changing substrate variable on *S. mutans* abundance, would help determine the robustness of the model. It would also help determine the relationship between changing substrate concentration on species invasion and the effect on the chemical environment within the reactor. Furthermore, this analysis would help better determine the predictive ability of the *in silico* model, which is important in directing *in vitro* strategy before conducting experiments. These *in vitro* systems are also subject to variability and conducting further repeats would help improve the robustness of conclusions on the ability of *S. mutans* to invade the commensal biofilm under different conditions. This

would require more experimental time. The use of MANOVA would help accounting for variation in growth between these repeats and experimental variability.

6.3 Concluding remarks

I have achieved my research aims of characterising the invasion of *S. mutans* into a 4-species oral commensal community, the factors underpinning invasion and the effect on the commensal biofilm. This work succeeded in combining *in vitro* and *in silico* approaches to understand the progression of the biofilm to a cariogenic state, in a defined environment which has not been done before in dental biofilm research. Agreement between the *in silico* and *in vitro* findings, particularly the dominance of *S. mutans* at high glucose concentration and *V. parvula* at low glucose concentration, demonstrates that models attempting to implement this strategy must consider pH in bacterial growth kinetics. This research and known literature underline the effect of pH on species behaviour. These models provide the option to test antimicrobial actives on the synthetic community and expand our understanding of the sensitive nature of a commensal biofilm in suboptimal environments. This would involve the synthetic community being exposed to antimicrobials and characterising the change in the community with the analytical techniques used in this research, including qPCR and viability testing. This would be used to validate *in silico* simulations of antimicrobial testing or integration of probiotic species within the biofilm using the IbM. The models, therefore, provide a powerful framework for informing safe product development in dental biofilm and caries research (Figure 6.1). Better defining the complex relationship between species through metabolic modelling and informing the *in silico* models with more data collected experimentally i.e., growth rates at different pH or different acid productions, will improve the model's ability to characterise dental biofilms. To conclude, I successfully developed combinatorial *in vitro* and *in silico* models using a defined synthetic community and a defined chemical environment, considering the influence of pH, to provide a powerful tool in understanding *S. mutans* invasion into a commensal oral community.



Figure 6.1 Strategy for using the modelling approaches to combat caries development. The continuum and IbM will be used to characterise *in vivo* findings, being informed by kinetic parameters of the bacteria species, and validated by the *in vitro* model. This will help inform safe product development and microbial risk assessment through testing antimicrobials and better understanding drivers of dysbiosis.

References

- Aas, J.A., Paster, B.J., Stokes, L.N., Olsen, I. & Dewhirst, F.E. (2005) 'Defining the normal bacterial flora of the oral cavity', *Journal of Clinical Microbiology*, 43(11), p. 5721.
- Abram, A.M., Szewczyk, M.M., Park, S.G., Sam, S.S., Eldana, H.B., Korja, F.J., Ferracciolo, J.M., Young, L.A., Qadir, H., Bonham, A.J., Yang, F., Zora, J.S., Abdulelah, S.A., Patel, N.A., Koleilat, A., Saleh, M.A., Alhabeil, J.A., Khan, S., Tripathi, A., *et al.*. (2022) 'A co-association of *Streptococcus mutans* and *Veillonella parvula/dispar* in root caries patients and *In Vitro* biofilms', *Infection and immunity*, 90(10), p1-8.
- Ajdic, D., McShan, W.M., McLaughlin, R.E., Savic, G., Chang, J., Carson, M.B., Primeaux, C., Tian, R., Kenton, S., Jia, H., Lin, S., Qian, Y., Li, S., Zhu, H., Najar, F., Lai, H., White, J., Roe, B.A. & Ferretti, J.J. (2002) Genome sequence of *Streptococcus mutans* UA159, a cariogenic dental pathogen, p 14434-14436
- Allaker, R.P., Silva Mendez, L.S., Hardie, J.M. & Benjamin, N. (2001) 'Antimicrobial effect of acidified', *Oral Microbiol Immunol*, 16, pp. 253–256.
- Amann, R.L., Krumholz, L. & Stahl, D.A. (1990) 'Fluorescent-Oligonucleotide probing of whole cells for determinative, phylogenetic, and environmental studies in microbiology', *Journal of Bacteriology*, 172 (2), pp 762-765.
- Ammann, T.W., Gmür, R. & Thurnheer, T. (2012) 'Advancement of the 10-species subgingival Zurich biofilm model by examining different nutritional conditions and defining the structure of the in vitro biofilms.', *BMC microbiology*, 12(1), pp. 1–13.
- An, S.Q., Hull, R., Metris, A., Barrett, P., Webb, J.S. & Stoodley, P. (2022) 'An *in vitro* biofilm model system to facilitate study of microbial communities of the human oral cavity', *Letters in applied microbiology*, 74(3), pp. 302–310.
- Angarita-Díaz, M. del P., Fong, C., Bedoya-Correa, C.M. & Cabrera-Arango, C.L. (2022) 'Does high sugar intake really alter the oral microbiota?: A systematic review', *Clinical and Experimental Dental Research*, pp 1376-1381
- Aruni, A.W., Dou, Y., Mishra, A. & Fletcher, H.M. (2015) 'The Biofilm Community: Rebels with a Cause', *Current Oral Health Reports* 2015 2:1, 2(1), pp. 48–56.
- Arweiler, N.B. & Netuschil, L. (2016) 'The Oral Microbiota', *Advances in experimental medicine and biology*, 902, pp. 45–60.
- Baca-Castañón, M.L., de la Garza-Ramos, M.A., Alcázar-Pizaña, A.G., Grondin, Y., Coronado-Mendoza, A., Sánchez-Najera, R.I., Cárdenas-Estrada, E., Medina-De la

- Garza, C.E. & Escamilla-García, E. (2015) 'Antimicrobial effect of *Lactobacillus reuteri* on cariogenic bacteria *Streptococcus gordonii*, *Streptococcus mutans*, and periodontal diseases *Actinomyces naeslundii* and *Tannerella forsythia*', *Probiotics and antimicrobial proteins*, 7(1), pp. 1–8.
- Baker, J.L. & Edlund, A. (2019) 'Exploiting the oral microbiome to prevent tooth decay: Has evolution already provided the best tools?' *Frontiers in Microbiology*, 10.
- Baker, J.L., Faustoferri, R.C. & Quivey, R.G. (2017a) 'Acid-adaptive mechanisms of *Streptococcus mutans*—the more we know, the more we don't'. *Molecular Oral Microbiology* 32 (2), pp. 107–117.
- Baker, J.L., Faustoferri, R.C. & Quivey, R.G. (2017b) 'Acid-adaptive mechanisms of *Streptococcus mutans*—the more we know, the more we don't'. *Molecular Oral Microbiology* 32 (2), pp. 107–117.
- Balhaddad, A.A., Kansara, A.A., Hidan, D., Weir, M.D., Xu, H.H.K. & Melo, M.A.S. (2019) 'Toward dental caries: Exploring nanoparticle-based platforms and calcium phosphate compounds for dental restorative materials'. *Bioactive Materials*, 4 (1), pp. 43–55.
- Bedoya-Correa, C.M., Rincón-Rodríguez, R.J. & Parada-Sanchez, M.T. (2021) 'Acidogenic and aciduric properties of *Streptococcus mutans* serotype c according to its genomic variability', *European journal of oral sciences*, 129(6), .
- Beheshti, S. (2021) 'Evaluation of caries risk reduction following preventive programs in orthodontic patients, using cariogram computer model: A quasi-experimental trial', *Dental Press J Orthod*, 26(5), p. 2120218.
- Belstrøm, D., Fiehn, N.E., Nielsen, C.H., Holmstrup, P., Kirkby, N., Klepac-Ceraj, V., Paster, B.J. & Twetman, S. (2014) 'Altered bacterial profiles in saliva from adults with caries lesions: A case-cohort study', *Caries Research*, 48(5), pp. 368–375.
- Bender, G.R., Thibodeau, E.A. & Marquis, R.E. (1985) 'Reduction of acidurance of *Streptococcal* growth and glycolysis by fluoride and gramicidin', *Journal of dental research*, 64(2), pp. 90–95.
- Bengtsson-Palme, J. (2020) 'Microbial model communities: To understand complexity, harness the power of simplicity'. *Computational and Structural Biotechnology Journal* 18, pp. 3987–4001.

- Bernabé, E. & Marcenés, W. (2020) 'Can minimal intervention dentistry help in tackling the global burden of untreated dental caries?', *British Dental Journal*, 229(7), pp. 487–491.
- Bibiloni, R. (2012) 'Rodent models to study the relationships between mammals and their bacterial inhabitants', *Gut Microbes*, 3(6), p. 536.
- Bogino, P.C., Oliva, M. de las M., Sorroche, F.G. & Giordano, W. (2013) 'The role of bacterial biofilms and surface components in plant-bacterial associations'. *International Journal of Molecular Sciences* 14 (8), pp. 15838–15859.
- Boisen, G., Davies, J.R. & Neilands, J. (2021a) 'Acid tolerance in early colonizers of oral biofilms', *BMC Microbiology*, 21(1), pp. 1–9.
- Bourgeois, D., David, A., Inquimbert, C., Tramini, P., Molinari, N. & Carrouel, F. (2017) 'Quantification of carious pathogens in the interdental microbiota of young caries-free adults', *PLoS ONE*, 12(10), .
- Bradshaw, D.J. & Marsh, P.D. (1998a) 'Analysis of pH-driven disruption of oral microbial communities *in vitro*', *Caries Research*, 32(6), pp. 456–462.
- Bradshaw, D.J., Marsh, P.D., Allison, C. & Schilling, K.M. (1996) 'Effect of oxygen, inoculum composition and flow rate on development of mixed-culture oral biofilms', *Microbiology*, 142 (3), pp. 623–629.
- Brown, J.L., Johnston, W., Delaney, C., Short, B., Butcher, M.C., Young, T., Butcher, J., Riggio, M., Culshaw, S. & Ramage, G. (2019) 'Polymicrobial oral biofilm models: Simplifying the complex', *Journal of Medical Microbiology*, 68(11), pp. 1573–1584.
- Brown, J.R., Jurcisek, J., Lakhani, V., Snedden, A., Ray, W.C., Mokrzan, E.M., Bakaletz, L.O. & Das, J. (2019) '*In Silico* modeling of biofilm formation by nontypeable *Haemophilus influenzae in vivo*', *mSphere*, 4(4), pp. 254–273.
- Buckel, W. (2021) 'Energy conservation in fermentations of anaerobic bacteria'. *Frontiers in Microbiology* 12.
- Burne, R.A. & Marquis, R.E. (2000) 'Alkali production by oral bacteria and protection against dental caries', *FEMS Microbiology Letters*, 193(1), pp. 1–6.
- Bustin, S.A., Benes, V., Garson, J.A., Hellems, J., Huggett, J., Kubista, M., Mueller, R., Nolan, T., Pfaffl, M.W., Shipley, G.L., Vandesompele, J. & Wittwer, C.T. (2009) 'The MIQE Guidelines: Minimum information for publication of quantitative real-time PCR experiments', *Clinical Chemistry*, 55(4), pp. 611–622.

- Cagetti, M.G., Mastroberardino, S., Milia, E., Cocco, F., Lingström, P. & Campus, G. (2013) 'The use of probiotic strains in caries prevention: A systematic review', *Nutrients*, pp 2530–2550.
- Cai, J.-N., Jung, J.-E., Lee, M.-H., Choi, H.-M. & Jeon, J.-G. (2018) 'Sucrose challenges to *Streptococcus mutans* biofilms and the curve fitting for the biofilm changes', *FEMS Microbiology Ecology*, 94, p. 91.
- Caous, J.S., Lövenklev, M., Fäldt, J. & Langton, M. (2013) 'Adhesion of *Streptococcus mitis* and *Actinomyces oris* in co-culture to machined and anodized titanium surfaces as affected by atmosphere and pH', *BMC Oral Health*, 13(1), pp. 1–10.
- Caselli, E., Fabbri, C., D'Accolti, M., Soffritti, I., Bassi, C., Mazzacane, S. & Franchi, M. (2020a) 'Defining the oral microbiome by whole-genome sequencing and resistome analysis: The complexity of the healthy picture', *BMC Microbiology*, 20(1), .
- Caselli, E., Fabbri, C., D'Accolti, M., Soffritti, I., Bassi, C., Mazzacane, S. & Franchi, M. (2020b) 'Defining the oral microbiome by whole-genome sequencing and resistome analysis: The complexity of the healthy picture', *BMC Microbiology*, 20(1), pp. 1–19.
- Castillo, A., Rubiano, S., Gutiérrez, J., Hermoso, A. & Liébana, J. (2000) 'Post-pH effect in oral *Streptococci*', *Clinical Microbiology and Infection*, 6(3), pp. 142–146.
- Cavalcanti, I.M.G., del Bel Cury, A.A., Jenkinson, H.F. & Nobbs, A.H. (2017) 'Interactions between *Streptococcus oralis*, *Actinomyces oris*, and *Candida albicans* in the development of multispecies oral microbial biofilms on salivary pellicle', *Molecular oral microbiology*, 32(1), pp. 60–73.
- Chathoth, K., Fostier, L., Martin, B., Baysse, C. & Mahé, F. (2022) 'A multi-skilled mathematical model of bacterial attachment in initiation of biofilms', *Microorganisms*, 10(4) .
- Chatzigiannidou, I., Teughels, W., van de Wiele, T. & Boon, N. (2020) 'Oral biofilms exposure to chlorhexidine results in altered microbial composition and metabolic profile', *Biofilms and Microbiomes*, 6(1).
- Chawhuaveang, D.D., Yu, O.Y., Yin, I.X., Lam, W.Y.H., Mei, M.L. & Chu, C.H. (2021) 'Acquired salivary pellicle and oral diseases: A literature review', *Journal of Dental Sciences*, 16(1), p. 523.
- Chenicheri, S., R, U., Ramachandran, R., Thomas, V. & Wood, A. (2017) 'Insight into oral biofilm: Primary, secondary and residual caries and phyto-challenged solutions', *The Open Dentistry Journal*, 11(1), p. 312.

- Ciric, L., Pratten, J., Wilson, M. & Spratt, D. (2010) 'Development of a novel multi-triplex qPCR method for the assessment of bacterial community structure in oral populations', *Environmental Microbiology Reports*, 2(6), pp. 770–774.
- Coenye, T., de Prijck, K., de Wever, B. & Nelis, H.J. (2008) 'Use of the modified robbins device to study the *in vitro* biofilm removal efficacy of NitrAdine™, a novel disinfecting formula for the maintenance of oral medical devices', *Journal of Applied Microbiology*, 105(3), pp. 733–740.
- Costa Oliveira, B.E., Ricomini Filho, A.P., Burne, R.A. & Zeng, L. (2021a) 'The Route of Sucrose Utilization by *Streptococcus mutans* Affects Intracellular Polysaccharide Metabolism', *Frontiers in Microbiology*, 12.
- Crielaard, W., Zaura, E., Schuller, A.A., Huse, S.M., Montijn, R.C. & Keijser, B.J.F. (2011) 'Exploring the oral microbiota of children at various developmental stages of their dentition in the relation to their oral health', *BMC Medical Genomics*, 4p. 22.
- Cristina Barbosa da Silva, A., dos Santos Cruz, J., Correia Sampaio, F. & Antônio Machado de Araújo, D. (2008) 'Detection of oral *Streptococci* in dental biofilm from caries-active and caries-free children', *Brazilian Journal of Microbiology*, 39, pp. 648–651.
- Crowley, P.J., Brady, L.J., Michalek, S.M. & Bleiweis, A.S. (1999) 'Virulence of a spaP mutant of *Streptococcus mutans* in a gnotobiotic rat model', *Infection and Immunity*, 67(3), p. 1201.
- Cugini, C., Shanmugam, M., Landge, N. & Ramasubbu, N. (2019) 'The role of exopolysaccharides in oral biofilms', *Journal of Dental Research*, 98(7), p. 739.
- Dame-Teixeira, N., de Lima, A.K.A., Do, T. & Stefani, C.M. (2021) 'Meta-analysis using NGS data: The *Veillonella* species in dental caries', *Frontiers in Oral Health*, 2.
- Dame-Teixeira, N., Parolo, C.C.F., Maltz, M., Tugnait, A., Devine, D. & Do, T. (2016b) 'Actinomyces spp. gene expression in root caries lesions', *Journal of Oral Microbiology*, 8(1), p. 32383.
- Daruich, P.M. & Brizuela, M. (2022) 'Remineralization of initial carious lesions', *StatPearls*,
- Dashper, S.G. & Reynolds, E.C. (2000) 'Effects of organic acid anions on growth, glycolysis, and intracellular pH of oral *Streptococci*', *J Dent Res* 79 (1).
- Dashper, S.G. & Reynolds, E.C. (1996) 'Lactic acid excretion by *Streptococcus mutans*'. *Microbiology* 142.

- Dawes, C. (2003) 'What is the critical pH and why does a tooth dissolve in acid?. *J Can Dent Assoc*, 69 (11), p 722-4.
- Decker, E.M., Klein, C., Schwindt, D. & von Ohle, C. (2014) 'Metabolic activity of *Streptococcus mutans* biofilms and gene expression during exposure to xylitol and sucrose', *International Journal of Oral Science*, 6(4), p. 195.
- Díaz-Garrido, N., Lozano, C.P., Kreth, J. & Giacaman, R.A. (2020) 'Competition and caries on enamel of a dual-species biofilm model with *Streptococcus mutans* and *Streptococcus sanguinis*', *Applied and Environmental Microbiology*, 86(21), .
- Dinis, M., Traynor, W., Agnello, M., Sim, M.S., He, X., Shi, W., Lux, R. & Tran, N.C. (2022) 'Tooth-specific *Streptococcus mutans* distribution and associated microbiome', *Microorganisms 2022, Vol. 10, Page 1129*, 10(6), p. 1129.
- Do, T., Sheehy, E.C., Mulli, T., Hughes, F. & Beighton, D. (2015) 'Transcriptomic analysis of three *Veillonella spp.* present in carious dentine and in the saliva of caries-free individuals', *Frontiers in Cellular and Infection Microbiology*, 5, p. 25.
- Doel, J.J., Benjamin, N., Hector, M.P., Rogers, M. & Allaker, R.P. (2005) 'Evaluation of bacterial nitrate reduction in the human oral cavity', *European Journal of Oral Sciences*, 113(1), pp. 14–19.
- Dong, L., Yin, J., Zhao, J., Ma, S. rui, Wang, H. rui, Wang, M., Chen, W. & Wei, W. qiang (2018) 'Microbial similarity and preference for specific sites in healthy oral cavity and esophagus', *Frontiers in Microbiology*, 9, .
- Dutra De Oliveira, R.V., Albuquerque, Y.E., Madalena, D., Spolidorio, P., Koga-Ito, Y., Maria, E., Giro, A. & Brighenti, F.L. (2016), Effect of dietary sugars on dual-species biofilms of *Streptococcus mutans* and *Streptococcus sobrinus*-A pilot study, *Revista de odontologia da unesp*.
- Dzianach, P.A., Dykes, G.A., Strachan, N.J.C., Forbes, K.J. & Pérez-Reche, F.J. (2019) 'Challenges of biofilm control and utilization: lessons from mathematical modelling', *Journal of the Royal Society Interface*, 16(155), .
- Egland, P.G., Palmer, R.J. & Kolenbrander, P.E. (2004) 'Interspecies communication in *Streptococcus gordonii*-*Veillonella atypica* biofilms: Signaling in flow conditions requires juxtaposition', *Proceedings of the National Academy of Sciences of the United States of America*, 101(48), p. 16917.
- Elias, S. & Banin, E. (2012) 'Multi-species biofilms: living with friendly neighbors', *FEMS Microbiology Reviews*, 36(5), pp. 990–1004.

- Erazo, D. & Whetstone, D.R. (2022) 'Dental Infections', *The 5-Minute Pediatric Consult, 8th Edition*, pp. 274–275.
- Escherichia coli* (ID 167) - Genome - NCBI. [online]. Available from: https://www.ncbi.nlm.nih.gov/genome/167?genome_assembly_id=1673556 (Accessed 14 October 2022).
- Fabregas, R. & Rubinstein, J. (2014) 'On the initial propagation of dental caries', *Journal of the Royal Society Interface*, 11(100), .
- Fakhruddin, K.S., Ngo, H.C. & Samaranayake, L.P. (2019) 'Cariogenic microbiome and microbiota of the early primary dentition: A contemporary overview', *Oral diseases*, 25(4), pp. 982–995.
- Fan, L. 4, Leyva-Ramos, R., Wisecarver, K.D. & Zehner, B.J. (1990) Diffusion of phenol through a biofilm grown on activated carbon particles in a draft-tube three-phase fluidized-bed bioreactor, *Biotechnology and Bioengineering*
- Feng, D., Neuweiler, I., Nogueira, R. & Nackenhorst, U. (2021) 'Modeling of symbiotic bacterial biofilm growth with an example of the *Streptococcus–Veillonella* sp. system', *Bulletin of Mathematical Biology*, 83(5), p. 48.
- Flemming, H.C. & Wuertz, S. (2019) 'Bacteria and archaea on earth and their abundance in biofilms', *Nature Reviews Microbiology*, 17(4), pp. 247–260.
- Fontana, M., Buller, T.L., Dunipace, A.J., Stookey, G.K. & Gregory, R.L. (2000) 'Antibodies to *Streptococcus mutans* surface proteins in preventing dental caries'. *Clinical and Diagnostic Laboratory Immunology*, 7 (1).
- Ganesh, K., Soumen, R., Ravichandran, Y. & Janarthanan (2017) 'Dynamic approach to predict pH profiles of biologically relevant buffers', *Biochemistry and Biophysics Reports*, 9pp. 121–127.
- German Collection of Microorganisms and Cell Cultures GmbH: Details. [online]. Available from: <https://www.dsmz.de/collection/catalogue/details/culture/DSM-17610> (Accessed 29 September 2022a).
- German Collection of Microorganisms and Cell Cultures GmbH: Details. [online]. Available from: <https://www.dsmz.de/collection/catalogue/details/culture/DSM-2008> (Accessed 29 September 2022b).
- Gedif Meseret, A. (2021) 'Oral biofilm and its impact on oral health, psychological and social interaction', *International Journal of Oral and Dental Health*, 7(1), .

- Gogulancea, V., González-Cabaleiro, R., Li, B., Taniguchi, D., Jayathilake, P.G., Chen, J., Wilkinson, D., Swailes, D., McGough, A.S., Zuliani, P., Ofiteru, I.D. & Curtis, T.P. (2019a) 'Individual-based model links thermodynamics, chemical speciation and environmental conditions to microbial growth', *Frontiers in Microbiology*, 10,
- Gogulancea, V., González-Cabaleiro, R., Li, B., Taniguchi, D., Jayathilake, P.G., Chen, J., Wilkinson, D., Swailes, D., McGough, A.S., Zuliani, P., Ofiteru, I.D. & Curtis, T.P. (2019b) 'Individual based model links thermodynamics, chemical speciation and environmental conditions to microbial growth', *Frontiers in Microbiology*, 0, p. 1871.
- Grainha, T., Magalhães, A.P., Melo, L.D.R. & Pereira, M.O. (2020) 'Pitfalls associated with discriminating mixed-species biofilms by flow cytometry', *Antibiotics*, 9(11), pp. 1–17.
- Gronow, S., Welnitz, S., Lapidus, A., Nolan, M., Ivanova, N., del Rio, T.G., Copeland, A., Chen, F., Tice, H., Pitluck, S., Cheng, J.F., Saunders, E., Brettin, T., Han, C., Detter, J.C., Bruce, D., Goodwin, L., Land, M., Hauser, L., *et al.*, (2010a) 'Complete genome sequence of *Veillonella parvula* type strain (Te3 T)', *Standards in Genomic Sciences*, 2(1), pp. 57–65.
- Gross, E.L., Beall, C.J., Kutsch, S.R., Firestone, N.D., Leys, E.J. & Griffen, A.L. (2012) 'Beyond *Streptococcus mutans*: Dental caries onset linked to multiple species by 16S rRNA Community Analysis', *PLoS ONE*, 7(10), .
- Guan, N. & Liu, L. (2020a) 'Microbial response to acid stress: mechanisms and applications', *Applied Microbiology and Biotechnology*, 104(1), p. 51.
- Guggenheim, B., Guggenheim, M., Gmür, R., Giertsen, E. & Thurnheer, T. (2004) 'Application of the Zürich biofilm model to problems of cariology', *Caries Research*, 38(3), pp. 212–222.
- Guo, L., Hu, W., He, X., Lux, R., McLean, J. & Shi, W. (2013) 'Investigating acid production by *Streptococcus mutans* with a surface-displayed pH-sensitive green fluorescent protein', *PLoS ONE*, 8(2), .
- Guo, Q., Ahn, S.J., Kaspar, J., Zhou, X. & Burne, R.A. (2014) 'Growth phase and pH influence peptide signaling for competence development in *Streptococcus mutans*', *Journal of Bacteriology*, 196(2), p. 227.
- Habibah, T.U., Amlani, D. v. & Brizuela, M. (2022) 'Hydroxyapatite dental material', *StatPearls*,

- Hamba, H., Nakamura, K., Nikaido, T., Tagami, J. & Muramatsu, T. (2020) Remineralization of enamel subsurface lesions using toothpaste containing tricalcium phosphate and fluoride: an *in vitro* μ CT analysis, *BMC Oral Health*, (20), 1-7
- He, X.-S. & Shi, W.-Y. (2009) 'Oral Microbiology: Past, present and future', *International Journal of Oral Science*, (2).
- Head, D., Devine, D.A. & Marsh, P.D. (2017) '*In silico* modelling to differentiate the contribution of sugar frequency versus total amount in driving biofilm dysbiosis in dental caries', *Scientific Reports 2017 7:1*, 7(1), pp. 1–10.
- Head, D., Marsh, P.D., Devine, D.A. & Tenuta, L.M.A. (2021) '*In Silico* modeling of hyposalivation and biofilm dysbiosis in root caries', *Journal of Dental Research*, 100(9), pp. 977–982.
- Head, D.A., Marsh, P.D. & Devine, D.A. (2014a) 'Non-lethal control of the cariogenic potential of an agent-based model for dental plaque', *PLOS ONE*, 9(8), p. 105012.
- Heijnen, J.J. & Kleerebezem, R. (2010) Bioenergetics of microbial growth, *Encyclopaedia of Industrial Biotechnology*
- Herzog, S.A., Blaizot, S. & Hens, N. (2017) 'Mathematical models used to inform study design or surveillance systems in infectious diseases: A systematic review', *BMC Infectious Diseases*, 17(1), .
- van der Hoeven, J.S., de Jong, M.H. & Rogers, A.H. (1985) 'Effect of utilization of substrates on the composition of dental plaque', *FEMS Microbiology Letters*, 31(3), pp. 129–133.
- van der Hoeven, J.S. & van den Kieboom, C.W.A. (1990) 'Oxygen-dependent lactate utilization by *Actinomyces viscosus* and *Actinomyces naeslundii*', *Oral Microbiology and Immunology*, 5(4), pp. 223–225.
- Høiby, N., Bjarnsholt, T., Givskov, M., Molin, S. & Ciofu, O. (2010) 'Antibiotic resistance of bacterial biofilms', *International journal of antimicrobial agents*, 35(4), pp. 322–332.
- van Holm, W., Verspecht, T., Carvalho, R., Bernaerts, K., Boon, N., Zayed, N. & Teughels, W. (2022) 'Glycerol strengthens probiotic effect of *Limosilactobacillus reuteri* in oral biofilms: A synergistic synbiotic approach', *Molecular Oral Microbiology*,
- Horst, J.A., Tanzer, J.M. & Milgrom, P.M. (2018) 'Fluorides and other preventive strategies for tooth decay'. *Dental Clinics of North America*, 62 (2) p.pp. 207–234.

- Huang, R., Li, M. & Gregory, R.L. (2011) 'Bacterial interactions in dental biofilm', *Virulence*, 2(5), p. 435.
- Hyde, E.R., Andrade, F., Vaksman, Z., Parthasarathy, K., Jiang, H., Parthasarathy, D.K., Torregrossa, A.C., Tribble, G., Kaplan, H.B., Petrosino, J.F. & Bryan, N.S. (2014) 'Metagenomic analysis of nitrate-reducing bacteria in the oral cavity: implications for nitric oxide homeostasis', *PloS one*, 9(3), .
- Ilie, O., van Loosdrecht, M.C.M. & Picioreanu, C. (2012) 'Mathematical modelling of tooth demineralisation and pH profiles in dental plaque', *Journal of Theoretical Biology*, 309pp. 159–175.
- Inquimbert, C., Bourgeois, D., Bravo, M., Viennot, S., Tramini, P., Llodra, J.C., Molinari, N., Dussart, C., Giraudeau, N. & Carrouel, F. (2019) 'The oral bacterial microbiome of interdental surfaces in adolescents according to carious risk', *Microorganisms* 2019,(7), p. 319.
- Invernici, M.M., Salvador, S.L., Silva, P.H.F., Soares, M.S.M., Casarin, R., Palioto, D.B., Souza, S.L.S., Taba, M., Novaes, A.B., Furlaneto, F.A.C. & Messoria, M.R. (2018) 'Effects of *Bifidobacterium* probiotic on the treatment of chronic periodontitis: A randomized clinical trial', *Journal of Clinical Periodontology*, 45(10), p. 1198.
- Iorgulescu, G. (2009) 'Saliva between normal and pathological. Important factors in determining systemic and oral health', *Journal of Medicine and Life*, 2(3), p. 303.
- Jakubovics, N.S., Gill, S.R., Vickerman, M.M. & Kolenbrander, P.E. (2008) 'Role of hydrogen peroxide in competition and cooperation between *Streptococcus gordonii* and *Actinomyces naeslundii*', *FEMS Microbiology Ecology*, 66(3), pp. 637–644.
- Jakubovics, N.S., Goodman, S.D., Mashburn-Warren, L., Stafford, G.P. & Cieplik, F. (2021) 'The dental plaque biofilm matrix', *Periodontology 2000*, 86(1), pp. 32–56.
- Jakubovics, N.S. & Kolenbrander, P.E. (2010) 'The road to ruin: The formation of disease-associated oral biofilms'. *Oral Diseases*, 16 (8) p.pp. 729–739.
- Janket, S.J., Benwait, J., Isaac, P., Ackerson, L.K. & Meurman, J.H. (2019) 'Oral and systemic effects of xylitol consumption', *Caries Research*, 53(5), pp. 491–501.
- Jauregui, C.E., Mansell, J.P., Jepson, M.A. & Jenkinson, H.F. (2013) 'Differential interactions of *Streptococcus gordonii* and *Staphylococcus aureus* with cultured osteoblasts', *Molecular Oral Microbiology*, 28(4), pp. 250–266.
- Jayathilake, P.G., Gupta, P., Li, B., Madsen, C., Oyebamiji, O., González-Cabaleiro, R., Rushton, S., Bridgens, B., Swailes, D., Allen, B., McGough, A.S., Zuliani, P., Ofiteru,

- I.D., Wilkinson, D., Chen, J. & Curtis, T. (2017) 'A mechanistic Individual-based model of microbial communities', *PLOS ONE*, 12(8), p. e0181965.
- Jensen, C.S., Norsigian, C.J., Fang, X., Nielsen, X.C., Christensen, J.J., Palsson, B.O. & Monk, J.M. (2020) 'Reconstruction and validation of a genome-scale metabolic model of *Streptococcus oralis* (iCJ415), a human commensal and opportunistic pathogen', *Frontiers in Genetics*, Op. 116.
- de Jesus, V.C., Khan, M.W., Mittermuller, B.A., Duan, K., Hu, P., Schroth, R.J. & Chelikani, P. (2021) 'Characterization of supragingival plaque and oral swab microbiomes in children with severe early childhood caries', *Frontiers in microbiology*, 12.
- Jijakli, K. & Jensen, P.A. (2019a) 'Metabolic modeling of *Streptococcus mutans* reveals complex nutrient requirements of an oral pathogen', *mSystems*, 4(5), .
- Jones, R.S. (2019) Combined chemical and physical approaches for oral biofilm control, PhD thesis submitted from Newcastle University.
- Joumal, A. I., & Bertolazzi, E. (2005). A Combination Formula of Michaelis-Menten-Monod Type. *Computers and Mathematics with Applications*, 50 (1), pp 201–215.
- Kalhan, T.A., Lin, Y.T., Kalhan, A.C., Lin, Y.T.J., Chou, C.C. & Hsu, C.Y.S. (2019) 'Dental plaque pH in predicting caries relapse after general anaesthesia – an exploratory study', *International Dental Journal*, 69(6), pp. 419–427.
- Kassebaum, N.J., Smith, A.G.C., Bernabé, E., Fleming, T.D., Reynolds, A.E., Vos, T., Murray, C.J.L., Marcenes, W., Abyu, G.Y., Alsharif, U., Asayesh, H., Benzian, H., Dandona, L., Dandona, R., Kasaeian, A., Khader, Y.S., Khang, Y.H., Kokubo, Y., Kotsakis, G.A., *et al.*, (2017) 'Global, regional, and national prevalence, incidence, and disability-adjusted life years for oral conditions for 195 Countries, 1990-2015: A Systematic analysis for the global burden of diseases, injuries, and risk factors', *Journal of Dental Research*, 96(4), pp. 380–387.
- Kawada-Matsuo, M., Oogai, Y. & Komatsuzawa, H. (2017) 'Sugar allocation to metabolic pathways is tightly regulated and affects the virulence of *Streptococcus mutans*', *Genes*, 8(1), .
- Keller, M.K., Kressirer, C.A., Belstrøm, D., Twetman, S. & Tanner, A.C.R. (2017) 'Oral microbial profiles of individuals with different levels of sugar intake', *Journal of Oral Microbiology*, 9(1), .
- Khan, R., Petersen, F.C. & Shekhar, S. (2019) 'Commensal bacteria: An emerging player in defense against respiratory pathogens', *Frontiers in Immunology*, 10, p. 1203.

- Khandelwal, R.A., Olivier, B.G., Röling, W.F.M., Teusink, B. & Bruggeman, F.J. (2013) 'Community flux balance analysis for microbial consortia at balanced growth', *PLOS ONE*, 8(5), p. 64567.
- Khoroushi, M. & Kachuie, M. (2017) 'Prevention and treatment of white spot lesions in orthodontic patients', *Contemporary Clinical Dentistry*, 8(1), p. 11.
- Kianoush, N., Adler, C.J., Nguyen, K.A.T., Browne, G. v., Simonian, M. & Hunter, N. (2014) 'Bacterial profile of dentine caries and the Impact of pH on bacterial population diversity', *PLoS ONE*, 9(3), .
- Kilian, M., Chapple, I.L.C., Hannig, M., Marsh, P.D., Meuric, V., Pedersen, A.M.L., Tonetti, M.S., Wade, W.G. & Zaura, E. (2016) 'The oral microbiome - An update for oral healthcare professionals', *British Dental Journal*, 221(10), pp. 657–666.
- Kim, M. & Or, D. (2016) 'Individual-based model of microbial life on hydrated rough soil surfaces', *PLOS ONE*, 11(1), p. e0147394.
- Klug, B., Santigli, E., Westendorf, C., Tangl, S., Wimmer, G. & Grube, M. (2016) 'From mouth to model: Combining *in vivo* and *in vitro* oral biofilm growth', *Frontiers in Microbiology*, 7(SEP), p. 1448.
- Knapp, R., Marshman, Z., Gilchrist, F. & Rodd, H. (2021) 'The impact of dental caries and its treatment under general anaesthetic on children and their families', *European Archives of Paediatric Dentistry*, 22(4), pp. 567–574.
- Koch, C.D., Gladwin, M.T., Freeman, B.A., Lundberg, J.O., Weitzberg, E. & Morris, A. (2017) 'Enterosalivary nitrate metabolism and the microbiome: Intersection of microbial metabolism, nitric oxide and diet in cardiac and pulmonary vascular health'. *Free Radical Biology and Medicine* 105, pp. 48–67.
- Könönen, E. & Wade, W.G. (2015) 'Actinomyces and related organisms in human infections', *Clinical Microbiology Reviews*, 28(2), p. 419.
- Kouidhi, B., al Qurashi, Y.M.A. & Chaieb, K. (2015) 'Drug resistance of bacterial dental biofilm and the potential use of natural compounds as alternative for prevention and treatment', *Microbial pathogenesis*, 80pp. 39–49.
- Kreft, J.-U., Picioreanu, C., Wimpenny, J.W.T. & van Loosdrecht, M.C.M. (2001) 'Individual-based modelling of biofilms', *Microbiology*, 147.
- Kreth, J., Hagerman, E., Tam, K., Merritt, J., Wong, D.T.W., Wu, B.M., Myung, N. v, Shi, W. & Qi, F. (2004) Quantitative analyses of *Streptococcus mutans* biofilms with quartz

- crystal microbalance, microjet impingement and confocal microscopy, *Biofilms*, (4), 277-280
- Kreth, J., Vu, H., Zhang, Y. & Herzberg, M.C. (2009) 'Characterization of hydrogen peroxide-induced DNA release by *Streptococcus sanguinis* and *Streptococcus gordonii*', *Journal of Bacteriology*, 191(20), p. 6281.
- Kreth, J., Zhu, L., Merritt, J., Shi, W. & Qi, F. (2008) 'Role of sucrose in the fitness of *Streptococcus mutans*', *Oral microbiology and immunology*, 23(3), pp. 213–219.
- Krishnan, K., Chen, T. & Paster, B.J. (2017) 'A practical guide to the oral microbiome and its relation to health and disease', *Oral diseases*, 23(3), p. 276.
- Kuhnert, W.L., Zheng, G., Faustoferri, R.C. & Quivey, R.G. (2004) 'The F-ATPase operon promoter of *Streptococcus mutans* is transcriptionally regulated in response to external pH', *Journal of Bacteriology*, 186(24), pp. 8524–8528.
- Lamont, E.I., Gadkari, A., Kerns, K.A., To, T.T., Daubert, D., Kotsakis, G., Bor, B., He, X. & McLean, J.S. (2021) 'Modified SHI medium supports growth of a disease-state subgingival polymicrobial community in vitro', *Molecular oral microbiology*, 36(1), pp. 37–49.
- Lamont, R.J., Koo, H. & Hajishengallis, G. (2018) 'The oral microbiota: dynamic communities and host interactions', *Nature reviews. Microbiology*, 16(12), p. 745.
- Lee, K.W.K., Periasamy, S., Mukherjee, M., Xie, C., Kjelleberg, S. & Rice, S.A. (2014a) 'Biofilm development and enhanced stress resistance of a model, mixed-species community biofilm', *The ISME Journal*, 8(4), p. 894.
- Lee, S.H. & Kim, Y.J. (2014) 'A comparative study of the effect of probiotics on cariogenic biofilm model for preventing dental caries', *Archives of microbiology*, 196(8), pp. 601–609.
- Levy, N. (2012) 'The use of animal as models: ethical considerations', *International journal of stroke : official journal of the International Stroke Society*, 7(5), pp. 440–442.
- Li, B., Taniguchi, D., Gedara, J.P., Gogulancea, V., Gonzalez-Cabaleiro, R., Chen, J., McGough, A.S., Ofiteru, I.D., Curtis, T.P. & Zuliani, P. (2019) 'NUFEB: A massively parallel simulator for individual-based modelling of microbial communities', *PLOS Computational Biology*, 15(12), p. e1007125.

- Li, H., Chen, S., Wu, L., Wang, H., Xiao, K., Gao, Y., Li, Y., Li, Huiqin, Xiao, B. & Zhu, Y. (2019) 'The effects of perineal disinfection on infant's oral microflora after transvaginal examination during delivery', *BMC pregnancy and childbirth*, 19(1), .
- Li, J., Helmerhorst, E.J., Leone, C.W., Troxler, R.F., Yaskell, T., Haffajee, A.D., Socransky, S.S. & Oppenheim, F.G. (2004) 'Identification of early microbial colonizers in human dental biofilm', *Journal of applied microbiology*, 97(6), pp. 1311–1318.
- Li, X., Shang, L., Brandt, B.W., Buijs, M.J., Roffel, S., van Loveren, C., Crielaard, W., Gibbs, S. & Deng, D.M. (2021) 'Saliva-derived microcosm biofilms grown on different oral surfaces in vitro', *npj Biofilms and Microbiomes* 2021 7:1, 7(1), pp. 1–8.
- Lim, B.S., Kim, B.H., Shon, W.J. & Ahn, S.J. (2020) 'Effects of caries activity on compositions of mutans *Streptococci* in saliva-induced biofilm formed on bracket materials', *Materials*, 13(21), pp. 1–11.
- Listl, S., Galloway, J., Mossey, P.A. & Marcenes, W. (2015) 'Global economic impact of dental diseases', *Journal of Dental Research*. [Online]. 1 October 2015 SAGE Publications Inc. pp. 1355–1361.
- Liu, G., Tang, C.M. & Exley, R.M. (2015) 'Non-pathogenic *Neisseria*: Members of an abundant, multi-habitat, diverse genus', *Microbiology*, 161(7), pp. 1297–1312.
- Liu, S., Chen, M., Wang, Y., Zhou, X., Peng, X., Ren, B., Li, M. & Cheng, L. (2020) 'Effect of *Veillonella parvula* on the physiological activity of *Streptococcus mutans*', *Archives of Oral Biology*, 109.
- Lories, B., Roberfroid, S., Dieltjens, L., de Coster, D., Foster, K.R. & Steenackers, H.P. (2020) 'Biofilm bacteria use stress responses to detect and respond to competitors', *Current Biology*, 30(7), p. 1231.
- Love, R.M. & Jenkinson, H.F. (2016) 'Invasion of dentinal tubules by oral bacteria', *Critical Reviews in Oral Biology and Medicine*, 13(2), pp. 171–183.
- Lund, P., Tramonti, A., de Biase, D., Pasteur-Fondazione, I. & Bolognetti, C. (2014) 'Coping with low pH: molecular strategies in neutralophilic bacteria', *FEMS Microbiology Reviews*, 38(6), pp. 1091–1125.
- Luo, T.L., Vanek, M.E., Gonzalez-Cabezas, C., Marrs, C.F., Foxman, B. & Rickard, A.H. (2022) 'In vitro model systems for exploring oral biofilms: From single-species populations to complex multi-species communities', *Journal of Applied Microbiology*, 132(2), pp. 855–871.

- Luppens, S.B.I., Kara, D., Bandounas, L., Jonker, M.J., Wittink, F.R.A., Bruning, O., Breit, T.M., ten Cate, J.M. & Crielaard, W. (2008) 'Effect of *Veillonella parvula* on the antimicrobial resistance and gene expression of *Streptococcus mutans* grown in a dual-species biofilm', *Oral Microbiology and Immunology*, 23(3), pp. 183–189.
- Lynge Pedersen, A.M. & Belstrøm, D. (2019) 'The role of natural salivary defences in maintaining a healthy oral microbiota', *Journal of Dentistry*, 80pp. S3–S12.
- Lyu, X., Wang, L., Shui, Y., Jiang, Q., Chen, L., Yang, W., He, X., Zeng, J. & Li, Y. (2021) 'Ursolic acid inhibits multi-species biofilms developed by *Streptococcus mutans*, *Streptococcus sanguinis*, and *Streptococcus gordonii*', *Archives of Oral Biology*, 125, p. 105107.
- Ma, L., Hu, L., Feng, X. & Wang, S. (2018) 'Nitrate and nitrite in health and disease', *Aging and Disease*, 9(5), p. 938.
- Mark Steven, W. & Charlie, L. (2009) 'The cariogenic dental biofilm: good, bad or just something to control?', *Brazilian Oral Research*, 23, pp. 31–38.
- Marsh, P.D. (2006) 'Dental plaque as a biofilm and a microbial community - Implications for health and disease', *BMC Oral Health*. [Online]. 2006
- Marsh, Philip D, Do, T., Beighton, D. & Devine, D.A. (2015) Influence of saliva on the oral microbiota, *Periodontology 2000*.
- Marsh, Phil D., Head, D.A. & Devine, D.A. (2015) 'Ecological approaches to oral biofilms: control without killing', *Caries research*, 49, pp. 46–54.
- Martin, B., Tamanai-Shacoori, Z., Bronsard, J., Ginguené, F., Meuric, V., Mahé, F. & Bonnaure-Mallet, M. (2017) 'A new mathematical model of bacterial interactions in two-species oral biofilms', *PLOS ONE*, 12(3), p. e0173153.
- Mashima, I. & Nakazawa, F. (2015) 'Interaction between *Streptococcus spp.* and *Veillonella tobetsuensis* in the early stages of oral biofilm formation', *Journal of Bacteriology*, 197(13), p. 2104.
- Mashima, I., Theodorea, C.F., Thaweboon, B., Thaweboon, S. & Nakazawa, F. (2016) 'Identification of *Veillonella* species in the tongue biofilm by using a novel one-step polymerase chain reaction method', *PLoS ONE*, 11(6), .
- Matsui, R. & Cvitkovitch, D. (2010) 'Acid tolerance mechanisms utilized by *Streptococcus mutans*', *Future microbiology*, 5(3), p. 403.
- Matsumoto-Nakano, M. (2018) 'Role of *Streptococcus mutans* surface proteins for biofilm formation', *Japanese Dental Science Review*, 54(1), pp. 22–29.

- Mazumdar, V., Snitkin, E.S., Amar, S. & Segrè, D. (2009) 'Metabolic network model of a human oral pathogen', *Journal of Bacteriology*, 91(1), pp. 74–90.
- McBain, A.J., O'neill, C.A., Amezcua, A., Price, L.J., Faust, K., Tett, A., Segata, N., Swann, J.R., Smith, A.M., Murphy, B., Hoptroff, M., James, G., Reddy, Y., Dasgupta, A., Ross, T., Chapple, I.L., Wade, W.G. & Fernandez-Piquer, J. (2019) 'Consumer safety considerations of skin and oral microbiome perturbation', *Clinical Microbiology Reviews*, 32(4), .
- McNeill, K. & Hamilton, I.R. (2003) 'Acid tolerance response of biofilm cells of *Streptococcus mutans*', *FEMS Microbiology Letters*, 221(1), pp. 25–30.
- Medjedovic, E., Medjedovic, S., Deljo, D. & Sukalo, A. (2015) 'Impact of fluoride on dental health quality', *Materia Socio-Medica*, 27(6), p. 395.
- Melaugh, G., Hutchison, J., Kragh, K.N., Irie, Y., Roberts, A., Bjarnsholt, T., Diggle, S.P., Gordon, V.D. & Allen, R.J. (2016) 'Shaping the growth behaviour of biofilms initiated from bacterial aggregates', *PLoS ONE*, 11(3), .
- Métris, A., Barrett, P., Price, L., Klamert, S. & Fernandez-Piquer, J. (2022) 'A tiered approach to risk assess microbiome perturbations induced by application of beauty and personal care products', *Microbial Risk Analysis*, 20.
- Meyer, F., Enax, J., Epple, M., Amaechi, B.T. & Simader, B. (2021) 'Cariogenic biofilms: Development, properties, and biomimetic preventive agents', *Dentistry Journal*, 9(8), .
- Miller, M., Rogers, J.C., Badham, M.A., Cadenas, L., Brightwell, E., Adams, J., Tyler, C., Sebahar, P.R., Haussener, T.J., Kanna Reddy, H.R., Looper, R.E. & Williams, D.L. (2020) 'Examination of a first-in-class bis-dialkyl-norspermidine-terphenyl antibiotic in topical formulation against mono and polymicrobial biofilms', *PLOS ONE*, 15(10), p. e0234832.
- Mishra, A., Das, A., Cisar, J.O. & Ton-That, H. (2007) 'Sortase-catalyzed assembly of distinct heteromeric fimbriae in *Actinomyces naeslundii*', *Journal of Bacteriology*, 189(8), pp. 3156–3165.
- Mishra, A., Wu, C., Yang, J., Cisar, J.O., Das, A. & Ton-That, H. (2010) 'The *Actinomyces oris* type 2 fimbrial shaft FimA mediates co-aggregation with oral *Streptococci*, adherence to red blood cells and biofilm development', *Molecular Microbiology*, 77(4), pp. 841–854.

- Mohammed, W.K., Krasnogor, N. & Jakubovics, N.S. (2018) '*Streptococcus gordonii* Challisin protease is required for sensing cell-cell contact with *Actinomyces oris*', *FEMS Microbiology Ecology*, 94(5), .
- Mombelli, A. & Décaillet, F. (2011) 'The characteristics of biofilms in peri-implant disease', in *Journal of Clinical Periodontology*. [Online]. March 2011 pp. 203–213.
- Muddugangadhar, B.C., Sangur, R., Rudraprasad, I. v., Nandeeshwar, D.B. & Dhanya Kumar, B.H. (2015) 'A clinical study to compare between resting and stimulated whole salivary flow rate and pH before and after complete denture placement in different age groups', *The Journal of the Indian Prosthodontic Society*, 15(4), p. 356.
- Muloiwa, M., Nyende-Byakika, S., & Dinka, M. (2020). *Comparison of unstructured kinetic bacterial growth models.*, *South African Journal of Chemical Engineering*, 33 (1). p 141-150
- Nairn, B.L., Lee, G.T., Chumber, A.K., Steck, P.R., Mire, M.O., Lima, B.P. & Herzberg, M.C. (2021) 'Uncovering roles of *Streptococcus gordonii* SrtA-processed proteins in the biofilm Lifestyle', *Journal of Bacteriology*, 203(2), .
- Nanda, J., Sachdev, V., Sandhu, M. & Deep-Singh-Nanda, K. (2015) 'Correlation between dental caries experience and mutans *Streptococci* counts using saliva and plaque as microbial risk indicators in 3-8 year old children. A cross sectional study', *Journal of Clinical and Experimental Dentistry*, 7(1), p. e114.
- Nascimento, M.M., Gordan, V. v., Garvan, C.W., Browngardt, C.M. & Burne, R.A. (2009) 'Correlations of oral bacterial arginine and urea catabolism with caries experience', *Oral Microbiology and Immunology*, 24(2), pp. 89–95.
- Nomura, R., Matayoshi, S., Otsugu, M., Kitamura, T., Teramoto, N. & Nakano, K. (2020) Contribution of severe dental caries Induced by *Streptococcus mutans* to the pathogenicity of infective endocarditis, *ASM Journals*.
- Norimatsu, Y., Kawashima, J., Takano-Yamamoto, T. & Takahashi, N. (2015) 'Nitrogenous compounds stimulate glucose-derived acid production by oral *Streptococcus* and *Actinomyces*', *Microbiology and Immunology*, 59(9), pp. 501–506.
- Nyvad, B. & Takahashi, N. (2020) 'Integrated hypothesis of dental caries and periodontal diseases'. *Journal of Oral Microbiology*, 12 (1).
- Ofițeru, I.D., Bellucci, M., Picioreanu, C., Lavric, V. & Curtis, T.P. (2014) 'Multi-scale modelling of bioreactor-separator system for wastewater treatment with two-dimensional activated sludge floc dynamics', *Water Research*, 50pp. 382–395.

- Oh, D.H., Chen, X., Daliri, E.B.M., Kim, N., Kim, J.R. & Yoo, D. (2020) 'Microbial etiology and prevention of dental caries: Exploiting natural products to inhibit cariogenic biofilms'. *Pathogens* 9 (7), pp. 1–15.
- O'Hagan-Wong, K., Enax, J., Meyer, F. & Ganss, B. (2022) 'The use of hydroxyapatite toothpaste to prevent dental caries', *Odontology*, 110(2), pp. 223–230.
- Orth, J.D., Thiele, I. & Palsson, B.O. (2010) 'What is flux balance analysis?' *Nature Biotechnology*, 28 (3) p.pp. 245–248.
- Otten, M.P.T., Busscher, H.J., Abbas, F., van der Mei, H.C. & van Hoogmoed, C.G. (2012) 'Plaque-left-behind after brushing: Intra-oral reservoir for antibacterial toothpaste ingredients', *Clinical Oral Investigations*, 16(5), pp. 1435–1442.
- Palmer, R.J. (2014) 'Composition and development of oral bacterial communities', *Periodontology 2000*, 64(1), pp. 20–39.
- Palmer, R.J., Diaz, P.I. & Kolenbrander, P.E. (2006) 'Rapid succession within the *Veillonella* population of a developing human oral biofilm in situ', *Journal of Bacteriology*, 188(11), pp. 4117–4124.
- Palmer, R.J., Gordon, S.M., Cisar, J.O. & Kolenbrander, P.E. (2003) 'Coaggregation-mediated interactions of *Streptococci* and *Actinomyces* detected in initial human dental plaque', *Journal of Bacteriology*, 185(11), pp. 3400–3409.
- Paredes, S.D.O., da Nóbrega, R.F., Soares, T.D.S., Bezerra, M.E.D., de Abreu, M.H.N.G. & Forte, F.D.S. (2021) 'Dental pain associated with untreated dental caries and sociodemographic factors in 5-year-old children', *Journal of Clinical and Experimental Dentistry*, 13(6), pp. 552–557.
- Park, S.H., Kim, K., Cho, S., Chung, D.H. & Ahn, S.J. (2022) 'Variation in adhesion of *Streptococcus mutans* and *Porphyromonas gingivalis* in saliva-derived biofilms on raw materials of orthodontic brackets', *Korean Journal of Orthodontics*, 52(4), pp. 278–286.
- Periasamy, S. & Kolenbrander, P.E. (2010) 'Central role of the early colonizer *Veillonella spp.* in establishing multispecies biofilm communities with initial, middle, and late colonizers of enamel', *Journal of Bacteriology*, 192(12), pp. 2965–2972.
- Petersson, J., Carlström, M., Schreiber, O., Phillipson, M., Christoffersson, G., Jägare, A., Roos, S., Jansson, E.Å., Persson, A.E.G., Lundberg, J.O. & Holm, L. (2009) 'Gastroprotective and blood pressure lowering effects of dietary nitrate are

- abolished by an antiseptic mouthwash', *Free radical biology & medicine*, 46(8), pp. 1068–1075.
- Philip, N., Suneja, B. & Walsh, L. (2018) Beyond *Streptococcus mutans*: clinical implications of the evolving dental caries aetiological paradigms and its associated microbiome Evolving paradigms of caries, *British Dental Journal*.
- Piciooreanu, C., Kreft, J.U. & van Loosdrecht, M.C.M. (2004) 'Particle-based multidimensional multispecies biofilm model', *Applied and Environmental Microbiology*, 70(5), pp. 3024–3040.
- Pitts, N.B., Twetman, S., Fisher, J. & Marsh, P.D. (2021) 'Understanding dental caries as a non-communicable disease', *British Dental Journal*, 231(12), pp. 749–753.
- Prasetyanto Wicaksono, D., Washio, J., Abiko, Y., Domon, H. & Takahashi, N. (2020) Nitrite production from bitrate and its link with lactate metabolism in oral *Veillonella spp.*
- Proctor, Di.M., Fukuyama, J.A., Loomer, P.M., Armitage, G.C., Lee, S.A., Davis, N.M., Ryder, M.I., Holmes, S.P. & Relman, D.A. (2018) 'A spatial gradient of bacterial diversity in the human oral cavity shaped by salivary flow', *Nature Communications* 2018 9:1, 9(1), pp. 1–10.
- Proctor, D.M. & Relman, D.A. (2017) 'The landscape ecology and microbiota of the human nose, mouth and throat', *Cell host & microbe*, 21(4), p. 421.
- Rath, H., Feng, D., Neuweiler, I., Stumpp, N.S., Nackenhorst, U. & Stiesch, M. (2017) 'Biofilm formation by the oral pioneer colonizer *Streptococcus gordonii*: an experimental and numerical study', *FEMS microbiology ecology*, 93(3), .
- Rath, S., Bal, S.C.B. & Dubey, D. (2021) 'Oral Biofilm: Development Mechanism, Multidrug resistance, and their effective management with novel techniques', *Rambam Maimonides Medical Journal*, 12(1), .
- Ratzke, C. & Gore, J. (2018) 'Modifying and reacting to the environmental pH can drive bacterial interactions', *PLoS Biology*, 16(3), .
- Reddersen, K., Güllmar, A., Tonndorf-Martini, S., Sigusch, B.W., Ewald, A., Dauben, T.J., Martin, K. & Wiegand, C. (2021) 'Critical parameters in cultivation of experimental biofilms using the example of *Pseudomonas fluorescens*', *Journal of Materials Science: Materials in Medicine*, 32(9), .
- Renye, J.A., Piggot, P.J., Daneo-Moore, L. & Buttaro, B.A. (2004) 'Persistence of *Streptococcus mutans* in stationary-phase batch cultures and biofilms', *Applied and Environmental Microbiology*, 70(10), p. 6181.

- Roberts, J.M., Bradshaw, D.J., Lynch, R.J.M., Higham, S.M. & Valappil, S.P. (2021) 'The cariogenic effect of starch on oral microcosm grown within the dual constant depth film fermenter', *PLOS ONE*, 16(10), p. 258881.
- Roberts, S., Wei, G. & Wu, C. (2002) Evaluating biofilm growth of two oral pathogens *Letters of Applied Microbiology*.
- Roberts, W.E., Mangum, J.E. & Schneider, P.M. (2022) 'Pathophysiology of demineralization, part II: Enamel white spots, cavitated caries, and bone infection'. *current osteoporosis Reports*, 20 (1), pp. 106–119.
- Rock, J.D., Thomson, M.J., Read, R.C. & Moir, J.W.B. (2007) 'Regulation of denitrification genes in *Neisseria meningitidis* by nitric oxide and the repressor NsrR', *Journal of Bacteriology*, 189(3), pp. 1138–1144.
- Roels, J.A. (1980) Application of macroscopic principles to microbial metabolism, *Biotechnology and Bioengineering*, pp. 2457-2505.
- Rosso, L., Lobry, J.R., Bajard, S. & Flandrois, J.P. (1995) 'Convenient model to describe the combined effects of temperature and pH on microbial growth', *Applied and Environmental Microbiology*, 61(2), p. 610.
- Rudney, J.D., Chen, R., Lenton, P., Li, J., Li, Y., Jones, R.S., Reilly, C., Fok, A.S. & Aparicio, C. (2012) 'A reproducible oral microcosm biofilm model for testing dental materials', *Journal of Applied Microbiology*, 113(6), pp. 1540–1553.
- Rusu, L.-C., Roi, A., Roi, C.-I., Tigmeanu, C.V., Ardelean, L.C., Rusu, L.-C., Roi, A., Roi, C.-I., Tigmeanu, C.V. & Ardelean, L.C. (2022) The Influence of Salivary pH on the Prevalence of Dental Caries, *Dental Caries*.
- van Ruyven', F.O.J., Lingström, P., van Houte, J. & Kene, R. (2000) 'Relationship among *Mutans Streptococci*, "Low pH" bacteria, and iodophilic polysaccharide-producing bacteria in dental plaque and early enamel caries in humans, *Journal of Dental Research*, (79), pp. 778-784.
- Salli, K.M. & Ouwehand, A.C. (2015) 'The use of *in vitro* model systems to study dental biofilms associated with caries: a short review', *Journal of Oral Microbiology*, (1), pp. 1–7.
- Salomão, P.M.A., Comar, L.P., Buzalaf, M.A.R. & Magalhães, A.C. (2016) 'In situ remineralisation response of different artificial caries-like enamel lesions to home-care and professional fluoride treatments', *BMC Oral Health*, 16(1), pp. 1–9.

- Sambunjak, D., Nickerson, J.W., Pericic, T.P., Johnson, T.M., Imai, P., Tugwell, P. & Worthington, H. v. (2019) 'Flossing for the management of periodontal diseases and dental caries in adults', *The Cochrane Database of Systematic Reviews*, 2019(4), .
- Sateriale, D., Imperatore, R., Colicchio, R., Pagliuca, C., Varricchio, E., Volpe, M.G., Salvatore, P., Paolucci, M. & Pagliarulo, C. (2020) 'Phytochemicals vs. dental plaque bacteria: *In vitro* effects of myrtle and pomegranate polyphenolic extracts against single-species and multispecies oral biofilms', *Frontiers in Microbiology*, 11, p. 2742.
- Sato, T., Watanabe, K., Kumada, H., Toyama, T., Tani-Ishii, N. & Hamada, N. (2012) 'Peptidoglycan of *Actinomyces naeslundii* induces inflammatory cytokine production and stimulates osteoclastogenesis in alveolar bone resorption', *Archives of Oral Biology*, 57(11), pp. 1522–1528.
- Schlafer, S., Raarup, M.K., Meyer, R.L., Sutherland, D.S., Dige, I., Nyengaard, J.R. & Nyvad, B. (2011) 'pH landscapes in a novel five-species model of early dental biofilm', *PLoS ONE*, 6(9), .
- Schluter, J., Nadell, C.D., Bassler, B.L. & Foster, K.R. (2015) 'Adhesion as a weapon in microbial competition', *The ISME journal*, 9(1), pp. 139–149.
- Schreiber, F., Stief, P., Gieseke, A., Heisterkamp, I.M., Verstraete, W., de Beer, D. & Stoodley, P. (2010) Denitrification in human dental plaque, *BMC Biology*, 24, pp. 1-8
- Seeliger, S., Janssen, P.H. & Schink, B. (2002) Energetics and kinetics of lactate fermentation to acetate and propionate via methylmalonyl-CoA or acrylyl-CoA, *FEMS Microbiology Letter*, pp. 65-70
- Senneby, A., Davies, J.R., Svensäter, G. & Neilands, J. (2017a) 'Acid tolerance properties of dental biofilms *in vivo*', *BMC Microbiology*, 17(1), .
- Senneby, A., Davies, J.R., Svensäter, G. & Neilands, J. (2017b) 'Acid tolerance properties of dental biofilms *in vivo*', *BMC Microbiology*, 17(1), .
- Seo, J., Sim, Y., Kim, J., Kim, H., Cho, I., Nam, H., Yoon, Y.G. & Chang, J.B. (2022) 'PICASSO allows ultra-multiplexed fluorescence imaging of spatially overlapping proteins without reference spectra measurements', *Nature Communications*, 13(1), .
- Sharma, D., Misba, L. & Khan, A.U. (2019) 'Antibiotics versus biofilm: an emerging battleground in microbial communities', *Antimicrobial Resistance & Infection Control* 2019 8:1, 8(1), pp. 1–10.

- Shi, D., Mi, G., Wang, M. & Webster, T.J. (2019) 'In vitro and ex vivo systems at the forefront of infection modeling and drug discovery', *Biomaterials*, 198p. 228.
- Simon-Soro, A., Ren, Z., Krom, B.P., Hoogenkamp, M.A., Cabello-Yeves, P.J., Daniel, S.G., Bittinger, K., Tomas, I., Koo, H. & Mira, A. (2022) 'Polymicrobial aggregates in human saliva build the oral biofilm', *mBio*, 13(1), .
- Simón-Soro, Á., Tomás, I., Cabrera-Rubio, R., Catalan, M.D., Nyvad, B. & Mira, A. (2013) 'Microbial geography of the oral cavity', *Journal of dental research*, 92(7), pp. 616–621.
- Singh, S., Singh, S.K., Chowdhury, I. & Singh, R. (2017) 'Understanding the mechanism of bacterial biofilms resistance to antimicrobial agents', *The Open Microbiology Journal*, 11(1), p. 53.
- Slot, D.E., Wiggelinkhuizen, L., Rosema, N.A. & van der Weijden, G.A. (2012) 'The efficacy of manual toothbrushes following a brushing exercise: a systematic review.', *International journal of dental hygiene*, 10(3), pp. 187–197.
- Socransky, S.S., Dzink, J.L. & Smith, C.M. (1985) 'Chemically defined medium for oral microorganisms'. *Journal Of Clinical Microbiology*, pp 303-305.
- Solsi, A., Findakly, D., Mihyaw, N. & Fath, A.R. (2020) 'An unusual case of *Neisseria flavescens/subflava* group tricuspid valve endocarditis in a patient with previously treated methicillin-resistant *Staphylococcus aureus* endocarditis', *Cureus*, 12(8), .
- Song, W.S., Lee, J.K., Park, S.H., Um, H.S., Lee, S.Y. & Chang, B.S. (2017) 'Comparison of periodontitis-associated oral biofilm formation under dynamic and static conditions', *Journal of Periodontal and Implant Science*, 47(4), pp. 219–230.
- Sotozono, M., Kuriki, N., Asahi, Y., Noiri, Y., Hayashi, M., Motooka, D., Nakamura, S., Machi, H., Iida, T. & Ebisu, S. (2021) 'Impacts of sleep on the characteristics of dental biofilm', *Scientific Reports*, 11(1), p. 138.
- Stoodley, P.W.J.M.A.B.P. (2022) 'Development of an *in vitro* model system for the investigation of oral healthcare active compounds', in <https://tt21c.org/wp-content/uploads/2019/06/Development-of-an-in-vitro-model-system-for-the-investigation-of-oral-antibacterial-technologies-and-active-compounds.pdf>. [Online]. 2022, pp. 1–14.
- Strauss, F.J., Espinoza, I., Stähli, A., Baeza, M., Cortés, R., Morales, A. & Gamonal, J. (2019) 'Dental caries is associated with severe periodontitis in Chilean adults: A cross-sectional study', *BMC Oral Health*, 19(1), pp. 1–8.

- Streptococcus gordonii* str. Challis substr. CH1 (ID 1021) - Genome - NCBI. [online]. Available from: https://www.ncbi.nlm.nih.gov/genome/1021?genome_assembly_id=300484 (Accessed 14 October 2022).
- Streptococcus mutans* (ID 856) - Genome - NCBI. [online]. Available from: https://www.ncbi.nlm.nih.gov/genome/856?genome_assembly_id=1918837 (Accessed 14 October 2022).
- Stubbenieck, R.M., Vargas-Bautista, C. & Straight, P.D. (2016) 'Bacterial communities: interactions to scale', *Frontiers in Microbiology*, 7(AUG), p. 1234.
- Sunde, P.T., Olsen, I., Göbel, U.B., Theegarten, D., Winter, S., Debelian, G.J., Tronstad, L. & Moter, A. (2003) 'Fluorescence in situ hybridization (FISH) for direct visualization of bacteria in periapical lesions of asymptomatic root-filled teeth'. *Microbiology* 149 (5) p.pp. 1095–1102.
- Sund-Levander, M., Forsberg, C. & Wahren, L.K. (2002) 'Normal oral, rectal, tympanic and axillary body temperature in adult men and women: a systematic literature review', *Scandinavian journal of caring sciences*, 16(2), pp. 122–128.
- Suzuki, N., Yoshida, A. & Nakano, Y. (2005) 'Quantitative analysis of multi-species oral biofilms by TaqMan Real-Time PCR', *Clinical Medicine & Research*, 3(3), pp. 176–185.
- Svensäter, G., Larsson, U.B., Greif, E.C.G., Cvitkovitch, D.G. & Hamilton, I.R. (1997) 'Acid tolerance response and survival by oral bacteria', *Oral microbiology and immunology*, 12(5), pp. 266–273.
- Tabenski, L., Maisch, T., Santarelli, F., Hiller, K.A. & Schmalz, G. (2014) 'Individual growth detection of bacterial species in an in vitro oral polymicrobial biofilm model', *Archives of Microbiology*, 196(11), pp. 819–828.
- Table of Acid and Base Strength*. [online]. Available from: <https://depts.washington.edu/eoopic/links/acidstrength.html> (Accessed 25 November 2022).
- Takahashi, N. (2015) 'Oral microbiome metabolism: From "who are they?" to "what are they doing?"', *Journal of Dental Research*, 94(12), pp. 1628–1637.
- Takahashi, N. & Nyvad, B. (2008) 'Caries Ecology Revisited: Microbial Dynamics and the Caries Process', *Caries Research*, 42(6), pp. 409–418.
- Takahashi, N. & Nyvad, B. (2016) 'Ecological hypothesis of dentin and root caries', *Caries Research*, 50(4), pp. 422–431.

- Takahashi, N & Yamada, T. (1999) 'Acid-induced acid tolerance', *Oral Microbiol Immunol*, 14pp. 43–48.
- Takahashi, N. & Yamada, T. (1999) 'Glucose and lactate metabolism by *Actinomyces naeslundii*', *Critical reviews in oral biology*, 10(4), pp. 487–503.
- Tanzer, J.M., Thompson, A., Sharma, K., Vickerman, M.M., Haase, E.M. & Scannapieco, F.A. (2012) '*Streptococcus mutans* out-competes *Streptococcus gordonii* in vivo', *Journal of Dental Research*, 91(5), p. 513.
- Tanzer, J.M., Thompson, A., Wen, Z.T. & Burne, R.A. (2006) *Streptococcus mutans*: Fructose Transport, Xylitol Resistance, and Virulence, *Journal of Dental Research*.
- Terleckyj, B., Willett, N.P. & Shockman, G.D. (1975) Growth of several cariogenic strains of oral *Streptococci* in a chemically defined medium, *Infection Immunology*, 11 (4).
- The Oral Microbiome & Systemic Disease | Semantic Scholar*. [online]. Available from: <https://www.semanticscholar.org/paper/The-Oral-Microbiome-%26-Systemic-Disease-Withers/6a229966a541d73b57bb910f01f52f1a114c9672> (Accessed 26 October 2022).
- Thurnheer, T., Gmur, R., Giertsen, E., Guggenheim, B. & Switzerland", S. (2001) 'Automated fluorescent in situ hybridization for the specific detection and quantification of oral *Streptococci* in dental plaque'. *Journal of Microbiological Methods*, 44.
- Thurnheer, T., Gmür, R. & Guggenheim, B. (2004) 'Multiplex FISH analysis of a six-species bacterial biofilm', *Journal of Microbiological Methods*, 56(1), pp. 37–47.
- TOPO™ TA Cloning™ Kit for Subcloning, with One Shot™ TOP10 chemically competent E. coli cells*. [online]. Available from: <https://www.thermofisher.com/order/catalog/product/K4500J10> (Accessed 29 September 2022).
- Valdebenito, B., Tullume-Vergara, P.O., González, W., Kreth, J. & Giacaman, R.A. (2018) '*In silico* analysis of the competition between *Streptococcus sanguinis* and *Streptococcus mutans* in the dental biofilm', *Molecular oral microbiology*, 33(2), pp. 168–180.
- Valm, A.M. (2019a) 'The structure of dental plaque microbial communities in the transition from health to dental caries and periodontal disease', *Journal of molecular biology*, 431(16), p. 2957.

- Valm, A.M., Mark Welch, J.L. & Borisy, G.G. (2012) 'CLASI-FISH: Principles of combinatorial labeling and spectral imaging', *Systematic and Applied Microbiology*, 35(8), pp. 496–502.
- Valour, F., Sénéchal, A., Dupieux, C., Karsenty, J., Lustig, S., Breton, P., Gleizal, A., Bousset, L., Laurent, F., Braun, E., Chidiac, C., Ader, F. & Ferry, T. (2014) 'Actinomycosis: Etiology, clinical features, diagnosis, treatment, and management'. *Infection and Drug Resistance*, 7, pp. 183–197.
- Vanhatalo, A., Blackwell, J.R., L'Heureux, J.E., Williams, D.W., Smith, A., van der Giezen, M., Winyard, P.G., Kelly, J. & Jones, A.M. (2018) 'Nitrate-responsive oral microbiome modulates nitric oxide homeostasis and blood pressure in humans', *Free radical biology & medicine*, 124pp. 21–30.
- Veillonella parvula* DSM 2008 (ID 2471) - Genome - NCBI. [online]. Available from: https://www.ncbi.nlm.nih.gov/genome/2471?genome_assembly_id=172451 (Accessed 14 October 2022).
- Volcke, E.I.P., van Hulle, S., Deksissa, T., Zaher, U. & Vanrolleghem, P. (2005), Calculation of pH and concentration of equilibrium components during dynamic simulation by means of a charge balance, *Biomath*.
- Wang, B.Y., Deutch, A., Hong, J. & Kuramitsu, H.K. (2011) 'Proteases of an early colonizer can hinder *Streptococcus mutans* colonization *in vitro*', *Journal of Dental Research*. [Online]. April 2011 pp. 501–505.
- Wasfi, R., Abd El-Rahman, O.A., Zafer, M.M. & Ashour, H.M. (2018) 'Probiotic *Lactobacillus sp.* inhibit growth, biofilm formation and gene expression of caries-inducing *Streptococcus mutans*', *Journal of Cellular and Molecular Medicine*, 22(3), p. 1972.
- Welin-Neilands, J. & Svensäter, G. (2007) 'Acid Tolerance of Biofilm Cells of *Streptococcus mutans*', *Applied and Environmental Microbiology*, 73(17), p. 5633.
- Willenborg, J. & Goethe, R. (2016a) 'Metabolic traits of pathogenic streptococci'. *FEBS Letters* 590 (21) p.pp. 3905–3919.
- Wimpenny, J.W.T. & Colasanti, R. (1997) 'A unifying hypothesis for the structure of microbial biofilms based on cellular automaton models', *FEMS Microbiology Ecology*, 22(1), pp. 1–16.
- Withers, S. (2019) *The Oral Microbiome & Systemic Disease*, Dental care, p4.

- Xiao, J., Hara, A.T., Kim, D., Zero, D.T., Koo, H. & Hwang, G. (2017) 'Biofilm three-dimensional architecture influences in situ pH distribution pattern on the human enamel surface', *International Journal of Oral Science*, 9(2), p. 74.
- Xu, W., Zhou, W., Wang, H. & Liang, S. (2020) 'Roles of *Porphyromonas gingivalis* and its virulence factors in periodontitis', *Advances in protein chemistry and structural biology*, 120p. 45.
- Yaws, C.L. (2009) Transport properties of chemicals and hydrocarbons : viscosity, thermal conductivity, and diffusivity of C1 to C100 organics and Ac to Zr inorganics, p. 597.
- Yin, W., Wang, Y., Liu, L. & He, J. (2019) 'Biofilms: The microbial "protective clothing" in extreme environments', *International Journal of Molecular Sciences*, 20(14), .
- Yoshida, A. & Kuramitsu, H.K. (2002) 'Multiple *Streptococcus mutans* genes are involved in biofilm formation', *Applied and Environmental Microbiology*, 68(12), p. 6283.
- Yoshida, A., Suzuki, N., Nakano, Y., Kawada, M., Oho, T. & Koga, T. (2003) 'Development of a 5' nuclease-based real-time PCR assay for quantitative detection of cariogenic dental pathogens *Streptococcus mutans* and *Streptococcus sobrinus*', *Journal of Clinical Microbiology*, 41(9), pp. 4438–4441.
- Zaura, E., Keijsers, B.J., Huse, S.M. & Crielaard, W. (2009), 'Defining the healthy "core microbiome" of oral microbial communities', *BMC Microbiology*, 9p. 259.
- Zeng, L. & Burne, R.A. (2021) 'Molecular mechanisms controlling fructose-specific memory and catabolite repression in lactose metabolism by *Streptococcus mutans*', *Molecular microbiology*, 115(1), p. 70.
- Zhang, H., Xia, M., Zhang, B., Zhang, Y., Chen, H., Deng, Y., Yang, Y., Lei, L. & Hu, T. (2022) 'Sucrose selectively regulates *Streptococcus mutans* polysaccharide by GcrR', *Environmental Microbiology*, 24(3), pp. 1395–1410.
- Zhang, X., Gao, X., Li, C., Luo, X. & Wang, Y. (2019) 'Fluoride contributes to the shaping of microbial community in high fluoride groundwater in Qiji County, Yuncheng City, China', *Scientific Reports 2019 9:1*, 9(1), pp. 1–10.
- Zhang, X. & Senpuku, H. (2013) 'Dynamic changes in the initial colonization of *Actinomyces naeslundii* and *Streptococcus gordonii* using a new animal model', *Japanese journal of infectious diseases*, 66(1), pp. 11–16.
- Zhang, Y., Ding, Y. & Guo, Q. (2022a) 'Probiotic species in the management of periodontal diseases: An overview', *Frontiers in Cellular and Infection Microbiology*, 12.

- Zhang, Y., Ding, Y. & Guo, Q. (2022b) 'Probiotic species in the management of periodontal diseases: An overview', *Frontiers in Cellular and Infection Microbiology*, 12p. 308.
- Zheng, L., Itzek, A., Chen, Z. & Kreth, J. (2011) 'Environmental influences on competitive hydrogen peroxide production in *Streptococcus gordonii*', *Applied and Environmental Microbiology*, 77(13), pp. 4318–4328.
- Zhou, P., Li, X., Huang, I.H. & Qi, F. (2017) 'Veillonella catalase protects the growth of *Fusobacterium nucleatum* in microaerophilic and *Streptococcus gordonii*-resident environments', *Applied and Environmental Microbiology*, 83(19), .
- Zhou, P., Manoil, D., Belibasakis, G.N. & Kotsakis, G.A. (2021a) 'Veillonellae: Beyond bridging species in oral biofilm ecology', *Frontiers in Oral Health*, 2.
- Zhou, Y., Millhouse, E., Shaw, T., Lappin, D.F., Rajendran, R., Bagg, J., Lin, H. & Ramage, G. (2018) 'Evaluating *Streptococcus mutans* strain dependent characteristics in a Polymicrobial Biofilm Community', *Frontiers in microbiology*, pp 1-5.

Appendix A- AFMC medium components

| Chemical | Concentration (g L ⁻¹) | Concentration (mol L ⁻¹) |
|---|------------------------------------|--------------------------------------|
| Monopotassium phosphate | 0.44 | 3.23 x 10 ⁻³ |
| Dipotassium phosphate | 0.30 | 1.72 x 10 ⁻³ |
| Ammonium sulfate | 0.60 | 4.54 x 10 ⁻³ |
| sodium phosphate | 3.15 | 1.92 x 10 ⁻² |
| Sodium dihydrogen phosphate monohydrate | 2.67 | 1.93 x 10 ⁻² |
| Sodium citrate | 0.26 | 9.93 x 10 ⁻⁴ |
| Magnesium sulfate heptahydrate | 0.39 | 3.24 x 10 ⁻³ |
| Sodium Chloride | 0.01 | 1.71 x 10 ⁻⁴ |
| Iron (II) Sulfate heptahydrate | 0.02 | 7.91 x 10 ⁻⁵ |
| Manganese Sulfate heptahydrate | 0.01 | 5.23 x 10 ⁻⁵ |
| Na acetate | 6.12 | 7.46 x 10 ⁻² |
| L-aspartic acid | 0.10 | 7.51 x 10 ⁻⁴ |
| L-phenylalanine | 0.10 | 6.05 x 10 ⁻⁴ |
| L-serine | 0.10 | 9.52 x 10 ⁻⁴ |
| L-proline | 0.20 | 1.74 x 10 ⁻³ |
| L-hydroxyproline | 0.20 | 1.53 x 10 ⁻³ |
| Glycine | 0.20 | 2.66 x 10 ⁻³ |
| L-methionine | 0.10 | 6.70 x 10 ⁻⁴ |
| L-leucine | 0.10 | 7.62 x 10 ⁻⁴ |
| DL-alanine | 0.10 | 1.12 x 10 ⁻³ |
| L-isoleucine | 0.10 | 7.62 x 10 ⁻⁴ |
| L-threonine | 0.10 | 8.39 x 10 ⁻⁴ |
| L-arginine.HCl | 0.24 | 1.38 x 10 ⁻³ |
| L-histidine.HCl.H2O | 0.27 | 1.26 x 10 ⁻³ |
| L-valine | 0.10 | 8.54 x 10 ⁻⁴ |
| L-lysine.HCl | 0.14 | 9.41 x 10 ⁻⁴ |
| L-glutamine | 0.01 | 3.42 x 10 ⁻⁵ |
| Nicotinamide | 9.00 x 10 ⁻⁴ | 7.37 x 10 ⁻⁶ |
| D-pantothenate | 7.20 x 10 ⁻⁴ | 2.98 x 10 ⁻⁶ |
| Thiamine.HCl | 3.36 x 10 ⁻⁴ | 9.96 x 10 ⁻⁷ |

| | | |
|---|-----------------------|-----------------------|
| p-aminobenzoic acid | 9.00×10^{-5} | 6.56×10^{-7} |
| Pyridoxamine.2HCl | 1.04×10^{-3} | 6.16×10^{-6} |
| L-glutamic acid | 0.27 | 1.84×10^{-3} |
| L-tyrosine | 0.18 | 9.94×10^{-4} |
| L-tryptophan | 0.20 | 9.79×10^{-4} |
| L-cystine | 0.20 | 8.32×10^{-4} |
| Riboflavin | 4.00×10^{-4} | 1.06×10^{-6} |
| Biotin | 1.00×10^{-4} | 4.09×10^{-7} |
| Folic acid | 1.00×10^{-4} | 2.27×10^{-7} |
| Adenine sulphate | 0.02 | 6.29×10^{-5} |
| Guanine | 0.01 | 8.70×10^{-5} |
| Uracil | 0.01 | 1.17×10^{-4} |
| Calcium chloride | 0.01 | 1.32×10^{-4} |
| Pimelic acid | 1.00×10^{-3} | 6.24×10^{-6} |
| Putrescine (1-4 Diaminobutane) | 0.01 | 1.13×10^{-4} |
| Lactic acid | 12.10 | 1.34×10^{-1} |
| Thioctic acid | 1.00×10^{-3} | 4.85×10^{-6} |
| Cysteine | 1.00 | 8.25×10^{-3} |
| Inositol | 2.00×10^{-3} | 1.11×10^{-5} |

Appendix B- Gibbs free energy of formation for chemical species

| Component | ΔG_f^0 (kJ/mol) | Reference |
|---|---|---|
| Glucose | -915.9 | (Heijnen and Kleerebezem 2010) Perry and Green (2008) |
| Acetic acid (CH ₃ COOH) | $\Delta G_{f, \text{CH}_3\text{COOH}} = -396.5$ $\Delta G_{f, \text{CH}_3\text{COO}^-} = -369.3$ | |
| Lactic acid (CH ₃ CHCOOH) | $\Delta G_{f, \text{CH}_3\text{CHCOOH}} = -430.62$ $\Delta G_{f, \text{CH}_3\text{CHCOO}^-} = -403$ | |
| Formic acid (HCOOH) | $\Delta G_{f, \text{HCOOH}} = -493.96$ $\Delta G_{f, \text{HCOO}^-} = -463$ | |
| Propionic acid (CH ₃ CH ₂ COOH) | $\Delta G_{f, \text{CH}_3\text{CH}_2\text{COOH}} = -291.36$ $\Delta G_{f, \text{CH}_3\text{CH}_2\text{COO}^-} = -263$ | |
| NH₃ | $-\Delta G_{f, \text{NH}_3} = -26.57$ $\Delta G_{f, \text{NH}_4^+} = -79.37$ | |
| O₂ | 16.40 | |
| CO₂ | $\Delta G_{f, \text{hydrolysis}} = -386.00$ $\Delta G_{f, \text{H}_2\text{CO}_3} = -623.16$ $\Delta G_{f, \text{HCO}_3^-} = -586.85$ $\Delta G_{f, \text{CO}_3^{2-}} = -527.8$ | |

Appendix C- Stoichiometry table for synthetic community species

| | <i>S. gordonii</i> (SGN) | | <i>S. mutans</i> (SMT) | | <i>A.Oris</i> (ACO) | | <i>N. subflava</i> (NSB) | | <i>V. parvula</i> (VPV) | |
|---|-----------------------------|------------|---------------------------|------------|------------------------|------------|-----------------------------|------------|----------------------------|------------|
| | <i>Cat</i> | <i>Ana</i> | <i>Cat</i> | <i>Ana</i> | <i>Cat</i> | <i>Ana</i> | <i>Cat</i> | <i>Ana</i> | <i>Cat</i> | <i>Ana</i> |
| Glu | -1 | -0.175 | -1 | -0.175 | -1 | -0.175 | -1 | -0.175 | - | - |
| AcH | - | - | - | - | - | - | 2 | - | 0.333 | - |
| LacH | 2 | - | 2 | - | 2 | - | - | - | -1 | -0.35 |
| ForH | - | - | - | - | - | - | 1 | - | - | - |
| PropH | - | - | - | - | - | - | - | - | 0.667 | - |
| NH₃ | - | -0.2 | - | -0.2 | - | -0.2 | - | -0.2 | - | -0.2 |
| O₂ | - | - | - | - | - | - | -1.5 | - | - | - |
| CO₂ | - | 0.05 | - | 0.05 | - | 0.05 | 2 | 0.05 | 0.333 | 0.05 |
| H₂O | - | 0.4 | - | 0.4 | - | 0.4 | - | 0.4 | - | 0.4 |
| H⁺ | 2 | 0.05 | 2 | 0.05 | 2 | 0.05 | 4 | 0.05 | 0.333 | 0.05 |
| CH_{1.8}O_{0.5}N_{0.2} | - | 1 | - | 1 | - | 1 | - | 1 | - | 1 |

Appendix D- Dissociation constants for chemical species

| Component | Dissociation constant | Reference |
|------------------------|---|---|
| Lactic acid | $10^{-3.86}$ | (Ilie, van Loosdrecht <i>et al.</i> , 2012) |
| Acetic acid | $10^{-4.76}$ | |
| Formic acid | $10^{-3.75}$ | |
| Propionic acid | $10^{-4.86}$ | |
| NH₃ | $5.6204 \cdot 10^{-10}$ | |
| H₂O | 10^{-14} | |
| CO₂ | $k_{eq,1} = 1.0081$ $k_{eq,2} = 5.0 \cdot 10^{-7}$ $k_{eq,3} = 7 \cdot 10^{-11}$ | |
| Phosphoric acid | $k_{eq,1} = 7.1 \cdot 10^{-3}$ $k_{eq,2} = 6.3 \cdot 10^{-8}$ $k_{eq,3} = 4.2 \cdot 10^{-13}$ | |

Appendix E- Code and functions for *in silico* models

0-D continuous model

Link to files:

<https://drive.google.com/file/d/1365wQn5FOngzuw36O63g6cn87yl8ar19/view?usp=sharing>

List of functions:

Assemble- Assembles the metabolic matrix and selects the species that participate in the reactor

MainStaggeredpH- Solves the reactor model

ReactorExtnopH- Solves pH (no pH correction)

ReactorExtpH- Solves pH (pH correction)

Read_conc- Reads chemicals from AFM in Repository excel sheet

Read_param- Reads kinetic parameters and chemical parameters from Repository excel

Solve- Solves the pH

Repository- Excel spreadsheet, including species stoichiometry, species charges, kinetic parameters etc.

2-D individual based model

Link to files:

https://drive.google.com/drive/folders/1ZNIInMNP8pB0x0GnDuqKej7xD2B-Tzu6p?usp=share_link

List of functions:

Call.m - This file initialises the simulation and calls the numerical solver.

loadModelXslx.m - Loads the parameters from the excel sheet and generates the structure of the model

R.mat- Contains the code for initial seeding of bacterial cells

integTime.m - Solver function. Solves the mass balance equations for:

- Liquid species: diffusion-reaction eq.
- Bacterial species: Monod growth eq.

out_integTime – Saves all the info after an integration step has been successfully completed

DiffMatrices.m – Computes the boundary layer position using the **b_layer.m** function.

Creates the domain decomposition for solving the diffusion equations (only the diffusion term, according to the numerical method)

massBal.m – Calls ***mykinetics.m*** to calculate the reaction term for the liquid species

mykinetics.m –Computes the yields, pH (**solve pH-embedded function**), liquid reaction rates and bacteria growth rates

bacteria.m – Checks for division (**bac_division.m**), maximum height of the biofilm

(**bac_elim.m**) and over-lapping (**bac_shovingloops.m**)

Updates the field with bacterial attributes in the R structure

boundary.m –Updates the boundary conditions in accordance with the CSTR performance

draw.m – Result processing function. Draws the bacteria position, number, concentration, liquid species concentration field, concentration in one grid cell, pH over computational domain, pH in a grid cell (function of time).